Issue 1 2015 | Volume 11

The Journal on Advanced Studies in Theoretical and Experimental Physics, including Related Themes from Mathematics

PROGRESS IN PHYSICS

"All scientists shall have the right to present their scientific research results, in whole or in part, at relevant scientific conferences, and to publish the same in printed scientific journals, electronic archives, and any other media." — Declaration of Academic Freedom, Article 8

ISSN 1555-5534

The Journal on Advanced Studies in Theoretical and Experimental Physics, including Related Themes from Mathematics

PROGRESS IN PHYSICS

A quarterly issue scientific journal, registered with the Library of Congress (DC, USA). This journal is peer reviewed and included in the abstracting and indexing coverage of: Mathematical Reviews and MathSciNet (AMS, USA), DOAJ of Lund University (Sweden), Zentralblatt MATH (Germany), Scientific Commons of the University of St. Gallen (Switzerland), Open-J-Gate (India), Referativnyi Zhurnal VINITI (Russia), etc.

Electronic version of this journal:
http://www.ptep-online.com

Postal Address

Department of Mathematics and Science,
University of New Mexico,
705 Gurley Ave., Gallup, NM 87301, USA

ISSN: 1555-5534 (print)
ISSN: 1555-5615 (online)

Standard Address Number: 297-5092
Printed in the United States of America

January 2015 **Vol. 11, Issue 1**

CONTENTS

Information for Authors and Subscribers

Progress in Physics has been created for publications on advanced studies in theoretical and experimental physics, including related themes from mathematics and astronomy. All submitted papers should be professional, in good English, containing a brief review of a problem and obtained results.

All submissions should be designed in LaTeX format using *Progress in Physics* template. This template can be downloaded from *Progress in Physics* home page http://www.ptep-online.com. Abstract and the necessary information about author(s) should be included into the papers. To submit a paper, mail the file(s) to the Editor-in-Chief.

All submitted papers should be as brief as possible. Short articles are preferable. Large papers can also be considered in exceptional cases. Letters related to the publications in the journal or to the events among the science community can be applied to the section *Letters to Progress in Physics*.

All that has been accepted for the online issue of *Progress in Physics* is printed in the paper version of the journal. To order printed issues, contact the Editors.

This journal is non-commercial, academic edition. It is printed from private donations. (Look for the current author fee in the online version of the journal.)

EDITORIAL MESSAGE

Progress in Physics: 10 Years in Print

In January, 2015, we celebrate first 10 years of our journal *Progress in Physics*. This is a good time to remember what events led to the idea of the journal, and how the journal was founded.

Ten years ago, in the fall of 2004, CERN Document Server has changed its policy so that it closed its door for all future pre-prints submitted by non-CERN employee. All other persons were advised to submit their papers to Cornell E-Print Archive (known as arXiv.org).

The main problem of this change was that Cornell E-Print Archive only accept papers from people who have a scientific institute affiliation. This policy continues to this day, and is a necessary condition for consideration of papers in almost all modern scientific journals.

This was a serious impact to the scientific community, where so many researchers continue their studies in between short-term grants, or even continue their scientific activity as independent researchers. They all are not affiliated to any scientific institution. So, they all loose their fundamental right to be published in scientific journals.

But it was not always. In already the beginning of the 20th century, every person was able to submit a paper to any scientific journal. And this paper was considered according to its real scientific importance, not the formal degree or scientific institute affiliation of the submitter. Otherwise, many great scientists such as Einstein and others would never have published their scientific works.

However, in the early 20th century, science was a matter of a very few people. With the progress of democracy and improved living mass of the people, in the 1950–1960's, science has become a professional field of activity of hundreds of thousands and even millions of people in the world. Massive investment in research activities have led to the fact that the scientific community is filled with people who do not view science as a search for truth but as "employment". Many scientific workers speak frankly to each other that we went to the science just in order "to get good income" thus doing some formal activities in the field which is a hard to understand for investors who pay for it all. Such "research staff", not being burdened with a large intellectual tension of the solution of scientific problems were much more socially active than the real scientists. Therefore, they quickly and systematically took formal positions in the scientific community, including scientific journals. As a matter of fact that they considered real scientists as potentially dangerous persons, who may potentially qualify for their sure and well-paid job positions. To defend themselves, they built a complicate bureaucratic system, where, as Grisha Perelman said very well, no one researcher who is really busy with research will waste so much time and effort to fill out all the paperwork for a grant. Only familiarity in the editorial board of the scientific journal, or belonging to the "friendly" scientific group gives the opportunity to publish your article.

In this way, the scientific bureaucracy was born. This situation continues in the scientific community until this day.

In this background, CERN Document Server was the solely possibility to publish research papers for the scientists, who are not joined into "groups" or do not belong to "scientific clans". In the fall of 2004, this window was closed.

It is comical, but even papers authored by Brian Josephson (Nobel Prize in Physics, 1973) were refused by Cornell E-Print Archive. As was claimed the reason was that he has right only to submit articles on his very particular field of physics, and has not rights to submit articles on other field of physics where he "cannot be an expert".

Correspondence among Josephson and other researchers, who were thinking of the future of the scientific community, has began. In the course of correspondence with Josephson, I met Florentin Smarandache. We both were active CERN E-Print Server users. I looked for another possibility to publish a series of research papers authored by me and Larissa Borissova, my closest colleague and friend. In our common discussion with Florentin, I told him that we must establish a new journal of physics: it is better and easier than to fight for influence in existing journals. Do you like to see this journal in print? — Florentin replied. So, *Progress in Physics* was established by our common power. It was January, 2005.

Then I wrote *Declaration of Academic Freedom*, to fix the fundamental rights and freedoms allowed among the scientific community. This text, known also as *Academic Bill of Rights* is now published in ten languages. All that we do in our journal, is according to the articles of the Bill.

During the first year, we had no many authors and readers. Nevertheless, ten years later, i.e. now, the journal has grown very much. We now have a stable traffic in the range from 25,000 to 35,000 downloaded papers per month, with some peaks in the months when a hot research is published.

Despite some difficulties, the journal is now stable. We allow every person to submit a paper, with the warranty that the submission will be reviewed according only to scientific judgements, independent on the personality of the submitter. Our personnel works on voluntary basis, to keep the author's fee as low as possible. I hope that first 10 years of *Progress in Physics* will be the beginning of the long term life of the journal, among the other respected journal of physics.

Dmitri Rabounski, Editor-in-Chief

Trapping Regions for the Navier-Stokes Equations

Craig Alan Feinstein

2712 Willow Glen Drive, Baltimore, Maryland 21209. E-mail: cafeinst@msn.com

In 1999, J. C. Mattingly and Ya. G. Sinai used elementary methods to prove the existence and uniqueness of smooth solutions to the 2D Navier-Stokes equations with periodic boundary conditions. And they were almost successful in proving the existence and uniqueness of smooth solutions to the 3D Navier-Stokes equations using the same strategy. In this paper, we modify their technique to obtain a simpler proof of one of their results. We also argue that there is no logical reason why the 3D Navier-Stokes equations must always have solutions, even when the initial velocity vector field is smooth; if they do always have solutions, it is due to probability and not logic.

1 Introduction

In this paper, we examine the three-dimensional Navier-Stokes equations, which model the flow of incompressible fluids:

$$\left.\begin{aligned} &\frac{\partial u_i}{\partial t}+\sum_{j=1,2,3} u_j\frac{\partial u_i}{\partial x_j}=\nu\Delta u_i-\frac{\partial p}{\partial x_i} \qquad i=1,2,3\\ &\sum_{i=1,2,3}\frac{\partial u_i}{\partial x_i}=0 \end{aligned}\right\}, \quad (1)$$

where $\nu>0$ is viscosity, p is pressure, u is velocity, and $t>0$ is time. We shall assume that both u and p are periodic in x. For simplicity, we take the period to be one. The first equation is Newton's Second Law, force equals mass times acceleration, and the second equation is the assumption that the fluid is incompressible.

Mattingly and Sinai [5] attempted to show that smooth solutions to 3D Navier Stokes equations exist for all initial conditions $u(x,0)=u^0(x)\in C^\infty$ by dealing with an equivalent form of the Navier-Stokes equations for periodic boundary conditions:

$$\frac{\partial\omega_i}{\partial t}+\sum_{j=1,2,3} u_j\frac{\partial\omega_i}{\partial x_j}=\sum_{j=1,2,3}\omega_j\frac{\partial u_i}{\partial x_j}+\nu\Delta\omega_i \quad i=1,2,3, \quad (2)$$

where the vorticity $\omega(x,t)=(\frac{\partial u_2}{\partial x_3}-\frac{\partial u_3}{\partial x_2},\frac{\partial u_3}{\partial x_1}-\frac{\partial u_1}{\partial x_3},\frac{\partial u_1}{\partial x_2}-\frac{\partial u_2}{\partial x_1})$.

Their strategy was as follows: Represent the equations (2) as a Galerkin system in Fourier space with a basis $\{e^{2\pi ikx}\}_{k\in\mathbb{Z}^3}$. A finite dimensional approximation of this Galerkin system can be associated to any finite subset $\mathcal{Z}$ of $\mathbb{Z}^3$ by setting $u^{(k)}(t)=\omega^{(k)}(t)=0$ for all k outside of $\mathcal{Z}$. For each finite dimensional approximation of this Galerkin system, consider the system of coupled ODEs for the Fourier coefficients. Then construct a subset $\Omega(K)$ of the phase space (the set of possible configurations of the Fourier modes) so that all points in $\Omega(K)$ possess the desired decay properties. In addition, construct $\Omega(K)$ so that it contains the initial data. Then show that the dynamics never cause the sequence of Fourier modes to leave the subset $\Omega(K)$ by showing that the vector field on the boundary of $\Omega(K)$ points into the interior of $\Omega(K)$.

Unfortunately, their strategy only worked for the 3D Navier-Stokes equations when the Laplacian operator Δ in (2) was replaced by another similar linear operator. (Their strategy was in fact successful for the 2D Navier-Stokes equations.) In this paper, we attempt to apply their strategy to the original equations (1).

2 Navier-Stokes equations in Fourier space

Moving to Fourier space where

$$\left.\begin{aligned} u_i(x,t)&=\sum_{k\in\mathcal{Z}} u_i^{(k)}(t)e^{2\pi ikx}\\ p(x,t)&=\sum_{k\in\mathcal{Z}} p^{(k)}(t)e^{2\pi ikx}\\ |k|&=\sqrt{\sum_{j=1,2,3}k_j^2} \end{aligned}\right\}, \quad (3)$$

let us consider the system of coupled ODEs for a finite-dimensional approximation to the Galerkin-system corresponding to (1),

$$\frac{du_i^{(k)}}{dt}=\Big(\sum_{\substack{q+r=k\\ q,r\in\mathcal{Z}}}\sum_{j=1,2,3}-2\pi iq_ju_i^{(q)}u_j^{(r)}\Big)- -4\pi^2\nu|k|^2u_i^{(k)}-2\pi ik_ip^{(k)} \qquad i=1,2,3, \quad (4)$$

$$\sum_{i=1,2,3}k_iu_i^{(k)}=0\,, \quad (5)$$

where $\mathcal{Z}$ is a finite subset of $\mathbb{Z}^3$ in which $u^{(k)}(t)=p^{(k)}(t)==0$ for each $k\in\mathbb{Z}^3$ outside of $\mathcal{Z}$. Like the Mattingly and Sinai paper, in this paper, we consider a generalization of this Galerkin-system:

$$\frac{du_i^{(k)}}{dt}=\Big(\sum_{\substack{q+r=k\\ q,r\in\mathcal{Z}}}\sum_{j=1,2,3}-2\pi iq_ju_i^{(q)}u_j^{(r)}\Big)- -4\pi^2\nu|k|^\alpha u_i^{(k)}-2\pi ik_ip^{(k)} \qquad i=1,2,3, \quad (6)$$

$$\sum_{i=1,2,3}k_iu_i^{(k)}=0\,, \quad (7)$$

where $\alpha \geqslant 2$. Multiplying each of the first three equations by k_i for $i = 1, 2, 3$ and adding the resulting equations together, we obtain

$$\sum_{\substack{q+r=k \\ q,r\in\mathcal{Z}}} \sum_{\substack{j=1,2,3 \\ l=1,2,3}} -2\pi i k_l q_j u_l^{(q)} u_j^{(r)} = 2\pi i |k|^2 p^{(k)}, \tag{8}$$

since $\sum_{i=1,2,3} k_i \frac{du_i^{(k)}}{dt} = 0$ (by equation (7)). Then substituting the above calculated expression for $p^{(k)}$ in terms of u into (6) we obtain

$$\frac{du_i^{(k)}}{dt} = \Big[\sum_{\substack{q+r=k \\ q,r\in\mathcal{Z}}} \sum_{\substack{j=1,2,3 \\ l=1,2,3}} 2\pi i \left(\frac{k_i k_l}{|k|^2} - \delta_{il}\right) q_j u_l^{(q)} u_j^{(r)}\Big] - - 4\pi^2 \nu |k|^\alpha u_i^{(k)} \qquad i = 1, 2, 3. \tag{9}$$

And since $\sum_{j=1,2,3} r_j u_j^{(r)} = 0$ and $q_j + r_j = k_j$, we can substitute k_j for q_j:

$$\frac{du_i^{(k)}}{dt} = \Big[\sum_{\substack{q+r=k \\ q,r\in\mathcal{Z}}} \sum_{\substack{j=1,2,3 \\ l=1,2,3}} 2\pi i \left(\frac{k_i k_l}{|k|^2} - \delta_{il}\right) k_j u_l^{(q)} u_j^{(r)}\Big] - - 4\pi^2 \nu |k|^\alpha u_i^{(k)} \qquad i = 1, 2, 3. \tag{10}$$

3 A new theorem

Now, we state and prove the following theorem:

Theorem: *Let $\{u^{(k)}(t)\}$ satisfy (10), where $\alpha > 2.5$. And let $1.5 < s < \alpha - 1$. Suppose there exists a constant $C_0 > 0$ such that $|u^{(k)}(0)| \leqslant C_0 |k|^{-s}$, for all $k \in \mathbb{Z}^3$. Then there exists a constant $C > C_0$ such that $|u^{(k)}(t)| \leqslant C|k|^{-s}$, for all $k \in \mathbb{Z}^3$ and all $t > 0$. (The constants, C_0 and C, are independent of the set $\mathcal{Z}$ defining the Galerkin approximation.)*

Proof: By the basic energy estimate (see [1,2,7]), there exists a constant $E \geqslant 0$ such that for each $t \geqslant 0$ and for any finite-dimensional Galerkin approximation defined by $\mathcal{Z} \subset \mathbb{Z}^3$, we have $\sum_{k\in\mathcal{Z}} \sum_{i=1,2,3} |u_i^{(k)}(t)|^2 \leqslant E$. Hence, for any $K > 0$, we can find a $C > C_0$ such that $|\Re(u^{(k)})| \leqslant C|k|^{-s}$ and $|\Im(u^{(k)})| \leqslant C|k|^{-s}$, for all $t \geqslant 0$ and $k \in \mathbb{Z}^3$ with $|k| \leqslant K$. Now let us consider the set,

$$\Omega(K) = \Big\{\Big(\Re(u^{(k)}), \Im(u^{(k)})\Big)_{k\in\mathbb{Z}^3} : |k| > K\,, \quad |\Re(u^{(k)})| \leqslant C|k|^{-s}, \quad |\Im(u^{(k)})| \leqslant C|k|^{-s}\Big\}. \tag{11}$$

We will show that if K is chosen large enough, any point starting in $\Omega(K)$ cannot leave $\Omega(K)$, because the vector field along the boundary $\partial\Omega(K)$ is pointing inward, i.e., $\Omega(K)$ is a trapping region. Since the initial data begins in $\Omega(K)$, proving this would prove the theorem.

We pick a point on $\partial\Omega(K)$ where $\Re(u_i^{(\bar{k})})$ or $\Im(u_i^{(\bar{k})}) = \pm C|\bar{k}|^{-s}$ for some $\bar{k} \in \mathcal{Z}$ such that $|\bar{k}| > K$ and some $i \in \{1, 2, 3\}$. (For definiteness, we shall assume that $\Re(u_i^{(\bar{k})}) = C|\bar{k}|^{-s}$, but the same line of argument which follows also applies to the other possibilities.) Then the following inequalities hold when K is chosen large enough:

$$\Big|\sum_{\substack{q+r=\bar{k} \\ q,r\in\mathcal{Z}}} \sum_{\substack{j=1,2,3 \\ l=1,2,3}} 2\pi \left(\delta_{il} - \frac{\bar{k}_i \bar{k}_l}{|\bar{k}|^2}\right) \bar{k}_j \Im(u_l^{(q)} u_j^{(r)})\Big| \leqslant$$

$$\sum_{\substack{q+r=\bar{k} \\ q,r\in\mathcal{Z}}} \sum_{\substack{j=1,2,3 \\ l=1,2,3}} 4\pi |\bar{k}_j| |u_l^{(q)}| |u_j^{(r)}| \leqslant$$

$$\sum_{\substack{j=1,2,3 \\ l=1,2,3}} 4\pi |\bar{k}_j| \Big(\sum_{q\in\mathcal{Z}} |u_l^{(q)}|^2\Big)^{1/2} \Big(\sum_{r\in\mathcal{Z}} |u_j^{(r)}|^2\Big)^{1/2} \leqslant$$

$$\sum_{\substack{j=1,2,3 \\ l=1,2,3}} 4\pi |\bar{k}_j| E < 4\pi^2 \nu |\bar{k}|^\alpha \frac{C}{|\bar{k}|^s} = 4\pi^2 \nu |\bar{k}|^\alpha |\Re(u_i^{(\bar{k})})|. \tag{12}$$

This establishes that the vector field points inward along the boundary of $\Omega(K)$ for all $t > 0$. So the trajectory never at any time leaves $\Omega(K)$. Then we have the desired estimate that $|u^{(k)}(t)| \leqslant C|k|^{-s}$ for all $t > 0$. ■

4 Discussion

Just as in the 1999 paper by Mattingly and Sinai [5], an existence and uniqueness theorem for solutions follows from our theorem by standard considerations (see [1, 2, 7]). The line of argument is as follows: By the Sobolev embedding theorem, the Galerkin approximations are trapped in a compact subset of L^2 of the 3-torus. This guarantees the existence of a limit point which can be shown to satisfy (10), where $\mathcal{Z} = \mathbb{Z}^3$. Using the regularity inherited from the Galerkin approximations, one then shows that there exists a unique solution to the generalized 3D Navier-Stokes equations where $\alpha > 2.5$.

The inequality (12) in the proof of our Theorem is not necessarily true when $\alpha = 2$. Because of this, there is nothing preventing the solutions to (10) from escaping the region $\Omega(K)$ when $\alpha = 2$. Hence, there is no logical reason why the standard 3D Navier-Stokes equations must always have solutions, even when the initial velocity vector field is smooth; if they do always have solutions, it is due to probability (see [6]) and not logic, just like the Collatz $3n + 1$ Conjecture and the Riemann Hypothesis (see [3, 4]). Of course, it is also possible that there is a counterexample to the famous unresolved conjecture that the Navier-Stokes equations always have solutions when the initial velocity vector field is smooth. But as far as the author knows, nobody has ever found such a counterexample.

Submitted on October 15, 2014 / Accepted on October 22, 2014

References

1. Constantin P., Foiaş C. Navier-Stokes Equations. University of Chicago Press, Chicago, 1988.

2. Doering C., Gibbon J. Applied analysis of the Navier-Stokes equations. Cambridge Texts in Applied Mathematics. Cambridge University Press, Cambridge, 1995.
3. Feinstein C. Complexity Science for Simpletons. *Progress in Physics*, 2006, issue 3, 35–42.
4. Feinstein C. The Collatz $3n+1$ Conjecture is Unprovable. *Global Journal of Science Frontier Research, Mathematics & Decision Sciences*, 2012, v. 12, issue 8, 13–15.
5. Mattingly J., Sinai Y. An elementary proof of the existence and uniqueness theorem for the Navier-Stokes equations. *Commun. Contemp. Math. 1*, 1999, no. 4, 497–516.
6. Montgomery-Smith S., Pokorny M. A counterexample to the smoothness of the solution to an equation arising in fluid mechanics. *Commentationes Mathematicae Universitatis Carolinae*, 2002, v. 43, issue 1, 61–75.
7. Temam R. Navier-Stokes equations: Theory and numerical analysis. Volume 2 of *Studies in Mathematics and its Applications*, North-Holland Publishing Co., Amsterdam-New York, revised edition, 1979.

Majorana Particles: A Dialectical Necessity and not a Quantum Oddity

Abdul Malek

980 Rue Robert Brossard, Québec J4X 1C9, Canada. E-mail: abdulmalek@qc.aibn.com

The confirmation of the existence of Majorana particles is the strongest ever imperative for a dialectical perspective for physics; and may have implications for epistemology from the sub-nuclear to the cosmic scale. As the Majorana particle suggests matter at its most fundamental level must be viewed as a composite of the "unity of the opposites" — a contradiction, the resolution of which imparts "motion" to matter and hence the dialectical assertion that "there can be no matter without motion and no motion without matter". The existence of Majorana particles show that the anti- dialectical conception of matter as composed of distinctive and unitary particles like the fermions and the bosons at the most fundamental level, is faulty and is untenable. These types of sharp distinctions and categories of matter are indeed to be found in nature, but with relative and conditional validity.

For dialectics, any tangible material existence is a composite of the unity of the two opposites; or an "Absolute Identity of identity and non-identity" — a contradiction and a rationale for its change, motion, development, evolution and so on. At the most fundamental level this contradiction is the unity of the opposites of "being" and "nothing" — an interpenetration of the opposites and/or their inter-conversion to each other. Any synthesis to a different level is infected with this and its own peculiar new contradictions. The newly confirmed [1] existence of the Majorana particle is an affirmation of this dialectical law and at the same time it is a negation of the (artificial) division into the absolute and the unitary categories of the fundamental particles in nature as bosons and fermions. This differentiation is indeed possible from an anti-dialectical perspective, but only with relative and conditional validity. The three laws of dialectics, namely i) the unity or the interpenetration of the opposites, ii) the inter-conversion of quality and quantity and iii) the negation of the negation mediated by chance and necessity; provide an essential basis for an understanding of nature from the microcosm to the macrocosm [2]. Any attribute, characteristics, manifestation, developments, etc. of matter in dialectical epistemology, therefore, must be found primarily within matter itself and through its contradictions and not through any external agency.

Official physics continues to operate under the perspective of what Hegel termed as the "view of understanding" which roughly corresponds to causality. This view follows the rules of formal logic, and Aristotle's doctrine of "unity, opposition and the excluded middle" and with the mutual exclusion of the opposites. The opposites in this view stand in absolute opposition to each other and remain the same forever once brought into existence by an external agency. This "good old commonsense" view of the world though approximate and faulty at human scale; was in essence satisfactory enough to serve humanity and natural science reasonably well. But the advent of the idea of evolution in biology and the quantum phenomenon in physics fundamentally undermined the validity of the notions of the "view of understanding" in epistemology, particularly in modern physics.

Even before the discovery of the quantum phenomena; thinkers starting from Heraclitus through Epicurus, Hegel, Marx and Engels showed that dialectics offers a better epistemological tool for an understanding of nature, life, history, society and thought. The existence of polarity and the "unity of the opposites" and hence motion, was shown to manifest itself in all aspects of the world But of course, dialectics that denies the stability or the permanence of what exists is inimical to a class based social structure, which insists on permanence, continuity, certainty etc. Of necessity, and because of its very nature as the conservative, the resisting and the preserving side of what exists; the "view of understanding" historically became the dominant epistemological tool, including that of the natural sciences. The anti-dialectical notion of the unitary and the absolutely defined "fundamental building blocks" or fundamental elementary particles in nature and their classification into fermions and bosons as developed through the quantum field theories of modern particle physics is a case in point.

The Italian physicist Ettore Majorana in his 1937 paper [3] raised serious doubt about such absolute categorization and forced the dialectical perspective on modern particle physics; shortly after Paul Dirac gave the relativistic formulation of quantum mechanics for the electron [4] and conceived the theoretical basis for describing the spin 1/2 particles that would divide all possible matter particles into two mutually exclusive groups known as fermions and bosons, based on their spin properties. Following the mathematical logic and the symmetry rules of Dirac; Majorana in contradiction to Dirac, showed that such an absolute differentiation is not possible, because both the fermions and the boson can contain their opposites within themselves as the dialectical unity of

the opposites.

Paul Dirac ushered in the revolutionary idea of the anti-particles in nature as a dialectical necessity. Dirac's epoch making discovery that anti-particles must exist as part of the real world in the context of a real/virtual dialectical category and that the quantum vacuum is seething with virtual particles with momentary existence and which can turn into real particles through quantum tunnelling; for the first time gave validity to the dialectical speculation of Hegel's fundamental triad of "being-nothing-becoming" as the mode of "coming into being and passing out of existence" of matter as elementary particles in nature [5].

The developments in particle physics from the turn of the 20th century led to the discovery of multitude of so-called "elementary particles" of matter/energy. These were eventually rationalized based on their integral or fractional electric charge and fractional/integral spin values into two groups of matter particles, namely Dirac fermions with fractional spin values and bosons (named after the Indian physicist S. N. Bose) with integral spin values. In his attempt to develop a theoretical framework for describing spin 1/2 particles, Dirac thereby made a revolutionary discovery of hitherto unknown dialectical realm of the "unity of the opposites" of matter/antimatter. To describe the spin 1/2 particles, Dirac found it necessary to incorporate imaginary and complex quantities in his equations that gave rise to the complex-conjugate field ϕ^* of the real field ϕ, where the complex- conjugate fields ϕ^* can accommodate the antiparticles. This is a new aspect of reality brought forth by the developments in quantum mechanics. Physics previously only dealt with integral spins of 0, 1 and 2 in its equations namely, the Klein-Gordon, Maxwell (electromagnetism) and Einstein (general relativity) equations, respectively; which readily accommodate real fields.

The concept of antiparticles in nature means that, as a dialectical necessity all particles must have or be their own antiparticles. This "unity of the opposites" may manifest either in the same body like the two poles of a magnet or on separate bodies like the positive and negative electric charge or in the same body simultaneously containing the opposites continuously exchanging into their opposite polarity; depending on the nature of the exchange force that keep the two opposites together and the external circumstances under which this force operates. The latter case is manifested for example in positronium or meson where (though very unstable) matter and antimatter reside together as the unity of the opposites. Both positronium and mesons can exist even as their dimmers like the dipositronium and the mystery meson (X3872) respectively. Even the most pure and holy of all things in the world, namely the light photon has opposite characteristics of a particle and a wave and also is a composite of two matter — antimatter particles and can be resolved into a pair of the particles such as the electron-positron pair if the photon has enough energy equivalent of the mass of the particle pair. All these particles probably exist in Majorana type formation where the two opposites exist in the same body through rapid inter-conversion of the one opposite to the other.

The conundrum for anti-dialectical official physics is that the existence of antiparticle itself is problematic. In the narrative of the big bang theory all matter (and admittedly now antimatter) was created in one fell swoop. Any antimatter that was created was conveniently annihilated by reaction with matter, so that only matter (which arbitrarily was in relative excess) now prevails in the universe. Any new antimatter can now only be produced in negligible quantity through secondary processes; but the existence of any tangible amount (or even in large scale equivalent to matter); of antimatter is therefore, impossible. This author has previously challenged this contention of official physics; as many cosmic phenomena and the dynamics of the galaxies can be attributed to large-scale presence of antimatter in the universe [6].

The existence of anti-particle as such is not a big problem for anti-dialectical official physics. Because neutral and integer spin particles (like bosons) can be viewed as their own antiparticles, as they must be created by fields ϕ that obey $\phi = \phi^*$ — that is, real fields, like electromagnetism and gravity discussed above. What is "fundamentally confusing" (to use the term expressed by some famous physicists) for official physics is that some fermions with electric charge and spin 1/2 must also be their own antiparticles as Majorana (and dialectics) asserted. These fermions already have their anti-particles that exist separately. For example the neutron even with 0 charge and spin 1/2 has its antiparticle — the anti-neutron, as electron and proton have their antiparticles as positron and anti-proton respectively. Why then the Dirac fermions still should behave as their own antiparticle in one single body as the unity of the opposites under special circumstances like for example positronium or pion? It is simply that matter and antimatter in the Majorana particles has undergone a qualitative change and now reside in the same entity (instead of different ones) like the two opposites poles of a magnet or to take the analogy further, like a transgender person. The matter and antimatter characteristics in the Majorana particle did not vanish, but are maintained in a different way, probably through rapid inter-conversion of the one to the other through the exchange of some force particles. This is the same as in the case of positronium or meson (or even in the inter-conversion of nucleons in the atomic nucleus). In meson for example (a simpler case) the quark and the antiquark must undergo rapid interchange of identity into each other (through exchange of force particles) to remain in a stable form. This seems evident; for example in the case of pi-meson, an up and anti-down quark combination has a mass-energy of only 140 MeV; yet the same quark combination but only with different spin in a rho-meson has a mass-energy of 770 MeV!

How the Majorana particle emerges in the experimental setup of Ali Yazdani's group described in [1] is a matter of

speculation at this stage. It seems that the super-conducting magnet (two opposing factors) somehow polarizes the electron, probably through some new kind of unifying electomagneton coupling interaction, forming the end-to-end linear chain of the polarized electrons within the magnet, turning them into particles like the neutrinos, or mesons or even photons with the unbalanced opposite polarity emerging at the two ends of the magnet

The random and catastrophic gamma ray bursts (GRBs) observed in the cosmos can be attributed to the chance accumulated cosmic scale Majorana type formation of matter and anti-matter clusters, or somewhat like speculated boson stars [7]; probably mediated by the magnatic fields of the host galaxies and their instant annihilations as gigantic cosmic "fire-balls"; emmiting high energy gamma rays, triggered sponteneously or by some outside events [2]. GRBs are short duration (10 milliseconds to several minutes) intense flashes of high energy (from KeV to MeV to GeV range) gamma rays associated with extremely energetic events in distant galaxies that appear from random locations isotropically distributed in the celestial sphere. The progenitors of these astrophysical phenomena remain largely unknown [8]. These energetic events mostly emmiting gamma ray photons probably occur from various scale matter-antimatter annihilation processes. Indeed in the lower energy range, the most dominant peak centered around ~ 1 MeV probably corresponds to the mass equivalent of the elctron-positron pair.

Like the quantum phenomena itself, dialectics and the Majorana particle are counter-intuitive for anti-dialectical physics. The discovery of the Majarona particle represents another blow to the anti-dialectical perspective of modern physics and shows the futility of hunting for absolutely unitary fundamental constituents of matter in nature, like the magnetic monopole.

Submitted on October 21, 2014 / Accepted on October 23, 2014

References

1. Nadj-Perge S., et al. Observation of Majorana fermions in ferromagnetic atomic chains on a superconductor. *Science Express*, published online October 02, 2014; doi: 10.1126/science.1259327.
2. Malek A. The Dialectical Universe — Some Reflections on Cosmology. Agamee Prakashani Publishers, Dhaka, 2012.
3. Majorana E. *Nuovo Cimento*, 1937, v. 5, 171–184.
4. Dirac P. A. M. *Proc. Royal Soc. Lond.*, 1928, v. A117, 610–624.
5. Malek A. The real/virtual exchange of quantum particles. *Progress in Physics*, 2014, v. 10, issue 4, 209–211.
6. Malek A. Ambartsumian, Arp and the breeding galaxies. *Apeiron*, 2005, v. 12, no. 2, 256–271.
7. Shunck F. E. and Mielke E. W. General relativistic boson stars. *Class. & Quantum Grav.*, 2003, v. 20, R301–R356.
8. Goldstein A. et al. The BATSE 5B gamma-ray burst spectral catalog. arXiv: 1311.7135.

LETTERS TO PROGRESS IN PHYSICS

An Essay on Numerology of the Proton to Electron Mass Ratio

Alexander Kritov
E-mail: alex@kritov.ru

There are few mathematical expressions for calculation proton to electron mass ratio presented. Some of them are new and some are not. They have been analysed in terms of their simplicity, numerical significance and precision. Expressions are listed in the structured manner with comments. The close attention should be paid to a comparison of the formula similarity via their precision. A brief review of the different attempts in similar search is given.

1 Introduction

The founding of the analytical expression for fundamental dimensionless constant was a dream of a physical science for many years. There are many papers in literature trying to derive or explain fine structure constant from pure numerical theories. Such hypothetical theories can be divided into two types. The first one proposes that the dimensionless constants of the Nature are not actually constant and suggests using some close numbers which deviate from the original ones. This type of the theories requires further experimental research because deviations of the dimensionless constants are still unknown with good precision. For example G. Gamov following Eddington's belief explained the fine structure constant suggesting that it is equal to exactly 137 but it differs from exact number because of some small quantum perturbations similar to those in the case of the Lamb-Rutherford effect [1]. The second type of the theories is less common, it suggests exact relation for the dimensionless constants which is close to current experimental value. Usually such hypotheses derive huge and unnatural formulas that lack of elegance and explain-ability. Moreover physical justification for such expressions doesn't have enough arguments or the physical model is absent. However some of such recent theories may look interesting and promising in the view of the the presented material [2–4].

The part of the physics which involves dimensionless constants is very prone to invasion of numerology. However such cooperation has not been shown to be efficient yet. Though it is worth to notice that numerology itself stays very close to algebra and number theory of mathematics. Numerology itself can be considered as ancient prototype of the modern algebra (as well as alchemy was a base for a modern chemistry) and as it was said by I. J. Good: "At one time numerology meant divination by numbers, but during the last few decades it has been used in a sense that has nothing to do with the occult and is more fully called physical numerology" [5]. At this perspective, physical numerology seems to be a way through back-door which researches also try to enter and finding a key by trying to pickup right numbers. Such attempts should not be ignored as they may provide not only new clues for the researchers, but also in case of null-result they might be an evidence for another consistent principle which can be explored further.

2 Background

The search for mathematical expression for this dimensionless number motivated many serious scientists. A sufficient theory on particle masses and their ratios is not yet ready. The mass ratio of proton to electron ($\mu = m_p/m_e$) — two known stable particles which belong to two different types (leptons and hadrons) — still remains the mystery among other dimensionless numbers.

In 1929 Reinhold Fürth hypothesized that μ can be derived from the quadratic equation involving the fine structure constant [6]. Later on in 1935, A. Eddington who accepted some of Fürth's ideas presented the equation for proton to electron mass ratio calculation ($10\mu^2 - 136\mu + 1 = 0$) which appeared in his book "New Pathways in Science" [17]. However both approaches can not be used nowadays as they give very high deviation from the currently known experimental value of μ, so they are not reviewed in present work. Later on in 1951, it was Lenz [7] (but not Richard P. Feynman!) who noted that μ can be approximated by $6\pi^5$. In 1990, I.J. Good, a British mathematician assembled eight conjectures of numerology for the ratio of the rest masses of the proton and the electron.

Nowadays proton to electron mass ratio is known with much greater precision: $\mu = m_p/m_e = 1836.15267245(75)$, with uncertainty of 4.1×10^{-10} (CODATA 2010, [4]). Recently the professional approach to mathematically decode m_p/m_e ratio was done by Simon Plouffe [8]. He used a large database of mathematical constants and specialized program to directly find an expression. Alone with his main remarkable result for the expression for μ via Fibonacci and Lucas numbers and golden ratio he also noted that expression for μ using π can be improved as $6\pi^5 + 328/\pi^8$, but he concluded that this expression: "hardly can be explained in terms of primes and composites".

Expression	Value	Ref.
$\mu = \left(\frac{7}{2}\right)^6$	**183**8.2656 (1×10^{-3})	1.
$\mu = \sin\left(\frac{\pi}{5}\right) \cdot 5^5$	**1836**.8289 (4×10^{-4})	2.
$\mu = \frac{17}{4}\,432$	**1836**.0000 (8×10^{-5})	3.
$\mu = 150^{\frac{3}{2}} - 1$	**1836.1**173 (2×10^{-5})	4.
$\mu = 6\pi^5$	**1836.1**181 (2×10^{-5})	5.
$\mu = \frac{200^{300}}{7^{103}}$	**1836.1**179 (2×10^{-5})	6.
$\mu = \frac{22}{(5 \cdot 3 \cdot \alpha)^2}$	**1836.15**56 (2×10^{-6})	7.
$\mu = \frac{5 \cdot 7^3}{6 \cdot 67} 137\pi$	**1836.15**14 (6×10^{-7})	8.
$\mu = \frac{2^4 3^5}{5\alpha^{-1}} 103\pi$	**1836.152**20 (3×10^{-7})	9.
$\mu = \frac{e^8 - 10}{\phi}$	**1836.15**301 (2×10^{-7})	10.
$\mu = \frac{40}{3}\alpha^{-1} + \frac{800}{9\pi^2}$	**1836.152**98 (2×10^{-7})	11.
$\mu = \frac{86^4}{31^3}$	**1836.152**39 (2×10^{-7})	12.
$\mu = \frac{2267^2}{5 \cdot 7 \cdot 11 \cdot \alpha^{-1}} 6\pi$	**1836.152**5639 $(6 * 10^{-8})$	13.
$\mu = \frac{11^2 5^{\frac{4}{5}} 7^{\frac{2}{5}} e^3}{6 \cdot 2^{\frac{4}{5}}}$	**1836.15267**03 (1×10^{-9})	14.
$\mu = \frac{55 \cdot 5^{\frac{3}{2}} 11^{\frac{15}{32}}}{\phi^{\frac{1}{16}}}$	**1836.15267**48 (1×10^{-9})	15.
$\mu = \frac{3^{\frac{15}{4}} 5^{\frac{9}{4}} 14^{\frac{3}{2}}}{\pi^3 e^{\frac{3}{4}}}$	**1836.15267**19 (1×10^{-10})	16.

3 Variability

During the last decade a subject of variability of μ appeared under heavy debate and serious experimental verifications. The main experimental task is to distinguish cosmological red-shift of spectral lines from the shift caused by possible variation of μ. There is also proposed method to observe absorption spectra in the laboratory using the high precision atomic clocks.

Reinhold et al. [9] using the analysis of the molecular hydrogen absorption spectra of quasars Q0405-443 and Q0347-373 concluded that μ could have decreased in the past 12 Gyr and $\Delta\mu/\mu = (2.4 \pm 0.6) \times 10^{-5}$. This corresponds to entry value of μ= 1836.19674. King et al. [9] re-analysed the spectral data of Reinhold et al. and collected new data on another quasar, Q0528-250. They estimated that $\Delta\mu/\mu = (2.6 \pm 3.0) \times 10^{-6}$, different from the estimates of Reinhold et al. (2006). So the corresponding value for maximal deviated μ to be something around 1836.1574. The later results from Murphy et al. [15] and Bagdonaite et al. [2] gave a stringent limit $\Delta\mu/\mu < 1.8 \times 10^{-6}$ and $\Delta\mu/\mu = (0.0 \pm 1.0) \times 10^{-7}$ respectively. However these deviations could be valid only for the half of the Universe's current age or to the past of 7 Gyr which may not be enough for full understanding of the evolution of such variation. The results obtained by Planck gave $\Delta\alpha/\alpha = (3.6 \pm 3.7) \times 10^{-3}$ and $\Delta m_e/m_e = (4 \pm 11) \times 10^{-3}$ at the 68% confidence level [13] which provided not so strong limit comparing to found in [9] and [10].

At first sight the variation, if confirmed, may seem to make the numerical search for the mathematical expression meaningless. However possible variability of the μ should not prevent such search further, because the variation means one has to find a mean value of its oscillation or the beginning value from where it has started to change. And such variation would give a wider space for the further numerical sophistication because such value can not be verified immediately as we currently lack experimental verification of the amount of such change. If the fundamental constants are floating and the Nature is fine-tuned by slight the ratio changes from time to time, even so, there should be middle value as the best balance for such fluctuations. In this sense numerologists are free to use more relaxed conditions for their search, and current the precision for μ with uncertainty of 2×10^{-6} (as discussed above) may suffice for their numerical experiments. The formulas listed after number 7 in the table below do fall into this range.

4 Comments to the table

1. This expression is not very precise and given for its simple form. Also the number (7/2) definitely has certain numerological significance. The result actually better fits to the value of the m_n/m_e ratio (relative uncertainty is 2×10^{-4}). It is not trivial task to improve the formula accuracy, but why not, for example: $\mu = \left(\frac{7}{2}\right)^8 \frac{9 \cdot 13}{10\pi \cdot \alpha^{-1}}$ (relative error: 10^{-6}).
2. It is well known [8] that m_p/m_n ratio can be well approximated as $\cos\left(\frac{\pi}{60}\right)$ with relative uncertainty of 6×10^{-6}. So this is an attempt to build the formula for m_p/m_e ratio of similar form. Next more precise formula of the same form would be: $\mu = \frac{17^{43}}{19^{37}} \sin\left(\frac{\pi}{674}\right) =$

1836.1526661 (relative error is 3×10^{-9}). In the table it would be placed between number 13 and 14.

3. It was Werner Heisenberg in 1935 [14] who suggested to use number $2^4 3^3$ (which is equal to 432) to calculate alpha as $\alpha^{-1} = 432/\pi$, so m_p/m_e ratio can be also obtained approximately via 432. The expression can be rewritten as $1836 = 17 \cdot 108$ (the number 108 was considered to be sacred by ancients). There are other possible representations for the number 1836 which were noticed in the past, for example: $1836 = (136 \cdot 135)/10$ (see review in [5] and [22]).
4. This expression has some certain theoretical base related to original R. Fürth ideas [6], but it won't be discussed here. The precision has the same order as famous $6\pi^5$.
5. This is a Lenz's formula and it remains the favorite among the physicists. Recently Simon Plouffe also suggested yet another adjustment to this formula as following: $\mu = \dfrac{1}{5\cosh(\pi)} + 6\pi^5 + \dfrac{1}{5\sinh(\pi)}$ which looks remarkably symmetric and natural. The relative error is also extremely good: 4×10^{-9}. This formula has not been published before, it definitely has to attract further attention of the researchers.
6. The simplest way to approximate m_p/m_e ratio using powers of 2 and 7. Similar formula: $\mu = \dfrac{3^5 7^{16}}{2^{42}}$.
7. The elegant expression which uses almost 'kabalistic' numbers 22, 5, 3 and fine structure constant. Other possible expression with similar look and with the same precision: $\mu = \dfrac{5^{76}}{2^{127}3^{25}}$. Being combined together one can derive approximation for fine structure constant as 137.035999761 (with good relative deviation of 5×10^{-9}): $\alpha^{-2} = \dfrac{5^{78}}{11 \cdot 2^{127}3^{23}}$.
8. Parker-Rhodes in 1981, see [21] and review in [5]. McGoveran D.O. [20] claimed that this formula does not have anything in common with numerology as it was derived entirely from their discrete theory.
9. This elegant expression uses only the fine structure constant α, powers of 2, 3, 5 and the number 103. As J.I. Good said: "the favoured integers seem all to be of the form $2^a 3^b$ " [5].
10. By unknown source. No comment.
11. The expression can be also rewritten in more symmetric form: $\mu = 2\left(\dfrac{20}{3}\alpha^{-1} + \left(\dfrac{20}{3\pi}\right)^2\right)$. It can be noted that the number (20/3) appears in the author previous work [18] in the expression for the gravitational constant G.
12. One of the found expressions by author's specialized program. The search was performed for the expression of the view: $\mu = p_1^{n_1} p_2^{n_2} p_3^{n_3} p_4^{n_4}$, where p_i — some prime numbers, n_i — some natural numbers. Also: $\mu = \left(\dfrac{19}{5}\right)^{21} \dfrac{1}{13^8}$.
13. Number 2267 has many interesting properties; it is a prime of the form $(30n-13)$ and $(13n+5)$, it is congruent to 7 mod 20. It is father primes of order 4 and 10 etc. In the divisor of this formula there are sequential primes 5, 7, 11. There are other possible expressions of the similar form with such precision (10^{-8}), for example: $\mu = \dfrac{45 * 49 * 53^2}{8 * 29 * \alpha^{-1}} 5\pi$. It is also hard to justify why in expressions 9 and 13 α^{-1} stays opposite to π as by definition they supposed to be on the same side: $\alpha^{-1} = \hbar c/ke^2$ or $(2\pi\alpha^{-1}) = hc/ke^2$. But the author did not succeed in finding similar expressions with α and π on the same side with the same uncertainty. There are some few other nice looking formulas which the use of big prime numbers, for example: $\mu = \sqrt{4^3 \cdot 52679}$ (9×10^{-8}).
14. Another possible expression was found using web based program Wolframalpha [23]. The precision is the same as in next formula.
15. Simon Plouffe's approximation using Fibonacci and Lucas numbers [8] - slightly adjusted from its original look. Another elegant form for this expression is following: $\mu^{32} = \dfrac{11^{47}5^{80}}{\phi^2}$.
16. This formula has the best precision alone the listed. Though, powers of π and e seem to despoil its possible physical meaning.

5 Conclusions

At the present moment big attention is paid to experimental verification of possible proton-electron mass ratio variation. If experimental data will provide evidence for the ratio constancy then only few expressions (14-16 from the listed) may pretend to express proton-electron mass ratio as they fall closely into current experimental uncertainty range (4.1×10^{-10} as per CODATA 2010). Of course Simon Plouffe's formula (14) seems as a pure winner among them in terms of the balance between it simplicity and precision. However, some future hope for the other formulas remains if the variability of the proton to electron mass ratio is confirmed. Important to note that there could be unlimited numbers of numerical approximations for dimensionless constant. Some of them may look more simple and "natural" than others. It is easy to see that expression simplicity and explain-ability in opposite determines its precision. As all formulas with uncertainty 10^{-8} and better become obviously more complex. And at the end: "What is the chance that seemingly impressive formulae arise

purely by chance?" [15].

Remembering mentioning words said by Seth Lloyd [19] "not to follow in Dirac's footsteps and take such numerology too seriously" the author encourages the reader to continue such mathematical experiments and in order to extend the table of the formulas and submit your expressions to the author. Special attention will be brought to simple expressions with relations to: power of two (2^n), prime numbers and properties of Archimedean solids. Besides that it may be interesting mathematical exercise it may also reveal some hidden properties of the numbers. But how complexity of the mathematical expression can be connected to the complexity of the numbers? What is the origin of the Universe complexity? How much we can encode by one mathematical expression?

The mass ratio of proton to electron — two stable particles that define approximately 95% of the visible Universe's mass — can be related to the total value Computational capacity of the Universe (see [19]). So as a pure numbers they supposedly have to be connected to prime numbers, entropy, binary and complexity. So, possibly, their property should be investigated further by looking through the prism of the algorithmic information theory.

Let's hope that presented material can be a ground for someone in his future investigation of this area.

Acknowledgements

I would like to express my gratitude to Simon Plouffe for his valuable guideline and advises.

Submitted on October 17, 2014 / Accepted on October 20, 2014

References

1. Gamov G. Numerology of the constants of Nature. *Proc. Natl. Acad. Sci. USA*, Feb. 1968, v. 59(2), 313–318.
2. Ionescu L.M. Remarks on Physics as Number Theory, arXiv: 0309981, 2011.
3. Kocik J. The Koide Lepton Mass Formula and Geometry of Circles. arXiv: 1201.2067, 2012
4. Rhodes C. K. Unique Physically Anchored Cryptographic Theoretical Calculation of the Fine-Structure Constant α Matching both the g/2 and Interferometric High-Precision Measurements. arXiv: 1008.4537, 2012.
5. Good I.J. A quantal hypothesis for hadrons and the judging of physical numerology. In G. R. Grimmett (Editor), D.J.A. Welsh (Editor), Disorder in Physical Systems. Oxford University Press, 1990, p.141.
6. Fürth R. Über einen Zusammenhang zwischen quantenmechanischer Unscharfe und Struktur der Elementarteilchen und eine hierauf begründete Berechnung der Massen von Proton und Elektron. *Zeitschrift für Physik*, 1929, v. 57, 429–446.
7. Lenz F. The ratio of proton and electron masses. *Physical Review*, 1851, v. 82, 554.
8. Plouffe S. A search for a mathematical expression for mass ratios using a large database. viXra:1409.0099, 2014.
9. Reinhold E., Buning R., Hollenstein U., Ivanchik A., Petitjean P., Ubachs W. Indication of a cosmological variation of the proton-electron mass ratio based on laboratory measurement and reanalysis of H_2 spectra. *Physical Review Letters*, 2006, v. 96(15), 151101.
10. King J., Webb J., Murphy M., Carswell R. Stringent null constraint on cosmological evolution of the proton-to-electron mass ratio. *Physical Review Letters*, 2008, v. 101, 251304.
11. Murphy M. et al. Strong limit on a variable proton-to-electron mass ratio from molecules in the distant Universe. arXiv:0806.3081, 2008.
12. Bagdonaite J. A Stringent Limit on a Drifting Proton-to-Electron Mass Ratio from Alcohol in the Early Universe. *Science*, 4 January 2013, v. 339, no. 6115, 46–48.
13. Ade P.A.R. et al. Planck intermediate results. XXIV. Constraints on variation of fundamental constants. arXiv: 1406.7482, 2014.
14. Kragh H. Magic number: A partial history of the fine-structure constant. *Arch. Hist. Exact Sci.*, 2003, v. 57, 395–431.
15. Barrow D. John. The Constants of Nature. Vintage Books, 2004, p.93.
16. CODATA Value: proton-electron mass ratio. The NIST Reference on Constants, Units, and Uncertainty. US National Institute of Standards and Technology, June 2011.
17. Eddington A. New Pathways in Science. Cambridge University Press, 1935.
18. Kritov A. A new large number numerical coincidences. *Progress in Physics*, 2013, v. 10, issue 2, 25–28.
19. Lloyd S. Computational capacity of the universe. arXiv:quant-ph/0110141, 2001.
20. McGoveran D.O., Noyes H. P. Physical Numerology? Stanford University, 1987.
21. Parker-Rhodes A.F. The Theory of Indistinguishables: A Search for Explanatory Principles below the level of Physics. Springer, 1981.
22. Sirag S.P. A combination [combinatorial] derivation of the proton-electron mass ratio. *Nature*, 1977, v. 268, 294.
23. www.wolframalpha.com

Ives-Stilwell Time Dilation Li^+ ESR Darmstadt Experiment and neo-Lorentz Relativity

Reginald T. Cahill

School of Chemical and Physical Sciences, Flinders University, Adelaide 5001, Australia. Email: reg.cahill@flinders.edu.au

Botermann *et al* in *Test of Time Dilation Using Stored Li^+ Ions as Clocks at Relativistic Speed*, *Physical Review Letters*, 2014, 113, 120405, reported results from an Ives-Stilwell-type time dilation experiment using Li^+ ions at speed 0.338c in the ESR storage ring at Darmstadt, and concluded that the data verifies the Special Relativity time dilation effect. However numerous other experiments have shown that it is only neo-Lorentz Relativity that accounts for all data, and all detect a 3-space speed $V \approx 470$ km/s essentially from the south. Here we show that the ESR data confirms both Special Relativity and neo-Lorentz Relativity, but that a proposed different re-analysis of the ESR data should enable a test that could distinguish between these two theories.

1 Introduction

Botermann *et al* [1] reported results from an Ives-Stilwell [2, 3] time dilation experiment using Li^+ ions at speed $v = 0.338c$ in the ESR storage ring at Darmstadt, and concluded that the data verifies the Special Relativity time dilation effect, in (1). However numerous other experiments [4, 5] have shown that it is only neo-Lorentz Relativity that accounts for all of the data from various experiments, all detecting a 3-space speed $V \approx 470$ km/s approximately from the south, see Fig. 3. Here we show that the ESR data confirms neo-Lorentz Relativity, and that the ESR Darmstadt experimental data also gives $V \approx 470$ km/s.

2 Special or Lorentz Relativity?

The key assumption defining Special Relativity (SR) is that the speed of light in vacuum is invariant, namely the same for all observers in uniform relative motion. This assumption was based upon the unexpectedly small fringe shifts observed in the Michelson-Morley experiment (MM) 1887 experiment, that was designed to detect any anisotropy in the speed of light, and for which Newtonian physics was used to calibrate the instrument. Using SR, a Michelson interferometer should not reveal any fringe shifts on rotation. However using LR, a Michelson interferometer [4] can detect such anisotropy when operated in gas-mode, i.e. with a gas in the light paths, as was the case with air present in the MM 1887 experiment. The LR calibration uses the length contraction, from (4), of the interferometer arms. This results in the device being some 2000 times less sensitive than assumed by MM who used Newtonian physics. Reanalysis of the MM data then led to a significant light speed anisotropy indicating the existence of a flowing 3-space with a speed of some 500 km/s from the south. This result was confirmed by other experiments: Miller 1925/26 gas mode Michelson interferometer, DeWitte 1991 coaxial cable RF speeds, Cahill 2009 Satellite Earth-flyby Doppler shift NASA data [6], Cahill 2012 dual coaxial cable RF speed [7], Cahill 2013-2014 [8, 9] Zener diode 3-space quantum detectors. These and other experiments are reviewed in [4, 10]. All these experiments also revealed significant space flow turbulence, identified as gravitational waves in the 3-space flow [10]. However there are numerous experiments which are essentially vacuum-mode Michelson interferometers in the form of vacuum resonant optical cavities, see [11], which yield null results because there is no gas in the light paths. These flawed experimental designs are quoted as evidence of light speed invariance. So the experimental data refutes the key assumption of SR, and in recent years a neo-Lorentz Relativity (LR) reformulation of the foundations of fundamental physics has been underway, with numerous confirmations from experiments, astronomical and cosmological observations [12–14].

However of relevance here are the key differences between SR and LR regarding time dilations and length contractions. In SR, these are

$$\Delta t = \Delta t_0 / \sqrt{1 - v^2/c^2} \tag{1}$$

$$\Delta L = \Delta L_0 \sqrt{1 - v^2/c^2} \tag{2}$$

where v is the speed of a clock or rod with respect to the observer, c is the invariant speed of light, and subscript 0 denotes at rest time and space intervals. In SR, these expressions apply to all time and space intervals. However in LR, the corresponding expressions are

$$\Delta t = \Delta t_0 / \sqrt{1 - v_R^2/c^2} \tag{3}$$

$$\Delta L = \Delta L_0 \sqrt{1 - v_R^2/c^2} \tag{4}$$

where v_R is the speed of a clock or rod with respect to the dynamical 3-space, and where c is the speed of light with respect to the dynamical 3-space. In LR, these expressions only apply to physical clocks and rods, and so the so-called time dilation in SR becomes a clock slowing effect in LR, caused by the motion of clocks with respect to the dynamical 3-space. Only

by using (4) in place of (2) does the data from the Michelson-Morley and Miller gas-mode interferometers agree with the results from using other experimental techniques [5].

The interpretation of (1) and (3), relevant to the experiment discussed herein, is that if a time interval Δt_0 corresponds to 1 cycle of an oscillatory system at rest with respect to an observer in SR, or at rest with respect to space in LR, then $\nu_0 = 1/\Delta t_0$ is the frequency of the emitted photon. When the system is moving with speed v with respect to an observer, or with speed v_R with respect to space, then the time internal Δt_0 is increased, and the emitted photon frequency is decreased to $\nu = 1/\Delta t$.

Here the LR effects are applied to the frequencies of photons emitted by the moving Li^+ ions, to the Doppler shifts of these photons, and to the clock slowing of the two detectors that measure the detected photon frequencies.

Fig. 1 shows the direction of the 3-space flow as determined from NASA satellite Earth-flyby Doppler shifts [6], revealing that the flow direction is close to being South to North, which is relevant to the ESR Darmstadt experiment in which the Li^+ ions travel also from South to North.

Fig. 2 shows the simple circuit for the quantum detection of the 3-space velocity, The measured 3-space speeds are shown in Fig. 3, and follow from measuring the time delay between two such detectors, separated by 25 cm and orientated such that the maximum time delay is observed for the 3-space induced quantum tunnelling current fluctuations.

3 Special Relativity and Li$^+$ ESR Darmstadt experiment

The Li^+ ESR Darmstadt experiment measured the photon frequencies ν_N and ν_S at the two detectors, emitted by the ions moving North at speed $v = 0.338c$, see Fig. 4 Top. In SR, there are two effects: time dilation of the emitting source, giving emitted photons with frequency $\nu_0\sqrt{1 - v^2/c^2}$, from (1), where ν_0 is the frequency when the ions are at rest with respect to the two detectors. The second effect is the Doppler shift factors $1/(1 \pm v/c)$, giving the detected frequencies

$$\nu_N = \nu_0\sqrt{1 - v^2/c^2}/(1 - v/c) \tag{5}$$

$$\nu_S = \nu_0\sqrt{1 - v^2/c^2}/(1 + v/c). \tag{6}$$

Then

$$\nu_N\nu_S/\nu_0^2 = 1 \tag{7}$$

and this result was the key experimental test reported in [1], with the data giving

$$\sqrt{\nu_N\nu_S/\nu_0^2} - 1 = (1.5 \pm 2.3) \times 10^{-9}. \tag{8}$$

On the basis of this result it was claimed that the Special Relativity time dilation expression (1) was confirmed by the experiment.

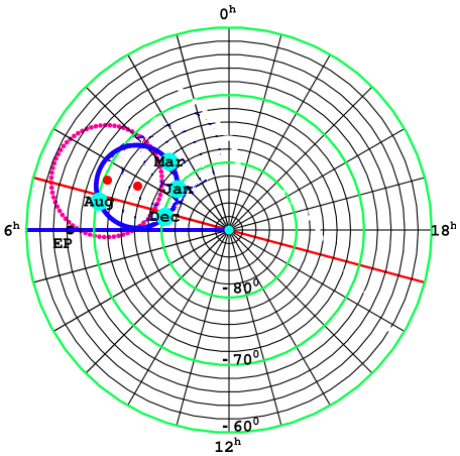

Fig. 1: South celestial pole region. The dot (red) at RA=4.3^h, Dec=75°S, and with speed 486 km/s, is the direction of motion of the solar system through space determined from NASA spacecraft Earth-flyby Doppler shifts [6], as revealed by the EM radiation speed anisotropy. The thick (blue) circle centred on this direction is the observed velocity direction for different months of the year, caused by Earth orbital motion and sun 3-space inflow. The corresponding results from the 1925/26 Miller gas-mode interferometer are shown by second dot (red) and its aberration circle (red dots). For December 8, 1992, the speed is 491km/s from direction RA=5.2^h, Dec=80°S, see Table 2 of [6]. EP is the pole direction of the plane of the ecliptic, and so the space flow is close to being perpendicular to the plane of the ecliptic.

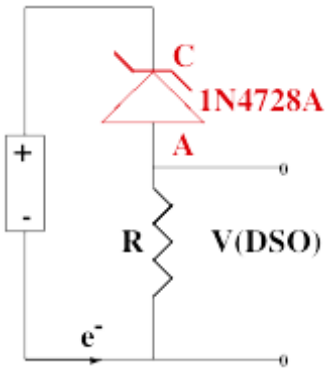

Fig. 2: Circuit of Zener Diode 3-Space Quantum Detector, showing 1.5 V AA battery, two 1N4728A Zener diodes operating in reverse bias mode, and having a Zener voltage of 3.3 V, and resistor R =10 KΩ. Voltage V across resistor is measured and used to determine the space driven fluctuating tunnelling current through the Zener diodes. Current fluctuations from two collocated detectors are shown to be the same, but when spatially separated there is a time delay effect, so the current fluctuations are caused by space speed fluctuations [8, 9]. Using more diodes in parallel increases S/N, as the measurement electronics has $1/f$ noise induced by the fluctuating space flow.

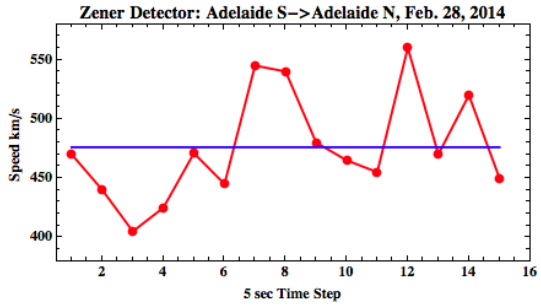

Fig. 3: Average speed, and speed every 5 sec, on February 28, 2014 at 12:20 hrs UTC, giving average speed = 476 ± 44 (RMS) km/s, from approximately S → N, using two Zener Diode detectors [9]. The speeds are effective projected speeds, and so do not distinguish between actual speed and direction effect changes. The projected speed = $V\cos\theta$, where θ is the angle between the space velocity V and the direction defined by the two detectors. V cannot be immediately determined with only two detectors. However by varying direction of detectors axis, and searching for maximum time delay, the average direction (RA and Dec) may be determined. As in previous experiments there are considerable fluctuations at all time scales, indicating a dynamical fractal structure to space.

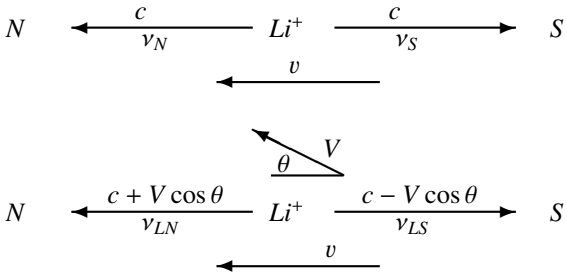

Fig. 4: **Top:** Special Relativity speed diagram with Li^+ ions travelling at speed v towards the North, emitting photons with speed c and frequency ν_N to the North, and speed c to the South with frequency ν_S, with all speeds relative to the detectors N and S frame of reference. The invariant speed of light is c. The photons are emitted with frequency ν_0 with respect to the rest frame of the ions.
Bottom: Neo-Lorentz Relativity speed diagram with space flow speed V at angle θ and Li^+ ions travelling at speed v towards the North, emitting photons with speed $c + V\cos\theta$ to the North and frequency ν_{LN}, and speed $c - V\cos\theta$ to the South and frequency ν_{LS}. $V\cos\theta$ is the projected space flow speed towards the North, with speeds relative to the detectors N and S frame of reference. The speed of light is c relative to the 3-space. The photons are emitted with frequency ν_0 with respect to the rest frame of the ions.

4 Lorentz Relativity and Li⁺ ESR Darmstadt experiment

In LR, expressions (5) and (6) are different, being

$$\nu_{LN} = \frac{\nu_0\sqrt{1-(v-V\cos\theta)^2/c^2-(V\sin\theta)^2/c^2}}{(1-v/(c+V\cos\theta))\sqrt{1-V^2/c^2}} \quad (9)$$

$$\nu_{LS} = \frac{\nu_0\sqrt{1-(v-V\cos\theta)^2/c^2-(V\sin\theta)^2/c^2}}{(1+v/(c-V\cos\theta))\sqrt{1-V^2/c^2}} \quad (10)$$

where $\nu_0\sqrt{1-(v-V\cos\theta)^2/c^2-(V\sin\theta)^2/c^2}$, from (3), is the expression for the lower emitted photon frequency with the ions moving at velocity

$$v_R = (v - V\cos\theta, -V\sin\theta) \quad (11)$$

with respect to the 3-space; with $1/(1-v/(c+V\cos\theta))$ and $1/(1+v/(c-V\cos\theta))$ being the Doppler shift factors as the photons have speed $c \pm V\cos\theta$ with respect to the detectors frame of reference; and $1/(1-V^2/c^2)$ being the time dilation effect for the clocks in the frequency measuring devices, as the slowing of these clocks, from (3), makes the detected frequency appear higher, as they have speed V with respect to the 3-space; see Fig. 4 Bottom. From (9) and (10) we obtain

$$\nu_{LN}\nu_{LS}/\nu_0^2 = 1 - \frac{v^2\sin^2\theta}{c^2(c^2-v^2)}V^2 + O[V^4] \quad (12)$$

which is identical to (7) to first order in V. We obtain

$$\sqrt{\nu_{LN}\nu_{LS}/\nu_0^2} - 1 = -\frac{v^2\sin^2\theta}{2c^2(c^2-v^2)}V^2 \quad (13)$$

and, for example, $V = 400$ km/s at an angle $\theta = 5°$, with $v = 0.338c$, gives

$$\sqrt{\nu_{LN}\nu_{LS}/\nu_0^2} - 1 = -0.9\times10^{-9} \quad (14)$$

which is nearly consistent with the result from [1] in (8). It is not clear from [1] whether the result in (8) is from the smallest values or whether it is from averaging data over several days, as the LR prediction varies with changing θ, as would be caused by the rotation of the earth. Here we have used $\theta = 5°$ which suggest the former interpretation of the data.

A more useful result follows when we examine the ratio ν_{LN}/ν_{LS} because we obtain a first order expression for V

$$V\cos\theta = \frac{c(c-v)^2}{2v^2}\left(\frac{c+v}{c-v} - \frac{\nu_{LN}}{\nu_{LS}}\right) \quad (15)$$

which will enable a more sensitive measurement of the projected $V\cos\theta$ value to be determined from the Li^+ ESR Darmstadt data. This result uses only the neo-Lorentz Doppler shift factors, and these have been confirmed by analysis of the Earth-flyby Doppler shift data [6]. $V\cos\theta$ will show space flow turbulence fluctuations and earth rotation effects, and over months a sidereal time dependence. The values are predicted to be like those in Fig. 3 from the 3-space quantum detectors. Indeed such a simple detection technique should be run at the same time as the Li^+ data collection. The data is predicted to give $V\cos\theta \approx 470$ km/s, as expected from Fig. 3. Then the Li^+ experiment will agree with results from other experiments [4–10].

Note that SR gives, from (5) and (6),

$$\left(\frac{c+v}{c-v}-\frac{\nu_N}{\nu_S}\right)=0 \qquad (16)$$

in contrast to (15).

5 Conclusions

The non-null experimental data, from 1887 to the present, all reveal the existence of a dynamical 3-space, with a speed $\approx$ 500 km/s with respect to the earth. Originally Lorentz proposed an aether moving through a static geometrical space. However the data and theory imply a different neo-Lorentz Relativity, with there being a dynamical fractal flowing 3-space, which possesses an approximate geometrical measure of distances and angles, which permits the geometrical description of relative locations of systems [5]. As well the dynamical theory for this 3-space has explained numerous gravitational effects, with gravity being an emergent quantum and EM wave refraction effect, so unifying gravity and the quantum [4, 10, 13–16]. An important aspect of Lorentz Relativity, which causes ongoing confusion, is that the so-called Lorentz transformation is an aspect of Special Relativity, but not Lorentz Relativity. The major result here is that the Li^+ ESR Darmstadt experimental data confirms the validity of both Special Relativity and neo-Lorentz Relativity, but only when the 3-space flow is nearly parallel to the NS orientation of the Li^+ beam. Then to distinguish between these two relativity theories one could use (15). This report is from the Flinders University Gravitational Wave Project.

Submitted on October 17, 2014 / Accepted on November 1, 2014

References

1. Botermann B., Bing D., Geppert C., Gwinner G., Hänsch T. W., Huber G., Karpuk S., Krieger A., Kühl T., Nörtershäuser W., Novotny C., Reinhardt S., Sánchez R., Schwalm D., Stöhlker T., Wolf A., and Saathoff G. Test of Time Dilation Using Stored Li^+ Ions as Clocks at Relativistic Speed. *Physical Review Letters*, 2014, v. 113, 120405
2. Ives H. E. and Stilwell G. R. An Experimental Study of the Rate of a Moving Atomic Clock. *Journal of the Optical Society of America*, 1938, v. 28, 215.
3. Ives H. E. and Stilwell G. R. An Experimental Study of the Rate of a Moving Atomic Clock II. *Journal of the Optical Society of America*, 1941, v. 31, 369.
4. Cahill R. T. Discovery of Dynamical 3-Space: Theory, Experiments and Observations - A Review. *American Journal of Space Science*, 2013, v. 1 (2), 77–93.
5. Cahill R. T. Dynamical 3-Space: Neo-Lorentz Relativity. *Physics International*, 2013, v. 4 (1), 60–72.
6. Cahill R. T. Combining NASA/JPL One-Way Optical-Fiber Light-Speed Data with Spacecraft Earth-Flyby Doppler-Shift Data to Characterise 3-Space Flow. *Progress in Physics*, 2009, v. 5 (4), 50–64.
7. Cahill R. T. Characterisation of Low Frequency Gravitational Waves from Dual RF Coaxial-Cable Detector: Fractal Textured Dynamical 3-Space. *Progress in Physics*, 2012, v. 8 (3), 3–10.
8. Cahill R. T. Nanotechnology Quantum Detectors for Gravitational Waves: Adelaide to London Correlations Observed. *Progress in Physics*, 2013, v. 9 (4), 57–62.
9. Cahill R. T. Gravitational Wave Experiments with Zener Diode Quantum Detectors: Fractal Dynamical Space and Universe Expansion with Inflation Epoch. *Progress in Physics*, 2014, v. 10 (3), 131–138.
10. Cahill R. T. Review of Gravitational Wave Detections: Dynamical Space, *Physics International*, 2014, v. 5 (1), 49–86.
11. Mueller H., Hermann S., Braxmaier C., Schiller S. and Peters A. Modern Michelson-Morley Experiment Using Cryogenic Optical Resonators *Physical Review Letters*, 2003, v. 91, 020401.
12. Cahill R. T. and Kerrigan D. Dynamical Space: Supermassive Black Holes and Cosmic Filaments. *Progress in Physics*, 2011, v. 7 (4), 79–82.
13. Cahill R. T. and Rothall D. P. Discovery of Uniformly Expanding Universe. *Progress in Physics*, 2012, v. 8 (1), 63–68.
14. Rothall D. P. and Cahill R. T. Dynamical 3-Space: Black Holes in an Expanding Universe. *Progress in Physics*, 2013, v. 9 (4), 25–31.
15. Cahill R. T. Dynamical Fractal 3-Space and the Generalised Schrödinger Equation: Equivalence Principle and Vorticity Effects. *Progress in Physics*, 2006, v. 2 (1), 27–34.
16. Cahill, R. T. Dynamical 3-Space: Emergent Gravity. In Should the Laws of Gravity be Reconsidered? Munera H. A., ed. Apeiron, Montreal, 2011, 363–376.

The Strong and Weak Forces and their Relationship to the Dirac Particles and the Vacuum State

William C. Daywitt

National Institute for Standards and Technology (retired), Boulder, Colorado. E-mail: wcdaywitt@me.com

This paper argues that the strong and weak forces arise from the proton and electron coupling to the Planck vacuum state. Thus they are not free space forces that act between free space particles, in contradistinction to the gravitational and electromagnetic forces. Results connect these four natural forces to the vacuum superforce.

1 Introduction

The Dirac particles (proton and electron) have been discussed in a number of previous papers [1] [2] [3] [4], where it is shown that they possess similar structures. Of interest here is the fact that they are both strongly coupled to the Planck vacuum (PV) state via a two-term coupling force that vanishes at their respective Compton radii. It is at these vanishing points where the strong and weak forces emerge. Consequently both forces are defined by the particle/PV coupling; i.e., they are not free space forces acting between free space particles.

What follows derives the strong and weak forces and calculates their relative strengths with respect to each other and with respect to the gravitational and electromagnetic forces. It is shown that these four forces are connected to the superforce associated with the PV (quasi-) continuum.

Strong Force

In its rest frame the proton core (e_*, m_p) exerts the following two-term coupling force (the Compton relations $r_e m_e c^2 = r_p m_p c^2 = r_* m_* c^2 = e_*^2$ are used throughout the calculations)

$$F_p(r) = \frac{(e_*)(-e_*)}{r^2} + \frac{m_p c^2}{r} = -F_s\left(\frac{r_p^2}{r^2} - \frac{r_p}{r}\right) \qquad (1)$$

on the PV continuum, where the proton Compton radius r_p ($= e_*^2/m_p c^2$) is the radius at which the force vanishes. The mass of the proton is m_p [3] and the bare charge e_* is massless. The radius r begins at the proton core and ends on any particular Planck-particle charge $(-e_*)$ at a radius r within the PV.

The strong force

$$F_s \equiv \left|\frac{(e_*)(-e_*)}{r_p^2}\right| = \frac{m_p c^2}{r_p} \qquad \left(= \frac{m_p m_* G}{r_p r_*}\right) \qquad (2)$$

is the magnitude of the two forces in the first sum of (1) where the sum vanishes. The (e_*) in (2) belongs to the free-space proton and the $(-e_*)$ to the separate Planck particles of the PV, where the first and second ratios in (2) are the vacuum polarization and curvature forces respectively. It follows that the strong force is a proton/PV force. The Planck particle mass m_* and Compton radius r_* are equal to the Planck Mass and Planck Length [5, p.1234].

Weak Force

The electron core $(-e_*, m_e)$ exerts the coupling force

$$F_e(r) = \frac{(-e_*)(-e_*)}{r^2} - \frac{m_e c^2}{r} = F_w\left(\frac{r_e^2}{r^2} - \frac{r_e}{r}\right) \qquad (3)$$

on the vacuum state and leads to the Compton radius r_e ($= e_*^2/m_e c^2$), where the first $(-e_*)$ in (3) belongs to the electron and the second to the separate Planck particles in the negative energy vacuum.

The weak force

$$F_w \equiv \frac{(-e_*)(-e_*)}{r_e^2} = \frac{m_e c^2}{r_e} \qquad \left(= \frac{m_e m_* G}{r_e r_*}\right) \qquad (4)$$

is the magnitude of the two forces in the first sum of (3) where the sum vanishes. Again, the first and second ratios in (4) are vacuum polarization and curvature forces. Thus the weak force is an electron/PV force.

2 Relative Strengths

The well known gravitational and electromagnetic forces of interest here are

$$F_g(r) = -\frac{m^2 G}{r^2} \qquad \text{and} \qquad F_{em}(r) = \pm\frac{e^2}{r^2} \qquad (5)$$

where r is the free-space radius from one mass (or charge) to the other.

The relative strengths of the four forces follow immediately from equations (2), (4), and (5):

$$\frac{F_w}{F_s} = \frac{r_p^2}{r_e^2} = \frac{m_e^2}{m_p^2} = \frac{1}{1836^2} \approx 3\times 10^{-7} \qquad (6)$$

$$\frac{|F_g(r_p)|}{F_s} = \frac{m_p^2 G/r_p^2}{e_*^2/r_p^2} = \frac{m_p^2(e_*^2/m_*^2)}{e_*^2} = \frac{m_p^2}{m_*^2} = \frac{r_*^2}{r_p^2} \approx 6\times 10^{-39} \qquad (7)$$

where $G = e_*^2/m_*^2$ [1] is used in the calculation, and

$$\frac{|F_{em}(r_p)|}{F_s} = \frac{e^2/r_p^2}{e_*^2/r_p^2} = \frac{e^2}{e_*^2} = \alpha \approx \frac{1}{137} \qquad (8)$$

where α is the fine structure constant.

3 Superforce

The relative strengths (6)–(8) agree with previous estimates and demonstrate that the free space forces

$$F_g(r_p) = -\frac{r_*^2}{r_p^2}\,F_s\,, \qquad F_g(r_e) = -\frac{r_*^2}{r_e^2}\,F_w \tag{9}$$

and

$$F_{em}(r_p) = \pm\alpha F_s\,, \qquad F_{em}(r_e) = \pm\alpha F_w \tag{10}$$

are related to the proton and electron coupling forces (1) and (3) through the strong and weak forces.

Equations (2) and (4) give precise definitions for the strong and weak forces, and are connected to the vacuum superforce via:

$$F_s = \left(\frac{r_*^2}{r_p^2}\right)\frac{e_*^2}{r_*^2} \qquad \text{and} \qquad F_w = \left(\frac{r_*^2}{r_e^2}\right)\frac{e_*^2}{r_*^2} \tag{11}$$

where

$$\text{superforce} \equiv \frac{e_*^2}{r_*^2} = \frac{m_* c^2}{r_*} \qquad \left(= \frac{m_*^2 G}{r_*^2}\right) \tag{12}$$

is the PV superforce to which Davies alludes [6, p.104]. The equality of the first and third ratios in (12) indicate that the degenerate vacuum state is held together by gravity-like forces.

The Newtonian force

$$-F_g(r) = \frac{m^2 G}{r^2} = \frac{(mc^2/r)^2}{c^4/G} =$$

$$= \frac{(mc^2/r)^2}{m_* c^2/r_*} = \left(\frac{mc^2/r}{m_* c^2/r_*}\right)^2 \frac{m_* c^2}{r_*} \tag{13}$$

is related to the superforce through the final expression, where $c^4/G\,(=\, m_* c^2/r_*)$ is the curvature superforce in the Einstein field equations [7]. The parenthetical ratio in the last expression is central to the Schwarzschild metrics [8] associated with the general theory.

Finally,

$$F_{em}(r) = \pm\frac{e^2}{r^2} = \pm\alpha\left(\frac{r_*^2}{r^2}\right)\frac{e_*^2}{r_*^2} \tag{14}$$

is the free space Coulomb force in terms of the vacuum polarization superforce.

Submitted on October 24, 2014 / Accepted on November 4, 2014

References

1. Daywitt W.C. The Planck Vacuum. *Progress in Physics*, v. 1, 20, 2009. See also www.planckvacuum.com.
2. Daywitt W.C. The Electron and Proton Planck-Vacuum Forces and the Dirac Equation. *Progress in Physics*, v. 2, 114, 2014.
3. Daywitt W.C. Why the Proton is Smaller and Heavier than the Electron. *Progress in Physics*, v. 10, 175, 2014.
4. Daywitt W.C. The Dirac Proton and its Structure. To be published in the International Journal of Advanced Research in Physical Science (IJARPS). See also www.planckvacuum.com.
5. Carroll B.W., Ostlie D.A. *An Introduction to Modern Astrophysics*. Addison-Wesley, San Francisco—Toronto, 2007.
6. Davies P. *Superforce: the Search for a Grand Unified Theory of Nature*. Simon and Schuster, Inc., New York, 1984.
7. Daywitt W.C. Limits to the Validity of the Einstein Field Equations and General Relativity from the Viewpoint of the Negative-Energy Planck Vacuum State. *Progress in Physics*, v. 3, 27, 2009.
8. Daywitt W.C. The Planck Vacuum and the Schwarzschild Metrics. *Progress in Physics*, v. 3, 30, 2009.

Lorentzian Type Force on a Charge at Rest. Part II

Rudolf Zelsacher

Infineon Technologies Austria AG, Siemensstrasse 2 A-9500 Villach. E-mail: Rudolf.zelsacher2@infineon.com

Some algebra and *seemingly* crystal clear arguments lead from the Coulomb force and the Lorentz transformation to the mathematical expression for the field of a moving charge. The field of a moving charge, applied to currents, has as consequences a magnetic force on a charge at rest, dubbed Lorentzian type force, and an electric field $\vec{E}$, the line integral of which, taken along a closed loop, is not equal to zero. Both consequences are falsified by experiment. Therefore we think that the arguments leading to the mathematical formulation of the field of a moving charge should be subject to a careful revision.

1 Citations

If someone asks me what time is, I do not know; if nobody asks me, I don't know either. [Rudolf Zelsacher]

2 Introduction

2.1 Miscellaneous

We will follow very closely the chain of thought taken by Edward Mills Purcell in [1]. We will use the Gaussian CGS units in order to underline the close relationship between electric field $\vec{E}$ and magnetic field $\vec{B}$.

Table 1: Definition of symbols

symbol	description
$j_x, \vec{J}$	current density
I	current
A, a	area
c	speed of light in vacuum
$v, \vec{v}$	speed, velocity
ϑ, α	angles
ω	anglular velocity
$N_e(x), n_e(x)$	current electron density, electron density
$\hat{R}$ etc.	unit vector in the direction of $\vec{R}$
$F(x, y, z, t)$, $F'(x', y', z', t')$	inertial systems in the usual sense as defined in e.g. [2]
β	$\frac{v}{c}$
$\vec{E}$	electric field
$\vec{B}$	magnetic field
q, Q, e, p	charge
h, a, r, R, s	distance
i, k, N, m	natural number variables
x, y, z	cartesian coordinates
t	time

2.2 The electric field $\vec{E}$ in F arising from a point charge q at rest in F′ and moving with $\vec{v}$ in F

The electric field $\vec{E}$ in F of a charge moving uniformly in F, at a given instant of time, is generally directed radially outward from its instantaneous position and given by [1]

$$\vec{E}(\vec{R}, \vartheta) = \frac{q(1-\beta^2)}{R^2(1-\beta^2 \sin^2 \vartheta)^{\frac{3}{2}}} \hat{R}. \tag{1}$$

R is the length of $\vec{R}$, the radius vector from the instantaneous position of the charge to the point of observation; ϑ is the angle between $\vec{v}\Delta t$, the direction of motion of charge q, and $\vec{R}$. Eq. 1, multiplied by Q, tells us the force on a charge Q at rest in F caused by a charge q moving in F (q is at rest in F').

3 Lorentzian type, i.e. magnetic like, force on a charge Q at rest

3.1 Boundary conditions that facilitate the estimation of the field characteristics

We have recently calculated the non-zero Lorentzian type force of a current in a wire on a stationary charge outside the wire by using conduction electrons all having the same speed [3]. We now expand the derivation given in [3] to systems with arbitrary conduction electron densities, i.e. to conduction electrons having a broader velocity range. Based on Eq. 1, describing the field of a moving charge, we derive geometric restrictions and velocity restrictions useful for our purposes. These boundary conditions allow the knowledge of important field characteristics, due to a non-uniform conduction electron density, at definite positions outside the wire.

3.1.1 The angular dependent characteristics of the field of a moving charge

For a given β, at one instant of time, the angle ϑ_c (theta change), between $\vec{R}$ and $\vec{v}\Delta t$, given by

$$\vartheta_c = \arcsin \frac{\left[1 - \left(1 - \beta^2\right)^{\frac{2}{3}}\right]^{\frac{1}{2}}}{\beta} \tag{2}$$

separates two regions: one where the absolute value of the field of the moving charge is less than $\frac{q}{R^2}$ and a second where the absolute value of the field of the moving charge is greater than $\frac{q}{R^2}$. For small velocities, e.g. $v = 2 \cdot 10^{-10}$ [cm/s], ϑ_c is $\approx \arcsin \sqrt{\frac{2}{3}}$ or about 54.7°. For $v = 2 \cdot 10^{10}$ [cm/s], ϑ_c is less than 60°. We will later need ϑ_c to estimate the effect of the field of conduction electrons at the position of a test charge Q. In Fig. 1 we have sketched in one quadrant the regions where the absolute value of the field of the moving charge is separated by ϑ_c. $2 \cdot 10^{10}$ cm/s or $2c/3$ is just an arbitrarily chosen and of course sufficiently high speed limit for conduction electrons to be used in our estimations.

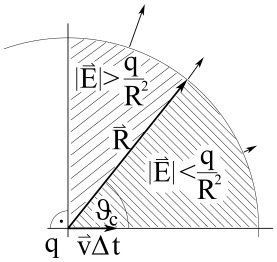

$$\vartheta_c = \arcsin \frac{\left(1 - \left(1 - \beta^2\right)^{\frac{2}{3}}\right)^{\frac{1}{2}}}{\beta}$$

for $v < c$

$$\vartheta_c \cong \arcsin\left(\sqrt{\frac{2}{3} + \frac{\beta^2}{9} + \frac{4\beta^4}{81} \cdots}\right)$$

(for $v = 2e^{10}[cms^{-1}]$ $\vartheta_c < 60°$)

(for $v \ll c$

$$\vartheta_c = \arcsin \frac{\sqrt{2}}{\sqrt{3}} \cong 54.7°$$

Fig. 1: The angle ϑ_c separates the region where the absolute value of the field of a moving charge is greater than $\frac{q}{R^2}$ from the region where the absolute value of the field of the moving charge is less than $\frac{q}{R^2}$.

3.1.2 The conduction electron density of a stationary current in a metal wire

We will use neutral wires and apply an electromotive force so that currents will flow in the wires. We also have in mind superconducting wires; at least we cool down the wires to near 0°[K] to reduce scattering. As in [1] we will restrict our investigation to a one dimensional current i.e. to velocities in one direction (v_x). A stationary current I, the number of electrons passing a point in a wire per unit of time, is then given by

$$I = \int \vec{j} d\vec{a} = A\,(-e)\,N_e\,(x)\,\bar{v}_x\,(x) \tag{3}$$

where A is the cross section of the wire, $\vec{j}$ or component j_x is the current density, $N_e(x)$ is the local conduction electron density and $\bar{v}_x(x)$ is the local mean velocity of the conduction electrons. For a stationary current $div\vec{j} = 0$. This indicates that there can be no permanent pile up of charges anywhere in the wire. From our discussion with regard to ϑ_c in section 3.1.1 we know that for restricted velocities v_x of the conduction electrons and restricted angles ϑ the absolute value of the field of the conduction electron $\frac{e(1-\beta^2)}{r^2(1-\beta^2 \sin^2 \vartheta)^{\frac{3}{2}}}$, at the position of the test charge Q, is either greater than $\frac{e}{r^2}$ or less than $\frac{e}{r^2}$.

3.1.3 The line integral of the field of a moving charge

The field of a moving charge at an instant t_0 cannot be compensated by any stationary distribution of charges. The reason is that for the field of a moving charge in general

$$\oint \vec{E} d\vec{s} \neq 0. \tag{4}$$

We will use this property to estimate whether a variable electron density $n_e(x)$ along a wire can compensate the field due to the moving conduction electrons. In addition we will use this fact to show that currents in initially neutral wires produce electric fields whose line integral along a closed loop is non-zero.

3.2 The force of a pair of moving charges on a resting charge

In Fig. 2 we show two charges q_n and q_p moving in lab and a test charge Q at rest in lab. The indices n & p were chosen to emphasize that we will later use a negative elementary charge and a positive elementary charge, and calculate the effect of such pairs, one moving and the other stationary, on a test charge Q at rest in lab.

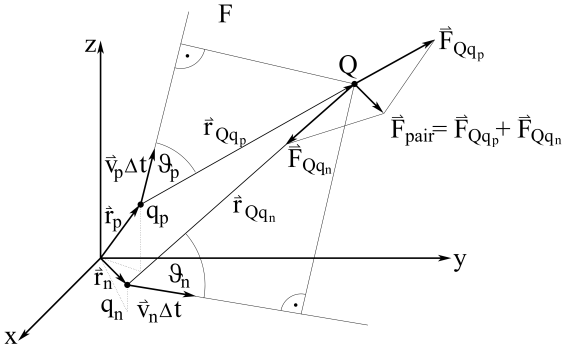

Fig. 2: The force $\vec{F}_{pair}$ on a resting charge Q caused by the two moving charges q_n and q_p. We assign the name $\vec{F}_{pair}$ to the result of the calculation of a force on a resting test charge Q, by at least two other charges having different velocities (including $\vec{v} = \vec{0}$).

The force $\vec{F}_{pair}$ exerted by this pair of charges, of q_n and

q_p, on the test charge Q is, according to Eq. 1, given by

$$\vec{F}_{pair} = \vec{F}_{Qq_p} + \vec{F}_{Qq_n} = \\ = \frac{q_p Q\left(1-\frac{\vec{v}_p^2}{c^2}\right)\hat{r}_{Qq_p}}{\vec{r}^2_{Qq_p}\left(1-\frac{\vec{v}_p^2}{c^2}\sin^2\vartheta_p\right)^{\frac{3}{2}}} + \frac{q_n Q\left(1-\frac{\vec{v}_n^2}{c^2}\right)\hat{r}_{Qq_n}}{\vec{r}^2_{Qq_n}\left(1-\frac{\vec{v}_n^2}{c^2}\sin^2\vartheta_n\right)^{\frac{3}{2}}}. \quad (5)$$

We are going to use such pairs of charges – specifically a conduction electron $(-e)$, and its partner, the nearest stationary proton (e) – in a current carrying wire and investigate the non vanishing field in lab produced by such pairs outside the wire. "Stationary" (or resting, or at rest) indicates that the "stationary charges" retain their mean position over time.

3.3 Lorentzian type force, part 1

We consider now two narrow wires isolated along their length, but connected at the ends, each having length 2a and lying in *lab* coaxial to the x-axis of F from $x = -a$ to $x = a$. In addition the system has a source of electromotive force applied so that a current I is flowing through the wires; in one of the wires I flows in the positive x direction and in the other wire I flows in the negative x direction. We also have in mind superconducting wires. On the z-axis of F fixed (stationary) at (0, 0, h) a test charge Q is located. The system is sketched in Fig. 3. We will now calculate the Lorentzian type force $\vec{F}_{Lt}$ on the stationary test charge Q fixed at (0, 0, h) exerted by the electrons of the current I and their nearest stationary protons at an instant t_0.

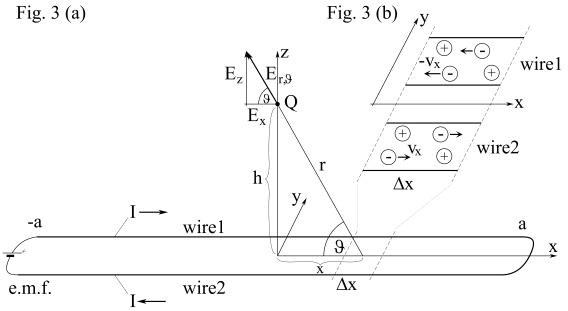

Fig. 3: (a) (b): We show in Fig. 3(a) the two wires carrying the current I extended along the x axis of F from $x = -a$ to $x = a$ and the charge Q at rest in F at (0, 0, h). Additionally on the right-hand side a magnification of a small element Δx containing the two wires and labeled Fig. 3(b) can be seen. Fig. 3(b) shows some moving electrons and for each of these the nearest neighboring proton situated in the tiny element. We calculate the force on Q by precisely these pairs of charges.

The two wires are electrically neutral before the current is switched on. Therefore after the current is switched on we have an equal number of N electrons and N protons in the system - the same number N, as with the current switched off. We look at the system at one instant of *lab* time t_0, after the current I is switched on and is constant. We consider the k electrons that make up the current I. For each of these k electrons e_i with $i = 1, 2, ..k$, having velocity $v_{x,i}$, we select the nearest neighboring stationary proton p_i with $i = 1, 2, ..k$. "Stationary" means that the charges labeled stationary retain their mean position over time. For each charge of the mobile electron-stationary proton pair, we use the same $\vec{r}_i$ as the vector from each of the two charges to Q. We use $\vartheta_i = \arcsin\frac{h}{r_i}$ as the angle between the x-axis and $\vec{r}_i$ for each pair of charges. As long as the velocity $v_{x,i}$ of a conduction electron is less than $2 \cdot 10^{10}[cm/s]$ and the angle $\vartheta_i = \arcsin\frac{h}{r_i}$, between the x-axis and the vector $\vec{r}_i$ from the current electron to test charge Q, is greater than 60°(and less than 120°), the contribution of the current electron to the absolute value of the field at (0,0,h) is, according to our discussion in section 3.1.1, greater than $\frac{e}{r_i^2}$. The contribution of the nearest proton that completes the pair is $\frac{e}{r_i^2}$. If we restrict ϑ_i to between 60°and 120°, we will have an electric field $\vec{E} \neq \vec{0}$ at the position of Q pointing towards the wire. The Lorentzian type force $\vec{F}_{Lt}$ on the stationary test charge Q is then given by

$$\vec{F}_{Lt} = Qe\sum_i\left\{\left|\frac{\cos\vartheta_i}{r_i^2}\right|(-1)^{m_i}\left(1-\frac{\left(1-\frac{v_{x,i}^2}{c^2}\right)}{\left(1-\frac{v_{x,i}^2}{c^2}\sin^2\vartheta_i\right)^{\frac{3}{2}}}\right)\hat{x}+ \right. \\ \left. +\frac{\sin\vartheta_i}{r_i^2}\left(1-\frac{\left(1-\frac{v_{x,i}^2}{c^2}\right)}{\left(1-\frac{v_{x,i}^2}{c^2}\sin^2\vartheta_i\right)^{\frac{3}{2}}}\right)\hat{z}\right\} = S_{Lt}\hat{S}. \quad (6)$$

The m_i ($m_i = 0$ if $x_{e_i} - x_Q < 0, m_i = 1$ if $x_{e_i} - x_Q > 0$) ensures the correct sign for the x-component of the force. Eq. 6 shows that an equal Number N of positive and negative elementary charges (the charges of the wire loop) produces a force on a stationary charge, when a current is flowing. This force can be written as

$$\vec{F}_{Lt} = F_{x,Lt}\hat{x} + F_{z,Lt}\hat{z} = \\ = \frac{\sqrt{F_{x,Lt}^2 + F_{z,Lt}^2}}{\sqrt{F_{x,Lt}^2 + F_{z,Lt}^2}}\left(F_{x,Lt}\hat{x} + F_{z,Lt}\hat{z}\right) = S_{Lt}\hat{S} \quad (7)$$

with the unit vector $\vec{\hat{S}}$ pointing from the position of the test charge $Q(0, 0, h)$ to a point $X(-a < X < a)$ on the x-axis. X will probably not be far from zero, but we leave this open as the resulting force vector $\vec{F}_{Lt} = S_{Lt}\vec{\hat{S}}$ depends on the local current electron density in the wire. Note that $\frac{\left(1-\frac{v_{x,i}^2}{c^2}\right)}{\left(1-\frac{v_{x,i}^2}{c^2}\sin^2\vartheta_i\right)^{\frac{3}{2}}}$ is greater than 1 as long as $v_{x,i} < 2 \cdot 10^{10}$ [cm/s] and 60°<

ϑ_i <120°, as was shown in section 3.1.1 This means the field at (0, 0, h) points to the wire.

3.4 Lorentzian type force, part 2

Next we place the stationary charge Q at the position $(b > a, 0, h)$, with $\vartheta_{max} = \arctan\frac{h}{b-a} < 54°$ (see Fig. 4).

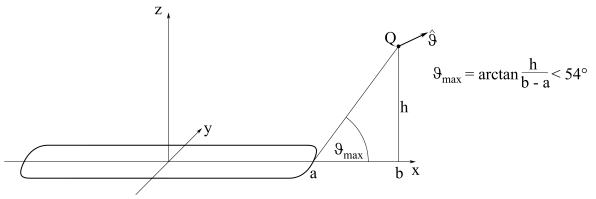

Fig. 4: If the test charge Q, is located at $(b, 0, h)$ as shown here, with $\vartheta_{max} = \arctan\frac{h}{b-a}$ <54°, then the absolute value of the field of each of the conduction electrons at $(b, 0, h)$ is less than that of a stationary charge for all velocities $0 < v_x < c$.

The force on the stationary test charge Q is given by Eq. 6. But now $\frac{\left(1-\frac{v_{x,i}^2}{c^2}\right)}{\left(1-\frac{v_{x,i}^2}{c^2}\sin^2\vartheta_i\right)^{\frac{3}{2}}}$ is less than 1 for $0 < v_{x,i} < 3\cdot 10^{10}$ [cm/s] and $0° < \vartheta_i < 54°$ or $136° < \vartheta_i < 180°$ as was shown in section 3.1.1. This means the field at $(b, 0, h)$ points away from the wire.

3.5 The line integral of the field of two parallel wires calculated at one instant t_0

We continue by estimating a specific line integral of the electric field outside the wire along the closed path shown in Fig. 5.

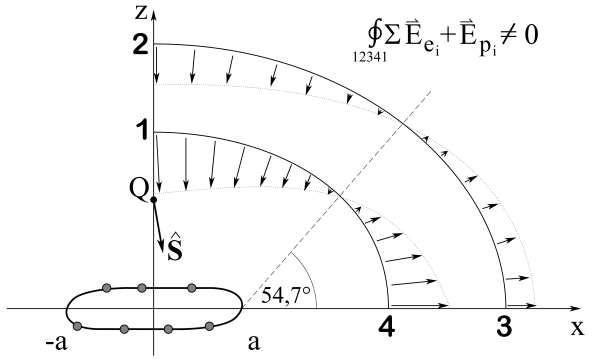

Fig. 5: Shows the electric field $\sum(\vec{E}_{e_i} + \vec{E}_{p_i})$ due to the moving conduction electrons and their partner protons of the system of Fig. 3. In addition the path 12341 is shown where the line integral of the electric field $\sum(\vec{E}_{e_i} + \vec{E}_{p_i})$ is estimated. $\vec{E}_s + \vec{E}_Q$, the field of the residual stationary charges of the system and the test charge Q, is not shown because the line integral of the field $\vec{E}_s + \vec{E}_Q$, along a closed path is zero.

The electric field of the system is a superposition of the field of the moving conduction electrons and their stationary partner protons $\sum(\vec{E}_{e_i} + \vec{E}_{p_i})$, the field $\vec{E}_s$ of the residual stationary electrons and protons of the wire and the field $\vec{E}_Q$ of the resting test charge Q. The line Integral of $\vec{E}_s + \vec{E}_Q$ along every closed path is zero. The line integral of the electric field $\sum(\vec{E}_{e_i} + \vec{E}_{p_i})$ due to the moving conduction electrons and their partner protons is, according to our discussion in section 3.1.1 and the results given by Eq. 6 at positions like (0, 0, h) and (b, 0, h), less than zero from 1 to 2, zero from 2 to 3 (because here we have chosen a path perpendicular to the field), less than zero from 3 to 4 and zero from 4 to 1 (because here we have again chosen a path perpendicular to the field).

$$\oint_{12341}\vec{E}d\vec{s} = \oint_{12341}\left(\sum\left(\vec{E}_{e_i}+\vec{E}_{p_i}\right)+\vec{E}_s+\vec{E}_Q\right)d\vec{s} = \\ = \left[\oint_1^2\left(\sum\vec{E}_{e_i}+\vec{E}_{p_i}\right)d\vec{s}+\oint_3^4\left(\sum\vec{E}_{e_i}+\vec{E}_{p_i}\right)d\vec{s}\right] < 0. \tag{8}$$

A wire bent like the loop 12341 might be a good device for the experimental detection of $\vec{F}_{Lt}$. As we have mentioned in section 3.1.2 we do not expect pile-up effects of charges in the wire because from experiment we know the extreme precision to which Ohm's Law, is obeyed in metals. But we expect a variable electron density $n_e(x)$ (not to be confused with the variable conduction electron density $N_e(x)$) on the wires resulting from capacitive and shielding effects, together with the field component of the moving conduction electrons directed along the wire. The estimation of the line integral of the electric field of the system, resulting in Eq. 8, shows, by being non-zero, that no "stationary" static charge distribution on the wires is able to compensate the field due to the moving conduction electrons.

3.6 The force on a charge at rest due to a superconducting ring

We consider now a superconducting current carrying ring, with radius a, and assume that one of its conduction electrons e_i at t_0, at rest in its local inertial frame, has constant velocity $\vec{v}_i = \vec{\omega}_i \times \vec{r}_i$. Then, according to Eq. 5 and Fig. 6 the Lorentzian type force on a charge Q at rest at $(0, 0, h)$ caused by this system is given by

$$\vec{F}_{Lt} = \sum_i \frac{Qe}{r_i^2+h^2}\left[1-\frac{1}{\left(1-\beta_i^2\right)^{\frac{1}{2}}}\right]\cos\arctan\frac{a}{h}\hat{z} \tag{9a}$$

or if $v \ll c$

$$\vec{F}_{Lt} \approx \sum_i \frac{Qe}{r_i^2+h^2}\left[1-1-\frac{\beta_i^2}{2}\right]\cos\arctan\frac{a}{h}\hat{z} = \\ = \sum_i -\frac{Qv_i}{c}\frac{ev_i}{2\left(r_i^2+h^2\right)c}\cos\arctan\frac{a}{h}\hat{z}. \tag{9b}$$

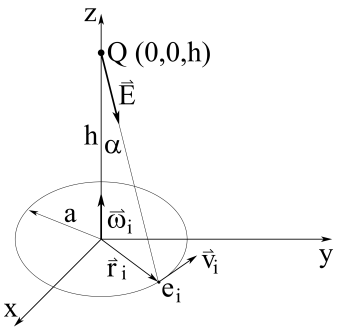

Fig. 6: The electrical field, at the position of a charge Q at rest, caused by one of the charges e_i of the current in a superconducting wire.

As stated above we assume that the current carriers are at rest in a succession of individual local inertial frames when circling in the loop; i.e. the movement of the charges is well described by a polygon, with as many line segments as you like it. This view is supported by the experimental fact that currents flow for years in such loops without weakening, showing that the passage from one inertial frame to the next happens without much radiation.

3.7 The Field due to a constant electron density in the parallel wires connected at the ends

We now proceed to the case where the current electron density $N_e(x)$ is constant along the wires *by definition* to get an analytic expression for the force $\vec{F}_{Lt}$ on a stationary charge. This was calculated in [3] and here we just rewrite the result. The Lorentzian type force on a charge Q at rest due to a system like that shown in Fig. 2 is, by assuming a constant current electron density, given by

$$\vec{F}_{Lt} = -\frac{Qv_x}{c}\frac{2I\cos\vartheta_{min}\sin^2\vartheta_{min}}{hc^2}\hat{z}. \qquad (10)$$

The force described by Eq. 10 is of the same order of magnitude as magnetic forces, as can be seen by comparing it to Eq. 11, the result of a similar derivation given in [1]

$$\vec{F} = \frac{qv_x}{c}\frac{2I}{rc^2}\hat{y}. \qquad (11)$$

4 Discussion

The one and only way to scientific truth is the comparison of theoretical conclusions with the experimental results. We have investigated the consequences of Eq. 1 - the elegant mathematical formulation of the field of a moving charge. By applying the field of a moving charge to currents in loops we derive a magnetic force on a charge at rest outside these loops. We have dubbed this force "Lorentzian type force" and state that such a force has never been observed in experiments. In addition such current-carrying systems, when investigated by using the mathematical expression for the field of a moving charge, show an electric field whose line integral along a closed loop is non-zero. Also this prediction has never been observed by experimental means. We find the example of the Lorentzian type, i.e. magnetic, force on a charge at rest due to the superconducting ring (as given in 3.6), which also has been never observed, to be especially instructive because nothing disturbs the intrinsic symmetry. The overall conclusion from our investigation is that the arguments leading to the formula for the field of a moving charge should be subject to a careful revision.

Acknowledgements

I am grateful to Thomas Ostermann for typesetting the equations and to Andrew Wood for correcting the English.

Submitted on November 20, 2014 / Accepted on November 22, 2014

References

1. Purcell E.M. Electricity and Magnetism, McGraw-Hill Book Company, New York, 1964.
2. Kittel C. et al, Mechanics 2^{nd} Edition, McGraw-Hill Book Company, New York, 1973.
3. Zelsacher R. Lorentzian Type Force on a Charge at Rest. *Progress in Physics*, 2014, v. 10(1), 45–48.

Gauge Freedom and Relativity: A Unified Treatment of Electromagnetism, Gravity and the Dirac Field

Clifford Chafin

Department of Physics, North Carolina State University, Raleigh, NC 27695. E-mail: cechafin@ncsu.edu

The geometric properties of General Relativity are reconsidered as a particular nonlinear interaction of fields on a flat background where the perceived geometry and coordinates are "physical" entities that are interpolated by a patchwork of observable bodies with a nonintuitive relationship to the underlying fields. This more general notion of gauge in physics opens an important door to put all fields on a similar standing but requires a careful reconsideration of tensors in physics and the conventional wisdom surrounding them. The meaning of the flat background and the induced conserved quantities are discussed and contrasted with the "observable" positive definite energy and probability density in terms of the induced physical coordinates. In this context, the Dirac matrices are promoted to dynamic proto-gravity fields and the keeper of "physical metric" information. Independent sister fields to the wavefunctions are utilized in a bilinear rather than a quadratic lagrangian in these fields. This construction greatly enlarges the gauge group so that now proving causal evolution, relative to the physical metric, for the gauge invariant functions of the fields requires both the stress-energy conservation and probability current conservation laws. Through a Higgs-like coupling term the proto-gravity fields generate a well defined physical metric structure and gives the usual distinguishing of gravity from electromagnetism at low energies relative to the Higgs-like coupling. The flat background induces a full set of conservation laws but results in the need to distinguish these quantities from those observed by recording devices and observers constructed from the fields.

1 Introduction

The theories (special and general) of relativity arose out of an extension of notions of geometry and invariance from the 19th century. Gauge freedom is an extension of such ideas to "internal" degrees of freedom. The gauge concept follow from the condition that quantities that are physically real and observable are generally not the best set of variables to describe nature. The observable reality is typically a function of the physical fields and coordinates in a fashion that makes the particular coordinates and some class of variations in the fields irrelevant. It is usually favored that such invariance be "manifest" in that the form of the equations of motion are evidently independent of the gauge. Implicit in this construction is the manifold-theory assumption that points have meaning and coordinate charts do not. We are interested in the largest possible extension of these ideas so that points themselves have no meaning and gauge equivalence is defined by mappings of one solution to another where the observers built of the underlying fields cannot detect any difference between solutions. This is the largest possible extension of the intuitive notion of relativity and gauge. It will be essential to find a mathematical criterion that distinguishes this condition rather than simply asserting some gauge transformation exists on the lagrangian and seeking the ones that preserve this. This leads us to consider a more general "intrinsic" reality than the one provided by manifold geometry but, to give a unified description of the gravitational fields and the fields that are seen to "live on top of" the manifold structure it induces requires we provide an underlying fixed coordinate structure. The physical relevance, persistence and uniqueness of this will be discussed, but the necessity of it seems unavoidable.

Initially we need to reconsider some aspects of the particular fields in our study: the metric, electromagnetic and Dirac fields. The Dirac equation is interesting as a spinor construction with no explicit metric but an algebra of gamma-matrices that induce the Minkowskii geometry and causal structure. There are many representations of this but the algebra is rigid. The general way to include spinors in spacetime is to use a nonholonomic tetrad structure and keep the algebra the same in each such defined space. We are going to suggest an initially radical alteration of this and abandon the spinor and group notions in these equations and derive something isomorphic but more flexible that does not require the vierbein construction. It is not obvious that this is possible. There are rigid results that would seem to indicate that curvature necessitates the use of vierbeins [1]. These are implicitly built on the need for ψ itself to evolve causally with respect to the physical metric (in distinction with the background metric). We will extend the lagrangian with auxiliary fields so that this is not necessary but only that the gauge invariant functions of the *collective* reality of these fields evolve causally. This is a subtle point and brings up questions on the necessity of the positive definiteness of energy, probability, etc. as defined by the underlying (but not directly observable) flat space.

Let us begin with a brief discussion of the Dirac equation and this modification. The Dirac equation is the fundamental description for electrons in quantum theory. It is typically derived in terms of causality arguments and the need for an equation of motion that is first order in time, as was Dirac's approach, or, more formally, in terms of representation theory of the Lorentz group. These arguments are discussed many places [2–4]. While this is a powerful description and has led to the first inclination of the existence of antiparticles, it has its own problems. Negative energy solutions have had to be reconciled by Dirac's original hole theory or through the second quantization operator formalism. Most are so steeped in this long established perspective and impressed by its successes that it gets little discussion.

A monumental problem today is that of "unification" of quantum theory and gravity. There are formal perturbative approaches to this and some string theory approaches as well. In quantum field theory we often start with a single particle picture as a "classical field theory" and then use canonical quantization or path integral methods. For this reason, it is good to have a thorough understanding of the classical theory to be built upon. We will show that, by making some rather formal changes in traditional lagrangians, some great simplifications can result. The cost is in abandoning the notions that the fields corresponding to nature are best thought of as evolving on the "intrinsic" geometry induced by a metric and that spacetime is a locally Lorentzian manifold. In place of this is a trivial topological background and a reality induced by fields which encodes the observable reality and apparent coordinates (induced by collections of objects) and metrical relationships in a non-obvious fashion. Usual objections to such a formalism in the case of a gravitational collapse are addressed by adherence to the time-frozen or continued collapse perspective.

A main purpose of this article is to illustrate an alternate interpretation of the Dirac equation. In the course of it, we will make gravity look much more like the other bosonic fields of nature and give a true global conservation law (that is generally elusive in GR). Our motivation begins with a reconsideration of the spinor transformation laws and the role of representation theory. This approach will greatly expand the gauge invariance of the system. In place of the metric $g_{\mu\nu}$ as the keeper of gravitational information, we will let the γ matrices become dynamic fields and evolve. Our motivation for this is that, for vector fields, the metric explicitly appears in each term and variation of it, gives the stress-energy tensor. The only object directly coupling to the free Dirac fields is γ. Additionally, γ^μ bears a superficial resemblance to A^μ and the other vector bosons. Since $g \sim \gamma\gamma$ we might anticipate that the spin of this particle is one rather than two as is for the graviton theories which are based explicitly on $g^{\mu\nu}$. It is because we only require our generalized gauge invariant functions to obey causality and that these conserved quantities, while exact, are not directly observable so do not have to obey positive definiteness constraints that this approach can be consistent.

We will be able to show that this construction can give GR evolution of packets in a suitable limit and obeys causal constraints of the physical metric. It is not claimed that the evolution of a delocalized packet in a gravitational field agrees with the spinor results in a curved spacetime. This will undoubtably be unsatisfactory to those who believe that such a theory is the correct one. In defense, I assert that we do not have any data for such a highly delocalized electron in a large nonuniform gravitational field and that the very concept of spinor may fail in this limit. As long as causality holds, this should be considered an alternate an viable alternative theory of the electron in gravity. The purely holonomic nature of the construction is pleasing and necessary for a theory built on a flat background. A unification of gravity in some analogous fashion to electroweak theory would benefit from having a its field be of the same type. One might naturally worry about the transformation properties of ψ_a and γ^μ_{ab} in this construction. Under coordinate transformations of the background, ψ_a behaves as a scalar not a spinor and γ^μ_{ab} is a vector. One should not try to assign to much physical meaning to this since these transformations of the structure are passive. Active transformations where we leave the reality of all the surrounding and weakly coupled fields the same but alter the electron of interest can be manifested by changes in both ψ and γ (and A) so that the local densities and currents describing it are boosted and those of the other fields are not. The usual active boost $\psi'_b = S(\Lambda)_{ba}\psi_a$ is included as a subset of this more general gauge change.

There has been work from the geometric algebra perspective before [5] in trying to reinterpret the Dirac and Pauli matrices as physically meaningful objects. Since the author has labored in isolation for many years searching for a physical meaning for the apparent geometric nature of physical quantities this did not come to his attention until recently. However, there are significant differences in the approach presented here and the easy unification with gravity that follows seems to depend on abandoning group representation theory in the formulation. Most importantly, one has a new notion of gauge freedom as it relates to the reality expressed by particle fields (i.e. the full gauge independent information associated with it). Coupling destroys the ability to associate the full "reality" of the electron with the wavefunction. We will see that this can get much more entangled when one includes gravity and, with the exception of phase information, the only consistent notion of a particle's reality comes from the locally conserved currents that can be associated with it. Here will involve multiple field functions not just ψ_a as in the free particle case.

The dominant approaches to fundamental physics has been strongly inspired by the mathematical theory of manifolds where a set of points is given a topology and local coordinate chart and metric structure. The points have a reality

in this construction and the charts are grouped into atlases so that coordinates are "pure guage" and no physical reality is associated with them. We frequently say that the invariance of the field's equations requires that we have a metric invariant action be a scalar. It can be shown somewhat easily [6] that this is not true and that most lagrangians that give many common (local) field equations are neither invariant nor local. In the following we enlarge the class of physically equivalent fields to the set of fields that evolve in such a fashion where the "observers" built from the fields cannot distinguish one description from another. This includes simple spacetime translations of a flat space of the entirety of fields and far more general deformations of the fields which do not preserve the underlying set of points.

The underlying space is chosen trivially flat with the $\eta^{\mu\nu}$ metric. This begs the question of how general curved coordinates resulting from the effective curvature induced by the field $g^{\mu\nu}(\gamma)$ relate to it and how the causally connected structure induced by the fields evolves through this flat background. In this picture the "physical coordinates" seen by observers are measures induced by "candles," specifically highly independent localized objects and radiators, that induce his perception of his surroundings. Clocks are induced by atomic oscillations and other local physical processes. Collective displacements and alterations of the fields on the underlying flat space that preserve the preserved reality are considered alternate representations of the same physical reality rather than an active transformation of it to a new and distinct one, as one would expect from the usual manifold founded perspective.

At the foundations of manifold inspired physics are tensors and their transformation rules under coordinate changes. In this case we have little interest in the transformations with respect to the underlying flat space and all fields are treated as trivial tensors with respect to it. The interesting case of apparent curvature must then be measured with respect to these local candles. The vector properties of functions of a field, like the current $j^{\mu}_{(0)} = \bar{\psi}_{(0)}\gamma^{\mu}\psi_{(0)}$, are then the collective result of active transformations of the $\psi_{(i)}$, γ and underlying coordinates that leave the nearby candles' (labelled by i) gauge invariant features unchanged and a transformation of the field $\psi_{(0)}$ so that the resulting current $j_{(0)}$ appears to move through a full set of Lorentz boosts and rotations relative to measurements using these candles.

This is a significant departure from the usual geometry inspired approach. Not surprisingly many formulas will appear (deceptively) similar to usual results despite having very different meaning since they will all be written with respect to the underlying flat structure not some "physical coordinates" with respect to some fixed point set induced by the candles. The mystery of how we arrive at a geometric seeming reality and at what energy scale we can expect this to fail is a main motivation for this article. Conservation laws follow from the usual ten Killing vectors of flat space but the meaning of these conservation laws (and their form in terms of observable quantities) is unclear. Even the positive definiteness of quantities like energy and mass density are not assured and failure of them do not carry the same consequences as in usual metric theories. The symmetry responsible for mass conservation is the same one as for probability so such a situation raises more questions that must be addressed along the way. We have been nonspecific about the details of what determines equivalent physical configurations. Aside from the geometry induced by candles the gauge invariant quantities that we presume are distinguishable by observers are those induced by conserved currents such as mass and stress-energy. It is not obvious why such should be the case. A working hypothesis is that all observers are made up of long lasting quasilocalized packets of fields that determine discrete state machines and these are distinguished by localized collections of mass, charge and other conserved quantities.

In this article we only discuss these as classical theories in a 4D spacetime. Of course, the motivation is for this to lead to a general quantum theory. There is a lot of work on reinterpretation of quantum theory as a deterministic one. Everyone who works on this has his favorite approach. The author here is no exception and has in mind a resolution that is consistent with the theory in [7] that gives QM statistics assuming that particular far-from-eigenstate wavefunctions describe classical matter that arise in an expanding universe with condensing solids. The motivations behind the following constructions is not just to get some insight on unification but to take steps to resolve some of the fundamental contradictions of quantum field theory, such as Haag's theorem, and to give a solid justification for the calculations of field theory that have been successful.

The structure of the article will be as follows. Invariance and the nature of causality are discussed and contrasted with the usual flat background approach in §2. This is especially subtle since the "physical" metric, reality and coordinate features are encoded in this construction in nonobvious ways, the gauge group is large and some conserved quantities and expected positive definiteness of quantities can change without altering the physically observable results. Next we will elaborate in §3 on the transformation properties of the fields and promotion of the gamma matrices to holonomically described proto-gravity fields in causally consistent manner and in §4 give a discussion on the "reality" induced by fields. In §5 we modify the Dirac lagrangian with an auxiliary field ϕ to replace the awkward $\bar{\psi} = \psi^*\gamma^0$ with its extra γ^0 factor uncontracted in any tensorial fashion, and demonstrate causality of the gauge invariant functions of the field.* In §6, a sister

*We typically vary ψ and ψ^* independently in the lagrangian to get equations of motion but then constrain them to be so related (though we should show this constraint is propagated as well). Here we make no such restriction and allow ψ and ϕ to be independent fields with no constraints on the initial data. In the flat space case, the case of $\phi = \gamma^0\psi^*$ gives the usual results and shows many other cases (i.e. ψ, ϕ initial data pairs) are gauge related to this.

field to γ is introduced that allows a similar lagrangian for the proto-gravity fields (when a Higgs-like construction is used) as for the electromagnetic field and that gives General Relativity in a suitable limit. This similarity suggests a pairing of the electromagnetic and proto-gravity fields in a manner reminiscent of the electroweak theory. §7 gives a discussion of the global conservation laws that arise due to symmetries of the flat background.

2 Roles of invariants in physics

The mathematical theory of invariants arose in the 19th century and the intuition derived from them made a physical appearance with the work of Mach [8] and Einstein [9]. Since then they have played a preeminent role both in formulating theory and solving particular problems. The geometrodynamic approach to General Relativity is to assume some underlying geometry that is locally special relativity and posit that this geometric structure and its associated transformation laws are the natural way to look at the world. "Flat background" approaches are generally to look at small post-Newtonian corrections to the universe for nearly flat spaces where gravity is playing a small role [10]. In more dramatic configurations this formalism seems hopelessly flawed. Wormholes are topologically forbidden from such a description. Black holes with their singularities have infinite metric curvature at the center and the interior of the event horizon causally decouples in one direction from the exterior.

There is an old and out-of-favor view of black holes that goes back to Oppenheimer [11] whereby the infalling matter gets redshifted to an effective asymptotic standstill so that no singularity or horizon ever forms. This is often called the "time-frozen" picture. For many this is considered equivalent to lagrangian evolution where the particles fall in finite proper time to the center. It is usually neglected that this implies a transfinite amount of external observer time must elapse for this to occur. This implies that we have assumed that in the entirety of external observer time, no collective action occurs to interfere with black hold formation before the event horizon forms. Furthermore, an infalling pair of charges on opposite nodes will be seen as a dipole field for all future time in the time-frozen case. The lagrangian approach would suggest that these fall to the center and form a spherically symmetric charge distribution as suggested by the "no-hair" conjecture. This latter picture has no physical relevance for the external observers, so the author is firmly in the time-frozen camp.

The importance of this point of view is that there are no exotic topologies to get in the way of assuming that one has a flat background. The "geometric" aspects of gravity are some yet to be explained feature of a field that evolves in an equivalent fashion to all the other fields of nature. Let us now take the point of view that there is a flat background and, rather that looking at perturbations of it as $g^{\mu\nu} = \eta^{\mu\nu} + \tilde{h}^{\mu\nu}$, the field h^{ab} sits on top of it and is coupled to the other fields, including the kinetic terms, in the fashion of a metric. Let this background have the flat space metric $\eta^{\mu\nu}$ so that coupling, for the electromagnetic case, is of the form

$$\mathcal{L} = \left(\partial_\alpha A_\beta - C^\gamma_{\alpha\beta} A_\gamma\right) h^{\alpha\alpha'} h^{\beta\beta'} \left(\partial_{\alpha'} A_{\beta'} - C^{\gamma'}_{\alpha'\beta'} A_{\gamma'}\right),$$

where the connection-like C tensor is yet to be defined. Importantly, these are *not* considered to be indices that transform as co and contravariant tensors under the metric h. All the objects here are flat space η-tensor objects. This seemingly bazaar construction gives causal cones for the evolution that are not the flat space cones defined by $\eta^{\mu\nu}$. The coordinate labels $\hat{t}, \hat{x}, \hat{y}, \hat{z}$ give coordinate directions. We expect that the (x, y, z) set are h-spacelike in the sense that $h^{ij}u_i u_j > 1$ for all u in the span of $\hat{x}, \hat{y}, \hat{z}$. The forward timelike direction has a positive projection on $\hat{t}$ even if the cone is so tilted that $h^{tt} > 0$. Thus it gives a positive evolution direction for a future on the background.

In general, any reasonable equation of motion for h should preserve this set of conditions and evolve in our coordinate time variable t for all values. In the case of black hole formation the metric tends to asymptotically converge on a degenerate state leading to a set of equations that are very ill-conditioned. How to treat this situation numerically is still unclear but the presence of a flat η-background means that we have a full set of conservation laws so these may provide an avenue to evolve without such problems [12]. We will not be answering the question of general persistence of evolution of the equations as it seems to be a very hard problem (as most nonlinear PDE solution existence problems are) but it is very important. Failure of this to hold would be destructive to such a theory. It is taken as an article of faith that such a set of initial data can be evolved for all coordinate time with time steps taken uniformly at all locations. In other words, cones may narrow and tilt but they will never intersect with our spatial coordinate slices.

The role of gauge invariance in physics is analogous to an equivalence class in mathematics. In mathematics we have some set of structures we wish to preserve and there can be classes of elements that act the same under them. In physics, we may have a set of fields that evolve under the equations of motion in such a way that there are classes that retain some set of properties under evolution. We usually describe the set by a gauge transformation that joins each subclass. It is not clear that nature is really blind to which element of the class we are choosing. One could choose a representative element and claim that this is the "correct" one and be no worse for it. In the case of the Dirac field ψ and the electromagnetic field A each has a set of gauge transformations as free fields. The Dirac field has only a global phase transformation however, when coupled to the electromagnetic field, it acquires some local gauge freedom $A \to A + \nabla\chi$ in that the phase $\varphi \to$

In the case of a nontrivial gravity field, we allow the possibility that no such mapping may exist.

$\varphi - \chi$. This is what we mean by "promoting" a global to a local symmetry.

In the following we will replace the quadratic lagrangian with a bilinear one by replacing $\bar{\psi} = \psi^* \gamma^0$ with a new field ϕ.* This is the motivation for the title. We are really only abandoning γ^0 in this sense as a factor in defining $\bar{\psi}$. The fields γ^μ are all retained as what might be loosely called a "spin 1" encoding of the gravitational field. We now need to ask what are the physically distinguishable states of the system. It is natural to argue that the conserved quantities give the only unambiguous physical quantities that we can distinguish. Phase is complicated in that it gives current and relative cancellation due to interference. One can define a ψ by the mass density ρ and the current j. When the density is over a compact set this is enough to fix the phase up to a constant. For our new set we will have conservation laws that depend on ψ, ϕ and γ. The γ^0 is still present but now a dynamical field. This trio of fields now collectively determines the conserved currents. Naturally this is a massive expansion of the gauge group. In the "flat space" case we can choose γ^μ to be the Dirac matrices in some representation and $\phi = \gamma^0 \psi^*$ and obtain the usual Dirac results.

The Noether charge symmetries here correspond to spacetime symmetries and phase transformations. When we consider the quantum analogs of such fields the importance of positive definite norm is important. This is because it is given the role of a probability for a measurement so must be positive definite and normalizable. This fails in the classical theory of Dirac particles but is "fixed up" in the quantum field theory by choices for the commutation relations of the operators and their action on the vacuum ground state (as with the Gupta-Bluer formalism [13]). In this classical theory we are not necessarily concerned with this for this reason but the same symmetry generates mass and charge conservation so it still is important. Interestingly, this symmetry holds in curved space as we propagate hyperbolic spacelike slices even when there is no spacetime symmetry.

One way the Dirac field is incorporated into curved spacetime is to fix γ^μ set to be a particular representation and use vierbein fields (tetrad formalism). This preserves the desired norm properties above and ensures local packets move correctly. There is little choice in this approach if one is to use wavefunction evolution from a quadratic lagrangian [1]. To be fair, no one knows what the evolution of an electron is on such scales. We expect packets to move along geodesics but if some negative norm or mass density entered we then must defer to experiment to validate or reject this. The probabilistic interpretation seems hopeless but consider that true "observers" as machines that measure the results are themselves built from such fields. If quantum evolution is a deterministic feature as decoherence advocates suggest, then the probability is unity by the evolution and a change in positive definite norm means that the action of our measurement devices must obey a modified rule that preserves this. This should be kept in mind when we consider questions about the conserved quantities. Negative energy and mass regions of quantum bodies in highly curved regions my not be forbidden by nature as much as we forbid it by our assumptions about the essential meaning of such quantities.

For evolution on such a flat η-background that mimics gravity, we must then ask what kinds of transformations correspond to the general coordinate transformations we are used to in GR. Firstly, just as information has come to be considered a physical state in quantum information theory, coordinates and time should be thought of as physical conditions given by the kinds of candles afforded by local atoms and clusters that triangulate our spacetime. We may as well think of "physical coordinates" (i.e. non η-background coordinate changes) as made of material bodies that are small enough to give insignificant perturbations to the general dynamics. To actively boost to another RF (reference frame) we consider a local current relative to some other standard currents that define the frame and choose the new current so the relative local motion matches. To passively boost to another RF we consider a transformation of the underlying η-background coordinates. Since the physically causal light cones induced by $h^{\mu\nu}$ in its coupling to the other fields A, ψ, etc. are not the cones induced by η we must take care to maintain the $\hat{t}$-forward direction of the cones under such changes. The tensor field constructions made with the usual forms $\bar{\psi}\gamma^\mu_D\psi$, etc. will now be of the form $j^\mu = \phi\gamma^\mu\psi$ so that their transformation properties under η-background coordinate changes are tensorial. This is, however, not very interesting because it does not relate to our physical observers and their physical coordinates that relate to the function $h^{\mu\nu}$. Many active transformation of the field trio ϕ, γ, ψ give the same boosted current. If we make the change purely with γ and assume our metric function $h^{\mu\nu}$ is built from them, this will change other terms in the equations of motion.

There remains the many possibilities of transforming the pair ψ, ϕ to give a new current function without altering the local observed geometry. Passive transformations based on allowable background coordinate changes can be done by changing the η-background coordinates or altering the fields ψ, ϕ in a manner that gives a shifted (on the background coordinates) set of currents and conserved densities that evolve in an isomorphic fashion to the original fields. The possibility of having shifted and deformed sets of fields on the background space with the same observable reality is a novel extension over the manifold approach where the points have reality and we assign and transform fields there based on coordinate changes and other gauges. It is analogous to having a set of fields on $\mathbb{R}^4$ and shifting the set by a 4-vector v^μ to give a new equivalent universe of solutions in the equivalence class; an obviously true equivalence that is not present by positing a

*Such a construction also introduces a large set set of nonlocal conservations laws. [6]

manifold with fields. We now allow this full set of equivalent representations of such a universe.

3 Transformation rules

The theory of spinors arose naturally out of Dirac's algebraic attempts to reconcile causality with the first order equations that seem to describe nonrelativistic electrons. Interestingly, Schrödinger originally attempted the, later named, Klein-Gordon equation to describe electrons but could not get the fine structure right [4]. He settled on a diffusion-like equation that was first order in time and second order in spatial derivatives. Pauli adapted it to include spin but, as for most such equations, signal propagation speeds diverge. Dirac introduced a pair of spinors and a linear first order operator that when "squared" gave the Klein-Gordon equation for each component, thus ensuring causality.

His treatment introduces a set of γ^{μ}_{ab} matrices that are considered fixed and constitute representations of the $SL(2,\mathbb{C})$ group which is a two-fold covering group of the $SO^{+}(3,1)$ group. More explicity, this gives a map of complex valued bi-spinors $\binom{a}{b}\binom{c}{d}$ to real 4-vectors so that each 4×4 complex matrix action corresponds to a Lorentz transformation and compositions among these is preserved by this mapping. In the humblest of terms, we can decompose a general free state ψ_a into a basis of free progressive wave solutions $e^{ik_\mu x^\mu}u_a(k)$ where we can define a general Lorentz transformation $\Lambda^{\mu'}_{\nu}$ through the coordinate *and* algebraic action $S(\Lambda)_{ab}\psi_b(\Lambda x)$. We define this action so that the current j^μ is transformed by a boost and interpret it as the actively boosted free plane wave of positive energy. Note that $S(\Lambda)_{ab}\psi_b(x) \neq \psi_a(\Lambda x)$.

The Dirac lagrangian has a (seemingly) symmetric form

$$\mathcal{L}_D = i\bar{\psi}\gamma^\mu\partial_\mu\psi - m\bar{\psi}\psi, \tag{1}$$

where $\bar{\psi} = \psi^*\gamma^0$. This inconvenient γ^0 is generally considered necessary to give Lorentz invariance. We can see that without it we would get inconsistent equations of motion for ψ and ψ^* if we vary them independently.

The operator $S(\Lambda)_{ab}$ performs a transformation of ψ_a so that the lagrangian is invariant and the resulting current is boosted as

$$\begin{aligned} j'^{\alpha}(x') &= \left(\psi'(x')^*\gamma^\alpha\psi'(x')\right) \\ &= \left((S\psi(x))^*\gamma^\alpha S\psi(x)\right) = \left(\psi(x)^*S^*\gamma^\alpha S\psi(x)\right) \\ &= \left(\psi(x)^*\gamma'^{\alpha}\psi(x)\right) = \Lambda^\alpha_\beta\left(\psi^*(x)\gamma^\beta\psi(x)\right) \\ &= \Lambda^\alpha_\beta j^\beta(x). \end{aligned} \tag{2}$$

The Dirac theory allows us to think of the complex 4-spinors ψ_a at each point as indicating the local direction of the local current of the particle corresponding to it. To achieve this it has been necessary to introduce negative energy solutions. The negative energy solutions are reinterpreted as positrons and given a positive mass through the details of canonical quantization since they are generally deemed undesirable. One reason to reconsider this point is that net positive energy initial data may maintain this property and negative energy states do not necessarily provide an avenue for some subset of the space to fall to negative infinite energy at the expense of heating the rest of the system. Such a result would depend on the details of the coupling and dynamics. Local net negative energy density in solutions arising from positive local energy physically arising states would produce problems but it is not clear that this ever arises except in extreme cases where pair production becomes available.

Other conservation laws such as the conservation of probability (which arise from the same global phase symmetry that give mass and charge conservation) have similar problems. In an "emergent" theory of quantum measurement we do not need a probability operator (or any operators at all). The probabilities arise from measurements with the kinds of macroscopic yet still quantum mechanical matter that constitutes the classical world [7]. In this approach, the initial data and evolution equations generate their dynamics in a deterministic fashion and the probabilistic features arise from the long lived partitioning of the classical world into subsets indexed by the delocalized objects that interact with it. Details of when this is a consistent procedure are discussed in ref. [7]. For this reason, we do not seek to validate or build upon arguments that start with an "interpretation" of particular expressions since we ultimately expect the evolution and interactions to independently determine the expressions that give all observable results.

One of the frustrating aspects of the Dirac equation as it stands is that it is not clear how we should alter its form in general coordinates. One can use the local frame approach and assume the Dirac matrices are members of the same representation in each one. A spinorial connection then indicates how nearby spinors are related as a consequence of geometry. If we allow the matrices to become functions of space and time with only the spacetime indices changing this gives a simple approach but then it is not clear how we recover local Klein-Gordon (KG) evolution of each component and what the locally boosted fields should be. If we continue with the spinor approach and let the $\gamma^\mu(x)$ matrices be fixed and alter the spinor fields instead then we need a transformation that is a kind of "square root" of the Lorentz vector transformation. This is how we get the actively boosted solutions in flat space. In curved spacetime, there is no global notion of a boost so the former perspective seems more valuable. Ultimately, we specify a configuration by the spacetime metric and the fields on it but the metric will be a function of the γ^μ matrix fields (and some associated dual fields) that only give geodesic motion below some energy bound.

In the early days of the Dirac equation, interpretations have evolved from a proposed theory of electrons and protons to that of electrons and positrons with positrons as "holes" in an infinitely full electron "sea" to that of electrons with

positrons as electrons moving "backwards in time." The first interpretation failed because the masses of the positive and negative energy parts are forced to be equal. The second was introduced out of fear that the negative energy solutions of the Dirac equations would allow a particle to fall to endlessly lower energies. The last was introduced as a computational tool. The negative mass solutions were to be reinterpreted as positive mass with negative charge. Necessary computational fixes associated with this idea are subtly introduced through the anticommutation relations used in the field theory approach to fermions and the properties of the supposed ground state [13]. If we are going to seek a classical field theory approach to this problem we need another mechanism.

For the moment, we assume the γ matrices are those of the Dirac representation. Standard treatments allow any selection of 4×4 matrices that represent the $SO^+(3,1)$ group. Here we choose a specific representation because we are going to let the γ's be fields and let these other choices be a kind of gauge freedom until some interaction restricts us to a specific subset. The Dirac lagrangian has a (seemingly) symmetric form

$$\mathcal{L}_D = i\bar{\psi}\gamma^\mu\partial_\mu\psi - m\bar{\psi}\psi \tag{3}$$

where $\bar{\psi} = \psi^*\gamma^0$. This is generally considered necessary to give Lorentz invariance. The Dirac matrices satisfy the condition

$$\{\gamma^\mu, \gamma^\nu\} = -2\eta^{\mu\nu}, \tag{4}$$

where η =Diag(−, +, +, +). This suggests that we could view the metrical properties of the space as encoded in γ rather than invoking a metric η. The metric has ten independent parameters at each point and γ has 4×10 or 4^3 parameters, depending on chosen symmetry constraints but we need to satisfy 4^4 equations. If we trace the suppressed spin indices then there are only 10 equations and a general metric can be encoded in the γ^μ set. However, eqn. 4 is the identity we require to convert the Dirac equation into a KG one that demonstrates causality in each component. This is a loose end in deriving geodesic motion for a packet to show that we get observed motion in the classical GR limit and an important consideration in what follows.

In anticipation of a future unification theory one cannot help but notice the greater similarity of $\gamma^\mu_{ab}(x)$ to $A^\mu(x)$ and the other vector boson fields than any of these to the metric $g_{\mu\nu}$. For now we simply leave this as constant but accept that it can have its own transformation properties as a one-vector. In contrast, all the "spinor" labels are considered as having only scalar transformation properties. The bispinors ψ_a now transform as scalars. To emphasize their new properties and that they still have a collective reality as a four-tuple of functions we term it a "spinplet." The mixed objects γ^μ_{ab} we consider a vector object with extra labels and, by analogy, label it a "vectorplet."

There are some surprising implications of this. The equations are unchanged but the transformation properties are now different. Since the γ^μ_{ab}'s can vary with position, we expect a much larger equivalence class of electron-gravity field pairs, $\{\psi, \gamma\}$, that correspond to the same underlying reality. We can boost the system by $\Lambda^\mu_\alpha\gamma^\alpha$. This gives the same ψ_a fields at every point but the physically measurable j^ν currents are altered. Of course we still have the traditionally boosted solutions $S(\Lambda)\psi^{(0)}(\Lambda x)$ that have this same current so we have a degeneracy in the pairs $(\Lambda\gamma, \psi^{(0)})$ and $e^{i\phi}(\gamma, S(\Lambda)\psi^{(0)})$ and all other states with the same current and net phase. This is not the result of a discrepancy in the active vs. passive coordinate transformations we observe in a fixed representation but an additional degeneracy in the equivalent physical descriptions. We have only used the current j^μ to distinguish states and we expect that there will be some other conserved quantities, like stress-energy, that will physically subdivide this set into distinct equivalence classes. Since there are so many degrees of freedom in the set of $\gamma^\mu_{ab}(x)$'s we anticipate that the set is still significantly enlarged.

4 Reality and gauge

The AB effect gives a simple example of how the "reality" of an electron is not sufficiently described by the wavefunction of the electron itself. In this case, the current is a function of both ψ and A as $J = i\hbar\nabla\psi + eA$. This construction is useful in sorting out various apparent contradictions in electromagnetism. If we want to investigate the radiation reaction or questions of "hidden momentum" [14, 15] one can build a packet that spreads slowly compared to the effects of external fields and see how the self field and lags contribute to the actual motion. The power of it is that there is no ambiguity in the gauge as for a hodge-podge lagrangian like $\frac{1}{2}mv^2 + jA - \frac{1}{4}FF$ [16] because the physical current of a packet is the gauge invariant J not the naive $j = mv$. The AB effect seems like a topological effect because it is viewed through the lens of ψ being the pure descriptor of the reality of the electron and as a stationary effect. In driving a solenoidal current to create a circulating A field we accelerate J with a transient circulating E field. Part of the current is made up of the phase gradient of ψ and part from A itself. The field and the acceleration moves outwards from the current source at the speed of light and the resulting equilibrated current becomes a function of the final magnetic flux. This circulating current must gain all of its curl from A. The ψ can only contribute to an irrotational flow so general charge packet motion requires a contribution from A. This suggests we might generally want a more nuanced distinction of particle reality than merely a function of each individual field in a lagrangian that has been nominally assigned to the particle type alone.

In flat space without gravity or interactions, we can consider packets of fields that are widely separated based on type. These can then evolve separately and the type of field and the reality implied by it are synonymous. There can still be some gauge freedom but the packets and any interesting properties

that one might observe are contained in the same support. The observables are, at best, the gauge invariant properties such as stress-energy or current. Allowing interactions, this reality gets complicated in two ways. Firstly, the conserved currents may now involve aspects of more than one kind of field and second, there are now constraints that must be obeyed. These are generally defined by elliptic PDEs such as $\nabla \cdot E = \rho$ that are propagated by the dynamic equations.*

If we now include gravity in the form of a γ_μ field that has some gauge freedom that mixes with the reality of the wavefuction ψ then we cannot make the above separation. The gravitational field is everywhere so no isolation of packets is possible. The reality of the electron is now a function of ψ and any γ-like fields that have global extent. This is in contrast with the case where the gravitational information is completely specified in the $g^{\mu\nu}$ field. Since this has no gauge freedom beyond that of coordinate changes, the packet motion of a wavefunction is affected by it yet the reality of the electron is still entirely determined by the values of ψ in the packet itself.

For the case where multiple fields determine a single reality, when is it really viable to call one set of quantities the "electron current" versus some combination of quantities that strictly depend on multiple types of fields? In the case of the Dirac and electromagnetic field (in flat space with constant γ matrices), the density of the field is only a function of ψ so that we have at least one component of the 4-current that is entirely specified by the wavefunction. This allows us a uniquely associate j^0 with the electron field ψ and so call it the "electron-density." The stress-energy terms similarly have T^{00} as a simple function of ψ alone. If every conserved quantity can be associated this way, we have a well-defined mapping between the fields and conserved quantities. If we are interested in more exotic lagrangians than can be formed by the "minimal" prescriptions from the free quadratic cases, we will need to be mindful of the possibility that the currents may not necessarily be so associated with one particular field.

Although this discussion may feel somewhat pedantic, it is important to make this distinction and not get trapped in the vague lore that sometimes accompanies discussions in physics. For example, it is often said that we must have "manifestly invariant" lagrangians to get relativistically consistent results. This is not true not only in the obvious sense that they can be rearranged in a nonobvious invariant form. One can conceivably write down a set of fields that gives a class of solutions whereby the degrees of freedom and invariance is with respect to the observers built of other physical fields. Here we can imagine inducing a set of "physical coordinates" based on local packets of long lasting separated objects that define a grid. With the right time evolution parameterization, we would expect the form of the equations to be invariant with respect to such a coordinate set. The overall class of equivalent solutions should allow for local field changes that induce independent observable current changes with the appropriate degrees of freedom for the observed dynamic freedom of the system. In general, we only need observers to see the world with such symmetry (such as Lorentz) but it need not hold with respect to the coordinates. As long as the constituent fields of the observers and the external reality "covary" together, then the observers see exactly the same thing. Allowing such dynamics can enlarge the equivalence classes at the cost of a more complicated relationship between coordinates and observable reality.

Generally we seek a quadratic free field lagrangian and then gauge and Lorentz invariant couplings between them. The Dirac lagrangian is usually presented in the superficially symmetric form

$$\mathcal{L}_D = i\bar{\psi}\gamma^\mu\partial_\mu\psi - m\bar{\psi}\psi. \tag{5}$$

The appearance of the γ^0 is displeasing if we are to interpret the μ indices as spacetime indices. This particular form is often considered important because it gives a positive definite probability density. In an "emergent" approach to quantum theory where the probabilities are defined by the evolution equations in a deterministic fashion, this is not important. Probability will automatically be conserved by the normalization over the resulting paths that bifurcate the histories of recording devices and observers as indexed by the delocalized particle's coordinates [7] regardless of whether there is a "nice" operator that describes it. More importantly, we need the eom of ψ and ψ^* to be consistent. This dictates that the γ^0 appear in this expression. By using a representation where $\gamma^0\gamma^\mu\gamma^0 = \gamma^\mu$ the variations of the action give equivalent equations of motion.

To achieve a lagrangian that is manifestly invariant using this "vector-plet" interpretation we introduce an auxiliary field ϕ that, in flat space, can be chosen to be $\psi^*\gamma^0$. For the usual Dirac equation this condition is propagated. One should wonder if this will give a true isomorphism with physical results. We are interested in the propagation of conserved quantities as mass, charge... and some local phase information. This brings us to a subtle point. Even in nonrelativistic quantum mechanics, the "reality" of interacting particles is not completely given by the corresponding fields themselves. This is most clearly observed in the AB effect. Often this is viewed as an important example of topology and gauge in

*This is purely a classical theory of delocalized fields so we do not have the problem of "self-energy" or the "particle not feeling its own fields." In the many body case, the fields presumably are made of many constituent ones with only the "center of mass" motion as visible to us. This allows us to have a wavefunction of a charged particle that does not spread under the influence of the field generated by it, as in the classical particle case [15]. However, the self force and momentum are subtle concepts in that such a composite charge must have both m_{bare} and m_{em} components. Only m_{bare} is localized and m_{em} is spread over the range the static fields. The contribution to the electromagnetic momentum in $Ma = (m_{bare} + m_{em})a = F_{ext}$ in the force law is actually provided by a self field of the radiation field traversing the support of the charge.

physics. It is more simply understood as an expression of the electron current being not simply a function of the electron wavefunction alone. A similar property is observed in the London skin depth in superconductors. The only way an electron current can obtain rotational flow is through the vector field $\vec{A}$ or through the appearance of discrete vortices. The moral here is that angular momentum, among other conserved quantities, is defined by a collective set of fields so it makes no sense to associate with one particular particle. "Spin" is now a kind of angular momentum that exists through the collective local reality of this new vector-plet graviton and two fermion spinplet fields. By abandoning this usual concept of a spinor we will obtain an isomorphic theory that has significant generalizations.

5 Bilinear modification

To resolve the complications arising from the hidden γ^0 in the usual Dirac lagrangian, let us replace $\bar{\psi}$ with an associated yet independent field ϕ and see when it evolves in a consistent fashion when we simplify to the Dirac representation. Consider the Dirac-limiting lagrangian density we can choose using only the complex valued ψ, ϕ and γ^α (with $g^{\mu\nu}$ an implicit function of it) is of the form

$$\mathcal{L} = i\left(\phi_a \gamma^\mu_{ab} \partial_\mu \psi_b - \partial_\mu \phi_a \gamma^\mu_{ab} \psi_b\right) - 2m\phi_a\psi_a. \tag{6}$$

For constant γ's chosen to be the Dirac representation, then variation $\delta\phi$ yields $i\gamma^\mu\partial_\mu\psi - m\psi = 0$. Variation by $\delta\psi$ yields $-i(\partial\phi)\gamma^\mu - m\phi = 0$. If we choose $\phi_a = \gamma^0_{ab}\psi^*_b$ then this is equivalent to the Dirac equation solution for ϕ.

When we consider the gauge equivalent states this introduces some additional considerations. For example, if the support of ψ and ϕ are disjoint then there is no net mass or current density. Such a state is evidently a vacuum despite the nontrivial values of the functions and evolution equations. Here we see that our notions of the physical meaning we attach to functions as describing the reality of a particle is less trivial than usual.

So far we have not explicitly included any measure or metric and the action of $\nabla_\mu\gamma^\nu$ is ambiguous without it. We can make formal definitions of these by using eqn. 4 as a guide. The pair of functions,

$$\left.\begin{aligned} g^{\mu\nu} &= -\frac{1}{4}\,\mathrm{Tr}_{ac}\gamma^{(\mu}_{ab}\gamma^{\nu)}_{bc} \\ g_{\mu\nu} &= \mathrm{Inv}\left(-\frac{1}{4}\,\mathrm{Tr}_{ac}\gamma^{(\mu}_{ab}\gamma^{\nu)}_{bc}\right) \end{aligned}\right\} \tag{7}$$

to define the metric in terms of γ are evidently complicated when explicitly constructed but they do give us trial definitions for $g^{\mu\nu}(\gamma)$ and its inverse in terms of γ^μ that can specify a completely general metric field. Another possible objections is that the form of γ^μ with indices raised as a contravariant object is opposite that of the covariant form that A_μ enters the lagrangian especially the interaction terms $q\bar{\psi}\gamma^\mu A_\mu\psi$ which gives us pause when considering the possibility of treating γ^μ and A_μ as analogous fields where no a priori metric exists.

Since we are interested in a theory that includes electrons, positrons, photons and gravity with the electromagnetic and gravitational fields on an equivalent footing we will will need to make a further modification. It will be convenient to let the natural form of γ be a lowered index object γ_μ and introduce a contravariant sister field λ^ν that generates $g^{\mu\nu}$ in the same fashion that γ_μ generates $g_{\mu\nu}$. It is not automatic that these be inverse functions despite the suggestive notation but we will show that they do so in sufficiently low energy cases for a particular lagrangian. We expect the following relations to be able hold in the flat space limit

$$\left.\begin{aligned} g^{\mu\nu}\delta_{ac} &= -\frac{1}{2}\{\lambda^\mu, \lambda^\nu\} = -\lambda^{(\mu}, \lambda^{\nu)} \\ g_{\mu\nu}\delta_{ac} &= -\frac{1}{2}\{\gamma_\mu, \gamma_\nu\} = -\gamma_{(\mu}, \gamma_{\nu)} \end{aligned}\right\}. \tag{8}$$

It is very important to distinguish between this case, which arises in deriving the Klein-Gordon results that demonstrate causality for the Dirac components and the traced result. The arbitrary metric field $g_{\mu\nu}(x) = -\frac{1}{8}\mathrm{Tr}\{\gamma_\mu(x), \gamma_\nu(x)\}$ can be defined in terms of $\gamma^\mu_{ab}(x)$'s but the untraced result for $g_{\mu\nu}(x)\delta_{ac}$ cannot. This will be central to what follows.

We like to have the metric appear explicitly in all the terms of the lagrangian for the reason it gives us something to vary in obtaining a conservation law for stress-energy. One way to do this is is to use the lagrangian

$$\mathcal{L}_e = i\left(g^{\mu\nu}\phi_a\gamma_{\mu:ab}\partial_\nu\psi_b - g^{\mu\nu}(\partial_\mu\phi_a)\gamma_{\nu:ab}\psi_b\right) - 2m\phi_a\psi_a, \tag{9}$$

where the colon separates spacetime from scalar indices. We define $g^{\mu\nu} = -\frac{1}{4}\mathrm{Tr}\lambda^{(\mu}, \lambda^{\nu)}$. The evolution equations are given by the variations $\delta\phi$

$$\left.\begin{aligned} &i\left(g^{\mu\nu}\gamma_{\mu:ab}\partial_\nu\psi_b + g^{\mu\nu}\nabla_\mu(\gamma_{\nu:ab}\psi_b)\right) - 2m\psi_a = 0 \\ &i g^{\mu\nu}\gamma_{\mu:ab}\partial_\nu\psi_b + \frac{1}{2}\,i g^{\mu\nu}(\nabla_\mu\gamma_{\nu:ab})\psi_b - m\psi_a = 0 \end{aligned}\right\} \tag{10}$$

and $\delta\psi$

$$i g^{\mu\nu}(\nabla_\mu\phi_b)\gamma_{\nu:ba} + \frac{1}{2}\,i g^{\mu\nu}\phi_b(\nabla_\mu\gamma_{\nu:ba}) + m\phi_a = 0 \tag{11}$$

so that ϕ evolves as ψ with $m \to -m$ and $\gamma \to \gamma^{\mathrm{T}}$.*

Since we are about to determine the motion of the conserved gauge invariant stress energy associated with the fields and it is deeply connected with geometry, we make a brief segue to derive this conserved quantity. A general action contains both a lagrangian and a measure that can be related to the metric

$$S = \int d^4x\,\mathcal{L}\sqrt{-g_{\cdot\cdot}}\,. \tag{12}$$

*Note that this does not mean that the energy of the rest field is m ($c = 1$). The energy is a function of the triple of fields (ψ, ϕ, γ) as we see next.

Incorporating general relativity, the lagrangian density is generally written

$$\mathcal{L} = \frac{1}{2\varkappa} R(g) + \mathcal{L}_{\text{fields}}, \tag{13}$$

where $\varkappa = 8\pi G$ and the first term gives the Riemann curvature and the second gives the field terms that do not depend only on the metric. The conservation laws arise from varying the metric $\delta g^{\mu\nu}$ from which we obtain

$$G^{\mu\nu} = 8\pi G T^{\mu\nu} = -\varkappa \frac{-2}{\sqrt{-g^{\cdot\cdot}})^{-1}} \frac{\delta \mathcal{L}_{\text{fields}}(\sqrt{-g^{\cdot\cdot}})^{-1}}{\delta g^{\mu\nu}}. \tag{14}$$

Since $\nabla_\mu G^{\mu\nu} = 0$ as an identity we have $\nabla_\mu T^{\mu\nu} = 0$. This is a local conservation law. To obtain a global one we need a spacetime with persistent Killing vectors corresponding to continuous symmetries. The action of gravity typically destroys these as global conservation laws, however, if $G \to 0$ *and* the initial data is chosen to be flat then these exist and persist so we have the usual global symmetric conservation laws. This justifies this as a general method of deriving conservation laws with symmetric stress-energy tensors for fields on flat space when all the fields present are tensorial. Of course, we expect any such conservation law to correspond to a symmetry. In this case, we can vary the coordinates locally and this leaves the quantity $\mathcal{L}\sqrt{g_{\cdot\cdot}}$ invariant. Since all the derivatives are covariant, we can replace a passive coordinate change on an open set with an active transformation of the metric field $g^{\mu\nu}$. Varying $g^{\mu\nu}$ is therefore equivalent to a general small variation in the local coordinates. Of course, we are considering these as fields on a flat background so that they change in a rather simple fashion relative to the coordinate changes and we should include a coordinate measure $\sqrt{-\eta}$ and this underlying space generates full set of ten conserved quantities (see §3).

The (symmetric) stress tensor is usually defined by*

$$\begin{aligned} T_{\mu\nu} = & -\frac{2}{(\sqrt{-g^{\cdot\cdot}})^{-1}} \frac{\delta\left(\mathcal{L}_{\text{fields}}\left(\sqrt{-g^{\cdot\cdot}}\right)^{-1}\right)}{\delta g^{\mu\nu}} \\ = & -2\frac{\delta(\mathcal{L}_{\text{fields}})}{\delta g^{\mu\nu}} + g_{\mu\nu}\mathcal{L}_{\text{fields}} \\ = & \; 2i\left(\phi_a \gamma_{(\mu:ab}\partial_{\nu)}\psi_b - (\partial_{(\mu}\phi_a)\gamma_{\nu):ab}\psi_b\right) \\ & + g_{\mu\nu}\Big[\, i\left(g^{\alpha\beta}\phi_a\gamma_{\alpha:ab}\partial_\beta\psi_b\right. \\ & \left. - g^{\alpha\beta}(\partial_\alpha\phi_a)\gamma_{\beta:ab}\psi_b\right) - 2m\phi_a\psi_a\Big] \\ = & \; 2i\left(\phi_a\gamma_{(\mu:ab}\partial_{\nu)}\psi_b - [\partial_{(\mu}\phi_a]\gamma_{\nu):ab}\psi_b\right), \end{aligned} \tag{15}$$

where we have varied with respect to $g^{\mu\nu}$ and assumed γ_μ is a field independent of it in anticipation of $g^{\mu\nu}$ being a function of λ^μ.

*Here we make the choice of taking the determinant with respect to the "contravariant" metric $g(\gamma^\mu)$ in anticipation of later work. This explains the power -1 this expression.

We can similarly examine the continuous symmetry given by the globally constant phase changes $\psi \to e^{i\theta}\psi$ and $\phi \to e^{-i\theta}\phi$ to get the conserved current

$$j^\nu = 2i g^{\mu\nu}\phi_a\gamma_{\mu:ab}\psi_b \tag{16}$$

so that $\nabla_\nu j^\nu = 0$. Here we see this current also depends on all three fields so that the vanishing of any one of them on a region necessitates the entirety of the physical reality vanish.

We will now consider the implications of packet motion given these two conservation laws. Firstly, when we say "packet" we are not referring to a packet of localized ψ or ϕ as much as a localized region where the reality associated with these fields through $T_{\mu\nu}$ and j^μ are nonzero. Let us also consider a packet that is devoid of internal stress and rotation and where the pressure is minimal. For such a packet with sufficiently uniform interior we can average over the current to give $\langle j^\mu\rangle \approx m v^\mu$ where m^2 is the averaged $g_{\mu\nu}j^\mu j^\nu$ density and, assuming the packet preserves its structure as it moves, v^i is the local coordinate velocity of the packet. We can then define v^0 by the relation $g_{\mu\nu}v^\mu v^\nu = -1$. The conservation law tells us that ρ is conserved. v^μ is well defined to the extent packet motion is so.

From $\langle T^{\mu 0}\rangle$ we can define a velocity u that carries the energy in a localized packet so that $\langle T^{\mu 0}\rangle \approx m' u^{(\mu}u^{0)}$. Since a vanishing of the current on a region implies vanishing of stress-energy as well we have that $v = u$ and that $\langle T^{\mu 0}\rangle \approx m'^{(\mu}v^{0)} = \alpha m^{(\mu}v^{0)}$. Since there are no internal stresses, $\langle T^{\mu\nu}\rangle \approx \alpha m v^\mu v^\nu$. By combining these expressions we derive that these "macroscopic" variables are

$$\left.\begin{aligned} v^\nu &= \frac{\langle T^{\mu\nu}\rangle}{\alpha\langle j^\mu\rangle} \\ m &= \alpha^2 \frac{\langle j^\mu\rangle\langle j^\nu\rangle}{\langle T^{\mu\nu}\rangle} \end{aligned}\right\}, \tag{17}$$

where these are actually several equations (repeated indices are not summed) that are all equal by the conditions above.

Now consider the parcel averaged stress-energy conservation law. Applying $\nabla_\mu j^\mu = 0$ we have

$$\begin{aligned} \langle \nabla_\mu T^{\mu\nu}\rangle &= \langle \nabla_\mu (j^\mu v^\nu)\rangle \\ &= \langle (\nabla_\mu j^\mu)v^\nu + j^\mu \nabla_\mu v^\nu\rangle \\ &= m' \langle \nabla_v v\rangle = 0, \end{aligned} \tag{18}$$

which indicates the gauge invariant aspects (i.e. the reality) of the parcel follows geodesic motion. This is not entirely surprising given that it is known that the conservation laws generally dictate that classical particles follow geodesics though the proofs are generally quite difficult [18]. The "geodesics" here are generally curved paths in our underlying coordinate space but appear as geodesics in the geometry most apparent to observers.

In the next section for a theory of "lepto-electro-gravity" we have two covariant gauge fields and one contravariant one.

These have trivial transformation laws in the flat background coordinates but we maintain this distinction because it seems more relevant for observers. In this sense we think of it as a "2+1" theory. One contravariant field is always necessary to match the covariant derivatives that must arise in any differential equation. The electron field is described by a (ϕ, ψ) pair of fields that embody its reality with a very large gauge group and the meaning of the reality they describe depends not only on the metric but the covariant gravity field γ_μ. We will see that these have properties that are distinct from the positive energy positrons so we will require another pair of fields for their description. Along the way we will introduce a lagrangian that exists as a purely polynomial expression and removes the need for complicated nonanalytic measures and rational inverse matrix functions.

6 Electro-gravity lagrangian

Here we seek a lagrangian that encompasses electrons, positrons, electromagnetism and gravity and seek to have equations that are polynomial rather than complicated rationals that arise from the operation of taking the inverse of the metric. For this reason we define the function $g : \mathcal{V} \to \mathcal{T}$ where $\mathcal{V}$ is the set of vector-plet objects λ^μ_{ab} and $\gamma_{\mu:ab}$ and $\mathcal{T}$ is the set of corresponding contravariant or covariant 2-tensors $g^{\mu\nu}$ and $g_{\mu\nu}$ respectively. Specifically,

$$g(A, B) = -\frac{1}{8}\,\mathrm{Tr}(AB + BA).$$

We will establish a lagrangian that gives Dirac particle motion in the flat space limit, electromagnetism and a form for GR that gives a simple parallel between the motion of the gravitational fields, γ_ν and the electromagnetic ones A_ν that allows gravity to obtain the nonlinear "geometric" features of GR.

Since we are interested predominantly in positive energy solutions we will need to introduce a separate action term Λ_p for positrons that have positive mass but a reversal of sign of the charge in the coupling. We can write the lagrangian for the covariant gravitational field γ by substitution into the Einstein-Hilbert lagrangian. Alternately, we can choose it to have a similar form of the action Λ'_g as the other vector potential Λ_A and the coupling terms $\Lambda_{e\lambda A}$, $\Lambda_{p\lambda A}$ will involve both the contravariant gravitational field λ and the vector potential. Finally, there will need to be some way for the covariant and contravariant gravitational fields to relate to one another. This will be accomplished by a Higgs-like interaction term Λ_c. The general action is then defined as

$$\begin{aligned} S &= \int d^4x \mathcal{L}\sqrt{-g} = \int d^4x\,\Lambda \\ &= \int d^4x\,(\Lambda_g + \Lambda_\lambda + \Lambda_A + \Lambda_e + \Lambda_p \\ &\qquad + \Lambda_{e\lambda A} + \Lambda_{p\lambda A} + \Lambda_c), \end{aligned} \tag{19}$$

where we will define Λ_λ shortly.

Since the measure is a nonanalytic function of the metric but this is not retained in the usual equations of motion. We will find that this is also true here. For reasons as above we use the λ fields in defining the measure.

The electron part of the action is given by the substitutions

$$\begin{aligned} \Lambda_e &= \mathcal{L}_e\left(\sqrt{g^{\cdot\cdot}(\lambda)}\right)^{-1} \\ &= \Big[\, i\left(g^{\mu\nu}(\lambda)\phi_a\gamma_{\mu:ab}\nabla_\nu\psi_b - g^{\mu\nu}(\lambda)(\nabla_\mu\phi_a)\gamma_{\nu:ab}\psi_b\right) \\ &\quad - 2m\phi_a\psi_a \,\Big]\left(\sqrt{g^{\cdot\cdot}(\lambda)}\right)^{-1} \end{aligned} \tag{20}$$

where we have, harmlessly, replaced the ordinary with covariant derivatives since the act on spinplet objects which are essentially scalars. Variation with the measure present allows their action on higher tensors to give the appropriate covariant connection terms. This is one indication of how the physics itself can generate the geometric aspects of gravity rather than imposing it by fiat in the formulation of the theory's foundations.

The positron portions of the lagrangian is of the same form as Λ_e but with a different pair of fields $\tilde\phi, \tilde\psi$. The distinction comes in the form of the interaction terms. The usual minimal coupling prescription gives

$$\left.\begin{aligned} \Lambda_{e\lambda A} &= -\,q\,\phi_a\lambda^\mu_{ab}A_\mu\psi_b \\ \Lambda_{p\lambda A} &= +\,q\,\tilde\phi_a\lambda^\mu_{ab}A_\mu\tilde\psi_b \end{aligned}\right\}. \tag{21}$$

It is only the sign of the charge in the interaction terms that distinguishes positrons from electrons and it only appears in the couplings.

The gravitational part of the action can be defined by a simple extension of the Einstein-Hilbert action

$$\Lambda_g = \frac{1}{2\varkappa}\,R\left(g_{\mu\nu}(\gamma), g^{\mu\nu}(\lambda)\right)\left(\sqrt{g^{\cdot\cdot}(\lambda)}\right)^{-1}. \tag{22}$$

R is defined in terms of $g_{\mu\nu}(\gamma)$, $g^{\mu\nu}(\lambda)$ and the connections implicit in the expression are defined by

$$\Gamma^\alpha_{\mu\nu} = \frac{1}{2}\,g^{\alpha\sigma}(\lambda)\left(g_{\mu\sigma,\nu}(\gamma) + g_{\sigma\nu,\mu}(\gamma) - g_{\mu\nu,\sigma}(\gamma)\right) \tag{23}$$

and their derivatives. We expect that some induced constraints force $g(\gamma)g(\lambda) = \delta$. To have this done as a result of field interactions we exploit a "Higgs-ish" mechanism with the coupling term

$$\Lambda_c = M\left|\, g_{\mu\nu}(\gamma)\, g^{\nu\rho}(\lambda) - \delta^\rho_\mu\right|^2 \tag{24}$$

for a sufficiently large mass M. When the energies in the other terms are much smaller this drives the relation between γ and λ to hold so that the solutions become "geometric." Specifically, while it is easy to enforce causality if all evolution fields obey some equation such as $g^{\mu\nu}\partial_\mu\partial_\nu\phi + \ldots$ where $g^{\mu\nu}$ is a metric with signature +2, the geometric case indicates that slowly spreading packets in regions of slowly varying spacetime move along geodesics. When such a relation holds

our lagrangian has a form that can be interpreted as coordinate invariant in that the derivatives act on the tensor fields with covariant derivatives with the Γs induced by the metric $g_{\mu\nu} = -4^{-1}\mathrm{Tr}\gamma_{(\mu}\gamma_{\nu)}$. In the next section we will see that we can also interpret the system to live on a flat background and derive global conservation laws.

The other gauge fields all come from lagrangians that have electromagnetic form $F^{\mu\nu}F_{\mu\nu}$ where $F_{\mu\nu} = \partial_\mu A_\nu - \partial_\nu A_\mu$. Specifically,

$$\begin{aligned}\Lambda_A = \; & g^{\mu\alpha}(\lambda)g^{\nu\beta}(\lambda)(\partial_\mu A_\nu - \partial_\nu A_\mu) \\ & \times (\partial_\alpha A_\beta - \partial_\beta A_\alpha)\left(\sqrt{-g^{\cdot\cdot}(\lambda)}\right)^{-1}.\end{aligned} \tag{25}$$

It is not necessary to use covariant derivatives here since antisymmetry cancels them. For example, we model the action contribution from the "dual field" λ as

$$\begin{aligned}\Lambda_\lambda = \; & \epsilon\, g^{\mu\alpha}(\lambda)\, g^{\nu\beta}(\lambda)\,\mathrm{Tr}(\partial_\mu\tilde{\lambda}_\nu - \partial_\nu\tilde{\lambda}_\mu) \\ & \times (\partial_\alpha\tilde{\lambda}_\beta - \partial_\beta\tilde{\lambda}_\alpha)\left(\sqrt{-g(\lambda)}\right)^{-1},\end{aligned} \tag{26}$$

where $\tilde{\lambda}_\mu = g_{\mu\nu}(\gamma)\lambda^\nu$.* where we have chosen the constant ϵ to be small so that the dynamics can be dominated by γ and the constraints induced by the Higgs-like term.

For a function $F_\mu(g_{\mu\nu}(\gamma))$ the variation under $\delta\gamma_\nu$ gives

$$\delta F_\mu = \frac{\delta F}{\delta g_{\mu\nu}}\,\delta\gamma_\nu \tag{27}$$

and similarly for $\delta\lambda$. Variation of Λ_g by $\delta\lambda$ gives

$$\frac{1}{2\varkappa}\left(R_{\mu\nu} - \frac{1}{2}\,R g_{\mu\nu}\right)\delta\lambda^\nu \tag{28}$$

or

$$G_{\mu\nu}\delta\lambda^\nu = \varkappa T_{\mu\nu}\delta\lambda^\nu, \tag{29}$$

where $T_{\mu\nu}$ is the stress-energy tensor for all the actions terms other that Λ_g. We have implicitly assumed that we are in a low enough energy regime and the initial data includes no "waves" of λ so that the contributions of Λ_λ can be ignored. Since the γ's contain gauge freedom that is independent of coordinate changes so that we can choose any γ_μ that give the same $g_{\mu\nu}(\gamma)$ field, this requires

$$G_{\mu\nu} = \varkappa T_{\mu\nu}\,. \tag{30}$$

7 Conservation laws

We can argue the whole structure exists on a flat background though this is just a convenient artifice among many. It is however a very convenient one. The appearance of geometric evolution via the additional Γ factors that make the derivatives seem "covariant" with respect to some induced geometry of these fields is an emergent byproduct of the kind of couplings present. It should be noted that these $\Gamma^\alpha_{\beta\gamma}$ factors are actual η-tensors on the background space instead of affine connections. Of course, we still need to know if our equations can be evolved for arbitrary times using this point of view. Some discussion of this, especially in the case of black hole formation is given in [12]. For now we assume that this is unlimited however, although other methods have attempted to justify working on a flat background [17] it is a delicate process to have this make sense as gravitational collapse ensues due to the trend of the equations to become ill conditioned here. One should not be overly comfortable with formalism in this case. A method to handle evolution on the large regions of nearly degenerate metric using conservation laws is proposed in [12]

The flat background has a natural set of Killing vectors that give global conservation laws. To elucidate this consider the lagrangian written in terms of ordinary derivatives and make the modification by defining $g(\gamma) = h(\gamma) \circ \eta$

$$\Lambda = \mathcal{L}\sqrt{-g} \to \Lambda\sqrt{h}\sqrt{-\eta}\,. \tag{31}$$

All actions on tensors induced by η-background coordinate transformations are of the form

$$\partial_\mu A^\alpha \to \nabla_\mu(\eta)A^\alpha = \partial_\mu A^\alpha - \Gamma^\alpha_{\mu\nu}(\eta)A^\nu \tag{32}$$

and so forth, where η is a metric (in any coordiates) that can be varied about the flat space case. Any covariant derivatives $\nabla_\mu(g)$ in terms of the metric induced connections are reinterpreted as formal couplings through $\Gamma(g)$ and the ∂_μ are converted by this prescription. We see a problem with eqn. 31 is that it is not invariant under general η-space coordinate transformations due to the factor $\sqrt{-g}$. It is, however, invariant under the isometries of flat spacetime that we use to generate global conservation laws.

Since the flat space contains a full set of ten Killing vectors we have a set of conserved global quantities that now includes the gravitational fields of the form

$$\partial_\mu T'^{\mu\nu} = 0 \tag{33}$$

with the Killing (co)vector fields $p_\nu = \hat{\omega}_\nu$, $M_{ijk} = \epsilon_{ijk}x_j\hat{\omega}_k$ and $b_i = x_0\hat{\omega}_i + x_i\hat{\omega}_0$. The globally conserved quantities in these coordinates are

$$\left.\begin{aligned} P^\nu &= \int d^3x\; p_\mu T'^{\mu\nu} \\ J^i &= \int d^3x\; M^i_{jk}T'^{ij} \\ C^j &= \int d^3x\; b_i T'^{ij} \end{aligned}\right\}. \tag{34}$$

8 Conclusions

The notions of invariance from differential geometry and invariance theory are imported into physics in a fashion that ranges from formal to ad hoc. Surprisingly, they have not

*We distinguish this field with a tilde because of the earlier convention that these are all tensor indices under the underlying flat space metric so that "lowering" an index with g must be new field to not be ambiguous.

been reconsidered from the more physical point of view that all configurations that are indistinguishable to observers built of the fields themselves should form the most general equivalence class of systems. This enlarged meaning of "gauge" requires some underlying structure. We have shown that many of the usual objections to a flat background can be overcome and that this allows the fields to have very simple transformation laws and a large set of conservation laws with respect to this flat background. The observers can then perceive a curved space with all its mathematical complexity as emerging from the nature of nonlinear and multilinear coupling among fields. Importantly, there is a classical lagrangian with a Higgs-like term that causes there to be such a strongly nonlinear and geometric theory of gravity to arise from the perspective of such observers at low energy.

An interesting by-product of this approach is that the apparent co and contravariant properties of the fields in the "physical coordinates" induced by objects for the observers obtain their transformation properties by the equations of motion not by a by-fiat assignment. This is another aspect of "geometry" that is determined by the physics itself. At high enough energies we expect this geometric association to fail and nonmetric features to become evident to the observers. In this case the induced constraints fail and evolution becomes potentially more difficult. One suggestion is that such a situation allows inconsistent light cone structures to be induced for different fields and that some intersection of these gives the proper causal structure for these fields when they are interacting.

The bilinear extension of the Dirac equation and promotion of the γ matrices to dynamical fields introduced a number of concerns related to positive definiteness of energy and probability and causality of the equations of motion. The latter has been verified for packets using gauge invariant functions of the fields. The former is seen to be not essential since these quantities, while rigidly conserved, are not necessarily the physical ones an observer perceives since they are derived from background coordinate symmetries. The probability function may be a nontrivial function of the fields in the case of gravity but normalization is assured in any theory of emergent measurement such as decoherence.

There are undoubtably many inequivalent such theories with the same low energy limit so we have presented only one of probably many such solutions. From here it is unclear how to extend this classical theory to a quantum one. The couplings are such that they determine the local notion of causality and it is not clear when or how well a perturbative scheme, which is generally built on free fields solutions, will work in the many body case. This is a direction for future work.

Submitted on November 4, 2014 / Accepted on November 24, 2014

References

1. Marquet P. Lichnierowicz's theory of spinors in General Relativity: the Zelmanov approach. *The Abraham Zelmanov Journal*, 2012 v. 5, 117–133.
2. Bjorken J.D., Drell S.D. Relativistic Quantum Mechanics and Relativistic Quantum Fields. McGraw-Hill, 1965.
3. Peskin M.E. and Schroeder D.V. An Introduction to Quantum Field Theory, Ed. Westview, Boulder, 1995.
4. Weinberg S. The Quantum Theory of Fields. Volumes I and II. Cambridge University Press, Cambridge, 1995.
5. Hestenes D. A unified language for Mathematics and Physics & Clifford algebra and the interpretation of quantum mechanics. In: Clifford Algebras and Their Applications in Mathematics and Physics. J.S.R. Chisholm & A.K. Common, eds., Reidel, Dordrecht, 1986, pp. 1–23 and pp. 321–346.
6. Chafin C. Automorphism Induced Nonlocal Conservation Laws. math-ph/arXiv: 1407.6782.
7. Chafin C. The Quantum State of Classical Matter I: Solids and Measurements. quant-ph/arXiv:1308.2305.
8. Mach E. The Science of Mechanics; a Critical and Historical Account of its Development. LaSalle, IL: Open Court Pub. Co., 1960.
9. Einstein A. On the electrodynamics of moving bodies. *Annalen der Physik*, 1905, v. 17, 891–921.
10. Misner C.W., Thorne K.S. and Wheeler J.A. Gravitation. Freeman, 1973.
11. Oppenheimer J.R. and Snyder H. On Continued Gravitational Contraction. *Physical Review*, 1939, v. 56(5), 455–459.
12. Chafin C. Globally Causal Solutions for Gravitational Collapse. gr-qc/arXiv:1402.1524.
13. Schweber S.S. An Introduction to Relativistic Quantum Field Theory. Harper and Row, 1962.
14. Jackson J. D. Classical Electrodynamics. Wiley, New York, 1962.
15. Rohrlich F. Classical Charged Particles. World Scientific, 2007.
16. Landau L. and Lifshitz E. M. The Classical Theory of Fields. Pergamon, Oxford, 1979.
17. Lasenby A. Doran C. and Gull S. Gravity, gauge theories and geometric algebra. *Philosophical Transactions of the Royal Society*, London, 1998, v. 356, 487.
18. Ehlers J. and Geroch R. Equation of motion of small bodies in relativity. *Annals of Physics*, 2004, v. 309, 232–239.

LETTERS TO PROGRESS IN PHYSICS

Bio-Precursors of Earthquakes and Their Possible Mechanism

Takhir R. Akhmedov

333 S. Webster Ave, Suite 4, Norman, OK 73069. E-mail: TakhirAkhmedov@yandex.com

People observed anomalous behavior of animals prior to powerful earthquakes since ancient times. Only in mid-20th century scientific community got interested in understanding what makes some animals "sensitive" to approaching earthquakes. Questions were raised of whether we are truly observing anomalous behavior or just interpreting it as such after the earthquake. Do animals actually "feel" the earthquakes? What are the stimuli impacting animal behavior? Scientists looked at chemical composition of ground water, release of some gases, sound booms and even electromagnetic activity as potential stimuli. With no comprehensive and systematic study of animal behavior prior to, during and after powerful earthquakes no plausible hypotheses explaining the sensitivity exist at this point. In this article, we propose a possible mechanism based on gravitational receptor, which each and every animal possess.

Accurate prediction of powerful earthquakes is one of the important problems faced by modern geophysics.

Rikitake (1979) presented extensive research data used for predicting earthquakes and tried to provide theoretical explanation [1]. While existing instrumental and statistical methods of predicting earthquakes allow identification of some patterns of future earthquakes, they do not answer the most important questions — the magnitude of future earthquake and its precise time. Geller (1997) states that "extensive searches have failed to find reliable precursors" [2]. He further notes that "theoretical work suggests that faulting is a non-linear process which is highly sensitive to unmeasurably fine details of the state of the Earth in a large volume, not just in the immediate vicinity of the hypocentre" [2].

Usually powerful earthquakes are accompanied with rapid increase in speed of vertical shift of Earth's crust in epicenter and adjacent areas. For example, after Ashkhabad, Turkmenistan, earthquake (October 5, 1948) as a result of leveling an increase in speed of vertical shift of Earth's crust with a maximum near Ashkhabad was identified. Similar observation made during Tashkent, Uzbekistan, earthquake (April 26, 1966).

Therefore, we can assume, that prior to powerful earthquakes an increase in speed of vertical shift of Earth's crust can be observed.

In recent years scientists got interested in the anomalous behavior of animals prior to powerful earthquakes. Even though anomalous behavior of animals is long known, scientific community only recently started researching this phenomenon. In late 1976, USA hosted the first conference on this subject.

The most important task facing scientists is identification of the physical nature of the processes, which lead to anomalous behavior of animals prior to powerful earthquakes.

Out of four types of forces (electromagnetic, gravitational, strong and weak) only electromagnetic and gravitational forces could be related to the mechanism of sensitivity of bio-precursors of earthquakes. Characteristics of Earth's electromagnetic field experience significant variations, which may impact sensitivity of the mechanism. Therefore, we will not consider electromagnetic force as the main force, which impacts the mechanism of sensitivity of bio-precursors of earthquakes. Let's consider gravitational force as the main force.

It is known that biological objects evolved within constant influence of gravitational field of the Earth. This lead to the creation of apparatus, gravitational receptor, allows biological objects to orient themselves in gravitational field [3]. Gravitational receptor basically consists of two main parts — "proof mass" with a mass m_p, which is capable of moving within the organ and around receptors that react to the changes of position of "proof mass".

One essential peculiarity of gravitational field is its constant presence and our inability to shield against its impact, i.e. all-pervading nature of the field.

One of the main characteristics of the gravitational field is free-fall acceleration g (analogous to the electric field intensity E). With changing characteristics of the field changes the force, which impacts the "proof mass" with the mass m_p. Such changes are possible prior to powerful earthquakes. However, there have not been successful measurements of such changes due to inadequate sensitivity of the instruments.

Biological objects, it seems, are able to react to the speed of changing free-fall acceleration parameter, which results from vertical shift of Earth's crust. If we consider the value of sensitivity of biological objects to such changes as m_p/M, where M is mass of the Earth, then biological objects are able to sense relative changes of the free-fall acceleration resulting from a vertical shift of Earth's crust, numerical value of

which exceeds m_p/M. Evaluations showed that speed of relative changes of free-fall acceleration, resulting from vertical shift of Earth's crust, exceeds maximum sensitivity of gravitational receptors of biological objects.

Thus, we conclude that biological objects, using signals from gravitational receptors, can react to the relative local changes of gravitational field prior to powerful earthquakes.

For experimental test of the proposed mechanism, we would suggest experiments with biological objects used as sensors of characteristics of gravitational field via continuous recording of bioelectric current from gravitational receptor during rapid increase in speed of vertical shift of Earth's crust in active seismic zones.

Submitted on December 1, 2014 / Accepted on December 4, 2014

References

1. Rikitake T. Prediction of Earthquakes. Mir Publishers, Moscow, 1979.
2. Geller R. J. Earthquake prediction: a critical review. *Geophys. J. Int.*, 1997, v. 131(3), 425–450.
3. Vinnikov Ya. A., Gazenko O. G., et al. Gravitational receptor. *Problems of Space Biology*, v. 12, Nauka, Leningrad, 1971.

Astrophysical Clock and Manned Mission to Mars

Takhir R. Akhmedov

333 S. Webster Ave, Suite 4, Norman, OK 73069. E-mail: TakhirAkhmedov@yandex.com

For many years scientists of different countries are engaged in research of biological processes, which have rhythms close to geophysical ones. The main objective of this research was finding the mechanism of time sensor, which leads to these rhythms. In the previous article (Akhmedov T.R. *Progress in Phys.*, 2014, v. 10, issue 1), based on the analysis of the known experimental data obtained from biological objects and in consideration of the original data obtained in Tashkent State University, we came to a conclusion that the time sensor of a biological clock is exogenous in nature. This means that clocks setting rhythms close to geophysical for biological processes exist outside of those biological objects. From this we conclude that there are no biological clocks, but rather there are astrophysical clocks (APhC), which form rhythms with periods close to geophysical within physical, chemical and biological processes.

1 Astrophysical Clocks (APhC)

Let us review the experimental data proving the existence of Astrophysical Clock. For this experiment we put assembled a system, schematics of which is plotted on Fig. 1.

Container (1) with distilled water was placed into the thermostated chamber (2), where stable temperature at $103 \pm 0.1^{\circ}$C was maintained. Water was boiling inside the container (1). The water vapor went through the cooling system (3) and precipitated into the container (4). The mass of the evaporated/precipitated water was measured every 15 min and a set of 4 measurements had been plotted on the Fig. 2 and Fig. 3. The experiments were carried out uninterruptedly by a number of series of 1 to 7 days of duration. In order to thoroughly investigate the rate of water vaporization power supply of the thermostat was carefully stabilized, all containers and tubes and connections were thermally insulated, mass was carefully measured and stability of the temperature was closely monitored. The data coming from the measurements strongly suggested the existence of CR in the physical process of distilled water evaporation from a thermostated container.

Initial experiments were carried out in 1974. During one of experiments it became necessary to obtain a stable flow of water vapor of low intensity (1.4×10^{-5} kg/s). This experimental data had been obtained in 1974 by a group of physicists conducted by Prof. M. A. Asimov. Author of the present article was a responsible head for the experiments.

2 Lunar rhythms

This study rises from my previous article [1], based on the analysis of the known experimental data obtained from biological objects and in consideration of the original data obtained in Tashkent State University. We came to a conclusion therein that the time sensor of a biological clock is exogenous in nature.

Scientific publications, dedicated to research of biological rhythms with periods close to geophysical ones, present much experimental data pointing at the existence of lunar

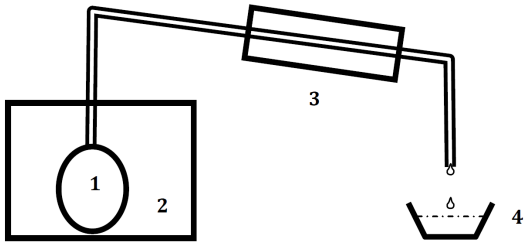

Fig. 1: (1) Container filled with distilled water; (2) Thermostated chamber with inside temperature of $103 \pm 0.1^{\circ}$C; (3) Cooling system; (4) Container where the water condensate was collected.

rhythms in biological processes [2, 3]. In 1974, a research group conducted by M. A. Azimov in Tashkent State University (Uzbekistan) identified lunar rhythms in chemical reaction of vapor conversion of methane at $T = 450^{\circ}$C. It is obvious that at such temperatures we can effectively exclude biological processes.

The stable vapor flow of low intensity was necessary for studying of chemical reaction of vapor conversion of methane. The reaction used in chemical industry to produce hydrogen is described by a formula:

$$CH_4 + 2H_2O \longrightarrow 450^{\circ}C \longrightarrow CO_2 + 4H_2 \,.$$

To investigate time dependence of the reaction speed there were provided stable flows of gaseous CH_4 and water vapor (deviations were $\pm 0.3\%$ and $\pm 3\%$, respectively). The experiment had been carried out for 540 hours in October and November of 1974.

In Fig. 3 the experimental measurements were plotted, y axis shows the fraction of residual methane in the converted dry gas at the output of the reactor.

Composition of the gas at the output was analyzed by the method of gas chromatography. Every 15 min three chromatographs were collected; results of 2-4 hour measurements were averaged and then plotted on the Fig. 3. Results of

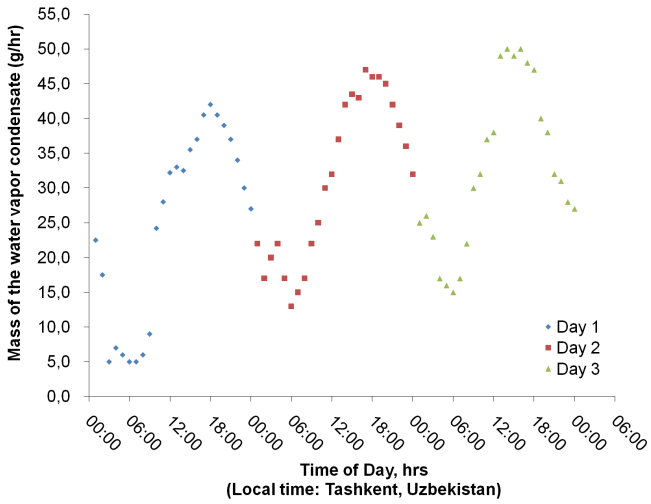

Fig. 2: Circadian periodicity of evaporation of water from a thermostated vessel at 103° (1974).

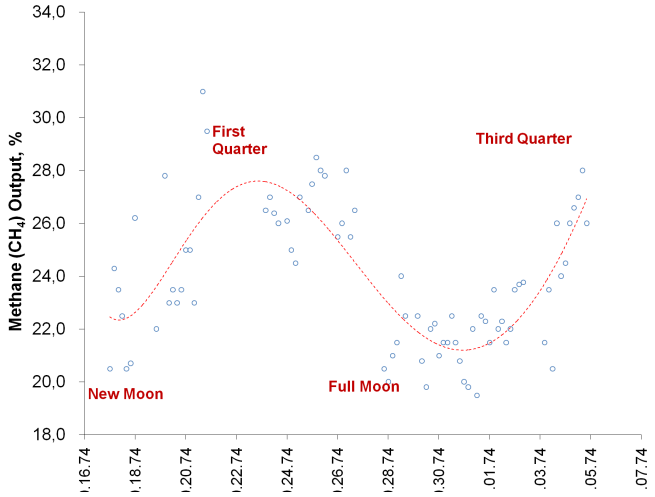

Fig. 3: Concentration of residual CH_4 in % in vapor conversion reaction output.†

these studies indicated on the existence of a lunar rhythm in the chemical reaction of vapor conversion of methane at $T = 450$°C. This temperature is noticeably higher than temperature of any known living organism.

3 Shnoll effect

One more argument in favor of existence of astrophysical clocks (APhC) is Shnoll Effect. It is shown that due to fluctuations, a sequence of discrete values is generated by successive measurement events whatever the type of the process measured. The corresponding histograms have much the same shape at any given time and for processes of a different nature and are very likely to change shape simultaneously for various processes and in widely distant laboratories. For a series of successive histograms, any given one is similar to its nearest neighbors and occurs repeatedly with a period of 24 hours, 27 days, and about 365 days, thus implying that the phenomenon has a very profound cosmophysical (or cosmogenic) origin [4, 5].

Substantial experimental material accumulated by biologists studying rhythms close to geophysical constitutes observations of the hands of astrophysical clock, which sets rhythms for biological processes. The rhythms for these processes are set by external forces.

Thus, from above described experimental data we conclude that rhythms close to geophysical, which occur in physical, chemical and biological processes, exist because of Astrophysical Clock (APhC).

4 How does Astrophysical Clock (APhC) work?

Let's analyze changing of kinetic and potential energy of atoms/molecule on the surface of the Earth. An atom/molecule on the surface of the Earth takes part in following motions:

1. Spinning of the Earth around its own axis with the surface speed $V_1 = 465 \cos\alpha$ m/s, where α is the geographic latitude;
2. Revolving with the Earth around the Sun with a linear speed of $V_2 = 3 \times 10^4$ m/s;
3. Moving with the Solar system around the center of the Galaxy with a linear speed of about $V_3 = 2.5 \times 10^5$ m/s;
4. Moving with the Galaxy from the center of the Universe with a linear speed of about $V_4 = 6 \times 10^5$ m/s.

It's known that total mechanical energy is the sum of kinetic energy E_K and potential energy U:

$$E_{\text{total}} = E_K + U(2).$$

And, if any of these components or both of them change according to a law, then the total energy will change according to the same law. And the change can be potentially affecting any physical, chemical or biological process. The factors 1-3 cause changing of kinetic energy of atoms/molecules on the surface of the Earth with periods, respectively, 24 hours (CR), a year (year rhythm), 180 million years (the Galaxy "year" rhythm). The existence of the rhythms has been mentioned above. Analysis of the kinetic energy changing leads us to the following formula:

$$E_{\max} - E_{\min} = 2m \times V_T \times V_E \cos\alpha\,,$$

where m is mass of an atom/molecule, V_T is thermodynamic speed of an atom/molecule, V_E is the orbital speed of the Earth's surface on the equator, α is the geographic latitude.

†Experimental data presented in this figure was obtained in 1972–1975, in Tashkent State University, Uzbekistan, by Azimov's group, headed by Takhir R. Akhmedov.

5 Conclusion

1. Experimental data on research of rhythmic processes with the periods close to geophysical (circadian rhythm — CR, lunar rhythm — LR, annual/year rhythm — YR) testify to existence of Astrophysical hours (APhC).

2. Rhythms with the periods close to the geophysical are experimentally observed in physical, chemical, and in biological processes. Furthermore, the circadian rhythm (CR) both in physical and in biological processes demonstrated a connection to local time.

3. Periods close to geophysical in all processes are formed Astrophysical Clock by change of a total energy (kinetic and potential) of atoms/ molecules located on the surface of Earth and moving with it in a space.

4. The Lunar Rhythm (LR) observed in chemical and biological processes is a result of a change of potential energy of atom (molecule), located on the surface of Earth. This change in potential energy is caused by movement of the Moon within the system Sun – Earth – Moon. All planets of the Solar System can have similar impact on processes taking place on Earth.

5. Biological objects (including humans) constantly have to receive signals of astrophysical clocks (APhC) for normal functioning. Thanks to APhC biological objects (almost closed systems) have an opportunity to exchange energy with environment, while maintaining their integrity.

6. During a long flight on low Earth orbit the time sensor of circadian rhythms is distorted for astronauts. This distortion could lead to imbalance of biochemical processes in astronaut's body, which could result in serious health issues. These issues may not manifest immediately.

7. During flight to Mars, human body stops receiving signals for setting circadian, lunar and yearly rhythms. This leads to total unbalancing of finely tuned biochemical reactions inside the body. At this point nobody knows what consequences this unbalancing may lead to. The difficulty of this problem is that experiments like Mars-500 cannot provide answers to these questions. One cannot turn off astrophysical clock during experiments on Earth.

8. To all those who desire and are able to carry out experiments studying the time dependence of water evaporation within a thermostatic vessel, further I provided the technical specifications:

- Thermostatic vessel to contain the liquid (8–10 litres of volume);
- Thermostatic liquid — motor or vegetable oil with temperature of 103±0.1°C;
- A system to distilled water, using typical chemical lab hardware;
- The flask with water to be evaporated should be located inside the thermostatic vessel;
- Cooling system for water vapor condensation;
- Water passing through the cooling system should be room temperature of 20°C with flow rate at 1 litre per minute;
- The frequency of measurements (time interval at which measurements are taken) is at the discretion of scientists setting up experiments (10 min, 15 min, etc.).

Objective: to plot the correlation of water vapor (condensate) with the time of day. Running experiment for 72 hrs is preferred. When publishing results of this experiment, the researcher needs to state geographical coordinates where experiment took place.

Submitted on December 1, 2014 / Accepted on December 4, 2014

References

1. Akhmedov T. R. Exogenous mechanism of the time sensor of biological clock. *Progress in Physics*. 2014, v. 10(1), 56–59.
2. Biological Clock. Transl. from Eng. with Introduction by S. E. Shnol, Mir Publishers, Moscow, 1964.
3. Biological Rhythms. Vols. 1-2, Ed. Achhoff J., Mir Publishers, Moscow, 1984.
4. Shnoll S. E., Kolombet V. A., Pozharskii E. V., Zenchenko T. A., Zvereva I. M., Konradov A. A. Realization of discrete states during fluctuations in macroscopic processes. *Physics Uspekhi*, 1998, v. 41, issue 10, 1025–1035.
5. Shnoll S. E. Cosmophysical Factors in Stochastic Processes. American Research Press, Rehoboth (NM), 2012.

Periodic Relativity: Deflection of Light, Acceleration, Rotation Curves

Vikram H. Zaveri

B-4/6, Avanti Apt., Harbanslal Marg, Sion, Mumbai 400022 INDIA. E-mail: zaverivik@hotmail.com

Vectorial analysis relating to derivation of deflection of light is presented. Curvilinear acceleration is distinguished from the Newtonian polar conic acceleration. The difference between the two is due to the curvature term. Lorentz invariant expression for acceleration is derived. A physical theory of rotation curves of galaxies based on second solution to Einstein's field equation is presented. Theory is applied to Milky Way, M31, NGC3198 and Solar system. Modified Kepler's third law yields correct orbital periods of stars in a galaxy. Deviation factor in the line element of the theory happens to be the ratio of the Newtonian gravitational acceleration to the measured acceleration of the star in the galaxy. Therefore this deviation factor can replace the MOND function.

1 Introduction

The article presented here is only a small element of a much larger formulation [1–6] proposed to arrive at a theory of quantum gravity and cosmology. Physicists have put in considerable efforts to unify general relativity and quantum mechanics but without success. The string theory and loop quantum gravity are still far from their goal.

Scientists are looking for a unified theory of creation. To achieve this objective, the physicists have set up two principal goals. First is the search for the fundamental building block of the universe. Second is the unification of four fundamental forces in nature. This constitutes the mainstream physics. The theory presented here regards these two principal goals as speculative and not plausible and hence the deviation from the mainstream physics.

Another feature of the mainstream physics is that most of the physicists if not all, consider consciousness [5, 6] as something outside the domain of physics and therefore when they talk about theory of everything, they really mean theory of everything excluding consciousness. As per the current understanding in the physical and life sciences, much of the scientific literature maintain strict distinction between consciousness and matter. The former is considered sentient and the later insentient. Many people are of the opinion that the existence of consciousness in this universe is a reality and the big bang theory could not be considered complete till it can account for the presence of consciousness along with the other forms of insentient matter.

Having rejected the two principal goals of the mainstream physics, this theory proposes that everything in the universe is reducible to energy. Therefore unity behind four forces (bosons), fermions and leptons should be sought in energy. Another point this theory makes is that the consciousness and energy are two states of one and the same thing which you may call the fundamental substance (Spirit) of the universe. Fundamental building block of the universe is assumed to be a micro entity, but the fundamental substance of the universe is all pervasive and ever remains undivided.

In this theory space and time does not have any physical existence, but they exist only in the human mind as imaginary artifacts. Comparatively, the energy has some real existence and it is found in myriads of forms. Again the energy is always associated with oscillations and motion, without exception. When these oscillation and motion of the energy subside, it gets transformed into the unmanifest which is not the energy and therefore does not gravitate. This unmanifest is motionless without any oscillations and therefore impossible to detect like empty space.

The idea of space-time arise in the human mind by way of delusion. When a particle wave is presented to a physicist, instead of seeing the oscillating energy, what he does is, superimposes the idea of wavelength and period on this wave and sees the space-time. All the geometrical theories in physics are founded upon such delusion. In periodic quantum gravity (PQG), the time does not flow in one direction, but one gets the sense of time by comparing one period of time with another. Hence time is a periodic phenomenon and periods are inverse of frequencies. Therefore in PQG, the Hubble parameter is associated with the frequency of the particle. Both have the same units. This eliminates the problem of time which plagues the Wheeler De Witt equation and its associated theories like loop quantum gravity, Hartle-Hawking wavefunction of the universe etc.

Advantage of Periodic relativity (PR) over general relativity can be seen in its use of revised principle of equivalence which states that the gravitational mass is equal to the relativistic mass. Application of this principle gives a very simple derivation for the orbital period derivative of the binary star [3]. And most important of all, allows the unification of periodic relativity with quantum mechanics. Because of this revised principle of equivalence, (modified) Newton's inverse square law of gravitation can be merged with the (modified) Schrodinger Wave equation which gives the basis for periodic quantum gravity and cosmology theory [4]. PR satisfies Einstein's field equations but does not utilize weak field approximation.

The reason general relativity (GR) got plagued with these two problems (the problem of time associated with Wheeler

De Witt equation and the inaccurate notion that the gravitational mass is equal to the inertial mass) is its dependence on the weak field approximation. The use of weak field approximation automatically locks the theory into having these two problems. When you depend on weak field approximation, you cannot treat time as a periodic phenomenon and you cannot introduce energy momentum invariant into Newton's inverse square law.

Another problem with GR is that the universe in this theory begins with a mixture of energy (radiation) and matter field. It doesn't even bother to explain where these two things come from. Another contradiction is that the equivalence of mass and energy is the biggest feature of GR at the same time they must have the universe begin with a mixture of energy (radiation) and the matter field. And all the physicists find it very comfortable to ignore the presence of life and consciousness in the universe. At the same time they must have a theory of everything.

Periodic quantum gravity and cosmology [4] is based on the idea that there is a connection between consciousness and energy [5]. Based on these ideas PQG proposes a unified field of consciousness (UFC) [6] underlying the entire universe from which comes the energy and matter fields of the big bang theory. In relating the consciousness and the energy the periodic nature of the time is the most essential factor. You don't need any clock operators of the Wheeler De Witt theory.

On the quantum mechanical side I don't think Dirac's linear representation of the wave function is very accurate because spin in that theory is not a part of the dynamics of motion but it is introduced as a perturbation just like in Darwin and Pauli theories. Also, the selection of the radial momentum operator is somewhat arbitrary and it isn't Hermitian as pointed out by several authors. These deficiencies are removed in the modified Schrodinger wave equation [2] in which spin is directly introduced in the Laplacian operator. This gives exactly same energy levels for hydrogen atom as in Dirac's theory and also it's application to heavy quarkonium spectra gives data which are spin dependent.

When these two theories, the periodic relativity and the relativistic wave mechanics are united, the result is the periodic quantum gravity and cosmology theory [4] which yields the entire table of standard model particles from a single formula. There is no other theory of quantum gravity that can do this.

Current article presents some corrections in previous article [1] and perfects the derivation for the deflection of light. It develops Lorentz invariant expression for the acceleration and provides solution for the rotation curves of galaxies which does not exist in GR. This solution does not have a discontinuity like the one in the MOND function. The transition from short distances to astronomical distances is continuous. This theory gives perfect fit for the rotation curves which MOND theory cannot give.

2 Curvilinear Gravity

In the earlier article "Periodic relativity: basic framework of the theory" [1], we obtained correct deflection of light in Newtonian theory by multiplying both sides of Newton's inverse square law of gravitation by the factor $(\cos\psi + \sin\psi)$. As shown in Figs. 1 and 2 of that article, ψ is the angle between the radial vector and the tangential velocity vector. Explanation given below makes it more clear that the theory is Lorentz invariant and factor $(\cos\psi + \sin\psi)$ introduces geodesic like trajectories. The details are as follows. After very elaborate analysis, we arrive at Newton's inverse square law given by

$$m_0 \frac{d^2\mathbf{r}}{dt^2} = -\frac{GM_0 m_0}{r^2}\,\hat{\mathbf{r}}, \tag{1}$$

where $GM_0 = \mu$. Here we introduce the dynamic weak equivalence principle which states that the gravitation mass is equal to the relativistic mass. Therefore Eq. 1 becomes

$$m \frac{d^2\mathbf{r}}{dt^2} = -\frac{\mu m}{r^2}\,\hat{\mathbf{r}}. \tag{2}$$

In classical mechanics, we have two different expressions for the acceleration acting on a body in motion. One is a general expression $d\mathbf{v}/dt$ in cartesian coordinates which include the curvature term, and another is for Newtonian gravity in polar coordinates $d^2\mathbf{r}/dt^2$ based on the angular momentum vector $\mathbf{h}$, which is supposed to be a constant in order to satisfy Kepler's third law of equal areas in equal times. In periodic relativity [1] we have shown that these two accelerations are not equal. At the same time we have maintained that the velocity vectors in both coordinate systems are equal, $\mathbf{v} = d\mathbf{r}/dt$. The reason for this is that the Newtonian gravity ignores the variation of angle ψ along the trajectory by assuming constant $\mathbf{h}$.

As shown in Fig. 1, this angle ψ is related to curvature through the expression

$$\phi = \theta + \psi, \tag{3}$$

where $d\phi/ds = \kappa$ is the curvature. Newtonian gravity ignores this curvature term by assuming constant $\psi = \pi/2$. This can be verified from following arguments.

$$\mathbf{h} = \frac{\mathbf{L}}{m} = \frac{\mathbf{p}\times\mathbf{r}}{m} \equiv \frac{|\mathbf{p}||\mathbf{r}|\sin\psi}{m}\,\hat{\mathbf{h}} = r^2\frac{d\theta}{dt}\sin\psi\,\hat{\mathbf{h}}. \tag{4}$$

From Eq. 4 we can see that $\mathbf{h}$ can be the desired constant only if $\sin\psi = 1$. This shows that the very foundation of Newtonian gravity ignores the curvature of the trajectory of the orbiting body. Hence in periodic relativity it is considered unreasonable to equate the cartesian acceleration $d\mathbf{v}/dt$ with the Newtonian polar acceleration $d^2\mathbf{r}/dt^2$.

In order to account for the variation of angle ψ along the trajectory, we propose that the absolute sum of vector and scalar products of $(\mu/r^2)\hat{\mathbf{r}}$ and $\hat{\mathbf{a}}$ is equal to magnitude

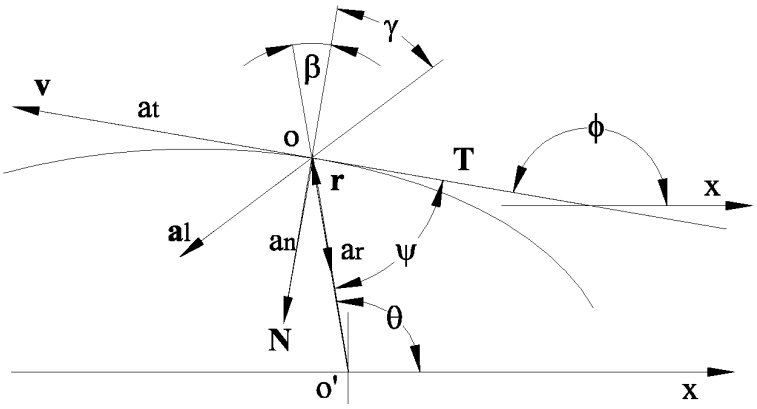

Fig. 1: Vectors in a two-body system.

of $d\mathbf{v}/dt$. The relation of these vectors to angle ψ is shown in Fig. 1

$$\left|\frac{d\mathbf{v}}{dt}\right| = \left|-\left|\hat{\mathbf{a}}\times\frac{\mu}{r^2}\hat{\mathbf{r}}\right| - \frac{\mu}{r^2}\hat{\mathbf{r}}\cdot\hat{\mathbf{a}}\right|, \tag{5}$$

$$\left|\frac{d\mathbf{v}}{dt}\right| = \left|\hat{\mathbf{a}}\right|\left|\frac{\mu}{r^2}\hat{\mathbf{r}}\right|\sin(\beta+\gamma)\hat{\mathbf{h}}\Big| + \left|\frac{\mu}{r^2}\hat{\mathbf{r}}\right|\left|\hat{\mathbf{a}}\right|\cos(\beta+\gamma), \tag{6}$$

where

$$\beta = \left(\frac{\pi}{2} - \psi\right), \tag{7}$$

$$\gamma = \tan^{-1}\left(\frac{a_t}{a_n}\right). \tag{8}$$

Various magnitudes of the parameters shown in Fig. 1 are as follows.

$$\mathbf{a}_l = \frac{d\mathbf{v}}{dt}, \tag{9}$$

$$a_t = \left(\frac{d^2s}{dt^2} + \frac{v}{\nu}\frac{d\nu}{dt}\right), \tag{10}$$

$$a_n = \kappa\left(\frac{ds}{dt}\right)^2, \tag{11}$$

$$a_r = -\frac{\mu}{r^2} = \left|\frac{d^2\mathbf{r}}{dt^2}\right|, \tag{12}$$

$$\mathbf{v} = \frac{d\mathbf{r}}{dt}. \tag{13}$$

Substitution of Eq. 7 in Eq. 6 gives

$$\left|\frac{d\mathbf{v}}{dt}\right| = \frac{\mu}{r^2}\left(\cos(\psi-\gamma) + \sin(\psi-\gamma)\right). \tag{14}$$

When the tangential component of the acceleration is absent then we have $a_t\widehat{\mathbf{T}} = 0$. This gives $\gamma = 0$ and Eq. 14 reduces to

$$\left|\frac{d\mathbf{v}}{dt}\right| = \frac{\mu}{r^2}\left(\cos\psi + \sin\psi\right). \tag{15}$$

Similarly we can show that

$$\left|\frac{d\mathbf{v}}{dt}\right| = \left|\frac{d^2\mathbf{r}}{dt^2}\right|\left(\cos(\psi-\gamma) + \sin(\psi-\gamma)\right). \tag{16}$$

The first term on the right of Eq. 14 can be interpreted as an angular acceleration vector with its axis perpendicular to the plane of motion. This could be the additional acceleration quantity responsible for the rotation of the velocity vector $\mathbf{v}$ about the coordinate origin o, causing the curvature of the trajectory.

2.1 Lorentz invariant acceleration

Little diversion here. In the earlier work [1], we introduced deviation to the flat Minkowski metric due to the gravitational field in the form,

$$\left(\frac{dt}{d\tau}\right)^2 = \gamma^{2n} = (1-\beta^2)^{-n}. \tag{17}$$

Here I propose a correction to our theory and change the method of introducing the deviation so that the deviation factor n is directly introduced in the Lorentz transformation equation as given below.

$$\left(\frac{d\tau}{dt}\right)^2 = \left(1 - n\beta^2\right), \tag{18}$$

where t is the coordinate time, τ the proper time of the orbiting body, n is a real number and $\beta = v/c$. The corresponding line element in polar coordinates is,

$$ds^2 = c^2dt^2 - ndr^2 - nr^2d\theta^2 - n(r^2\sin^2\theta)d\phi^2. \tag{19}$$

We showed [1] that the line element Eq. 19 satisfies Einstein's field equations for any constant value of n. For any constant value of n, metric 19 always remain flat. This is similar to the line element in Friedmann model when curvature factor $K = 0$. The change made in equation 18 does not alter any of the previous derivations.

Coming back to the main topic, in relativity we can either write our equations in terms of proper time or alternatively we can write them in terms of relativistic mass. Eq. 18 can be written as

$$\left(\frac{d\tau}{dt}\right)^2 = \left(1 - n\beta^2\right) = \left(\frac{m_0}{m}\right)^2 = \left(\frac{E_0}{E}\right)^2, \tag{20}$$

where $E = mc^2 = h\nu$. This gives

$$E = \left(E_0^2 + nE^2\beta^2\right)^{1/2}. \tag{21}$$

Differentiating w.r.t. time we get

$$\frac{dE}{dt} = \hat{\mathbf{v}}F = n\left(m\mathbf{a} + \frac{h\mathbf{v}}{c^2}\frac{d\nu}{dt}\right). \tag{22}$$

Here we arrive at the same relation that we described as true force in the previous article [1] except that now we have introduced the deviation factor n. I like to further point out a correction that this true force is same as the Lorentz force. Here we have used the relation $E = mc^2 = h\nu$. Therefore

$$\mathbf{F} = \frac{d\mathbf{p}}{dt} = \frac{dm\mathbf{v}}{dt} = n\left(m\mathbf{a} + \frac{h\mathbf{v}}{c^2}\frac{d\nu}{dt}\right), \tag{23}$$

where $\mathbf{F}$ is the Lorentz force and $\mathbf{v}$ the velocity vector and $\mathbf{a}$ is the classical acceleration of the particle given by

$$\mathbf{a} = \left(\frac{d^2s}{dt^2}\widehat{\mathbf{T}} + \kappa\left(\frac{ds}{dt}\right)^2\widehat{\mathbf{N}}\right). \tag{24}$$

Therefore, Lorentz force = Classical force + de Broglie force. From Eq. 23 we can define Lorentz invariant acceleration $\mathbf{a}_l$ as

$$n\mathbf{a}_l = n\left(\left(\frac{d^2s}{dt^2} + \frac{v}{\nu}\frac{d\nu}{dt}\right)\widehat{\mathbf{T}} + \kappa\left(\frac{ds}{dt}\right)^2\widehat{\mathbf{N}}\right). \tag{25}$$

The de Broglie force acts along the tangent vector. Now we equate Lorentz force with the gravitational force given by Eq. 14

$$\begin{aligned} |nm\,\mathbf{a}_l| &= \left|m\frac{d\mathbf{v}}{dt}\right| \\ &= nm\left(\left(\frac{d^2s}{dt^2} + \frac{v}{\nu}\frac{d\nu}{dt}\right)\widehat{\mathbf{T}} + \kappa\left(\frac{ds}{dt}\right)^2\widehat{\mathbf{N}}\right) \\ &= \frac{\mu m}{r^2}\left(\cos(\psi-\gamma) + \sin(\psi-\gamma)\right), \end{aligned} \tag{26}$$

$$\begin{aligned} |\mathbf{a}_l| &= \left|\frac{1}{n}\frac{d\mathbf{v}}{dt}\right| = \left(\left(\frac{d^2s}{dt^2} + \frac{v}{\nu}\frac{d\nu}{dt}\right)\widehat{\mathbf{T}} + \kappa\left(\frac{ds}{dt}\right)^2\widehat{\mathbf{N}}\right) \\ &= \frac{\mu}{nr^2}\left(\cos(\psi-\gamma) + \sin(\psi-\gamma)\right). \end{aligned} \tag{27}$$

2.2 Bending of light in periodic relativity

For the bending of light around the sun, we introduce light parameters $v = ds/dt = c$, $d^2s/dt^2 = 0$ and $cdt = ds$, along with $\kappa = d\phi/ds$ for the curvature of the trajectory in Eq. 27. In this case we will have $d\nu/dt = 0$ because the ray is equally blue shifted and then red shifted, and the frequency shift is 0 at the limb of the sun. This gives,

$$\left|\frac{c^2}{\nu}\frac{d\nu}{ds}\widehat{\mathbf{T}} + c^2\frac{d\phi}{ds}\widehat{\mathbf{N}}\right| = \frac{\mu}{nr^2}\left(\cos(\psi-\gamma) + \sin(\psi-\gamma)\right). \tag{28}$$

Multiplying both sides by $d\psi$, we get

$$\begin{aligned} &\left|\frac{1}{\nu}d\nu d\psi\widehat{\mathbf{T}} + d\phi d\psi\widehat{\mathbf{N}}\right| \\ &= \frac{\mu}{nc^2r^2}\left(\cos(\psi-\gamma) + \sin(\psi-\gamma)\right)ds d\psi. \end{aligned} \tag{29}$$

We integrate both sides with proper limits. For the star light approaching the sun we get,

$$\begin{aligned} &\left|\int_{\nu_1}^{\nu_2}\int_{\pi}^{\frac{\pi}{2}}\frac{1}{\nu}d\nu d\psi\widehat{\mathbf{T}} + \int_{-\phi}^{0}\int_{\pi}^{\frac{\pi}{2}}d\phi d\psi\widehat{\mathbf{N}}\right| \\ &= \frac{\mu}{nc^2}\int_{-\infty}^{0}\int_{\pi}^{\frac{\pi}{2}}\frac{1}{r^2}\left(\cos(\psi-\gamma) + \sin(\psi-\gamma)\right)d\psi ds. \end{aligned} \tag{30}$$

For the star light approaching earth from the limb of the sun we get,

$$\begin{aligned} &\left|\int_{\nu_2}^{\nu_1}\int_{\frac{\pi}{2}}^{0}\frac{1}{\nu}d\nu d\psi\widehat{\mathbf{T}} + \int_{0}^{-\phi}\int_{\frac{\pi}{2}}^{0}d\phi d\psi\widehat{\mathbf{N}}\right| \\ &= \frac{\mu}{nc^2}\int_{0}^{\infty}\int_{\frac{\pi}{2}}^{0}\frac{1}{r^2}\left(\cos(\psi-\gamma) + \sin(\psi-\gamma)\right)d\psi ds, \end{aligned} \tag{31}$$

$$\begin{aligned} &\left|(\ln\nu_2 - \ln\nu_1)\widehat{\mathbf{T}} + \phi\widehat{\mathbf{N}}\right| \\ &= \frac{\mu}{nc^2}\int_{-\infty}^{0}\int_{\pi}^{\frac{\pi}{2}}\frac{1}{r^2}\left(\cos(\psi-\gamma) + \sin(\psi-\gamma)\right)d\psi ds, \end{aligned} \tag{32}$$

$$\begin{aligned} &\left|(\ln\nu_1 - \ln\nu_2)\widehat{\mathbf{T}} + \phi\widehat{\mathbf{N}}\right| \\ &= \frac{\mu}{nc^2}\int_{0}^{\infty}\int_{\frac{\pi}{2}}^{0}\frac{1}{r^2}\left(\cos(\psi-\gamma) + \sin(\psi-\gamma)\right)d\psi ds. \end{aligned} \tag{33}$$

If we add l.h.s. of Eqs. 32 and 33 we get,

$$\text{l.h.s.} = \left|0.\widehat{\mathbf{T}} + 2\phi\widehat{\mathbf{N}}\right|. \tag{34}$$

From Eq. 34 we see that the magnitude of the tangential component is zero. Therefore $\gamma = 0$. Hence substituting $r^2 = s^2 + \Delta^2$ in Eqs. 32 and 33 we get

$$2\phi = \frac{4\mu}{nc^2\Delta}. \tag{35}$$

It is obvious from Eq. 35 that the value of constant n is 1 and not 0 as was assumed in earlier article [1]. $n = 1$ corresponds to the flat Minkowski metric therefore both the bending of light and the gravitational frequency shift can be explained corresponding to $n = 1$. Not only that, but no matter what gets measured in future experiments such as LATOR, the new measurement can easily be made to fit Eq. 35 by adjusting the constant n.

2.3 Curvic and conic gravity

Newtonian gravity is based on the constant vector **h** which yields the conic sections. Therefore we can distinguish the gravity that uses the Lorentz invariant acceleration as the curvilinear (or curvic) gravity and the Newtonian gravity with constant **h** as the conic gravity. Accelerations of the curvic and conic gravity are related by Eq. 16. It also needs to be understood that $d^2\mathbf{r}/dt^2$ is a radial vector but $d\mathbf{r}/dt$ is not a radial vector which acts along the velocity vector **v**. Moreover, the constant vector **h** does not play any role in defining the velocity vector **v**. Therefore factor $(\cos\psi + \sin\psi)$ does not appear in this expression of velocity $\mathbf{v} = d\mathbf{r}/dt$ which remains unaltered. This can be verified from following analysis. By definition we have

$$\cos\psi = \frac{dr}{ds}, \quad \text{and} \quad \sin\psi = \frac{rd\theta}{ds}, \tag{36}$$

$$\frac{d\mathbf{r}}{dt} = \left(\frac{dr}{dt}\hat{\mathbf{r}} + \frac{rd\theta}{dt}\hat{\theta}\right), \tag{37}$$

$$\frac{d\mathbf{r}}{dt} = \frac{ds}{dt}\left(\cos(\psi+\theta)\mathbf{i} + \sin(\psi+\theta)\mathbf{j}\right). \tag{38}$$

Substitution of Eq. 3 gives

$$\frac{d\mathbf{r}}{dt} = \frac{ds}{dt}\sqrt{\left(\cos^2\phi + \sin^2\phi\right)}\widehat{\mathbf{T}} = \frac{ds}{dt}\widehat{\mathbf{T}} = \mathbf{v}. \tag{39}$$

From Fig. 1 we can verify that the unit vector acting at an angle ϕ is $\widehat{\mathbf{T}}$. Therefore Eq. 39 is not influenced by the constant **h** assumption.

3 Rotation curves of galaxies

Earlier [1] we obtained two solutions to Einstein's field equations,

$$\left(\frac{r}{n}\frac{\partial n}{\partial r}\right) = 0 \qquad \text{and} \qquad \left(\frac{r}{n}\frac{\partial n}{\partial r}\right) = -4. \tag{40}$$

So far we have seen the application of the first solution which requires n to be any real number constant. Now we look at the second solution which we can write as

$$\int \frac{\partial n}{n} = -4\int \frac{\partial r}{r}, \tag{41}$$

$$\ln(nr^4) = C, \tag{42}$$

where C is a constant of integration. This gives

$$n = \frac{e^C}{r^4} = \frac{k}{r^4}, \tag{43}$$

where

$$k = e^C = \text{constant}. \tag{44}$$

In this second solution n need not be a constant. We make use of Eq. 27 in order to apply the second solution to rotation curves of a galaxies. Assuming circular orbit we substitute $\psi = \pi/2$ and $\gamma = 0$. This gives

$$|\mathbf{a}| = \frac{\mu}{nr^2} = \frac{\mu r^2}{k} = \frac{v^2}{r}, \tag{45}$$

$$k = \frac{\mu r^3}{v^2}. \tag{46}$$

We can write Eq. 45 as

$$v^2 = \frac{4\pi^2 r^2}{P^2} = \frac{\mu}{nr}, \tag{47}$$

$$P = \frac{2\pi r}{v}, \tag{48}$$

$$P^2 = \frac{4\pi^2 r^3 n}{\mu}. \tag{49}$$

For $n = 1$, Eq. 49 reduces to Kepler's third law, where P is the orbital period. Substituting Eq. 46 in Eq. 43 and Eq. 18 we can compute the ratio $d\tau/dt$. We can apply these equations of stellar motion to Blue Horizontal-Branch (BHB) halo stars of the Milky Way [8]. The circular velocity estimates are based on Naab's simulation [9]. To this data, one additional data point for solar radius of $8kpc$ [10] is added and the results obtained from Eqs. 46, 43 and 18 are shown in Table 1. Computed values are based on the stellar mass at the galactic center, which is $5.0924 \times 10^{10} M_\odot$ [11, 12]. Observed values of r and circular velocities constrain the integration constant k which provides a measure of non-uniform distribution of the galactic matter and the cold dark matter at a given radius. Hence it is appropriate to describe k as a galactic matter distribution constant. We also find that Eqs. 48 and 49 both yield exactly the same orbital period when velocity and deviation n along with the galactic stellar mass are used from the Tables. For the Sun, both yield 223.4 million years.

Table 1: Milky Way rotation curve based on proper time. r(kpc), v(km/s).

r	v	$k \times 10^{-81}$	n	$(1 - d\tau/dt)$
7.5	216	1.79546	0.62593	1.6246×10^{-7}
8.0	220	2.10050	0.56566	1.5231×10^{-7}
12.5	227	7, 52624	0.34004	9.748×10^{-8}
17.5	179	33.2129	0.39061	6.9628×10^{-8}
22.5	168	80.1362	0.34490	5.4155×10^{-8}
27.5	183	123.309	0.23782	4.43091×10^{-8}
32.5	143	333.332	0.32956	3.7492×10^{-8}
37.5	170	362.322	0.20210	3.2493×10^{-8}
42.5	183	455.160	0.15388	2.8670×10^{-8}
47.5	165	781.650	0.16936	2.5652×10^{-8}
55	183	986.474	0.11891	2.2154×10^{-8}

Table 2 shows solar system data from NASA planet fact sheets. Radial distance equal to semi major axis and mean

Table 2: Solar system rotation curve based on proper time. r(m), v(km/s).

Planet	$r \times 10^{-9}$	v	k	n
Mercury	57.91	47.87	1.12×10^{43}	1.000103
Venus	108.21	35.02	1.37×10^{44}	1.000059
Earth	149.6	29.78	5.01×10^{44}	1.000332
Mars	227.92	24.13	2.69×10^{45}	1.000065
Jupiter	778.57	13.07	3.66×10^{47}	0.997876
Saturn	1433.53	9.69	4.16×10^{48}	0.985986
Uranus	2872.46	6.81	6.78×10^{49}	0.99627
Neptune	4495.06	5.43	4.08×10^{50}	1.00136
Pluto	5869.66	4.72	1.20×10^{51}	1.014912
Moon	0.3844	1.023	2.16×10^{34}	0.990824

Table 3: M31 rotation curve. k in m^4, r(kpc), v(km/s), P in billions of yrs, $x = k \times 10^{-81}$.

r	v	x	n	$(1 - d\tau/dt)$	P
8.5	232	6.23	1.316	3.94×10^{-7}	0.225
12.5	251	16.89	0.763	2.68×10^{-7}	0.305
16.5	251	38.74	0.576	2.03×10^{-7}	0.402
20.5	227	90.94	0.568	1.63×10^{-7}	0.553
24.5	226	156.89	0.480	1.367×10^{-7}	0.665
28.5	218	263.96	0.441	1.175×10^{-7}	0.80
32.5	224	371.15	0.367	1.030×10^{-7}	0.888
36.5	240	460.47	0.286	9.178×10^{-8}	0.933

Table 4: NGC3198 rotation curve. k in m^4, r(kpc), v(km/s), P in billions of yrs, $x = k \times 10^{-79}$.

r	v	x	n	$(1 - d\tau/dt)$	P
0.68	55	0.202	10.45	1.76×10^{-7}	0.0759
1.36	92	0.579	1.868	8.79×10^{-8}	0.0908
2.72	123	2.593	0.522	4.39×10^{-8}	0.1358
5.44	147	14.52	0.183	2.2×10^{-8}	0.2273
8.16	156	43.52	0.108	1.466×10^{-8}	0.3213
13.6	154	206.78	0.066	8.79×10^{-9}	0.5425
19.04	148	614.36	0.0515	6.28×10^{-9}	0.7903
24.48	148	1305.7	0.040	4.88×10^{-9}	1.016
29.92	149	2352.1	0.0323	3.99×10^{-9}	1.233

orbital velocity are used. k and n are computed using Eqs. 46 and 43. $(1 - d\tau/dt)$ are of order 10^{-8} to 10^{-12} and not shown in the table. In case of moon, earth mass 5.9736×10^{24} Kg. is used. Value of n for Mercury shown in Table 2 should not be compared with that used in the derivation of perihelic precession [1] because here we have used second solution of Einstein's field equations with constant k, where as perihelic precession is derived from the first solution of Einstein's field equations with constant n. These two solutions are derived from two roots of a quadratic equation. The purpose of presenting the solar system data is only to show that there is no discontinuity like the MOND function. One should not look for precision in Table 2 because it is based on circular orbit approximation. It is sufficient to note that $n = 1$ for flat Minkowski metric is recovered at small distances.

We can also apply these equations of stellar motion to rotation curves of M31 [13] and NGC3198 [14]. The results obtained from Eqs. 46, 43 and 18 are shown in Tables 3 and 4. Computed values are based on the stellar mass at the galactic center, which is $1.4 \times 10^{11} M_\odot$ for M31 and $5.0 \times 10^9 M_\odot$ for NGC3198.

From Eq. 27, we can see that n is a ratio of Newtonian gravitational acceleration to the measured acceleration which is 1 for flat Minkowski metric. From Eq. 45 we get the same relation for circular orbits.

$$n = \frac{\mu/r^2}{v^2/r}. \tag{50}$$

Substitution of n in Eq. 18 gives

$$d\tau^2 = \left(1 - \frac{\mu}{rc^2}\right) dt^2. \tag{51}$$

Therefore metric 51 becomes singular for the limiting radius

$$r_l = \frac{\mu}{c^2}. \tag{52}$$

This is the same expression which we derived earlier [1] for a black hole.

4 Conclusion

We have presented derivation for the deflection of light from fundamentals by introducing vectors. Here we can relate the additional component of acceleration with the rotation of the velocity vector which causes the curvature of the trajectory. We have distinguished the cartesian curvilinear acceleration from the polar conic acceleration and explained why they are not equal even though they are derived from the same velocity vector. We have derived expression for the Lorentz invariant acceleration. We have presented a theory of rotation curves of galaxies which is based on the second solution of Einstein's field equations which yields much better results than the earlier one based on the first solution with constant n [7]. Deviation factor n appears in the expression for acceleration as well as the modified Kepler's third law which now yeilds correct orbital periods for the stars of galaxies. Deviation factor n plays the same role as the MOND function in the expression for acceleration. This kind of solution cannot be obtained in general relativity because of the weak field approximation, which is a different way of introducing deviation to the flat Minkowski metric.

Acknowledgments

Author is grateful to Robert Low, Gerard t'Hooft, Stam Nicolis, Christopher Eltschka, Bruce Rout and Thiago C. Junqueira for useful discussion and comments.

Submitted on November 24, 2014 / Accepted on November 28, 2014

References

1. Zaveri V.H. Periodic relativity: basic framework of the theory. *Gen. Relativ. Gravit.*, 2010, v. 42 (6), 1345–1374. https://www.researchgate.net/publication/225712819.
2. Zaveri V.H. Quarkonium and hydrogen spectra with spin dependent relativistic wave equation. *Pramana — J. Phys.* 2010, v. 75 (4), 579–598.
3. Zaveri V.H. Orbital period derivative of a binary system using an exact orbital energy equation. arXiv:0707.4544v3.
4. Zaveri V.H. Periodic quantum gravity and cosmology. Submitted, *Grav. Cosmol.* May 2014, https://www.researchgate.net/publication/262492889.
5. Zaveri V.H. Consciousness and energy. In: The Big Bang: Theory, Assumptions and Problems, eds. O'Connell J.R., Hale A.L. 275–284. Nova Science Publishers, New York, 2012, https://www.researchgate.net/publication/262494186.
6. Zaveri V.H. Unified field of consciousness. 2014. https://www.researchgate.net/publication/266618399.
7. Zaveri V.H. Rotation curves of galaxies in periodic relativity. arXiv: 0805.2233v4.
8. Xue X.-X., Rix H.-W., Zhao G., Fiorentin P.R., Naab T., Steinmetz M., Van den Bosch F.C., Beers T.C., Lee Y.S., Bell E.F., Rockosi C., Yanny B., Newberg H., Wilhelm R., Kang X., Smith M.C., Schneider D.P. The Milky Way's Rotation Curve to 60 kpc and an Estimate of the Dark Matter Halo Mass from Kinematics of 2500 SDSS Blue Horizontal Branch Stars. *Astrophys. J.*, 2008, v. 684, 1143–1158. arXiv:0801.1232v3[astro-ph].
9. Naab T., Johansson P.H., Ostriker J.P., Efstathiou G. Formation of Early-Type Galaxies from Cosmological Initial Conditions. *Astrophys. J.*, 2007, v. 658, 710N.
10. Eisenhauer F., Schoedel R., Genzel R., Ott T., Tecza M., Abuter R., Eckart A. Alexander T. A Geometric Determination of the Distance to the Galactic Center. *Astrophys. J. Lett.*, 2003, v. 597, L121–L124.
11. Wu X., Famaey B., Gentile G., Perets H., Zhao H.S. Milky Way potentials in CDM and MOND. Is the Large Magellanic Cloud on a bound orbit? *Mon. Not. R. Astron. Soc.*, 2008, v. 386 (4), 2199–2208. arXiv:0803.0977v1[astro-ph].
12. Robin A.C., Reyle C., Derriere S., Picaud S. A synthetic view on structure and evolution of the Milky Way. *Astron. Astrophys.*, 2003, v. 409 (2), 523.
13. Corbelli E., Lorenzoni S., Walterbos R., Braun R., Thilker D. A wide-field H I mosaic of Messier 31 — II. The disk warp, rotation, and the dark matter halo. *Astron. Astrophys.*, 2010, v. 511, A89.
14. Begeman K.G. H I rotation curves of spiral galaxies. I — NGC 3198. *Astron. Astrophys.*, 1989, v. 223, 47–60.

Motion-to-Motion Gauge for the Electroweak Interaction of Leptons

Felix Tselnik

Ben-Gurion University of the Negev, P.O.B. 653 Beer-Sheva 84105, Israel. E-mail: tselnik@ee.bgu.ac.il

Comprised of rods and clocks, a reference system is a mere intermediary between the motion that is of interest in the problem and the motions of auxiliary test bodies the reference system is to be gauged with. However, a theory based on such reference systems might hide some features of this actual motion-to-motion correspondence, thus leaving these features incomprehensible. It is therefore desirable to consider this correspondence explicitly, if only to substantiate a particular scheme. To this end, the very existence of a (local) top-speed signal is shown to be sufficient to explain some peculiarities of the weak interaction using symmetrical configurations of auxiliary trajectories as a means for the gauge. In particular, the unification of the electromagnetic and weak interactions, parity violation, $SU(2)_L \times U(1)$ group structure with the values of its coupling constants, and the intermediate vector boson are found to be a direct consequence of this gauge procedure.

1 Introduction

We shall apply a direct motion-to-motion gauge to the electroweak interactions. In so doing, our sole tool is the counting of the numbers of the top-speed signal oscillations in order to arrange test particles in special configurations of their trajectories possessing a particular symmetry. First we shortly review the basics of the motion-to-motion measurements (Sec. 1). Second we introduce compact symmetric configurations suitable for the gauge (Secs. 2, 3). Third we apply this gauge to construct a regular lattice suitable to unambiguously transport the (integer) value of the electric charge unit over the space-time and find that parity violating weak interaction is a necessary component of this (Sec. 4). In the Sec. 5, we describe some other applications of the gauge. The burden of the argument is as follows. The cube-star arrangement of electron and positron trajectories allows for the construction of a regular gauging lattice only under some conditions. In particular, it turns out that the particle charges must be altered, so as to let them leave the gauging cell intact notwithstanding the residual uncertainty pertinent to the gauge. Aiming at the finest lattice, we have found its minimal cell size required for the gauge. This size defines the range which is free to introduce an additional ("weak") interaction having no effect on the gauge itself. We can use this additional interaction to realize the necessary charge conversion (the electrons into the neutrinos). However, the top-speed signal oscillation numbers define not a single but two trajectories, and we have to provide the weak interaction with the property to select one of them. This interaction must depend on spin and contains parity violation as a necessary ingredient of electric charge gauge and transport.

2 Motion gauged with auxiliary motion

Ultimately, mechanics is based on comparing a trajectory of the body which is of interest in a problem to the trajectories of test bodies that are measuring force in the related points. Applications of the scheme also require a means to follow motions of the body. Otherwise, one could never be sure (in the absence of instant communication) that at a later moment it is the same body rather than a similar one. To this end, a top speed signal must exist in the scheme for not to loose the object upon its possible accelerations. In the conventional version, the required comparison is being carried out via an intermediate reference system comprised of rods and clocks. However, finally the real devices designed to measure the trajectories of bodies are to be gauged with the use of some standard motions. Thus, narrow light rays or free fall are used to determine whether or not the rod is rectilinear, and clock readings are to agree with astronomical and/or atomic processes. So, a reference system comprised of rods and clocks is just an intermediary in the comparison of one motion to another. One could guess that this intermediary might either add some features of its own to the gauge or, on the contrary, hide some important information in cases when the standard procedure is used beyond its traditional scope. It is therefore desirable to dispense with any intermediary so as to gauge motions directly, if only to obtain a criterion of suitability of the intermediary. To this end, many authors attempted to define the structure of space-time solely in terms of trajectories. In particular, natural topologies have been proposed to conform to the special role of the time axis [1-5]. A drawback of some of these approaches is the premise of a four-dimensional differentiable manifold for the space-time a topology to be introduced in. (However, the very idea to construct open subsets out of all trajectories, rather than of only free ones, and to deduce space-time properties, e.g., its dimension, out of their intersections was already considered [2].) Furthermore, topology is a too general structure, and practice requires more details. Thus, in order to define metrics based on a subset of trajectories, it was proposed to eliminate rigid rods (see, e.g., [6] and references therein); still clocks, at least in the form of affine parameters, seemed unavoidable.

But then, trajectories cannot be taken as primary entities in a theory to be developed from scratch, even though they might be considered directly observed (contrary to empty space-time!). It must be explained why just the trajectories of bodies are of particular interest rather than arbitrary changes in nature. Already in the Einstein's picture of the space-time, the event is defined as the intersection point of world lines of particles or of light pulses. This approach was further developed by Marzke and Wheeler [7]. In actual fact, primary definitions must be substantiated by the intended application of the theory, and therefore they must arise directly from the desirable statement of the problem, that is, to be axioms rather than hypotheses. Of course, a general uncertain concept of event cannot be basic for technical use that aims at a method to provide predictions, and therefore mechanics offers a particular kind of event, namely, contact (collision). The idea is to leave aside the question as to what results from the contact, assuming instead that nothing will happen, provided the contact does not occur. Whereas the notion "material point", i.e. "infinitesimal body", requires a preliminary concept of metric, the concept of contact is self-contained: the contact either exists or not. Only such problems are allowed for the analysis in mechanics. To this end, we define trajectories merely as a means to predict whether or not the contact of interest will occur in a particular problem upon detecting only some auxiliary contacts to be appropriately selected. Each trajectory possesses its own linear order, since it is introduced just for step-to-step predictions. This order introduces the topology of a simple arc on the trajectory to provide the basis for emerging structures. For this to be possible, we have to prepare a set of auxiliary (standard) trajectories in order to encode final, initial and intermediary states (contacts) solely in terms of these. Yet the choice of standard trajectories needs an explanation of its own. Can we dispense with geodesics? What properties of these are actually necessary for the scheme? Might these properties be deduced from meager information?

A reliable concept to begin with is the communication of bodies with a top speed signal (which is necessary anyway to follow motions of the body, while ensuring its unambiguous identification). Top speed signal can be defined independently of any general concept of speed. Consider two bodies A and B, the problem being stated of whether or not they will come into contact. Let A contact with an auxiliary body X which then contacts with B. Among these X's we look for the first to reach B, whatever ways they go. Only the order of these contacts matters, e.g., an X might put a mark on B, so that all the X's, except the first, find B already marked. It is this top-speed body that will serve as the signal. Let further there be a triple contact (B,X,Y), such that Y is, in turn, the first to meet A afterwards. If the contact (A,B) occurs, the number of these oscillations (multiple "echo") is infinite, corresponding to the so-called Zeno sequence. Otherwise, the last oscillation would occur before (A,B), and then this last oscillating body would not be a top-speed one. We could reverse this argument, suggesting that tending the number of oscillations to infinity could be used to predict the occurrence of (A,B), if in the absence of this contact the number of oscillations were not infinite as well. In conventional notions this implies infinite time of oscillations, but we cannot introduce space-time terms a priori aiming at a solution solely in terms of contacts. For this purpose, let us provide in our scheme some auxiliary X, such that (B,X) does occur. Then we can state that (A,B) occurs, provided the ratio of the (infinite) numbers of oscillations between A and B to that between B and X tends to a finite limit. For this to be actually used, one begins to count oscillation numbers at a moment, and the value of the ratio is determined as its limit when the number of oscillations as measured for the contacts of the signal with, e.g., A tends to infinity. This limit does not depend on the moment it starts from or on the reciprocal positions of the signals coming to A from B and X within one oscillation cycle [8]. We emphasize, that only local existence of the top speed signals is important (no cm/sec and no free trajectories to appear from the outset!). The counting of such ratios will be our sole tool in the sequel; however in some cases also finite oscillation numbers are suitable. (Finite numbers of top-speed signal oscillations were already used to compare distances [6, 7].)

We *define* space-time R not as something pre-existing but rather as an envelope of combination of all possible trajectories, the occurrence of contacts between which can be determined by means of top speed signal. In fact a (single!) reference system does exist in this approach, comprising an appropriate subset of trajectories – X's – chosen under the following conditions: i. Any pair of them either have no common contact or have only one (at least locally – with respect to their own topology); ii. If some trajectory A has a contact with some other trajectory B, there exists some X with the triple contact (A,B,X); iii. Although X's might have multiple contacts with trajectories not belonging to the subset, any pair of such contacts could be separated to insert a sequence of the top-speed signal oscillations for each of them. Moreover, just multiple contacts determine dynamics in terms of X's upon using an additional subset of "charged" test bodies, the trajectories of which are also encoded via X's. Under these conditions, infinite oscillation numbers provide the space-time with differential topology as a means to clearly separate possible contacts. Moreover, space-like hyper-surfaces S and the projections of trajectories thereon ("paths") might also be defined in these terms. The condition for a so defined contact scheme to represent any finite arrangement of the projections with their mutual intersections, while excluding any unnecessary for this purpose subsets, defines the topology of S. In the framework of traditional topology [1-5], dim R=ind R=1, but S is *not* a sub-space of R, though the set of its neighborhoods can be induced by trajectories from R: Each neighborhood of a point of the trajectory defines the corresponding neighbor-

hood of this point in S, consisting of all its points connected with top-speed signal to this neighborhood of the trajectory. However, S is not a topological image of R, and its dimension is to be defined independently of R.

Unlike the trajectory itself, its projection on S need not be a simple arc, and it might have various self-intersections. However, according to the Nöbeling-Pontryagin embedding theorem, any n-dimensional metrizable topological space with a countable base of open subsets can be embedded into the (2n+1)-dimensional Euclidean space. In fact, the theorem states that in this space its n-dimensional subspaces are free to intersect or not, while a space of a lower dimension might be too "dense" forcing some of them to intersect necessarily, and a space of a higher dimension would add nothing to this freedom. This is particularly clear for n=1: In only two dimensions a line cannot pass a closed boundary line without crossing it, whereas in three dimensions this is always possible (traffic interchange, say), while the fourth dimension would be redundant. For a finite (and even for a countable) array of trajectories its map in S has n=1, so dim S = 3. It follows that each contact might be encoded with only three X's. This fact could never be understood unless the space-time is defined as a union of actual trajectories [2] rather than being accepted in advance. In this version, the extension of bodies should itself be regarded just as their property to obstruct some trajectories or their paths.

Upon focusing in this presentation only on some features of motion-to-motion measurements relevant for weak interactions, further analysis of geometrical properties of the space-time that arise from this approach is left for discussion elsewhere.

3 Compact arrangements of trajectories

Consider a set of trajectories with their common contact. We can choose some triple of them to provide a basis, so that any other member of the set can be specified with its oscillation numbers ratios with those of the basis. *However, there exists the twin to any so defined trajectory.* Indeed, let us consider for the sake of visualization such decomposition in the rest frame of one of bodies of the basis. Then the other two define a surface, e.g., a plane, and the dual to a trajectory is its mirror image with respect to this plane. In order to specify the trajectory uniquely, we have to add some internal degree of freedom, a doublet, in close analogy to the spin variable.

Among all such sets we select a particular subset – *spheres* – that is defined as follows. It is convenient to introduce an additional body for the center of the sphere. The sphere is comprised of a finite number of trajectories with equal oscillation numbers with respect to the center body, that is, their ratio equals 1 for each pair of the sphere members. The sphere might be viewed as a compact arrangement of trajectories which are specified solely by their mutual angles. While the ratios of the oscillations numbers between the members themselves to those between them and the center are in general different, we can define for each trajectory its neighbors as those for which this ratio is maximal. The spheres might be used to specify a condition for forces that are permitted to act on bodies over their trajectories. If we accept that everything in sight must be described in terms of signals, we have to define forces in these terms as well. Such a rule must be independent of the space-time point, i.e. to require the force not to alter oscillation number ratios.

Let us take the sphere consisting of A, B, C and use conventional variables in order to reveal the familiar forces that satisfy this condition. The ratio ${}_A\Gamma_{BC}$ of the oscillation numbers between the bodies A and B to that of A and C is [8]:

$$ {}_A\Gamma_{BC} = \lim_{n_{AB}\to\infty} \frac{n_{AB}}{n_{AC}} = \frac{\ln\left(u_{Ai}u_{Bi} + \sqrt{(u_{Ai}u_{Bi})^2 - 1}\right)}{\ln\left(u_{Ai}u_{Ci} + \sqrt{(u_{Ai}u_{Ci})^2 - 1}\right)} \qquad (1) $$

where u_{Ai} and others are the four-velocities of the bodies, and summation over i is implied. Evidently the ratio ${}_A\Gamma_{BC}$ will not change under a force if the scalar products of the four-velocities do not.

Consider the electromagnetic force, F_{ik}. Then for velocity of light c, the charges and masses of the bodies e and m:

$$ du_{Ai} = \frac{e}{mc} F_{ik}u_{Ak}ds_A \,. \qquad (2) $$

Hence:

$$ d(u_{Ai}u_{Bi}) = \frac{e_A}{m_Ac} F_{ik}u_{Ak}u_{Bi}ds_A + \frac{e_B}{m_Bc} F_{ki}u_{Bi}u_{Ak}ds_B \,. \qquad (3) $$

But $ds_A = ds_B$ since A and B are the members of a sphere. Then, $d(u_{Ai}u_{Bi}) = 0$, if $F_{ik} = -F_{ki}$ and also $e_A/m_A = e_B/m_B$. Apart from electromagnetic field, anti-symmetry of which can be expressed, in the connected space-time manifold, via potentials as $F_{ik} = \partial A_i/\partial x_k - \partial A_k/\partial x_i$, a field might also include commutators $[A_i, A_k]$ if the components of the potential do not commute. (Quanta of these fields must be bosons, whereas fermions would require only anti-commutators.) We can then reverse the argument to state that only fields preserving the ratios of the oscillation numbers can appear in the theory as bosons. Moreover, propagation of the fields can also be expressed via appropriate contact schemes by means of Green functions [9]. To complete the method, we stay in need of a condition, in terms of contacts, for the constancy of charge and mass in (3) everywhere, and in order to find this condition we need a means to translate these values over the whole space- time. For this purpose consider a particular subset of spheres, in which the oscillation number ratios with its neighbors are the same for each member of the sphere. Such a sphere will be called a star. In three-dimensional space only five stars are possible. These are known as Platonic solids. Note that the definition of star doesn't imply that its bodies move uniformly.

4 Star-based gauge of electric charge

Eventually, all that is actually measured in experiments relates to motion under electromagnetic force of, e.g., particles, products of their interactions etc. It is therefore this force proportional to the electric charge of the particle it acts upon that must be gauged in the first place. The value of this charge is commonly accepted to be the same everywhere. Still a method is needed to detect this identity in terms of contacts. We want to use the stars for gauging electric charge without any intermediary. To this end, we have to specify the charge not only locally but also to develop some motion-to-motion gauge for its translation to any point the body of interest might occupy along its trajectory. This should be based on the symmetries of stars, which can easily be expressed in terms of equality of some oscillation numbers.

Suppose all the members of a star (in the gauge procedure we will call them particles) are electrically charged with equal e/m values and move only under mutual electromagnetic interaction. In any star comprised of identical particles they move along straight lines repelling each other, and the particles cannot reach the center. Moreover, the trajectories might become curved, provided some of the particles differ from others in charges or masses, and for this reason they miss the center as well. But in a symmetry-based charge gauging procedure, it is the disparity of charges and masses that is detected as a star symmetry breaking. If the particles miss the star center anyway, we cannot be sure that the symmetry is not broken just at the closer vicinity of the center, still being observed far from it. We must therefore use for the gauge only neutral as a whole stars with equal numbers of positive and negative particles. Of all Platonic solids, the center is reached only in the cube with opposite signs of the charges between the tetrahedrons the cube is comprised of. Although in the cube star the particles keep moving along straight lines (even if the absolute values of their charges differ between its two tetrahedrons, while being identical within each of them), the symmetry will be broken because the tetrahedrons are being differently accelerated by mutual attraction.

Starting the counting of the oscillation numbers between the particle and an introduced, for the sake of simplicity, imaginary central particle at a moment before the contact, we detect the symmetry breaking if these numbers, as measured at the center, differ at least by one oscillation. In the limit of the smallest star size, defining the highest precision of electromagnetic gauge, one tetrahedron nears the center over only one oscillation while another — over two oscillations. At a smaller initial radius the second oscillation has no time to occur. Since we detect only integer numbers of signal oscillations, the values of charge to be detected must be discrete. Indeed, suppose that the charges differ by some infinitesimal value. However close to the center the symmetry was detected, we cannot be sure that asymmetry could still be detected upon continuing the counting, since nothing is being registered in between the neighboring contacts. So, we are able to detect with our method only discrete values of charge (and/or mass), hence a minimum value of charge e can be registered, the next value being $2e$. Now, whereas in a given external field acceleration depends on e/m, for a case of interacting particles it depends on e^2/m, and in order to observe the symmetry of a star the masses and the absolute values of the charges of its particles are to be equal.

The particles of the tetrahedron having the charge $2e$ experience smaller acceleration as compared to the tetrahedron having the charge e. The related symmetry breaking gauge condition — one extra oscillation — is reached at some final radius r_{min}. Smaller radii are not involved in the gauge procedure, leaving this region free to introduce a new interaction under our general trend to regard possible in mechanics everything described with the motion-to-motion schemes. In the next section, we will find such an interaction to be necessary for the gauge itself.

5 Application to electroweak interactions

With the basic cube star at hand we proceed to develop the whole regular lattice, along which the value of the electric charge can be transported to a point of the trajectory in question. Along our general lines, the regular lattice must comprise elementary cube-star cells. For this purpose, we use some particles of one star, after they pass its center, as a seed for the next star. According to Sec. 2, just three stars are sufficient to completely define their next star. As a matter of fact, this simple picture cannot be trusted, because deviation of the charge at radii that are smaller than those involved in the gauge for the finest lattice might either prevent electrons and positrons from escaping the star against the exit potential barrier formed by the attraction of the other members of the star or to have a final energy differing from what is needed as the input energy of the next star. Even small charge deviation are important, since the energy near the minimal radius is typically much higher than the energies of the particles at the star entrance, and momentum conservation would yield large final fluctuations there; moreover, the deviation might be collected over a sequence of stars. In particular, even low level radiation that has a small effect on the matching of incoming to outgoing energies in a single star might cause large deviations over long sequences.

Radiation is negligible in stars comprising large bodies, and our gauge is quite feasible in this case. Long sequences might then be directly arranged, in which the outgoing bodies are directly used in the next star, since their velocity return to the initial values being decelerated after passing the star center. This is impossible in the limit of elementary particles. If, however, a new — "weak" — interaction converts the charge of the particles to zero at the smallest radius of the symmetry detection, the gauge becomes independent of radiation. Being constrained to radii that are smaller than those involved in the

electric charge gauge, such a conversion doesn't obstruct the gauge. Over a larger scale, one could consider stars consisting, e.g., of ions, which can change their charge via charge exchange or stripping. We, however consider the limiting case of the finest lattice comprised of stars having the smallest possible size, still allowing the motion-to-motion charge gauge. Then only elementary particles might participate in the lattice, and an elementary neutral particle must complete the collection. It is just in this extreme case the weak interaction with its parity violation appears.

In order to form the lattice, this newborn particle, the "neutrino", has then to be converted back into the electron of the next star. This can happen under the same weak interaction, provided the neutrino collides with the anti-neutrino to create the electron-positron pair. Though never observed in practice, such a limiting process, as well as the charged star itself — with its eight particles' simultaneous collision, should be considered a feature of our formal language to question nature, providing as concepts for theories so also rules for experiments. We need therefore to introduce intermediate cube stars made up of only neutrinos and anti-neutrinos and positioned at the corners of the charged cube. These neutral stars are "blind" in the sense that their symmetry cannot be detected electromagnetically. Still, suitability of the whole regular lattice might be detected, provided the following charged star is found to repeat the original symmetry. So, we need a doublet consisting of electrons and neutrinos to prepare a regular lattice. The doublet corresponds to two charge states that convert one into another at the vertices, suggesting the SU(2) group for transformations of the inner (charge) space in the gauge field theory, but now it appears as an indispensable mechanism to realize the regular lattice by means of the motion-to-motion gauge.

Our next step is to define all the members of the next star starting with the trajectories that are continuations of its three preceding stars. For any star, it is sufficient to take a basis of three trajectories to determine all the others. In order to visualize this construction, it is convenient to proceed using the conventional picture, that is, to imagine the cube star in its center-of-mass (CM) reference system as eight particles at its vertices moving toward the center with equal velocities v ($\beta = v/c$). Let us take, for example, the trajectory A and its neighbors B and C as the basis for the star to be constructed and choose the line of A for the x-axis, the line through the cube center parallel to the line between the vertices B and C for the y-axis, and the z-axis as orthogonal to these two. We have to find D as the third neighbor of A. In so chosen coordinates, the decomposition coefficients of the basis are:

$$\left.\begin{aligned} &\beta_{Ax} = \beta, \quad \beta_{Ay} = \beta_{Az} = 0 \\ &\beta_{Bx} = \beta_{Cx} = \frac{\beta}{3}, \quad \beta_{By} = -\beta_{Cy} = \beta\sqrt{\frac{2}{3}} \\ &\beta_{Bz} = \beta_{Cz} = \beta\,\frac{\sqrt{2}}{3} \end{aligned}\right\}, \qquad (4)$$

and those of D:

$$\beta_{Dx} = \frac{\beta}{3}, \quad \beta_{Dy} = 0, \quad \beta_{Dz} = -\beta\,\frac{2\sqrt{2}}{3}. \qquad (5)$$

But we know from Sec. 2 that via the oscillation number ratios counting — our sole means — the basis A, B, C defines actually two trajectories, that is, there exists another trajectory E besides D with the same ratios of the oscillations. In order to determine the coordinates of E, we transform (4) and (5) to the reference system, in which A is at rest, to find E there as the mirror image of D, and then to return to the CM system to find the coordinates of E there. From the relativistic transformation formulae for velocities, we find:

$$\left.\begin{aligned} &\beta'_{Ax} = \beta'_{Ay} = \beta'_{Az} = 0 \\ &\beta'_{Bx} = \beta'_{Cx} = -\beta\,\frac{2}{3-\beta^2} \\ &\beta'_{By} = -\beta'_{Cy} = \beta\,\frac{\sqrt{6(1-\beta^2)}}{3-\beta^2} \\ &\beta'_{Bz} = \beta'_{Cz} = \beta\,\frac{\sqrt{2(1-\beta^2)}}{3-\beta^2} \\ &\beta'_{Dx} = -\beta\,\frac{2}{3-\beta^2}, \quad \beta'_{Dy} = 0 \\ &\beta'_{Dz} = -\beta\,\frac{2\sqrt{2(1-\beta^2)}}{3-\beta^2} \end{aligned}\right\}. \qquad (6)$$

Using (6), we obtain the mirror image E of D trajectory with respect to the plane defined by the transformed B and C velocities as:

$$\left.\begin{aligned} &\beta'_{Ex} = -\beta\,\frac{2(3-5\beta^2)}{(3-\beta^2)^2} \\ &\beta'_{D'y} = 0 \\ &\beta'_{D'z} = \beta\,\frac{2\sqrt{2(1-\beta^2)}\,(3+\beta^2)}{(3-\beta^2)^2} \end{aligned}\right\}. \qquad (7)$$

Upon back transforming (7) to the laboratory reference frame, we find finally:

$$\left.\begin{aligned} \beta_{Ex} &= \frac{\beta\left((3-\beta^2)^2 - 2(3-5\beta^2)\right)}{(3-\beta^2)^2 - 2\beta^2(3-5\beta^2)} \\ \beta_{Ez} &= \frac{2\sqrt{2}\,\beta(1-\beta^2)(3+\beta^2)}{(3-\beta^2)^2 - 2\beta^2(3-5\beta^2)} \end{aligned}\right\}. \qquad (8)$$

Though in our example (D placed between B and C) E moves in the same xz plane as D, (8) does not define a vertex of the cube. Even the absolute values of the D and E velocities differ already in the order of β, though their oscillations numbers with respect to the basis are the same. So, upon constructing the next star we must introduce some additional — internal — degree of freedom, helicity, to define just D but not E by means of choosing a particular order in the basis A,

B, C. Mathematically, this is similar to the spin variable, the spin being directed either in the direction of the momentum of the particle or oppositely. So, parity violation turns out to be a necessary property of the motion-to-motion gauge, since only the projection of spin on the momentum direction conveys the necessary information to select the appropriate trajectory out of the two. In the electron/positron cube star, the opposite sense particles belong to different tetrahedrons, and of the two particles on each main diagonal of the cube one is the electron while another – the positron. Therefore the order of the basis for the electron is seen as reversed from its opposite positron, and the product of parity and charge conjugation is the same for both (CP conservation).

We are able now to use parity in the electric charge gauge as performed solely with photon oscillations counting. In the symmetric cube star magnetic field is zero on the trajectories, hence there is no orbital angular momentum, and only the spin of the particle defines its total angular momentum. Then our electric charge gauge fails to distinguish between particles with left and right orientations, letting both enter the weak interaction zone. In order to define the fourth trajectory, the neutrinos must be provided with a definite, e.g., left, helicity, and therefore the charged star must generate only these. To this end, the weak interaction must be spin-dependent to create only left-handed neutrinos (and right-handed antineutrinos) in the collision of the particles in the charged star. It is sufficient to consider only the electron and its neutrino, the argument being similar for their antiparticles. In the blind star the neutrino will turn into the electron with the same projection of its spin in virtue of the angular momentum conservation.

For the left-handed electrons in the charged star, the function of the weak interaction is dual. On the one hand, the weak interaction for the left-handed electrons possesses its own dynamics, since it should match the output and input energies in the sequence of charged stars over the whole lattice. On the other hand, its intensity defines charge conversion probability, scaling as $\gamma^2 = (1-\beta^2)^{-1}$ according to the general properties of all acceptable fields as satisfying the condition (1), and the same field should also accelerate the electrons to maximize the cross-section of charge conversion along with minimizing that of annihilation. (The latter scales as γ^{-2}; so the ratio of the related probabilities (however small) is proportional to γ^4.) This relationship of the dynamics and the charge conversion implies their common coupling constant. For the same reason charged particles created in the neutral star are to leave the weak interaction region avoiding annihilation.

When the left-handed electron passes the weak interaction region of the star, it has some probability either to turn into the neutrino or to annihilate or to cross this region intact. In the latter case this left-handed electron might be reflected by the exit potential to pass the star center in the opposite direction now as a right-handed one. Being reflected once again, this electron can turn into the neutrino becoming left-handed again, thus sharing the total neutrino flux. This cannot be allowed for the gauge, since the time moment of this electron would differ from that of the normally leaving star electron to result further on in the incorrect initial moment of the newborn electron in the next star. This unwanted process can be suppressed by annihilation of the electron-positron pair when the reflected particles flip their helicity. The related probabilities depend on the value of the weak coupling constant g_L, given the electromagnetic coupling constant e (the subscript L refers to the left-handed electron).

Let us first consider the energy matching dynamics ignoring radiation. In the charged star, the electron is being accelerated from γ_i at the radius r_i, as defined by the finest star cell still possible for the gauge of electron charge, up to some γ_f at $r_{min} \ll r_i$ [10]. As any field satisfying the general motion-to-motion condition (1), the weak field has to satisfy a wave equation [9]. In particular, the finite range weak interaction could be expressed via the Yukawa potential $gr^{-1}\exp(-r/r_{min})$ satisfying the wave equation with an additional "mass" term. For not to disturb the charge gauge, the weak potential should be at most of the order of the Coulomb potential e^2/r at the minimal gauge-defined radius r_{min}. Apart from the short range, parity violation and electric neutrality, the dynamical behavior of weak field should be quite similar to that of electric field, as prescribed by (1). For the estimations let us approximate the weak field Yukawa potential with its averaged factor g^2/r, analogous to the electromagnetic e^2/r, though defined only within the weak field range $r/r_{min} \sim 1$: For $r/r_{min} < 1$, the potential $gr^{-1}\exp(-r/r_{min}) \approx g/r - g/r_{min}$ constant second term being immaterial. We introduce therefore a combined radius r_L, $r_L = (e^2+g_L^2)/mc^2$ to write the following equation for γ in the CM reference system:

$$\gamma^3 = \gamma_f^3 + 3Ar_L\left(\frac{1}{r} - \frac{1}{r_{min}}\right) \tag{9}$$

where $A \approx 10$ represents the force created by all the other particles of the cube star together [10]. In dimensionless variables $\eta_L = 3Ar_L/r_{min}$ and $x = r/r_{min}$ (8) reads:

$$\gamma^3 = \gamma_f^3 + \eta_L\left(x^{-1} - 1\right). \tag{10}$$

In the transition from one star to the next, the electron starting with $\gamma = \gamma_f$ is accelerated by both the electromagnetic and weak forces from r_{min} down to some smaller r', where it turns into the neutrino, which moves to some r'' on the opposite end of the weak region under the weak force only, then this neutrino moves freely to start being accelerated by the weak field of the neutral star at r_{min}, where it turns into the new electron at r'', which finally decelerates by both the electromagnetic and weak fields to become a member of the next star, now at its own r_i, where it must have $\gamma = \gamma_i$. In this oversimplified scenario the total contribution of the weak field over the whole path from the output of one

charged star to the input of the next charged star is zero, and it is the sole electric field, which is active only over its parts, defines the final velocity. In order to obtain a non-zero result also for the weak field, we have to switch it on and off over some parts of the transition. A natural means to realize this switch is to include an intermediate particle with a different mass as its carrier. This is the typical situation for a random process (at least, for a local one [11]), e.g., for quantum mechanics: the described with the wave function particle can be found (with some probability) anywhere at the same moment, still remaining point-like. The required intermediate particle will then have some mass M, the value of which must be large, being defined only within the short weak field range $\Lambda = \hbar/Mc \sim r_{min}$, so describing the transition solely in terms of the charge gauge.

For the energies relevant in our gauge procedure such a massive particle can only be a virtual one, its sole role consisting in correctly transporting the momentum, charge and spin data. For this to be possible, this meson must possess its own charge and polarization, having the spin equal to 1 to preserve the total angular momentum in the charge conversion, since the two other particles — the electron and the neutrino — have spin 1/2. Similarly, transporting the value of momentum as encoded by means of the boson properties implies its motion. Then the moments of creation and decay of the boson must be separated by a time interval, however short due its small velocity for the large mass. The whole transition between the charged stars will now look as follows. In electron at r_{min} having $\gamma = \gamma_f$ is being accelerated to reach the energy $mc^2\gamma'$ at $r = r'$. Here the electron turns into the intermediate boson, non-relativistic because of its large mass, moving with the velocity $v = c(\gamma' 2m/M)^{1/2}$.

Over the characteristic time Λ/c the boson moves a distance of the order $\Lambda(\gamma' 2m/M)^{1/2} \sim r_{min}(\gamma' 2m/M)^{1/2}$ (neglecting acceleration due to its large mass) to turn into the neutrino, moving with the same energy the distance $\sim r_i$ with velocity c to turn back into the boson at $r = r''$ (now measured from the center of the neutral star). Here the newborn electron is being decelerated, again by the electromagnetic and weak forces to reach $\gamma = \gamma_i$ at $r = r_i$ as measured from the center of the next charged star. In order to get in the course of the transition to the required γ_i given γ_f, we put $r'' = r' - r_{min}(\gamma' 2m/M)^{1/2}$ to obtain for the whole transition:

$$\gamma_i^3 = \gamma_f^3 + \eta_L \left(x'^{-1} - \frac{1}{x' - \sqrt{2m/M\gamma'}} \right). \qquad (11)$$

This equation should be supported with the equation for $\gamma' = \gamma(x')$:

$$\gamma'^3 = \gamma_f^3 + \eta_L \left(x'^{-1} - 1 \right). \qquad (12)$$

We eliminate x' from the system of (11) and (12) to obtain:

$$\begin{aligned} F(\gamma', \eta_L) = {} & \gamma_f^3 - \gamma_i^3 \\ & - \frac{\left(\eta_L + \gamma'^3 - \gamma_f^3\right)\sqrt{2m/M\,\gamma'}}{\eta_L - \left(\eta_L + \gamma'^3 - \gamma_f^3\right)\sqrt{2m/M\,\gamma'}} \\ = {} & 0. \end{aligned} \qquad (13)$$

Still, the condition of reducing γ from γ_f to γ_i in the course of the whole transition doesn't define the points r' and r'' of the charge flips uniquely, unless the charge conversion is connected with the related dynamics (otherwise the flip might occur at any point within the weak interaction region), and we look for the maximum of γ' to achieve the maximal ratio (increasing as γ') of the charge conversion cross section to that of the dominating (two-photon) electron/positron annihilation.

The equation (13) implicitly defines $\gamma'(\eta)$ given γ_f and γ_i, and the condition for its maximum $d\gamma'(\eta_L)/d\eta_L = \partial F/\partial\eta_L = 0$ (provided $\partial F/\partial\gamma' \neq 0$ at $\eta_L = \eta_{L(max)}$) yields:

$$\eta_{max} = \left(\gamma'^3_{max} - \gamma_f^3\right)\frac{1 + \sqrt{2m/M\,\gamma'_{max}}}{1 - \sqrt{2m/M\,\gamma'_{max}}}. \qquad (14)$$

Substituting (14) in (13), we obtain the equation for γ'_{max}, given γ_f and γ_i:

$$\gamma'^3_{max} - \left(\gamma_f^3 - \gamma_i^3\right)\frac{\left(1 - \sqrt{2m/M\,\gamma'_{max}}\right)^2}{4\sqrt{2m/M\,\gamma'_{max}}} - \gamma_f^3 = 0. \qquad (15)$$

For the finest lattice as defined by the electron charge gauge, the equation for γ_f is similar to (9), in which, however, the electric force, introduced via $r_e = e/mc$, acts alone:

$$\gamma_f^3 = \gamma_i^3 + 3Ar_e\left(\frac{1}{r_{min}} - \frac{1}{r_i}\right). \qquad (16)$$

In the gauge procedure, the value of γ_i is of great importance, because it is this lowest velocity that mainly contributes to the sensitivity of asymmetry detection in the stars: Since $r_i \gg r_{min}$, it will be: $\gamma_f \gg \gamma_i$ and the exact value of γ_f (since β_f is very close to 1) is but of minor importance in the integration of the disparity between the tetrahedrons [10]. However, γ_f is important in equations (9)-(15).

With resulting from the gauge condition [10] $\gamma_i \sim 3$ and $r_{min} \sim 3\times10^{-3}r_e$, we find from (16): $\gamma_f \sim 30$. Then from (15) and (14): $\gamma'_{max} \sim 50$ and $\eta_{L(max)} \sim 10^5$. This value of $\eta_{L(max)}$ corresponds to $g \sim 2e$, in agreement with the experimental data: $\sin\theta_w \sim 0.5$.

Until now we ignored radiation, and we have to consider its importance. In the gauge process itself, i.e. for $r_i > r > r_{min}$, radiation decreases the value of γ_f, and in the weak field regions, $r_{min} > r > r'$ and $r'' < r < r_{min}$, radiation is active as well. Both effects decrease the related γ's and therefore the probability of the charge conversions.

Whereas only the mean values of mechanical variables (behaving classically) are important in our gauge, as based solely on the top-speed signal oscillations, the analysis of the role of radiation requires the full quantum theory. Indeed, it was shown [10] that in the classical limit, corresponding to multiple soft-photons emission [11], radiation restricts the size of the star for the finest lattice down to the order of r_e. But it is well known that the classical field theory is no longer valid at these distances. Instead, we are bound to calculate only the cross sections for the emission of single photons.

Contrary to the classical limit, single photon radiation in QED occurs only with some probability, i.e. there is also a finite probability for the absence of emission. Only this case is relevant for our gauge, since radiation decreasing the related γ accordingly decreases the proportional to γ ratio of charge conversion cross section to that of annihilation. If the radiation cross section is not too close to unity, the charge conversion events which are not accompanied by radiation might be isolated as providing correct γ_f to γ_i transitions in accord with (11).

In the close vicinity of the star center only some small central part of the wave packet can take a part in the interaction, which is the source of radiation. Therefore, only a small part of the infinite range Coulomb interaction is actually involved, behaving there like a short range interaction. A similar effect in scattering on (neutral) atoms is accounted for by means of "screening" the potential [11, 12]. When the particle interacts with atom, this screening appears as a form factor effectively reducing the range of Coulomb potential to the size of the atom. In the same way, the short range Yukawa potential could be regarded as a screened initially long range fictitious potential, and we consider also the electromagnetic interaction to be screened as well, because now the flux of incoming particles should be normalized for a wave packet of the relevant size rather than for a plane wave. We start with the ultra- relativistic case for the radiation cross section formula in the center-mass system [11]:

$$d\sigma_{rad} = 4\alpha r_e^2 \frac{df}{f}\left(1 - \frac{2}{3}(1-f) + (1-f)^2\right) \times \left(\ln 4\gamma_0^2\left(\frac{1}{f} - 1\right) - \frac{1}{2}\right), \tag{17}$$

where $\alpha = e^2/\hbar c \sim 1/137$ is the fine structure constant $f = \hbar\omega/\epsilon_0$ (ω is the frequency of the emitted photon, ϵ_0 is the energy of the incident electron in the CM system, $\gamma_0 = \epsilon_0/m$). Integrating (17), we find σ_{rad}. The integral diverges for small f. For a simple estimation let us replace $\ln(1/f - 1)$ with its average value Q. Integrating f from some f_{min}, (to be determined later) to 1:

$$\sigma_{rad} = 4\alpha r_e^2\left(Q - \frac{1}{2} + 2\ln 2\gamma_0\right) \times \left(\frac{5}{6} - \frac{4}{3}(\ln f_{min} - f_{min}) - \frac{1}{2}f_{min}^2\right). \tag{18}$$

In the scattering matrix theory, the analysis is carried out over the infinite distances from the interaction region both for initial and final states of the system, so that the incoming and outgoing wave functions are plain waves over the whole continuum, and in the derivation of (17), the integral for the Fourier component of the infinite range Coulomb potential is taken from 0 to ∞. In our case, only radiation events within the star are important, e.g., for $r_i > r > r'$ in the charged star and for $r'' < r < r_{min}$ in the neutral one. We shall therefore accept a model, in which the wave functions outside the interaction regions are still plain waves though bounded laterally to the interaction radii. These functions are given in advance, not taking care of how they were actually prepared. Then we can replace r_e^2 with r_i^2 for the gauge region in (17) and (18), so normalizing the plane wave spinors in the S-matrix element with one particle in r_i^3 rather than in the unit volume, in accord with the flux density of one electron per r_i^2. Similarly, r_{min} will replace r_e for the weak field region. We have also to modify α to account for the weak potential: $\alpha_L = e(e+g_L)/\hbar c$.

It will then be possible to use the Feynman diagram technique to calculate the radiation cross sections. Considering the interactions as existing only in these regions, we calculate the related interaction potential in the momentum representation. In particular, for the pure Coulomb potential $eA_0(q)$ (the time component of the four-vector eA_i) in the gauge region ($r_i > r > r_{min}$) we write (see, e.g., [11]):

$$\begin{aligned} A_0(q) &= -4\pi e\int_{r_{min}}^{r_i} dr\ \exp(iqr) \\ &= \frac{4\pi e}{q^2}\left(\cos(qr_i) - \cos(qr_{min})\right), \end{aligned} \tag{19}$$

where we put the boundary radii instead of usual ∞ and 0. (If r_i were to tend to infinity, the exponential factor with a negative real power should be included in the integrand (to be set zero at the end in order to cancel the first term in the parenthesis, while and the second term becomes unity). In the derivation of (17) (see, e.g., [11, 12]), the argument q has to be set equal to the absolute value of the recoil momentum according to the total four-momentum conservation. In the ultra-relativistic case $q \approx mc/\hbar$, so for the gauge region ($r_i \sim r_e \gg r_{min}$), $qr_i \sim e^2/\hbar c = \alpha \ll 1$, and it follows from (19):

$$A_0(q) = -\frac{2\pi e}{q^2}\alpha^2. \tag{20}$$

Since the S-matrix element is proportional to (20), the radiation cross section (17), proportional to the S-matrix element squared, becomes modified by the additional factor $\alpha \sim 10^{-9}$. In order to obtain the total probability w_{rad} of emission in the interval ($r_i > r > r_{min}$) of a single photon with $f_{min} < f < 1$, the modified according to (20) cross section (18) is to be multiplied by the flux $j = 2v/V$ ($v \approx c$ is the velocity in the CM system, and $V \sim r_i^3$ is the gauge region volume) to obtain the probability for unit time, and then multiplying by r_i/v to find the probability for this region. With all

these substitutions:

$$w_{rad} \approx 4\alpha^5 \left(Q - \frac{1}{2} + 2\ln 2\gamma_0 \right) \times \left(\frac{5}{6} - \frac{4}{3}\left(\ln f_{min} - f_{min}\right) - \frac{1}{2} f_{min}^2 \right). \quad (21)$$

Due to the factor α^5, this probability is very low, unless f_{min} is sufficiently small. For w_{rad} to be of the order of unity, it must be: $\ln(1/f_{min}) \sim \alpha^{-5}$, whatever all other factors in (21) might be. Evidently, such soft photons cannot bring about any changes in the value of γ_f in the gauge region. The same reasoning and with the same conclusion holds in the weak field region for γ'_{max} and η_{max}.

The factor α^4 in (21) suppresses radiation of the electron that does not pass the star center, the nearest vicinity of which provides main contribution to radiation. However, for the electron that passes the center without turning into the neutrino the full radiation cross section must be accounted for. As it follows from (18), the probability of emitting even rather high energy photons is of the order of unity, and it will be collected over a sequence of stars, since radiation can only decelerate the electron. Loosing even a small part of its final energy ($\geq mc^2\gamma_i$), this electron either reaches a lower value of γ_i than allowed for the next stars, or even fails to overcome the exit potential barrier of the last star of a short star sequence, so destroying the gauge lattice.

Although the right-handed electrons take no part in the charge conversion, they might ruin the charge gauge. Indeed, their helicity becomes opposite if they are reflected by the output electromagnetic barrier of the star, and the initially right-handed electron becomes a source of the left-handed neutrino as well. Such oppositely moving neutrinos would make uncertain the choice of the charge sign in the next star, being admixed to the proper antineutrinos generated by the positrons. The flux of these neutrinos could be somewhat suppressed by the electromagnetic electron-positron annihilation, provided the weak interaction acts against the electromagnetic acceleration. So, for the right-handed electron the weak interaction also receives some dynamical meaning.

In order to determine the value of the corresponding coupling constant g_R in the Yukawa potential, we have to find the probability w_{an} of the two-photon electron-positron annihilation when they are decelerated from $\gamma = \gamma_f$ down to $\gamma = 0$ at the turning point. We start with the well-known Dirac's formula for the annihilation cross section in the CM system. In our case it looks:

$$\sigma_{an} = \frac{2\pi r_{min}^2}{\gamma^4\sqrt{\gamma^2-1}}\left[\left(\gamma^4+\gamma^2-\frac{1}{2}\right)\ln\left(\gamma+\sqrt{\gamma^2-1}\right) - \frac{1}{2}\gamma\left(\gamma^2+1\right)\sqrt{\gamma^2-1}\right]. \quad (22)$$

The probability of annihilation w_{an}, increasing with deceleration, depends on the function $\gamma(r)$, which, in turn, depends on r:

$$\gamma^3 = \gamma_f^3 - \eta_R\left(\frac{1}{x} - 1\right) \quad (23)$$

where $\eta_R = 30r_R/r_{min}$, $r_R = (g_R^2 - e^2)/mc^2$, $x = r/r_{min}$. Annihilation probability dw an over the interval dx is:

$$dw_{an} = \sigma_{an}\frac{2v}{r_{min}^2}\,dx. \quad (24)$$

From (22), (23) and (24) we obtain:

$$w_{an} = 12\pi\eta_R\int_1^{\gamma_f} d\gamma \times \frac{\left(\gamma^4-\gamma^2-\frac{1}{2}\right)\ln\left(\gamma+\sqrt{\gamma^2-1}\right)-\frac{1}{2}\gamma\left(\gamma^2+1\right)\sqrt{\gamma^2-1}}{\gamma^2\sqrt{\gamma^2-1}\left(\gamma_f^3+\eta_R-\gamma^3\right)^2}. \quad (25)$$

Given γ_f, this equation defines a function $w_{an}(\eta_R)$, which possesses a maximum. A simple numerical calculation with $\gamma_f \approx 30$ gives: $w_{an}(max) = 0.12$ for $\eta_R(max) \approx 2500$. This value of $\eta_R(max)$ corresponds to $g_R \approx 1.15e$, again in close correspondence with the experimental value of $\cos\theta_w$. In a standard probabilistic approach, this 12% difference is sufficient to reliably discern between particles and antiparticles.

6 Conclusion

In summary, our argument goes as follows:

i. A direct gauge of electric charge using motion-to-motion measurements might be based on the very existence of a (local) top-speed signal, no matter how high this speed is in any units whatsoever.

ii. Letting this signal oscillate between test particles and counting the ratios of the (infinite) numbers of these oscillations, we are able to detect the symmetry of the stars arranged as Platonic solids.

iii. Of the five Platonic solids, only the neutral as a whole cube-symmetrical star, consisting of the two tetrahedrons – one for the electron and another for the positron – is suitable for the electric charge gauge, since it is the only symmetry in which the particles move under electrical interaction along straight lines to cross at their common center.

iv. In order for the electron charge to be gauged as having the same value everywhere, the stars must be arranged in a lattice extended over the whole space-time, in which the initial star arrangement gives rise to its followings by means of the same signal oscillations counting.

v. For this to be possible, the method must uniquely define the transitions in the star sequences; however, the oscillation ratios counting method defines two trajectories rather than only one, and some internal degree of freedom (spin) should be given the particle to make the choice unique.

vi. With our gauge confined to integer charge values and sensitive to deviation from these, however small, beyond the

gauge region, transitions between the stars in the lattice becomes uncertain; however, our charge gauge leaves free some vicinity of the star center, where an additional interaction not destroying the gauge might exist, and it could be used for charge conversion to make this uncertainty immaterial.

vii. The weak interaction realizes the necessary charge conversion with the neutrino that must also provide the necessary information to select a single trajectory out of the two in the next star, their spin projection onto the momentum direction being the sole source for this selection. The transition within the lattice also requires appropriate matching between the in and out energies of the electrons in the succeeding stars; this can be reached only with an intermediate vector boson.

viii. The design of the lattice requires only one conversion of the electric charge, so involving only two charge eigenstates (the SU(2) doublet).

ix. The charge gauge naturally combines the weak and electromagnetic interactions in a single interaction as pertaining to the common cube star, and the numerical relationships between the three coupling constants directly follow from this gauge.

It is fascinating that just the existence of top-speed signals is sufficient to predict the existence of the weak interactions with its range, parity violation and even the intermediate boson, basing solely on Platonic symmetries. The electroweak segment in the standard model suggesting $SU(2)_L \times U(1)$ group with adjusted coupling constants to account for the previously observed in experiments data including parity violation (while PC is still preserved for the leptons) provides good predictions as well. One should appreciate, however, the difference between a theory predicting these features from its own "first principles" and a developed ad hoc theory that only explains, however successfully, already known experimental results. Moreover in other applications, the existence of top-speed signal is sufficient to construct the non-singular part of the Green function (the so-called Huygens' tail) in general relativity [9]. Also, motion-to-motion measurements are relevant in stochastic approach to quantum mechanics [13], in which random scattering on the measuring device, that is realized as a set of macroscopic bodies moving so as to correspond on average to that of the particle in question, leads to the Schrodinger equation: In the form of the Madelung's fluid with its "quantum potential" depending on the same wave function, the external force vector corresponds to the total average acceleration of the particle, that is, the "scattering medium" itself depends also on the own motion of the particle under measurement. One more application of the motion-to-motion gauge helps to explain the existence and masses of the heavy μ- and τ-mesons [14]: In the cube cell, the same gauge regular lattice might occur if one (for the τ) or two (for the μ) electron/positron pairs are being replaced by the heavy mesons. These two sub-symmetries of the cube star may form the whole regular lattice, provided these "foreign" entries move under the mutual acceleration in the cell nearly identically to other electrons and positrons. This situation was found to exist only for some particular values of the mesons' masses, found to be close to experimental data.

We deduce therefore that the pure motion-to-motion gauge eliminating all artificial ingredients (even free falling bodies) and basing only on the (local) existence of top-speed signals provides not only its own interpretation of observations, but it can predict experimental results, otherwise hidden. This is not surprising, since such a gauge is based solely on the very statement of practical problems, and the attached theoretical scheme merely prescribes appropriate notions to address nature. Experiments, as carried out along these lines, can give then nothing but what these notions already imply, in accord with the viewpoint of I. Kant [15] (see also H. Bergson [16]).

Submitted on November 24, 2014 / Accepted on November 28, 2014

References

1. Zeeman E.C. *Topology*, 1967, issue 6, 161.
2. Tselnik F. *Sov. Math. Dokl.*, 1968, v. 9, 1151.
3. Hawking S.W., King A.R., McCarty P.J. *J. Math. Phys.*, 1976, v. 17, 174.
4. Gobel R. *Comm. Math. Phys.*, 1976, v. 46, 289.
5. Fullwood D.T. *J. Math. Phys.*, 1992, v. 33, 2232 and references therein.
6. Ehlers J., Pirani F.A.E. and Schild A. In: General Relativity, ed. by L. O'Raifeartaigh, 1972.
7. Marzke R.F., Wheeler J.A. In: Gravitation and Relativity, ed. by H.Y. Chiu and W.F. Hoffmann, New York, 1964.
8. Tselnik F. Preprint N89-166, Budker Institute of Nuclear Physics, Novosibirsk, 1989.
9. Tselnik F. *Nuovo Cimento*, 1995, v. 110B(12), 1435.
10. Tselnik F. *Communications in Nonlinear Science and Numerical Simulation*, 2005, v. 12(8), 1427.
11. Berestetskii V.B., Lifshitz E.M., Pitaevskii L.P. Relativistic Quantum Theory. Pergamon Press, 1971.
12. Gingrich D.M. Practical Quantum Electrodynamics. Taylor & Francis, 2006.
13. Tselnik F. *Sov. Phys. Dokl.*, 1989, v. 34(7), 634.
14. Tselnik F. Cube star gauge implies the three lepton families (to be published).
15. Kant I. Prolegomena to Any Future Methaphysics. New York, Bobbs-Merrill, 1950.
16. Bergson H. Creative Evolution. London Macmillan, 1911.

Mixed Ion-Electron Conductivity and Superconductivity in Ceramic Electrolytes

Sebastiano Tosto
Retired Physicist. E-mail: stosto44@gmail.com

The paper concerns a theoretical model on the transport mechanisms occurring when the charge carriers generated during the working conditions of a fuel cell interact with point and line defects in a real lattice of solid oxide electrolyte. The results of a model previously published on this topic are here extended to include the tunnelling of carriers within the stretched zone of edge dislocations. It is shown that at temperatures appropriately low the charge transport turns into a frictionless and diffusionless mechanism, which prospects the chance of solid oxide fuel cells working via a superconductive effect.

1 Introduction

The electric conductivity of ceramic electrolytes for solid oxide fuel cells (SOFC) has crucial importance for the science and technology of the next generation of electric power sources. Most of the recent literature on solid oxide electrolytes concerns the effort to increase the ion conductivity at temperatures as low as possible to reduce the costs and enhance the portability of the power cell. The efficiency of the ion and electron transport play a key role in this respect.

In general different charge transfer mechanisms are active during the working conditions of a fuel cell, depending on the kind of microstructure and temperature of the electrolyte. The ion migration in the electrolyte is consequence of the chemical reactions at the electrodes, whose global free energy change governs the charge flow inside the electrolyte and the related electron flow in the external circuit of the cell. Aliovalent and homovalent chemical doping of the oxides affects the enthalpy of defect formation, whose kind and amount in turn control the diffusivity of the charge carriers and thus their conductivity. Particularly interesting are for instance multi-ion [1] and super-ion [2] conduction mechanisms.

Yet in solid oxide electrolytes several reasons allow also the electronic conduction; are important in this respect the non-stoichiometric structures originated by appropriate heat treatments and chemical doping. In general an oxygen vacancy acts as a charge donor, because the two electrons related to O^{-2} can be excited and transferred throughout the lattice. Oxygen deficient oxides have better conductivity than stoichiometric oxides. Typical case is that of oxygen deficient oxides doped with lower valence cations, e.g. ZrO_2 with Y or Ca. As a possible alternative, even oxide doping with higher valence cations enables an increased amount of electrons while reducing the concentration of oxygen vacancies. Besides, an oxide in equilibrium with an atmosphere of gas containing hydrogen, e.g. H_2O, can dissolve neutral H or hydride H^- or proton H^+; consequently the reaction of hydrogen and hydrogen ions dissolved in the oxide with oxygen ions releases electrons to the lattice in addition to the proton conduction.

Mixed ionic–electronic conductors (MIECs) concern in general both ion, σ_i, and hole/electron, σ_{el},conductivities of the charge carriers. Usually the acronym indicates materials in which σ_i and σ_{el} do not differ by more than 2 orders of magnitude [3] or are not too low (e.g. $\sigma_i, \sigma_{el} \geq 10^{-5}$ S cm^{-1}). According to I. Riess [4], this definition can be extended to intend that MIEC is a material that conducts both ionic and electronic charges. A review of the main conduction mechanisms of interest for the SOFC science is reported in [5]. Anyway, regardless of the specific transport mechanism actually active in the electrolyte, during the work conditions of the cell the concentration profiles of the charges generated by the chemical reactions at the electrodes look like that qualitatively sketched in the figure 1.

It is intuitive that the concentration of each species is maximal at the electrode where it is generated. The con-

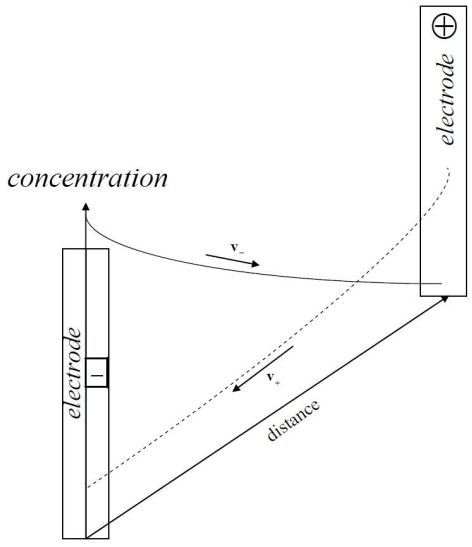

Fig. 1: Qualitative sketch of the concentration profiles of two carriers with opposite charges in the electrolyte as a function of their distance from the electrode where either of them was generated. The profiles represent average diffusion paths, regardless of the local microscopic lattice jumps around the average paths.

centration gradients are sustained by the free energy change of the global reaction in progress; so the charges are subjected to a diffusive driving force $\mathbf{F}_c$ and electric potential gradient driving force $\mathbf{F}_\phi$, the latter being related to the non-uniform distribution of charges at the electrodes. In general both forces control the dynamics of all charge carriers.

This picture is however too naive to be realistic. Dopant induced and native defects in the lattice of the electrolyte can interact together and merge to form more complex defects, in particular when the former and the latter have opposite charges, until an equilibrium concentration ratio of single to complex defects is attained in the lattice. Moreover, in addition to the vacancies and clusters of vacancies, at least two further crystal features are to be taken into account in a real material: the line defects and the grain boundaries, which act as potential barriers to be overcome in order that the ions perform their path between the electrodes. The former include edge and screw dislocations that perturb the motion of the charge carriers because of their stress field; the latter have a very complex local configuration because of the pile up of dislocations, which can result in a tangled dislocation structure that can even trap the incoming ions and polygonized dislocation structure via appropriate annealing heat treatments. For instance hydrogen trapping in tangled dislocations is reported in [6]. Modelling these effects is a hard task; exists in the literature a huge amount of microscopic [7] and macroscopic [8] models attempting to describe the transport mechanisms of the charge carriers through the electrolyte.

The former kind of models implements often quantum approaches to get detailed information on a short range scale of phenomena; their main problem is the difficulty of theoretical approach that often requires drastic approximations, with results hardly extrapolable to the macroscopic behaviour of a massive body and scarcely generalizable because of assumptions often too specific.

The latter kind of models regards the electrolyte as a continuous medium whose properties are described by statistical parameters like temperature, diffusion coefficient, electrical conductivity and so on, which average and summarize a great variety of microscopic phenomena; they typically have thermodynamic character that concerns by definition a whole body of material, and just for this reason are more easily generalized to various kinds of electrolytes and transport mechanisms.

A paper has been published to model realistically the electrical conductivity in ceramic lattices used as electrolytes for SOFCs [9]; the essential feature of the model was to introduce the interaction between charge carriers and lattice defects, in particular as concerns the presence of dislocations. It is known that the diffusion coefficient D of ions moving in a diffusion medium is affected not only by the intrinsic lattice properties, e.g. crystal spacing and orientation, presence of impurities and so on, but also by the interaction with point and line defects. The vacancies increase the lattice jump rate and decrease the related activation energy, thus enhancing the diffusion coefficient; this effect is modelled by increasing purposely the value of D, as the mechanism of displacement of the charge carriers by lattice jumps is simply enhanced but remains roughly the same. More complex is instead the interaction with the dislocation; thinking for simplicity one edge dislocation, for instance, the local lattice distortion due to stress field of the extra-plane affects the path of the ions between the electrodes depending on the orientation of the Burgers vector with respect to the applied electric field. Apart from the grain boundaries, where several dislocations pile up after having moved through the core grain along preferential crystal slip planes, the problem of the line defects deserves a simulation model that extends some relevant concepts of the dislocation science: are known in solid state physics phenomena like dislocation climb and jog, polygonization structures and so on.

From a theoretical point of view, the problem of ion diffusion in real lattices is so complex that simplifying assumptions are necessary. The most typical one introduces a homogeneous and isotropic ceramic lattice at constant and uniform temperature T; in this way D is given by a unique scalar value instead of a tensor matrix. Also, the dependence of D and related conductivity σ upon T are described regardless of their microscopic correlation to the microstructure, e.g. orientation and spacing of the crystal planes with respect to the average direction of drift speed of the charge carriers. Since the present paper represents an extension of the previous results, a short reminder of [9] is useful at this point. The starting points were the mass flow equations

$$\mathbf{J} = -D\nabla c = c\mathbf{v} : \tag{1}$$

the first equality is a phenomenological law that introduces the proportionality factor D, the latter is instead a definition consistent with the physical dimensions of matter flow i.e. $mass/(surface \times time)$. The second Fick law is straightforward consequence of the first one under the additional continuity condition, i.e. the absence of mass sinks or sources in the diffusion medium. Strictly speaking one should replace the concentration with the activity, yet for simplicity the symbol of concentration will be used in the following. The model focuses on a solid lattice of ceramic electrolyte, assumed for simplicity homogeneous and isotropic, where charge carriers are allowed to travel under concentration gradient and electric potential field. It is interesting in this respect the well known Nernst-Einstein equation linking σ to D/k_BT, which has general valence being inferred through elementary and straightforward thermodynamic considerations shortly commented below; so, in the case of mixed electronic-ionic conduction, it holds for ions and expectedly for electrons too, being in effect direct consequence of the Ohm law. Is known the dependence of D on T; the Arrhenius-like form $D = D_0 \exp(-\Delta G/kT)$ via the activation free energy ΔG is due not only to the direct T-dependence of the frequency of lattice jumps inherent D_0, but also to the fact that the temperature controls the amount

and kind of point defects that affect ΔG. The Nernst-Einstein equation has conceptual and practical importance, as it allows calculating how the electrolytes of SOFCs conduct at different temperatures; yet it also stimulates further considerations about the chance of describing the interactions of charges in a crystal lattice via the concept of "effective mass" and the concept of diffusion coefficient in agreement with the Fick laws. This point is shortly highlighted as follows.

It is known that the effective mass m^{eff} of an electron with energy E moving in a crystal lattice is defined by $m^{\text{eff}} = \hbar^2\left(\partial^2 E(k)/\partial k^2\right)^{-1}$, being $k = 2\pi/\lambda$ and λ the wavelength of its De Broglie momentum $p = h/\lambda = \hbar k$. The reason of this position is shortly justified considering the classical energy $E = p^2/2m + U$, which reads $E = \hbar^2 k^2/2m + U$ from the quantum standpoint; $U = U(k)$ is the electron interaction potential with the lattice. If in particular $U = 0$, then m^{eff} coincides with the ordinary free electron rest mass m. Instead the interacting electron is described by an effective mass $m^{\text{eff}} \neq m$; putting $U = \hbar^2 u(k)/m$ and replacing in E, one finds instead $m^{\text{eff}} = m(1 + \partial^2 u/\partial k^2)^{-1}$. In fact the deviation of m^{eff} from m measures the interaction strength of the electron with the lattice; it is also known that by introducing the effective mass, the electron can be regarded as a free particle with good approximation. Owing to the physical dimensions $length^2 \times time^{-1}$ of $\hbar/m$, the same as the diffusion coefficient, it is formally possible to put $D = \hbar q_m/m$ and $D^{\text{eff}} = \hbar q_{m^{\text{eff}}}/m^{\text{eff}}$ via appropriate coefficients q_m and q_m^{eff} able to fit the experimental values of D and D^{eff}.

Rewrite thus m^{eff}/m as

$$\frac{D^{\text{eff}}}{D^*} = 1 + \frac{\partial^2 u}{\partial k^2} \qquad D = \frac{\hbar q_m}{m} \qquad D^* = qD \qquad q = \frac{q_{m^{\text{eff}}}}{q_m}, \quad (2)$$

which calculate D^* and thus D^{eff} as a function of the physical D actually measurable. So, once taking into account the interaction of the electron with the lattice, one could think that the real and effective electron masses correspond to the actual D and effective D^{eff} related to its interaction with the electric field and lattice. Note that the first eq (2) reads

$$D^{\text{eff}} = D^* + D^{\S} \qquad D^{\S} = D^* \frac{\partial^2 u(k)}{\partial k^2}. \quad (3)$$

Clearly the contribution of $D^{\S}$ to the actual diffusion coefficient D^{eff} is due to the kind and strength of interaction of the charge carrier with the lattice; thus D^{eff}, and not the plain D, has physical valence to determine the electrical conductivity of the electrolyte during the operation conditions of the cell: the electron in the lattice is not a bare free particle, but a quasi-particle upon which depends in particular its conductivity. It is known indeed that electrons in a conductor should be uniformly accelerated by an applied electric field, but attain instead a steady flow rate because of their interaction with the lattice that opposes their motion; the resistivity is due to the electron-phonon scattering and interaction with lattice ions, impurities and defects, thermal vibrations. Any change of these mechanisms affects the resistivity; as a limit case, even the superconducting state with null resistivity is due itself to the formation of Cooper pairs mediated just by the interaction between electrons and lattice. Write thus the Nernst-Einstein equation as follows

$$\sigma^{\text{eff}} = \frac{1}{\rho^{\text{eff}}} = \frac{(ze)^2 c D^{\text{eff}}}{k_B T}. \quad (4)$$

The crucial conclusion is that all this holds in principle for any charge carrier, whatever U and m might be. To understand this point, suppose that the interaction potential U depends on some parameter, e.g. the temperature, such that $u = u(k, T)$ verifies the condition $\lim_{T \to T_c} \partial^2 u/\partial k^2 = \infty$ at a critical temperature $T = T_c$. Nothing excludes "a priori" such a chance, as this condition does not put any physical constrain on the macroscopic value of the diffusion coefficient D nor on the related D^*: likewise as this latter is simply D affected by the applied electric field via the finite factor q, the same holds for D^{eff} affected by the lattice interaction upon which depends m^{eff} as shown in the eq (2). Thus the limit $\lim_{T \to T_c} (D^{\text{eff}}/D) = \infty$ concerns $D^{\S}$ only. Being $q_m > 0$ and $q_m^{\text{eff}} > 0$ but anyway finite, the divergent limit is not unphysical, it merely means that at $T = T_c$ the related carrier/lattice interaction implies a new non-diffusive transport mechanism; this holds regardless of the actual value of D, which still represents the usual diffusion coefficient in the case of carriers ideally free or weakly interacting with the lattice in a different way, e.g. via vacancies only. In conclusion are possible two diverse consequences of the charge carrier/lattice defect interactions: one where $D^{\S} \neq D$, i.e. the presence of defects simply modifies the diffusion coefficient, another one where the usual high temperature diffusive mechanism is replaced by a different non-diffusive mechanism characterized by $D^{\S} \to \infty$, to which corresponds $\rho^{\text{eff}} \to 0$ at $T = T_c$. Two essential remarks in this respect, which motivate the present paper, concern:

(i) The quantum origin of both eqs (1) is inferred in [10]; this paper infers both equations as corollaries of the statistical formulation of quantum uncertainty. Has been contextually inferred also the statistical definition of entropy $S = -\sum_j \pi_j \log(\pi_j)$ in a very general way, i.e. without hypotheses about the possible gaseous, liquid or solid phase of the diffusion medium. It has been shown that the driving force of diffusion is related to the tendency of a thermodynamic system in non-equilibrium state because of the concentration gradients towards the equilibrium corresponding to the maximum entropy, whence the link between diffusion propensity and entropy increase.

(ii) The result $D^{\text{eff}} = D^{\S} + D^*$, actually inferred in [9]: the interaction of the charge carrier with the stress field of one edge dislocation defines an effective diffusion coefficient D^{eff} consisting of two terms, D^* related to its interaction with the

electric potential of the cell and $D^{\S}$ related to its chemical gradient and interaction with the stress field of the dislocation.

The concept of D^{eff} is further concerned in the next section to emphasize that the early ideas of Fick mass flow, which becomes now effective mass flow, and Einstein D^{eff}-dependent conductivity are extendible to and thus still compatible with the limit case $D^{\S} \to \infty$.

In summary $D_{id} \to D \to D^{*} \to D^{\text{eff}}$ are the possible diffusion coefficients of each charge carrier concerned in [9]: D_{id} is that in an ideal defect free lattice, D that in a lattice with point defects only, D^{*} in the given lattice with an applied electric potential, D^{eff} in a real lattice with dislocations under an applied electric potential. The chance of extrapolating the equation (4) to the superconducting state, despite this latter has seemingly nothing to do with the diffusion driven charge displacement, relies on two logical steps.
The first step is to acknowledge that $D^{\text{eff}} = D^{\S} + D$ is required by the presence of dislocations, because D^{eff} cannot be defined simply altering the value of the plain D; the reason of it has been explained in [9] and is also summarized in the next section for clarity.

To elucidate the second step, consider preliminarily $D \to D^{\text{eff}}$ simply because $D^{\S} \gg D$: in this case the finite contribution $D^{\S}$ due to the charge/dislocation interaction can be accepted without further problems.

Suppose that a valid physical reason allows a charge carrier to move as a free particle in the lattice, regardless of the concentration gradient or applied potential difference or force $\mathbf{F}$ of any physical nature; in this extreme case, the condition $\rho^{\text{eff}} \to 0$ necessarily results by consequence and requires itself straightforwardly $D^{\S} \to \infty$ in the Nernst-Einstein equation. In other words, the second step to acknowledge the divergent value of $D^{\S}$ is to identify the peculiar interaction mechanism such that the charge carrier behaves effectively in the lattice as a free particle at a critical temperature T_c: the existence of such a mechanism plainly extrapolates to the superconducting state the eq (4), which is thus generalized despite the link between σ and D is usually associated to a diffusive mechanism only.

The present paper aims to show that thanks to the fact of having introduced both point and line lattice defects in the diffusion problem, the previous model can be effectively extended to describe even the ion superconducting state in ceramic electrolytes. It is easy at this point to outline the organization of the present paper: the section 2 shortly summarizes the results exposed in [9], in order to make the exposition clearer and self-contained; the sections 3 and 4 concern the further elaboration of these early results according to the classical formalism. Eventually the section 5 reviews from the quantum standpoint the concepts elaborated in section 4. Thus the first part of the paper concerns in particular the usual mechanism of charge transport via ion carriers, next the results are extended to the possible superconductivity effect described in the section 5. A preliminary simulation test in the section 5.1 will show that the numerical results of the model in the particular case where the charge carrier is just the electron match well the concepts of the standard theory of superconductivity.

2 Physical background of the model

The model [9] assumes a homogeneous and isotropic electrolyte of ceramic matter at uniform and constant temperature everywhere; so any amount function of temperature can be regarded as a constant. The electrolyte is a parallelepiped, the electrodes are two layers deposited on two opposite surfaces of the parallelepiped. The following considerations hold for all charge carriers; for simplicity of notation, the subscript i that numbers the i-th species will be omitted. Some remarks, although well known, are shortly quoted here because useful to expose the next considerations in a self-contained way. Merging the flux definition $\mathbf{J} = c\mathbf{v}$ and the assumption $\mathbf{J} = -D\nabla c$ about the mass flux yields $\mathbf{v} = -D\nabla \log(c)$. Introduce then the definition $\mathbf{v} = \beta\mathbf{F}$ of mobility β of the charge carrier moving by effect of the force $\mathbf{F}$ acting on it; one infers both $D = k_B T\beta$ and $\mathbf{F} = -\nabla\mu$ together with $\mu = -k_B T \log(c/c_o)$. An expression useful later is

$$\mathbf{F} = \frac{k_B T}{D}\mathbf{v} = \frac{k_B T}{Dc}\mathbf{J}. \tag{5}$$

So the force is expressed through the gradient of the potential energy μ, the well known chemical potential of the charge carrier. The arbitrary constant c_o is usually defined as that of equilibrium; when c is uniform everywhere in the diffusion medium, the driving force of diffusion vanishes and the Fick law predicts a null flow of matter, which is consistent with $c \equiv c_o$. Another important equation is straightforward consequence of the link between mass flow and charge flow; since the former is proportional to the number of charged carriers, each one of which has charge ze, one concludes that $\mathbf{J}_{ch} = ze\mathbf{J}$ and so $\beta_{ch} = ze\beta$. Let the resistivity ρ be summarized macroscopically by Ohm's law $\rho\mathbf{J}_{ch} = -\nabla\phi = \mathbf{E}$; i.e. the charge carrier interacts with the lattice while moving by effect of the applied electric potential ϕ and electric field $\mathbf{E}$. The crucial eq (4) is inferred simply collecting together all statements just introduced in the following chain of equalities

$$\mathbf{J}_{ch} = \sigma\mathbf{E} = zec\mathbf{v} = zec\beta_{ch}\mathbf{E} =$$

$$= (ze)^2 c\beta\mathbf{E} = \frac{(ze)^2\mathbf{E}cD}{k_B T} = -\frac{cDze\nabla\phi}{k_B T}. \tag{6}$$

Moreover the effect of an electric field on the charge carriers moving in the electrolyte is calculated through the last sequence of equalities recalling that the electric and chemical forces are additive. Consider thus the identity

$$\mathbf{F}_{tot} = -\nabla\mu - \alpha ze\nabla\phi = -\frac{k_B T}{c}\left(\nabla c + \alpha\frac{zec\nabla\phi}{k_B T}\right)$$

where α is the so called self-correlation coefficient ranging between 0.5 to 1; although usually taken equal to 1 and omitted [11], it is quoted here by completeness only. Recalling the mobility equation $k_BT/c = D/\beta c$ and noting that $\mathbf{F}\beta c$ is just a mass flow, the result is

$$\mathbf{J}_{tot} = -D\left(\nabla c + \alpha\frac{zec}{k_BT}\nabla\phi\right) = \frac{cD}{k_BT}\left(\nabla\mu - \alpha ze\nabla\phi\right). \qquad (7)$$

So far D has been introduced without mentioning the diffusion medium, in particular as concerns its temperature and the presence of lattice defects of the ceramic crystal. As the point defects simply increase the frequency of lattice jumps [12] and thus the value of the diffusion coefficient, in these equations D is assumed to be just that already accounting for the vacancy driven enhancement. As concerns the presence of edge and screw dislocations also existing in any real crystal, the paper [9] has shown that in fact the dislocations modify significantly the diffusion mechanism in the electrolyte: their stress field hinders or promotes the charge transfer by creating preferential paths depending on the orientation of the dislocation stress field with respect to the electrode planes. In particular the dislocation affects the mobility of the charge carriers, as it is intuitive to expect: phenomena like the climbing, for instance, occur when a dislocation or isolated atoms/ions move perpendicularly to the extra plane of another dislocation to overcome the compression field due to the local lattice distortion. Moreover, in the case of edge dislocations the figure 2 shows the possibility of confinement of light atoms, e.g. typically C and N, along specific lattice directions perpendicular to the Burgers vector; this emphasizes the importance of the orientation of grains and dislocations with respect to the average path of the charges between the electrodes.

Assume first one lonely dislocation in a single crystal lattice; this case allows a preliminary assessment of the interaction between charge carriers travelling the lattice in the presence of an applied potential field. In the case of edge dislocation the shear stress component on a plane at distance y above the slip plane is known to be $\sigma_{xy} = [8\pi y(1-\nu)]^{-1}Gb\sin(4\theta)$, being ν the Poisson modulus, G the shear modulus, $b = |\mathbf{b}|$ and $\mathbf{b}$ the Burgers vector, θ is the lattice distortion angle induce by the extra plane on the neighbour crystal planes [13]. Moreover the modulus of the force per unit length of such dislocation is $F^{(d)} = b\sigma_{xy}$, where the superscript stands for dislocation. Hence, calling $l^{(d)}$ the length of the extra plane, the force field due to one dislocation is

$$\mathbf{F}^{(d)} = [8\pi y(1-\nu)]^{-1}Gb^2 l^{(d)}\sin(4\theta)\mathbf{u}_b$$

where $\mathbf{u}_b$ is a unit vector oriented along the Burger vector, i.e. normally to the dislocation extra plane. It is known that atom exchange is allowed between dislocations; the flow $\mathbf{J}$ of these atoms within a lattice volume Ω is reported in the literature to be

$$\mathbf{J} = D_L\nabla\mu/(\Omega k_BT) \qquad \mu = -kT\log(c_\Omega),$$

being μ the chemical potential and D_L the appropriate diffusion coefficient; for clarity are kept here the same notations of the original reference source [14]. Actually this flow is straightforward consequence of the Fick law, as it appears noting that the mass m_Ω of atoms within the volume Ω of lattice corresponds by definition to the average concentration $c_\Omega = m_\Omega/\Omega$; so the atom flow between dislocations at a mutual distance consistent with the given Ω is nothing else but the diffusion law $\mathbf{J}_\Omega = -D_L\nabla c_\Omega$ itself, as it is shown by the following steps

$$\begin{aligned}\mathbf{J}_\Omega &= -D_L\nabla c_\Omega = -c_\Omega D_L\nabla\log(c_\Omega)\\ &= \frac{c_\Omega D_L}{k_BT}\nabla\mu = \frac{m_\Omega}{\Omega}\frac{D_L}{k_BT}\nabla\mu.\end{aligned} \qquad (8)$$

Thus the flow $\mathbf{J} = \mathbf{J}_\Omega/m_\Omega$ reported in the literature describes the number of atoms corresponding to the pertinent diffusing mass. The key point of the reasoning is the appropriate definition of the diffusion coefficient D_L, which here is that of a cluster of atoms of total mass m_Ω rather than that of one atom in a given matrix. Once having introduced $\mathbf{F}^{(d)}$, it is easy to calculate how the flow of the charge carriers is influenced by this force field via the related quantities $D^{(d)} = k_BT\beta^{(d)}$ and $\mathbf{v}^{(d)} = \beta^{(d)}\mathbf{F}^{(d)}$; in metals, for instance, it is known that the typical interaction range of a dislocation is of the order of 10^{-4} cm [13]. The contribution of this exchange to the charge flow is reasonably described by $\mathbf{J}^{(d)} = \mathbf{F}^{(d)}D^{(d)}c/k_BT$ according to the eq (5). Consider now $\mathbf{F}^{(d)}$ as the average field due to several dislocations, while the same holds for $\beta^{(d)}$ and $D^{(d)}$, which are therefore related to the pertinent $\sigma^{(d)}$; omitting the superscript to simplify the notation, eq (7) reads thus

$$\mathbf{J}_{tot} = -D\left(\nabla c + \alpha\frac{zec}{k_BT}\nabla\phi - \frac{c\mathbf{F}}{k_BT}\right)$$

$$\mathbf{F} = <\mathbf{F}^{(d)}(G,\nu,l^{(d)},\mathbf{b})>. \qquad (9)$$

In this equation D has the usual statistical meaning in a real crystal lattice and includes the electric potential as well. Here the superscript has been omitted because also $\mathbf{F}$ denotes the statistical average of all the microscopic stress fields $\mathbf{F}^{(d)}$ existing in the crystal. One finds thus with the help of the continuity condition

$$\nabla\cdot\left[D\left(\nabla c + \alpha\frac{zec}{k_BT}\nabla\phi - \frac{c\mathbf{F}}{k_BT}\right)\right] = \frac{\partial c}{\partial t} \qquad D = D(T,c,t) \quad (10)$$

where c and $\mathbf{v}$ are the resulting concentration and drift velocity of the i-th charge carrier in the electrolyte. In general the diffusion coefficient depends on the local chemical composition and microstructure of the diffusion medium. Moreover the presence of $\mathbf{F}$ into the general diffusion equation is required to complete the description of the charge drift through a real ceramic lattice by introducing a generalized thermodynamic force, justified from a microscopic point of view and

thus to be regarded also as a statistical macroscopic parameter. This force, considered here as the average stress field resulting from the particular distribution of dislocation arrays in the lattice, accounts for the interaction of a charge carrier with the actual configuration of lattice defects and is expected to induce three main effects: (i) to modify the local velocity $\mathbf{v}$ of the charge carrier, (ii) to modify the local concentration of the carriers (recall for instance the "Cottrel atmospheres" that decorate the dislocation), (iii) to modify the local electric potential because altering the concentration of charged particles certainly modifies the local ϕ. Accordingly, considering again the average effects of several dislocations in a macroscopic crystal, it is reasonable to write

$$\frac{c\mathbf{F}}{k_BT} = \frac{mc\dot{\mathbf{v}}}{k_BT} + a\nabla c + \mathbf{\Gamma}$$
$$\dot{\mathbf{v}} = \dot{\mathbf{v}}(c) \qquad \mathbf{\Gamma} = \mathbf{\Gamma}(c, \phi_o) \qquad c = c(x, y, z, t, T)$$

being a a proportionality constant. The first addend at right hand side accounts for the effect (i), the second for the effect (ii), the vector $\mathbf{\Gamma}$ for the effect (iii) because it introduces the local potential ϕ_o due to the charges piled up around the dislocation; the dependence of these quantities on c of the pertinent carrier emphasizes the local character of the respective quantities depending on the time and space coordinates. The final step is to guess the form of $\mathbf{\Gamma}$ in order to introduce in the last equation the electrochemical potential $\alpha\phi + \mu/ze$ inferred from the eq (7) . As motivated in [9], $\mathbf{\Gamma}$ is defined as a local correction of ϕ because of the concentration of the charge carriers; with the positions

$$\mathbf{\Gamma} = \frac{c\alpha}{k_BT}\nabla(ze\phi + \mu) - \frac{ze\phi_o\alpha}{k_BT}\nabla c \qquad a = 1 - \alpha$$

eq (10) turns into

$$\nabla \cdot \left[\frac{m\mathbf{v}}{k_BT}\frac{\partial(cD)}{\partial t} + \frac{ze\phi_o\alpha}{k_BT}D\nabla c\right] = \frac{\partial C}{\partial t} \tag{11}$$

where

$$C = c + \frac{m}{k_BT}\nabla \cdot (cD\mathbf{v}) \qquad \phi_o = \phi_o(x, y, z, t).$$

The function ϕ_o has physical dimensions of electric potential. Eventually, owing to this definition of C, the last equation reads

$$\nabla \cdot \left[(D^* + D^{\S})\nabla C\right] = \frac{\partial C}{\partial t} \tag{12}$$

being

$$D^* = \frac{ze\phi_o}{k_BT}\alpha D \qquad \frac{m}{k_BT}\frac{\partial(cD)}{\partial t}\mathbf{v} = D^*\nabla(C - c) + D^{\S}\nabla C.$$

These considerations show that it is possible to define an effective diffusion coefficient in the presence of an applied potential ϕ and taking into account the presence of point and line defects

$$D^{\text{eff}} = D^* + D^{\S}. \tag{13}$$

This equation is equal to that inferred via the effective mass of the charge carrier interacting with the lattice, see the eq (3); $D^{\S}$ is defined by the last eq (12) accounting via C for the presence of dislocations in a real ceramic electrolyte. Accordingly, the equation (13) is modified as follows

$$\frac{D^{\text{eff}}}{D} = \alpha\frac{ze\phi_o}{k_BT} + \frac{D^{\S}}{D} \qquad \sigma^{\text{eff}} = \frac{1}{\rho^{\text{eff}}} = \frac{D^{\text{eff}}}{D}\sigma. \tag{14}$$

The solution of the eq (10) via the eq (12) to find the analytical form of the space and time profile of c is described in [9]; it is not repeated here because inessential for the purposes of the present paper. Have instead greater importance the result (13) and the following equations inferred from the eqs (11) and (12)

$$\nabla \cdot (cD\mathbf{v}) = 0, \qquad C \equiv c, \qquad \mathbf{v} = \frac{k_BT}{m}\frac{D^{\S}}{\partial(cD)/\partial t}\nabla c. \tag{15}$$

The consistency of the first equation with the eq (12) has been therein shown. This condition requires that the vector $cD\mathbf{v}$, having physical dimensions of energy per unit surface, is solenoidal i.e. the net flow of carriers crossing the volume enclosed by any surface is globally null; this holds for all carriers and means absence of source or sinks of carriers around any closed surface. Note that this condition is fulfilled by

$$\mathbf{v} = \frac{\mathbf{B}}{cD} \tag{16}$$

with

$$\mathbf{B} = \mathbf{i}B_x(y, z, t) + \mathbf{j}B_y(x, z, t) + \mathbf{k}B_z(x, y, t) \qquad |\mathbf{B}| \to \frac{energy}{surface}.$$

The vector $\mathbf{B}$ is defined by arbitrary functions whose arguments depend on the coordinate variables as shown here: at any time and local coordinates the functions expressing the components of $\mathbf{B}$ can be appropriately determined in order to fit the corresponding values of $\mathbf{v}cD$ resulting from the solution of the eq (10). Hence the positions (15) do not conflict with this solution, whatever the analytical form of $\mathbf{v}$ and c might be; the third equality (15) defines $D^{\S} = D^{\S}(c, D, \mathbf{v}, T)$. The central result to be implemented in the present model is

$$\mathbf{v} = \frac{k_BT}{\eta}D^{\S}\frac{\nabla c}{m} = \Omega D^{\S}\nabla n \tag{17}$$

where

$$\eta = \frac{\partial(cD)}{\partial t} \qquad n = \frac{c}{m} \qquad \Omega = \frac{k_BT}{\eta}$$

with n numerical density of the given carrier and η energy density corresponding to the time change of cD; the volume Ω results justified by dimensional reasons and agrees with the fact that the diffusion process is thermally activated. Moreover one finds

$$\mathbf{v} = \frac{\mathbf{B}}{cD} = \frac{\Omega}{m}D^{\S}\nabla c = D^{\S}\frac{\nabla c}{c} \qquad m = c\Omega. \tag{18}$$

Owing to the importance of the third eq (15) for the purposes of the present paper, it appears useful to verify its validity; this check is shortly sketched below by demonstrating its consistency with relevant literature results.

First of all, the eq (17) leads itself to the literature result (8); the key points are the definition of mobility β and its relationship to the diffusion coefficient $\beta = D/kT$ previously reported in the eq (5). Let the atom exchange between dislocations be thermally activated, so that holds the last eq (17). Being $\mathbf{v} = D^{\S}\nabla\mu/k_BT$ according to the eq (18), then $D_L\mathbf{F}/k_BT = -D^{\S}\nabla\mu/k_BT$ specifies $D_L \equiv D^{\S}$, i.e. the diffusion coefficient is that pertinent to the interaction of atoms with the concerned dislocations; moreover the force $\mathbf{F} \equiv -\nabla\mu$ acting on the atoms corresponds to the change of chemical potential related to the migration of the atoms themselves. Since these relationships are directly involved in the Fick equation inferred in section 1, it follows that the eq (15) fits well the model of concentration gradient driven diffusion process.

Furthermore let us show that eq (15) implies the link between $\nabla\mu$ and the stress τ that tends to move preferentially dislocations with Burgers vector favourably oriented in a crystal matrix, e.g. perpendicularly to a tilt boundary plane [14]; this stress produces thus a chemical potential gradient between adjacent dislocations having non-perpendicular component of the Burgers vector. Once more D to be implemented here is just the diffusion coefficient $D^{\S}$ pertinent to the interaction with the dislocation and thus appropriate to this specific task. Assuming again $k_BT/\eta \approx \Omega$, then $\mathbf{F} = -\nabla\mu$ yields $\mathbf{F}\Omega = -(k_BT/\eta)\nabla\mu$. If two dislocations are at a distance d apart, then $\Omega = Ad/2$ for each dislocation, being A the surface defined by the length L of the dislocations and the height of their extra-planes; so Ad is the total volume of matrix enclosed by them, whereas $Ad/2$ is the average volume defined by either extra-plane and its average distance from an equidistant atom, assumed $d/2$ apart from each dislocation. Being $2\mathbf{F}\Omega/(Ad) = -\nabla\mu$, the conclusion is that $2\tau\Omega/d = -\nabla\mu$ with $\tau = \mathbf{F}/A$, which is indeed the result reported in [14].

Finally let us calculate with the help of the eq (15) also the atom flux $\mathbf{I} = A\mathbf{J}/m$ between dislocations per length of boun-dary of cross section A in direction parallel to the tilt axis. The following chain of equations

$$\mathbf{I} = -\frac{AD_L\nabla c}{m} = -\frac{AD_L\nabla c}{c\Omega} = -\frac{AD_L\nabla\log(c)}{\Omega} =$$

$$= \frac{D_LA\nabla\mu}{k_BT\Omega} = -\frac{2D_L\mathbf{F}}{k_BTd} = -\frac{2D_LL\tau}{k_BT} \qquad \tau = \frac{\mathbf{F}}{Ld}$$

yields the literature result $-2D_L\tau/kT$ per unit length of dislocation [14].

All considerations carried out from now on are self-contained whatever the analytical form of c might be. In the following the working temperature T of the cell is always regarded as a constant throughout the electrolyte.

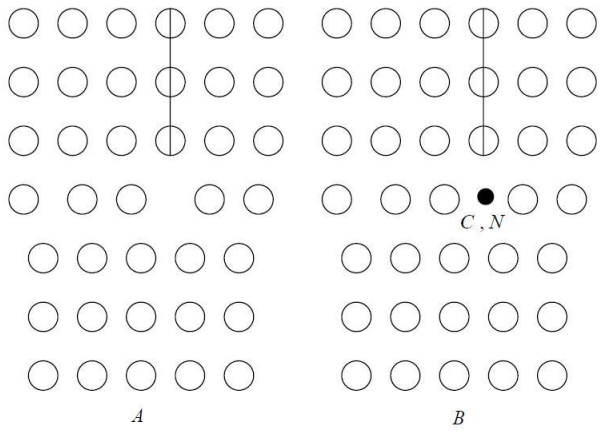

Fig. 2: A: Cross section of the stretched zone of an edge dislocation at the interface between the lower boundary of the extra plane and the perfect lattice. B: Equilibrium position of an atom, typically carbon or nitrogen, in the stretched zone after stress ageing.

3 Outline of the charge transport model

In general, the macroscopic charge flow within the electrolyte of a SOFC cell is statistically represented by average concentration profiles of all charges that migrate between the electrodes. The profiles of the ions during the working condition of the cell, qualitatively sketched in the fig. 1, are in effect well reproduced by that calculated solving the diffusion equation (12) [9]. The local steps of these paths consist actually of random lattice jumps dependent on orientation, structure and possible point and line defects of the crystal grains forming the electrolyte, of course under the condition that the displacement of the charge carriers must be anyway consistent with the overall formation of neutral reaction products. So $\mathbf{v}$ and ∇n of the eqs (17) are average vectors that consist actually of local jumps dependent on how the charge carriers interact each other and with lattice defects, grain boundaries and so on. The interaction of low sized light atoms and ions with the lattice distortion due to the extra plane of a dislocation has been concerned in several papers, e.g. [15]: the figure 2A shows the cross section of the stretched zone of an edge dislocation, the fig. 2B the location of a carbon atom in the typical configuration of the Cottrell atmosphere after strain ageing of bake hardenable steels. The segregation of N and C atoms, typically interstitials, on dislocations to form Cottrell atmospheres is a well known effect; it is also known that after forming these atmospheres, energy is required to unpin the dislocations: Luders bands and strain ageing are macroscopic evidences of the pinning/unpinning instability. These processes are usually activated by temperature and mechanical stresses.

Of course the stress induced redistribution and ordering of carbon atoms has 3D character and has been experimentally

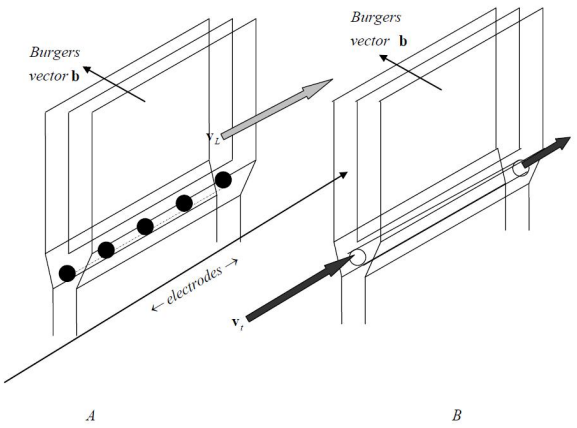

Fig. 3: 3D representation of the static Cottrell configuration of several carbon atoms after interaction with the stress field of an edge dislocation. B: dynamical flow of charge carriers that tunnel along the length of the extra plane of the dislocation.

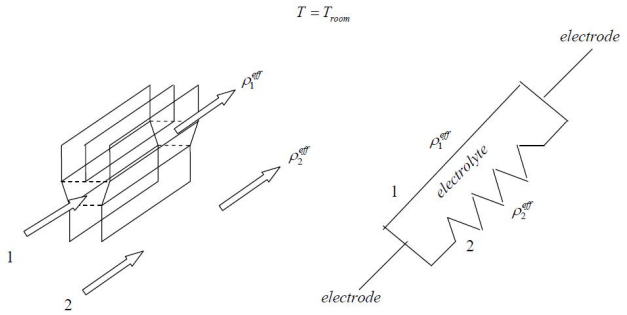

Fig. 4: Shunt effect of charge carriers between dislocation path and lattice path of different resistivity. On the left is sketched the possible path within and in proximity of the stretched zone of an edge dislocation; on the right is shown the corresponding electric circuit of the currents crossing the electrolyte.

verified in ultra low carbon steels; the configuration reported in the literature and redrawn in fig 3A explains the return to the sharp yield point of the stress-strain curve of iron [16].

The chance that light atoms line up into the strained zone of an edge dislocation is interesting for its implications in the case of mixed conductivity in ceramic electrolytes. It is reasonable to guess that the aligned configuration sketched in fig. 3A is in principle also compatible with the path of mobile charge carriers displacing along this transit trail, as represented in the fig. 3B. Among all possible paths, the next section concerns in particular the conduction mechanism that occurs when low atomic number ions tunnel along the stretched zone at the interface between the extra-plane of an edge dislocation and the underlying perfect lattice. The mechanism related to this specific configuration of charges involves directly the interaction of the carriers with the dislocation and thus is described by the eq (15), which indeed depends explicitly upon $D^{\S}$. From a classical point of view, is conceivable in principle an ideal fuel cell whose electrolyte is a ceramic single crystal with one edge dislocation spanning the entire distance between the electrodes; in this particular case, therefore, is physically admissible a double conduction mechanism based on the standard diffusive process introduced in [9] plus that of ion tunnelling throughout the whole electrolyte size. Regarding the tunnel path and the whole lattice path as two parallel resistances, the Kirchhoff laws indicate how the current of charge carriers generated at the electrodes shunts between either of them. This is schematically sketched in the figure 4.

The tunnel mechanism appears reasonable in this context considering the estimated electron and proton classical radii, both of the order of 10^{-15} m, in comparison with the lattice spacing, of the order of some 10^{-10} m. A short digression about the atom and ion sizes with respect to the crystal cell parameter deserves attention. Despite neither atoms nor ions have definite sizes because of their electron clouds lack sharp boundaries, their size estimate allowed by the rigid sphere model is useful for comparison purposes; as indeed the Cottrel atmospheres of C and N atoms have been experimentally verified, the sketch of the fig. 3A suggests by size comparison a qualitative evaluation about the chance of an analogous behaviour of ions of interest for the fuel cells. The atomic radius is known to be in general about 10^4 times that of the nucleus, the radii of low atomic number elements typically fall in the range $1 \div 100$ pm [17]. Specifically, the covalent values for C, N and O atoms are 70, 65 and 60 pm respectively; it is known that they decrease across a period. The ionic radii of low atomic number elements are typically of the order of 100 pm [18]; they are estimated to be 0.1 and 0.14 nm for Na^+ and $O^=$. It is known that the average lattice parameters of solid oxides increase about linearly with cationic radii [19]; typical values of lattice average spacing are of the order of 0.5-0.6 nm. As the stretched zone of a dislocation has size necessarily greater than the unstrained spacing, one reasonably concludes that, at least in principle, not only the proton and nitrogen and carbon atoms but even oxygen ions have sizes compatible with the chance of being accommodated in the stretched zone underlying the dislocation extra-plane. These estimates suggest by consequence that even low atomic number ion conduction via channelling mechanism along the stretched zone of the dislocation is reasonably possible. It is known that proton conducting fuel cells typically work with protons crossing of polymer membranes from anode to cathode, whereas in-SOFCs oxygen ions migrate through the ceramic electrolyte from cathode to anode; yet the tunnelling mechanism seems in principle consistent with both kinds of charge carriers in typical SOFC electrolytes.

Consider now the case where the driving energy of the segregation process of atoms to dislocations is not only the lattice strain of the ceramic electrolyte but, during the working cycle of a fuel cell, also the free energy that generates ions at the electrodes and compels them migrating by effect of the electric potential; the alignment of several ions confined along the dislocation length sketched in fig. 3A has thus a dynamical valence, i.e. it suggests the specific displacement mechanism that involves the tunnelling of ions throughout the stretched zone of an edge dislocation at its boundary with the perfect lattice. In other words, one can think that the line of foreign light ions along this zone is also compatible with the particular migration path of such ions generated at either electrode; certainly the proton is a reasonable example of carrier compliant with such particular charge transport mechanism, as qualitatively sketched in fig. 3B. These considerations explain the difference between D, the usual diffusion coefficient of a given ion in a given lattice with or without point defects, and D^{eff}, which in this case is the effective diffusion coefficient of the same ion that moves confined in the stretched zone of the dislocation. This conclusion agrees with and confirms the idea that the electric conductivity is related to D^{eff} and not to D, because the former only accounts for this particular kind of interaction between charge carrier and dislocation. Also, just for this reason in the fig. 4 the resistivity of ions with different kind of interaction with the dislocation, i.e. inside it along the stretched zone and outside it in the lattice compression zone, have been labelled respectively ρ_1^{eff} and ρ_2^{eff}. Despite D^{eff} is related generically to any interaction mechanism possible when charge carriers move in the presence of dislocations, it will be regarded in the following with particular reference to the charge tunnelling mechanism just introduced.

4 Classical approach to elaborate the early results [9]

The experimental situation described in this section, in principle possible, is the one of a unique edge dislocation crossing throughout the single crystal ceramic electrolyte and arbitrarily inclined with respect to plane parallel electrodes. The following discussion concerns the eq (17) and consists of two parts: the first part has general character, i.e. it holds at any point of the ceramic lattice, in which case the presence of the dislocation merely provides a reference direction to define specific components of $\mathbf{v}$; the second part aims to describe the particular mechanism of transport of charges that tunnel along the stretched zone of the dislocation, which in fact is the specific case of major interest for the present model.

4.1 Charge transport in the electrolyte lattice

Regard in general the drift velocity $\mathbf{v}$ of a charge carrier as due to a component $\mathbf{v}_\parallel$ parallel to the tunnelling direction and a component $\mathbf{v}_\perp$ perpendicular to $\mathbf{v}_\parallel$; so the eq (17) yields

$$\mathbf{v} = \mathbf{v}_\parallel + \mathbf{v}_\perp \qquad \mathbf{v}_\parallel \eta = k_B T D_\parallel^{\S} \nabla n \pm \eta' \mathbf{v}_a \tag{19}$$

$$\mathbf{v}_\perp \eta = k_B T D_\perp^{\S} \nabla n \mp \eta' \mathbf{v}_a \qquad D_\parallel^{\S} + D_\perp^{\S} = D^{\S}$$

where η' has physical dimensions of energy per unit volume and $\mathbf{v}_a$ is an arbitrary velocity vector: with the given signs, the third equation is fulfilled whatever $\mathbf{v}_a$ and η' might be. Of course the components of $\mathbf{v}$ are linked by

$$\mathrm{v} = \sqrt{\mathrm{v}_\parallel^2 + \mathrm{v}_\perp^2} \qquad \mathbf{v}_\perp = \left(\mathbf{u}_\parallel - \frac{\mathbf{u}_o}{\mathbf{u}_o \cdot \mathbf{u}_\parallel}\right)\mathrm{v}_\parallel \qquad \mathbf{u}_\parallel = \frac{\mathbf{v}_\parallel}{\mathrm{v}_\parallel} \tag{20}$$

with $\mathrm{v} = |\mathbf{v}|$ given by the solution of the set (12) of diffusion equations; the same notation holds for the moduli $\mathrm{v}_\parallel$ and $\mathrm{v}_\perp$. The arbitrary unit vector $\mathbf{u}_o$ is determined in order to satisfy the first equation; trivial manipulations yield indeed

$$\mathrm{v} = \frac{\mathrm{v}_\parallel}{\cos\varphi} \qquad \mathrm{v}_\perp^2 = \mathrm{v}_\parallel^2 \left(\frac{1}{\cos^2\varphi} - 1\right) \qquad \mathbf{u}_o \cdot \mathbf{u}_\parallel = \cos\varphi, \tag{21}$$

which fits v^2 via an appropriate value of $\cos\varphi$. Moreover the eq (17) yields

$$\mathrm{v}_\parallel = \Omega D^{\S} \mathbf{u}_\parallel \cdot \nabla n, \tag{22}$$

which in principle is fulfilled by an appropriate value of Ω whatever the actual orientation of $\mathbf{u}_o$ and related value of $\cos\varphi$ in the eqs (21) might be. Consider now that also the thermal energy $k_B T = m\mathrm{v}_T^2/2$ contributes to the velocity of the carriers crossing the electrolyte, and thus must someway appear in the model; v_T defined in this way is the average modulus of the velocity vector $\mathbf{v}_T$, whose orientation is by definition arbitrary and random. During the working conditions of the cell it is reasonable to expect that the actual dynamics of charge transport is described combining $\mathbf{v}_T$, due to the heat energy of the carrier in the electrolyte, with $\mathbf{v}$, due to its electric and concentration gradient driving forces. Let us exploit $\mathbf{v}_a$ of the eqs (19) to introduce into the problem just the vector $\mathbf{v}_T$ of the carriers; hence

$$\mathbf{v}_\parallel = \frac{D_\parallel^{\S}}{D^{\S}}\mathbf{v} \pm \frac{\eta'}{\eta}\mathbf{v}_T \qquad \mathbf{v}_\perp = \frac{D_\perp^{\S}}{D^{\S}}\mathbf{v} \mp \frac{\eta'}{\eta}\mathbf{v}_T \qquad \mathbf{v}_a \equiv \mathbf{v}_T. \tag{23}$$

These equations express the components of $\mathbf{v}$ along the tunnel direction and perpendicularly to it. Of course $\mathbf{v}$ is the actual velocity of the charge carrier resulting from the solution of the eq (12), $\mathbf{v}_\parallel$ and $\mathbf{v}_\perp$ are the components of $\mathbf{v}$ affected by the thermal perturbation consequently to either sign of $\mathbf{v}_T$; the notations $\mathbf{v}_\parallel^{\pm}$ and $\mathbf{v}_\perp^{\mp}$, in principle more appropriate, are implied and omitted for simplicity. So in general

$$\mathbf{v}_\parallel = r_\parallel \mathbf{v} \pm r\mathbf{v}_T \qquad \mathbf{v}_\perp = r_\perp \mathbf{v} \mp r\mathbf{v}_T \qquad r = \frac{\eta'}{\eta} \qquad r_\parallel = \frac{D_\parallel^{\S}}{D^{\S}} \tag{24}$$

$$r_\perp = \frac{D_\perp^{\S}}{D^{\S}} \qquad r_\parallel + r_\perp = 1.$$

As expected, the velocity components result given by the respective linear combinations of $\mathbf{v}$ and $\mathbf{v}_T$. Here it is reasonable to put $r = 1$ in order that $\mathbf{v}_\parallel \to \pm\mathbf{v}_T$ and $\mathbf{v}_\perp \to \mp\mathbf{v}_T$ for

$\mathbf{v} \to 0$; as this reasonably occurs for $T \to 0$, it means that both components of $\mathbf{v}$ tend to the respective values consistent with the zero point energy of the charge carrier. Note in particular that the second eq (24) $\mathbf{v}_T = \pm(r_\perp \mathbf{v} - \mathbf{v}_\perp)$ yields thanks to the eqs (21) $\mathrm{v}_T^2 = (r_\perp \mathrm{v})^2 + \mathrm{v}_\perp^2 - 2r_\perp \mathbf{v} \cdot \mathbf{v}_\perp$, i.e.

$$\mathrm{v}_T^2 = r_\perp^2 \frac{\mathrm{v}_\parallel^2}{\cos^2\varphi} + \mathrm{v}_\parallel^2 \tan^2\varphi - 2r_\perp \mathrm{v}_\perp^2 = \qquad (25)$$

$$= \left(\frac{r_\perp^2}{\cos^2\varphi} + (1 - 2r_\perp)\tan^2\varphi \right) \mathrm{v}_\parallel^2 \qquad \mathbf{v} \cdot \mathbf{v}_\perp = \mathrm{v}_\perp^2$$

Let us specify now the considerations hitherto carried out to describe the behaviour of a charge carrier moving inside the stretched zone of the dislocation; the next part of this section concerns in particular just the charge transport via tunnelling mechanism.

4.2 Charge transport along the stretched zone of the dislocation

Both possible chances $r_\parallel \mathbf{v}_\parallel + \mathbf{v}_T$ and $r_\parallel \mathbf{v}_\parallel - \mathbf{v}_T$ of the first equation (24) yield an average velocity vector still consistent with the possible tunnelling of the ion. The corresponding chances of the second equation, where instead the vector $\mathbf{v}_T$ sums and subtracts to $r_\perp \mathbf{v}_\perp$, are more interesting and critical. The components $r_\perp \mathbf{v}_\perp \mp \mathbf{v}_T$ of $\mathbf{v}$ show indeed that the thermal agitation summed up to the transverse component of ion velocity could possibly avert the tunnelling conduction mechanism; this linear combination implies the possibility for the ion path to deviate from the tunnel direction and flow outwards the tunnel. Moreover, even the Coulomb interaction of the carriers with the charged cores of the lattice closely surrounding the tunnel is to be considered: as the cores are in general electrically charged, their interaction with the flow of mobile carriers is expectable. The second condition for a successful tunnelling path of the carriers concerns just this interaction: if for instance the charge carrier is an electron, it is likely attracted to and thus neutralizes with the positive cores; so the tunnel path through the whole distance L is in practice impossible. If instead the carrier is a proton, its Coulomb repulsion with the positive cores is consistent with the chance of travelling through L and coming out from the dislocation tunnel: in the case of a ceramic single crystal and dislocations crossing throughout it, the charge carrier would start from one electrode and would reach the other electrode entirely in the confined state. This tunnel transport mechanism is coupled with the usual lattice transport mechanism. This situation is represented in the figure 5.

Let us analyze both effects. Let $\delta t = L/\mathrm{v}_\parallel$ be the time necessary for the carrier to tunnel throughout the length L of the stretched zone. Then, as schematically sketched in fig. 6, all possible trajectories are included in a cone centred on the entrance point of the carrier whose basis has maximum total size $2\delta r = 2(r_\perp \mathrm{v}_\perp + \mathrm{v}_T)\delta t$.

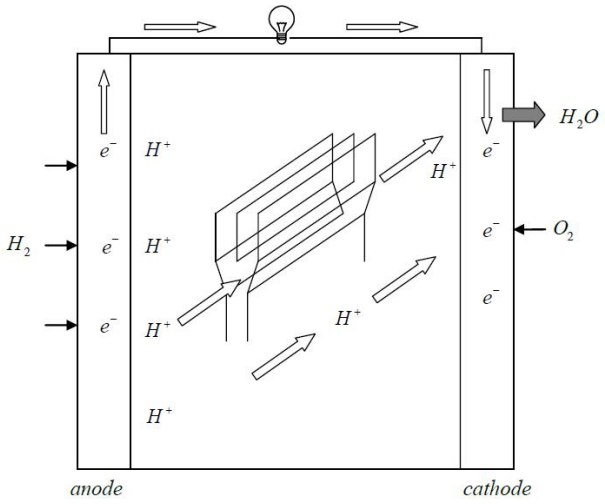

Fig. 5: Schematic sketch of a cell where is operating the proton conduction mechanisms.

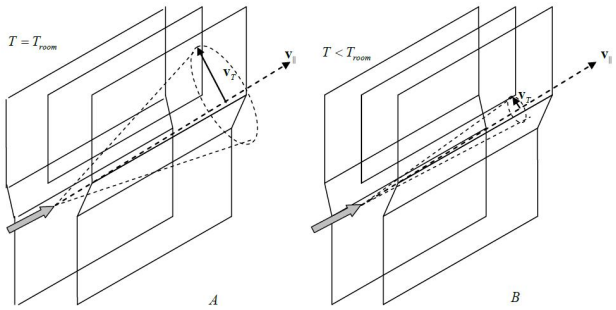

Fig. 6: The figure shows qualitatively the effect of the thermal velocity, solid arrow, on the tunnelling of a charge carrier that travels within the stretched zone of an edge dislocation. In A the vector sum of $\mathbf{v}_\parallel$ and $\mathbf{v}_T$ occurs at a temperature preventing the chance for the carrier to tunnel throughout the dislocation length; in B the reduced value of $\mathbf{v}_T$ at lower T allows the tunnelling effect.

As $\mathbf{v}_T$ has by definition random orientation, here has been considered the most unfavourable case where $\mathbf{v}_T$ is oriented just transversally to $\mathbf{v}_\parallel$ in assessing the actual chance of confinement of the carrier within the stretched zone of the dislocation. In general the tunnel effect is expectable at temperatures appropriately low only, in order that the width of the cone basis be consistent with the average size δl of the stretched zone: during δt the total lateral deviation $2\delta r$ of the ion path with respect to $\mathbf{v}_\parallel$ must not exceed δl, otherwise the ion would overflow in the surrounding lattice. In other words, the charge effectively tunnels if $\mathrm{v}_\parallel$ is such to verify the condition $(r_\perp \mathrm{v}_\perp + \mathrm{v}_T)L/\mathrm{v}_\parallel \leq \delta l$ only.
In conclusion, considering the worst case with the plus sign where $\mathbf{v}_T$ and $r_\perp \mathbf{v}_\perp$ sum up correspondingly to the maximum

deviation of the charge, it must be true that, whatever the component $\mathrm{v}_\parallel$ of the actual ion displacement velocity might be,

$$T \leq \frac{m}{2k_B}\left(\mathrm{v}_\parallel \frac{\delta l}{L} - r_\perp \mathrm{v}_\perp\right)^2 \qquad k_B T = \frac{m\mathrm{v}_T^2}{2}. \tag{26}$$

Two interesting equations are obtained merging the general eq (5) and the eqs (24). Specifying for instance that the modulus of velocity is $\mathrm{v}_\perp$ and D is actually $D^{\S}_\perp$, one finds $D^{\S}_\perp = \mathrm{v}_\perp k_B T/F_\perp$; so, multiplying both sides by $\mathrm{v}_\perp/D^{\S}$ and repeating identical steps also for $\mathrm{v}_\parallel$, the results are

$$r_\perp \mathrm{v}_\perp = \frac{k_B T}{F_\perp D^{\S}}\mathrm{v}_\perp^2 \qquad r_\parallel \mathrm{v}_\parallel = \frac{k_B T}{F_\parallel D^{\S}}\mathrm{v}_\parallel^2. \tag{27}$$

These equations introduce the confinement forces $F_\perp$ and $F_\parallel$ that constrain the carrier path within the tunnel and correspond to the interaction of the charge carrier with the neighbours lattice cores surrounding the stretched zone of the dislocation. Also, as the eqs (21) yield $\mathrm{v}_\perp = \pm \mathrm{v}_\parallel \tan\varphi$, one finds

$$T \leq \frac{m\mathrm{v}_\parallel^2}{2k_B}\left(\frac{\delta l}{L} - \frac{k_B T \mathrm{v}_\parallel}{F_\perp D^{\S}}\tan^2\varphi\right)^2$$

which is more conveniently rewritten as follows

$$\frac{T}{T_c} \leq \frac{m\mathrm{v}_\parallel^2}{2k_B T_c}\left(\frac{\delta l}{L} - \frac{T}{T_c}\frac{\mathrm{v}_\parallel}{\mathrm{v}_c} w\left(\frac{\delta l}{L}\right)^2\right)^2 \tag{28}$$

$$F_\perp D^{\S} = \mathrm{v}_c k_B T_c \qquad \tan\varphi = \pm w\frac{\delta l}{L} + \ldots .$$

The meaning of the second equation is at the moment merely formal, aimed to obtain an expression function of T/T_c and $\mathrm{v}_\parallel/\mathrm{v}_c$; as concerns the third position, is attracting the idea of writing the expression in parenthesis as a power series expansion of $\delta l/L$ truncated at the second order, in which case the proportionality constant w defines the series coefficient $T\mathrm{v}_\parallel w/(T_c \mathrm{v}_c)$. Note that this coefficient should expectably be of the order of the unity, in order that the series could converge; indeed this conclusion will be verified in the next subsection 5.2. Clearly v_c is definable as the transit critical velocity of the charge carrier making equal to 1 the right hand side of the first eq (28). Anyway both positions are acceptable because neither of them needs special hypotheses, being mere formal ways to rewrite the initial eq (26). This equation emphasizes that even when $\mathbf{v}_\perp = 0$, i.e. in the particular case where the entrance path of the charge carrier is exactly aligned along $\mathbf{v}_\parallel$, the mere thermal agitation must be consistent itself with the available tunnel cross section: the greater the latter, the higher the critical temperature below which the tunnelling is in fact allowed to occur. This equation links the lattice features δl and L to the operating conditions of the cell, here represented by the ion properties m and $\mathrm{v}_\parallel$. Hence it is reasonable to expect that v_T and thus T must not exceed a critical upper value in order to allow the tunnelling mechanism. If T and m, and thus v_T, are such that $\mathrm{v}_\parallel \delta t$ really corresponds to the whole length L of the dislocation, then the eqs (17) describe the flow of ions that effectively tunnel in the stretched zone of the dislocation.

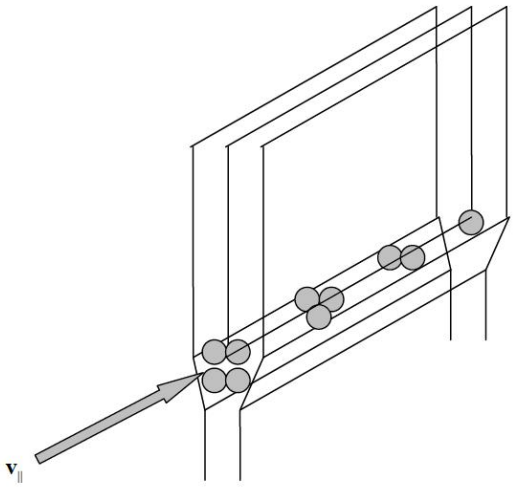

Fig. 7: The figure highlights that the arising of a concentration gradient along the tunnel is hindered by the size of the stretched zone of the dislocation.

4.3 The superconducting charge flow

The main feature of these results is that $D^{\S}$ and ∇n characterize the charge tunnelling path. In general the occurring of concentration gradient requires by definition a volume of electrolyte so large to allow the non-equilibrium distribution of a statistically significant number of charge carriers unevenly distributed among the respective lattice sites. Yet $\nabla n \neq 0$ is in fact inconsistent with the size of the dislocation stretched zone here concerned; in particular, the existence of the component $\mathbf{u}_\parallel \cdot \nabla n$ of this gradient would require a configuration of charges like that qualitatively sketched in fig. 7.

This chance seems however rather improbable because of the mutual repulsion between charges of the same sign in the small channel available below the dislocation extra plane. So the gradient term at right hand side of the eq (22) should intuitively vanish inside the tunnel. Assume thus the component $\mathbf{u}_\parallel \cdot \nabla n = 0$, i.e the carriers travel the stretched zone with null gradient within the tunnel path. To better understand this point, note that in the eq (22) appears the product $D^{\S}\nabla n$; moreover, in the eqs (27) appear the products $F_\perp D^{\S}$ and $F_\parallel D^{\S}$. These results in turn suggest two chances allowed at left hand side of eq (22):

(i) $\mathrm{v}_\parallel = 0$, i.e. all charges are statistically at rest in the stretched zone; the eq (22) trivially consisting of null terms at both sides is nothing else but the particular case of the Cottrell

atmosphere sketched in fig. 3A. The ions that decorate the dislocation prevent the tunnelling of further ions provided by the lattice. The charge flow in the cell is merely that described by the usual bulk lattice ion transport under concentration and electric potential gradients, already concerned in [9].

(ii) The left hand side of the eq (22) is non-vanishing: $\mathrm{v}_{\|} \neq 0$ reveals actual dynamics of charges transiting within the tunnel zone. This is closely related to the previous statement of the section 1 according which, for instance, a bare electron of mass m_e interacting with the dislocation can be described by a free electron of effective mass m_e^{eff}: owing to the eqs (2), this reasoning is identically expressed in general via D^{eff} instead of m^{eff} of any charge carrier.

The latter case is interesting, because the finite value of $\mathrm{v}_{\|} \neq 0$ requires that $D^{\S} \to \infty$ in order that the undetermined form $\infty \times 0$ makes finite the corresponding limit value of $D^{\S}\mathbf{u} \cdot \nabla n$. This also means that $D^{\mathrm{eff}} = D^{*} + D^{\S}$ tends to infinity as well, which compels the resistivity $\rho^{\mathrm{eff}} \to 0$ according to eq (4). Moreover, for the same reason this mechanisms implies both $F_{\perp} \to 0$ and $F_{\|} \to 0$ for $D^{\S} \to \infty$, which implies $D^{\S}_{\perp} \to \infty$ and $D^{\S}_{\|} \to \infty$; this in turn means null interaction of the charge carrier with the lattice surrounding the tunnel zone. Hence the eqs (28) and (27) yield

$$\frac{T}{T_c} = \frac{m\mathrm{v}_{\|}^2}{2k_B T_c}\left(\frac{\delta l}{L} - \frac{T}{T_c}\frac{\mathrm{v}_{\|}}{\mathrm{v}_c} w\left(\frac{\delta l}{L}\right)^2\right)^2 \qquad (29)$$

$$\lim_{\substack{D^{\S}\to\infty \\ F_{\perp}\to 0}} \frac{F_{\perp} D^{\S}}{k_B} = \mathrm{v}_c T_c \qquad \lim_{\substack{D^{\S}\to\infty \\ F_{\|}\to 0}} \frac{F_{\|} D^{\S}}{k_B} = \mathrm{v}'_c T_c .$$

In the eqs (28) T_c and v_c were in general arbitrary variables; here instead they are fixed values uniquely defined by the limit of the second and third equations; the same holds for v'_c related to $\mathrm{v}_{\|}$. So the transport mechanism in the stretched boundary zone of the dislocation extra plane is different from that in other zones of the ceramic crystal: clearly the former has nothing to do with the usual charge displacement throughout the lattice concerned by the latter. While the concentration gradient is no longer the driving force governing the charge transport, $F_{\perp} \to 0$ and $F_{\|} \to 0$ consequently obtained mean that the charge carrier moves within the tunnel as a free particle: the lack of friction force, i.e. electrical resistance, prevents dissipating their initial access energy into the dislocation stretched zone. This appears even more evident in the eq (5), where $D \equiv D^{\S}$ at $T = T_c$ yields $\mathbf{J} \neq 0$ compatible with $\mathbf{F} = 0$.

Simple considerations with the help of fig. 8, inferred from the fig. 4 but containing the information $\rho^{\mathrm{eff}} \to 0$, show the electric shunt between zones of different electrical resistivity and highlight why the charge carriers tend to privilege the zero resistance tunnel path: this answers the possible question about the preferential character of this conduction mechanism of the charge carriers. Further quantum considerations are necessary to complete the picture essentially classical so far carried out. On the one hand the expectation of a superconducting flow of charges cannot be certainly regarded as an unphysical result, despite its derivation has surprisingly the classical basis hitherto exposed. In this respect however it is worth recalling the quantum nature of both eqs (1), which indeed have been obtained as corollaries of the statistical formulation of the quantum uncertainty [10]; the fact that the Fick equations have been obtained themselves as corollaries of a quantum approach to the gradient driven diffusion force, shows that actually all results have inherently quantum physical meaning. Then, by definition, even a classical approach inferred from these equations has intrinsic quantum foundation. On the other hand, the heuristic character of this section requires being completed with further concepts more specifically belonging to the quantum world.

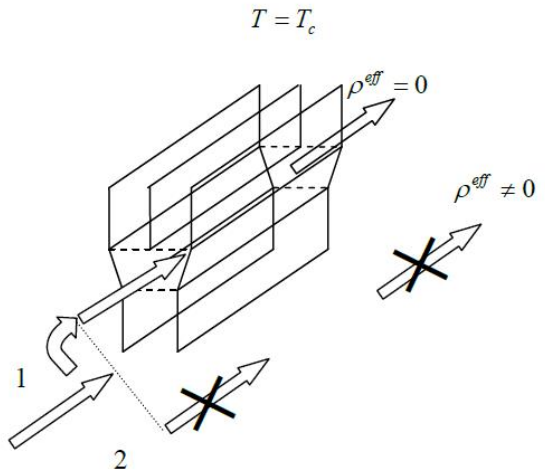

Fig. 8: Schematic sketch showing that at the ion current shunts to the zero resistivity path inside the tunnel with electrical resistivity $\rho^{\mathrm{eff}} = 0$ rather than to any lattice path with $\rho^{\mathrm{eff}} \neq 0$.

5 Quantum approach

This section aims to understand why the results of the classical model of a unique dislocation crossing through one single grain are actually extendible to a real grain with several disconnected dislocations of different orientations and to the grain boundaries consisting of several tangled dislocations inordinately piled up at the interface with other grains.

5.1 Grain bulk superconductivity

Define $\delta\varepsilon = \varepsilon_{tu} - \varepsilon_{la}$, being ε_{tu} the energy of the ion travelling the tunnel along the stretched zone of the edge dislocation and ε_{la} that of the ions randomly moving in the lattice before entering the tunnel; $\delta\varepsilon$ represents thus the gap between the energy of the ion in either location, which in turn suggests

the existence of an energy gap for a charge carrier in the superconducting and non-superconducting state. This conclusion is confirmed below. The fact of having introduced the tunnelling velocity components $\mathbf{v}_\perp$ and $\mathbf{v}_\parallel$, suggests introducing the respective components of De Broglie momentum of the ion corresponding to ε_{tu}. Being $p_\parallel = h/\lambda_\parallel$ and $p_\perp = h/\lambda_\perp$ these components, then $|\mathbf{p}| = h\sqrt{\lambda_\perp^{-2} + \lambda_\parallel^{-2}}$ in the tunnel state; $\lambda_\perp$ and $\lambda_\parallel$ are the wavelengths corresponding to the respective velocity components. Let us specify $n_\perp\lambda_\perp = \delta l$ and $n_\parallel\lambda_\parallel = L$, in order to describe steady waves with $n_\perp$ and $n_\parallel$ nodes along both tunnel sizes; then, with $n_\perp = 1$ and $n_\parallel = 1$,

$$p_{tu} = |\mathbf{p}| = \gamma h/\delta l \qquad \gamma = \sqrt{1 + (\delta l/L)^2}.$$

Note that $\gamma \approx 1$ approximates well p_{tu} even if L corresponds to just a few lattice sites aligned to form the extra-plane of the edge dislocation, i.e. even in the case of an extra-plane extent short with respect to the lattice spacing stretched to δl: indeed $(\gamma h/\delta l - h/\delta l)/(\gamma h/\delta l) \approx (\delta l/L)^2/2$ yields $\gamma \approx 1$ even for values $L \gtrsim \delta l$. Anyway with $p_{tu} = \gamma h/\delta l$ one finds $\varepsilon_{tu} = (h\gamma)^2/2m\delta l^2$. According to this result, the momentum is essentially due to the small cross section of the stretched zone that constrains the transverse velocity component $\mathbf{v}_\perp$ of the ion in the tunnel with respect to that of the ion randomly moving in the lattice; this means that remains instead approximately unchanged the component $\mathbf{v}_\parallel$ of velocity along the tunnel. Put now $\varepsilon_{la} = \vartheta\varepsilon_{tu}$, being θ an appropriate numerical coefficient such that $\delta\varepsilon = (\vartheta - 1)\varepsilon_{tu}$. In principle both chances $\vartheta \gtrless 1$ are possible, depending on whether $\varepsilon_{la} \gtrless \varepsilon_{tu}$: as neither chance can be excluded "a priori" for an ion in the two different environments, this means admitting that in general to the unique ε_{la} in the lattice correspond two energy levels spaced $\pm\delta\varepsilon$ around ε_{tu}, one of which is actually empty depending on either situation energetically more favourable. This is easily shown as the eqs (24) yield two chances for the energy of the charge carrier in the tunnel, depending on how $\mathbf{v}_T$ combines with $\mathbf{v}_\parallel$ and $\mathbf{v}_\perp$. These equations yield $\varepsilon_2 = \left((r_\parallel\mathbf{v} + \mathbf{v}_T)^2 + (r_\perp\mathbf{v} - \mathbf{v}_T)^2\right)m/2$ and $\varepsilon_1 = \left((r_\parallel\mathbf{v} - \mathbf{v}_T)^2 + (r_\perp\mathbf{v} + \mathbf{v}_T)^2\right)m/2$; trivial manipulations via the eqs (21) yield thus $\delta\varepsilon = \varepsilon_2 - \varepsilon_1 = 2m\mathbf{v}\cdot\mathbf{v}_T(r_\parallel - r_\perp)$ showing indeed a gap between the levels $\varepsilon_2 = \varepsilon_0 + m\mathbf{v}\cdot\mathbf{v}_T(r_\parallel - r_\perp)$ and $\varepsilon_1 = \varepsilon_0 - m\mathbf{v}\cdot\mathbf{v}_T(r_\parallel - r_\perp)$ with $\varepsilon_0 = \left((r_\parallel^2 + r_\perp^2)\mathrm{v}^2/2 + \mathrm{v}_T^2\right)m$: this latter corresponds thus to the Fermi level between the occupied and unoccupied superconducting levels defining the gap. As the ion dwell time δt in the tunnel is of the order of

$$\delta t = \frac{\hbar}{|\delta\varepsilon|} = 2\frac{m\delta l^2\hbar}{|\vartheta - 1|\,(\gamma h)^2},$$

the extent L of the extra-plane controlling the time range of ion transit at velocity $\mathrm{v}_\parallel$ requires

$$L = \mathrm{v}_\parallel\delta t = \frac{m\mathrm{v}_\parallel\delta l^2}{|\vartheta - 1|\,\pi h\gamma^2}.$$

So, supposing that n_{tu} electrons ξ apart each other transit simultaneously within the tunnel,

$$L = \frac{\mathrm{v}_\parallel\hbar}{|\delta\varepsilon|} = \frac{\mathrm{v}_\parallel\hbar}{|\vartheta - 1|\,\varepsilon_{tu}} \qquad L = (n_{tu} - 1)\xi \qquad \mathrm{v}_\parallel = \frac{\gamma h}{m\delta l}$$

suggest that

$$\xi = \frac{\mathrm{v}_\parallel\hbar}{(n_{tu} - 1)\,|\delta\varepsilon|} = \frac{\mathrm{v}_\parallel\hbar}{|\vartheta - 1|\,(n_{tu} - 1)\varepsilon_{tu}}.$$

Define now the tunnel volume V available to the transit of the ions as $V = \chi L\delta l^2$, being χ a proportionality constant of the order of the unity related to the actual shape of the stretched zone; if for instance the tunnel would be simulated by a cylinder of radius $\delta l/2$, then $\chi = \pi/4$. Hence

$$V = \chi\delta l^2\mathrm{v}_\parallel\delta t = \frac{\chi}{|\vartheta - 1|\,\pi}\frac{m}{h}\frac{\mathrm{v}_\parallel\delta l}{\gamma^2}\delta l^3.$$

Note that $\mathrm{v}_\parallel\delta l$ has the same physical dimensions of a diffusion coefficient; so it is possible to write $\mathrm{v}_\parallel\delta l = \psi D_\parallel$, being ψ an appropriate proportionality constant. Moreover recall that the diffusion coefficient has been also related in the section 1 to h/m via a proportionality constant, once more because of dimensional reasons; so put $D_m = q_m h/m$ via the proportionality factor q_m, as done in the section 1, whereas the subscript emphasizes that the diffusion coefficient is by definition that related to the mass of an ion or electron tunnelling in the stretched zone of the dislocation. So one finds

$$V = \frac{\chi\psi}{|\vartheta - 1|\,\pi\gamma^2}\frac{D_\parallel}{q_m D_m}\delta l^3.$$

Note eventually that it is certainly possible to write $V/\delta l^3 = \theta(1 + \zeta)$ with $\zeta > 1$ appropriate function and θ proportionality constant: indeed the tunnel can be envisaged as a series of cells of elementary volumes $L_0\delta l^2$, where L_0 corresponds to the lattice spacing of atoms aligned along the dislocation extra plane. Replacing these positions in the equation of V one finds

$$\frac{D_\parallel}{qD_m} = 1 + \zeta \qquad q = \frac{|\vartheta - 1|\,\theta\pi q_m}{\chi\psi}\gamma^2.$$

This result compares well with the eq (2) previously obtained in an independent way, simply identifying $\zeta = \partial^2 u(k)/\partial k^2$ and all constants with q; as expected here $D_\parallel$ plays at $T = T_c$ the role of $D^\S$ introduced in the section 1, whereas qD_m is just D^* previously obtained as electric potential driven enhancement of the plain diffusion coefficient $D \equiv D_m$. This agreement supports the present approach. This also suggests some more considerations about the nature of the superconducting charge wave propagating along the tunnel zone. It is intuitive that the quantum states of the charge carriers within the tunnel must correspond to an ordered flow of particles, all travelling the tunnel with the same velocity $\mathrm{v}_\parallel$; any perturbation of the motion of these charges would increase the total

Coulomb energy of the flow and could even spoil the flow; the low temperature helps in this respect. This requires in turn a sort of coupling between the carriers, because several fermions cannot have the same quantum state; in effect it is known that a small contraction of positive charges of the lattice cores around the transient electrons in fact couples two electrons. Actually, in this case the contraction is that of the lines of lattice cores delimiting the tunnel stretched by the dislocation plane around the transient charges. In other words, electron pairs or proton pairs travel through the tunnel as bosons with a unique quantum state.

5.2 Computer simulation

Some estimates are also possible considering a ceramic lattice whose average spacing is a; this is therefore also the order of magnitude expected for the size $\delta l \gtrsim a$ of the stretched zone. Consider first the case where the charge carrier is an electron, which requires negatively charged ion cores delimiting the tunnel cross section; this assumption reminds the familiar case of electron super-conduction and thus helps to check reliability and rationality of the estimates. To assess the previous results, put $m = 9 \times 10^{-28}$ g and consider the reasonable simulation value $\delta l = 5 \times 10^{-8}$ cm, consistent with a typical lattice spacing quoted in the section 3; one finds $\mathrm{v}_\parallel \approx 1.5 \times 10^8$ cm/s with the approximation $\gamma = 1$. Moreover putting $L = 10^{-4}$ cm, i.e. considering an edge dislocation that crosses through a test grain average size of the typical order of 1 μm, one finds a gap $\delta\varepsilon = \mathrm{v}_\parallel \hbar / L = 10^{-3}$ eV between the ion energies in the tunnel and in the lattice. Note that the zero point energy of a free ion in such a test lattice would be of the order of $\varepsilon_{la} \approx 3\hbar^2/2ma^2 \approx 0.3$ eV, quite small with respect to the definition value 1 eV of one electron or unit charge ion in a ceramic electrolyte of a cell operating with 1 V. To ε_{la} corresponds the zero point vibrational frequency $\nu = 2\varepsilon_{la}/h$, i.e. $\nu \approx 2 \times 10^{14}$ s^{-1}; with such a frequency the wavelength $\lambda_\parallel = L$ corresponds to a total charge wave due to $L\nu/\mathrm{v}_\parallel$ electrons. So one finds $\approx 10^2$ electrons, whose mean mutual distance is thus 10 nm about. Eventually the critical temperature compatible with the arising of the superconducting state given by the eq (26) is 0.02 K with $\mathrm{v}_\perp = 0$ or even smaller for $\mathrm{v}_\perp \neq 0$. Compare now this result obtained via the eq (26) with that obtainable directly through the eq (25)

$$\mathrm{v}_T^2 = \left(\frac{r_\perp^2}{\cos^2\varphi} + (1 - 2r_\perp)\tan^2\varphi \right) \mathrm{v}_\parallel^2 .$$

Note that v_T^2 has a minimum as a function of $r_\perp$. If $\varphi = \pi/2$ this minimum corresponds to $r_\perp^{\min} = 1$, to be rejected because it would imply $D_\perp^{\S} = D^{\S}$ and $D_\parallel^{\S} = 0$. If instead $\varphi \neq \pi/2$, then the minimum corresponds to $r_\perp^{\min} = \sin^2\varphi$, which yields in turn $\mathrm{v}_T^2 = \mathrm{v}_\parallel^2 \sin^2\varphi$; hence $k_B T_c = m\mathrm{v}_T^2/2$ yields

$$T_c = \frac{m}{2k_B} \mathrm{v}_\parallel^2 \sin^2\varphi .$$

With $\mathrm{v}_\parallel = 1.5 \times 10^8$ cm/s the electron mass would yield $T = 6.2 \times 10^6 \sin^2\varphi$ K. Comparing with the previous result, one infers that $10^{-8} \gtrsim \sin^2\varphi$; so being $\sin^2\varphi \approx \tan^2\varphi$ with good approximation, one also infers that the second position (28) is verified with w such that $T\mathrm{v}_\parallel w/(T_c \mathrm{v}_c)$ is of the order of unity for $\delta l/L = 10^{-4}$, as in fact it has been anticipated in the previous subsection 4.3. Of course the actual values of these order of magnitude estimates depend on the real microstructure of the ceramic lattice; yet the aim of this short digression concerning the electron is to emphasize that the typical properties of the test material used for this simulation are consistent with the known results of electron superconduction theory. The simulation can be repeated for the proton, considering that the proton velocity $\mathrm{v}_\parallel$ is now m_e/m_{prot} times lower than before; so, despite m is m_{prot}/m_e larger than before, $m\mathrm{v}_\parallel^2$ of the eq (26) predicts a critical T smaller than that of the electron by a factor m_e/m_{prot} for $r_\perp \mathrm{v}_\perp \ll \mathrm{v}_\parallel \delta l/L$.

5.3 Grain bulk and grain boundary superconductivity

As concerns the chance of superconduction in the grain bulk with several disconnected dislocations at the grain boundaries, it is necessary to recall the Josephson effect concurrently with the presence of tangled dislocations and pile up of dislocations. The former concerns the transfer of superconducting Cooper pairs existing at the Fermi energy via quantum tunnelling through a thin thickness of insulating material: it is known that the tunnelling current of a quasi-electron occurs when the terminals of two dislocations, e.g. piled up or tangled, are so close to allow the Josephson Effect. If some terminals are a few nanometers apart, then superconduction current is still allowed to occur even though the dislocation break produces a thin layer of ceramic insulator. In other words, the terminal of the superconducting channel of one dislocation transfers the pair to the doorway of another dislocation and so on: in this way a superconduction current can tunnel across the whole grain. An analogous idea holds also at the grain boundary. Of course the chance that this event be actually allowed to occur has statistical basis: due to the high number of dislocations that migrate and accumulate at the grain boundaries after displacement along favourable slip planes of the bulk crystal lattice, the condition favourable to the Josephson Effect is effectively likely to occur. As the same holds also within the grain bulk between two different dislocations close enough each other, e.g. because they glide preferentially along equal slip planes and pile up on bulk precipitates, the conclusion is that the pair tunnelling allows macroscopic superconduction even without necessarily requiring the classical case of a unique dislocation spanning throughout a single crystal electrolyte.

6 Discussion

It is commonly taken for granted that the way of working of the fuel cells needs inevitably high temperatures, of the or-

der of some hundreds C degrees, so as to promote adequately the ion conductivity; great efforts are addressed to reduce as much as possible this temperature, down to a few hundreds C degrees, yet still preserving an acceptable efficiency of the cell compatibly with the standard mechanisms of ion conduction.

The present paper proposes however a new approach to the problem of the electric conduction in solid oxide electrolytes: reducing the operating temperature of SOFCs down to a few K degrees, in order to promote a superconducting mechanism.

Today the superconductivity is tacitly conceived as that of the electrons only; the present results suggest however that at sufficiently low temperatures, even the low atomic number ions are allowed to provide an interaction free conduction thanks to their chance of tunnelling in the stretched zone of edge dislocations. Note that although the electron and ion superconduction occur at different temperatures, as it is reasonable to expect, the nature of the lattice cores appears able to filter either kind of mechanism during the working conditions of the cell for the reasons previously remarked: for instance positively charged cores hinder the electron superconduction by attractive Coulomb effect, while promoting instead the proton superconduction via the repulsive effect that keeps the proton trajectory in the middle of the stretched channel. The results obtained in this paper support reasonably the chance that, at least in principle, this idea is practicable. Of course other problems, like for instance the catalysis at the electrodes, should be carefully investigated at the very low temperatures necessary to allow the ion superconduction. However this side problem, although crucial, has been deliberately waived in the present paper: both because of its different physicochemical nature and because the foremost aim of the model was (i) to assess the chance of exploiting the superconductivity not only for the electric energy transmission but also for the electric energy production and (ii) to bring this intriguing topic of the quantum physics deeply into the heart of the fuel cell science.

Moreover other typical topics like the penetration depth of the magnetic field and the critical current have been skipped because well known; the purpose of the paper was not that of elaborating a new theory of superconductivity, but to ascertain the feasibility of an ion transport mechanism able to bypass the difficulties of the high temperature conductivity. Two considerations deserve attention in this respect. The first one concerns the requirement $\mathbf{u}_{\|} \cdot \nabla n = 0$ characterizing the superconductive state with $D \to \infty$. At first sight one could naively think that the eq (4) should exclude a divergent diffusion coefficient. Yet the implications of a mathematical formula cannot be rejected without a good physical reason. Actually neither the chain of equations (6) nor the eq (19) exclude $D \to \infty$: the former because it is enough to put the lattice-charge interaction force $\mathbf{F} \to 0$ whatever $\mathbf{v}$ and $k_B T$ might be, the latter provided putting concurrently $\nabla\phi = -\mathbf{E}e \to 0$. The product $\infty \times 0$ is in principle not necessarily unphysical despite D diverges, because this divergence is always counterbalanced by some force or energy or concentration gradient concurrently tending to zero; rather it is a matter of experience to verify whether the finite outcomes of these products, see for instance the eqs (29), have experimental significance or not. In this respect, however, this worth is recognized since the times of Onnes (1913). In fact, the electron superconductivity is nothing else but a frictionless motion of charges, somehow similar to the superfluidity. Coherently, both equations (29) and (10) suggest simply a free charge carrier moving without need of concentration gradient or applied potential difference or electric field or force $\mathbf{F}$ of any physical nature. The essence of the divergent diffusion coefficient is thus the lack of interaction between lattice and charge carrier. In this sense the Nernst-Einstein equation is fully compatible even with $D^{eff} \to \infty$: in fact is hidden in this limit, and thus in the eq (4) itself, the concept of superconductivity, regarded as a peculiar charge transport mechanism that lacks their interactions and thus does not need any activation energy or driving force.

These results disclose new horizons of research as concerns the solid oxides candidate for fuel cell electrolytes. The choice of the best oxides and their heat treatments is today conceived having in mind the best high temperature conductivity only. But besides this practical consideration, nothing hinders in principle exploring the chance of a fuel cell realized with MIEC solid oxides designed to optimize the ion superconducting mechanism. The prospective is that MIECS with poor ionic conductivity at some hundreds degrees could have excellent superconductors at low temperatures. It seems rational to expect that the optimization of the electrolytes for a next generation of fuel cells compels the future research not to lower as much as possible the high temperatures but to rise as much as possible the low temperatures.

7 Conclusion

The model has prospected the possibility of SOFCs working at very low temperatures, where superconduction effects are allowed to occur. Besides the attracting importance of the basic and technological research aimed to investigate and develop high temperature superconductors for the transport of electricity, the present results open new scenarios as they concern the production itself of electric power via zero resistivity electrolytes. Of course the chance of efficient fuel cells operating according to these expectations must be verified by the experimental activity; if the theoretical previsions are confirmed at least in the frame of a preliminary laboratory activity, as it is legitimate to guess since no ad hoc hypothesis has been introduced in the model, then the race towards high Tc electrolytes could allow new goals of scientific and applicative interest.

Submitted on December 9, 2014 / Accepted on December 12, 2014

References

1. Murch G.E. Atomic diffusion theory in highly defective solids. Trans Tech Publications, Limited, 1980
2. Kontturi K., Murtomäki L., Manzanares J.A. Ionic Transport Processes in Electrochemistry and Membrane Science, 2008, Oxford University Press, Oxford, UK.
3. Gellings P.J., Bouwmeester H.J.M. (Eds.), CRC Handbook of Solid State Electrochemistry, CRC Press, 1997.
4. Riess I. Mixed ionic–electronic conductors - material properties and applications. *Solid State Ionics*, 157, (2003).
5. Eoin M. NMR studies of conduction mechanisms in electrolyte materials for fuel cells. PhD Thesis, University of Dublin, School of chemical Sciences, 2007.
6. Hong G.W., Lee J.Y. The interaction of hydrogen with dislocations in iron. *Acta Metallurgica*, 1984, v. 32(10), p. 1581.
7. Rice M.J., Roth W.L. Ionic transport in super ionic conductors: a theoretical model. *Journal of Solid State Chemistry*, 1972, v. 4(2), p. 294.
8. Boris B., Bokshtein S., Zhukhovitskii A. Thermodynamics and kinetics of diffusion in solids, 1985, Oxonian Press, NY.
9. Tosto S. Correlation model of mixed ionic-electronic conductivity in solid oxide lattices in the presence of point and line defects for solid oxides fuel cells *International Journal of Energy Research*, 2011, v. 35(12), p. 1056.
10. Tosto S. Fundamentals of diffusion for optimized applications, 2012, ENEA Ambiente Innovazione, p. 94.
11. Freemann S.A., Booske J.H., Cooper R.F., Modeling and numerical simulations of microwave induced ion transport. Journal of Applied Physics, 1998, v. 83(11), 2979.
12. Karger J., Heitjans P., Haberlandt R. Diffusion in Condensed Matter, 1998, Friedr. Vieweg and Sohn Verlagsgesell. mbH Braunschweig.
13. Kittel C. Introduction to solid state physics, 2005, J. Wiley and Sons, Hoboken, NJ, USA.
14. Sutton A.P. and Balluffi R.W. Interfaces in Crystalline Materials. 1995 Clarendon Press, Oxford, UK.
15. Zhao J.Z., De A.K., De Cooman B.C. Formation of the Cottrell Atmosphere during Strain Ageing of Bake-Hardenable Steels, *Metallurgical and Materials Transactions*, 2001, v. 32A, p. 417.
16. Conrad H., Schoeck G. Cottrell locking and the flow stress in iron. *Acta Metallurgica*, 1960, v. 8(11), 791–796.
17. Slater J.C. Atomic Radii in Crystals. *Journal of Chemical Physics*, 1964, v. 41(10), 3199–3205.
18. Lande A. *Zeitschrift fur Physik*, 1920, v. 1(3), p. 191.
19. Otobe H. and Nakamura A. Lattice Parameters and Defect Structure of the Fluorite and C-Type Oxide Solid Solutions between MO2 and M2O3, in Solid Oxide Fuel Cells (SOFCs VI): Proc. Of the Sixth International Congress, S.C. Singhal and M. Dokiya Eds, 1999, p. 463, The Electrochemical Society, Pennington, N.J., USA.

Weinberg Angle Derivation from Discrete Subgroups of SU(2) and All That

Franklin Potter

Sciencegems.com, 8642 Marvale Drive, Huntington Beach, CA 92646 USA. E-mail: frank11hb@yahoo.com

The Weinberg angle θ_W of the Standard Model of leptons and quarks is derived from specific discrete (i.e., finite) subgroups of the electroweak local gauge group $SU(2)_L \times U(1)_Y$. In addition, the cancellation of the triangle anomaly is achieved even when there are four quark families and three lepton families!

1 Introduction

The weak mixing angle θ_W, or Weinberg angle, in the successful theory called the Standard Model (SM) of leptons and quarks is considered traditionally as an unfixed parameter of the Weinberg-Salam theory of the electroweak interaction. Its value of ~30° is currently determined empirically.

I provide the only first principles derivation of the Weinberg angle as a further application of the discrete symmetry subgroups of SU(2) that I used for the first principles derivation of the mixing angles for the neutrino mixing matrix PMNS [1] in 2013 and of the CKM quark mixing matrix [2] in 2014. An important reminder here is that these derivations are all done within the realm of the SM and no alternative theoretical framework beyond the SM is required.

2 Brief review of neutrino mixing angle derivation

The electroweak component of the SM is based upon the local gauge group $SU(2)_L$ x $U(1)_Y$ acting on the two SU(2) weak isospin flavor states $\pm\frac{1}{2}$ in each lepton family and each quark family. Its chiral action, i.e., involving LH doublets and RH singlets, is dictated by the mathematics of quaternions acting on quaternions, verified by the empirically determined maximum parity violation. Consequently, instead of using SU(2) generators acting on SU(2) weak isospin states, one can equivalently use the group of unit quaternions defined by q = a + bi + cj + dk, for a, b, c, d real and $i^2 = j^2 = k^2 =$ ijk = −1. The three familiar Pauli SU(2) generators σ_x, σ_y, σ_z, when multiplied by i, become the three generators k, j, i, respectively, for this unit quaternion group.

In a series of articles [3–5] I assigned three discrete (i.e., finite) quaternion subgroups (i.e., SU(2) subgroups), specifically 2T, 2O, 2I, to the three lepton families, one to each family (ν_e, e), (ν_μ, μ), (ν_τ, τ). These three groups permeate all areas of mathematics and have many alternative labelings, such as [3,3,2], [4,3,2], [5,3,2], respectively. Each of these three subgroups has three generators, $R_s = iU_s$ (s = 1,2,3), two of which match the two SU(2) generators, U_1 = j and U_3 = i, but the third generator U_2 for each subgroup is not k [6]. This difference between the third generators and k is the true source [1] of the neutrino mixing angles. All three families must act together to equal the third SU(2) generator k.

The three generators U_2 are given in Table 1, with $\phi = (\sqrt{5}+1)/2$, the golden ratio. The three generators must add to make the generator k, so there are three equations for three unknown factors. The arccosines of these three normalized factors determine the quaternion angles 105.337°, 36.755°, and 122.459°. Quaternion angles are double angle rotations, so one uses their half-values for rotations in R^3, as assumed for the PMNS matrix. Then subtract one from the other to produce the three neutrino mixing angles $\theta_{12} = 34.29°$, $\theta_{23} = -42.85°$, and $\theta_{13} = -8.56°$. These calculated angles match their empirical values $\theta_{12} = \pm 34.47°$, $\theta_{23} = \pm(38.39° - 45.81°)$, and $\theta_{13} = \pm 8.5°$ extremely well.

Table 1: Lepton Family Quaternion Generators U_2

Fam.	Grp.	Generator	Factor	Angle°
ν_e, e	332	$-\frac{1}{2}\,i - \frac{1}{2}\,j + \frac{1}{\sqrt{2}}\,k$	−0.2645	105.337
ν_μ, μ	432	$-\frac{1}{2}\,i - \frac{1}{\sqrt{2}}\,j + \frac{1}{2}\,k$	0.8012	36.755
ν_τ, τ	532	$-\frac{1}{2}\,i - \frac{\phi}{2}\,j + \frac{\phi^{-1}}{2}\,k$	−0.5367	122.459

Thus, the three mixing angles originate from the three U_2 generators acting together to become the k generator of SU(2). Note that I assume the charged lepton mixing matrix is the identity. Therefore, any discrepancy between these derived angles and the empirical angles could be an indication that the charged lepton mixing matrix has off-diagonal terms.

The quark mixing matrix CKM is worked out the same way [2] by using four discrete rotational groups in R^4, [3,3,3], [4,3,3], [3,4,3], [5,3,3], the [5,3,3] being equivalent to $2I \times 2I$. The mismatch of the third generators again requires the linear superposition of these four quark groups. The 3×3 CKM matrix is a submatrix of a 4×4 matrix. However, the mismatch of 3 lepton families to 4 quark families indicates a triangle anomaly problem resolved favorably in a later section by applying the results of this section.

3 Derivation of the Weinberg angle

The four electroweak generators of the SM local gauge group $SU(2)_L \times U(1)_Y$ are typically labeled W^+, W^0, W^-, and B^0, but they can be defined equivalently as the quaternion generators i, j, k and b. But we do not require the full SU(2) to act upon the flavor states $\pm\frac{1}{2}$ for discrete rotations in the unitary plane C^2 because the lepton and quark families represent specific discrete binary rotational symmetry subgroups of SU(2).

That is, we require just a discrete subgroup of $SU(2)_L \times U(1)_Y$. In fact, one might suspect that the 2I subgroup would be able to perform all the discrete symmetry rotations, but 2I omits some of the rotations in 2O. Instead, one finds that $2I \times 2I'$ works, where 2I′ provides the "reciprocal" rotations, i.e., the third generator U_2 of 2I becomes the third generator U_2' for 2I′ by interchanging ϕ and ϕ^{-1}:

$$U_2 = -\frac{1}{2}\, i - \frac{\phi}{2}\, j + \frac{\phi^{-1}}{2}\, k, \quad U_2' = -\frac{1}{2}\, i - \frac{\phi^{-1}}{2}\, j + \frac{\phi}{2}\, k. \quad (1)$$

Consider the three SU(2) generators i, j, k and their three simplest products: $i \times i = -1$, $j \times j = -1$, and $k \times k = -1$. Now compare the three corresponding $2I \times 2I'$ discrete generator products: $i \times i = -1$, $j \times j = -1$, and

$$U_2\, U_2' = -0.75 + 0.559i - 0.25\, j + 0.25k, \quad (2)$$

definitely not equal to -1. The reverse product $U_2' U_2$ just interchanges signs on the i, j, k, terms.

One needs to multiply this product quaternion $U_2 U_2'$ by

$$P = 0.75 + 0.559i - 0.25\, j + 0.25k \quad (3)$$

to make the result -1. Again, P′ has opposite signs for the i, j, k, terms only.

Given any unit quaternion $q = \cos\theta + \hat{n} \sin\theta$, its power can be written as $q^\alpha = \cos\alpha\theta + \hat{n} \sin\alpha\theta$. Consider P to be a squared quaternion $P = \cos 2\theta + \hat{n} \sin 2\theta$ because we have the product of two quaternions U_2 and U_2'. Therefore, the *quaternion* square root of P has $\cos\theta = \sqrt{0.75} = 0.866$, rotating the U_2 (and U_2') in the unitary plane C^2 by the quaternion angle of 30° so that each third generator becomes k. Thus the Weinberg angle, i.e., the weak mixing angle,

$$\theta_W = 30^\circ. \quad (4)$$

Therefore, the Weinberg angle derives from the mismatch of the third generator of $2I \times 2I'$ to the SU(2) third generator k.

The empirical value of θ_W ranges from 28.1° to 28.8°, values less than the predicted 30°. The reason for the discrepancy is unknown (but see [7]), although one can surmise either (1) that in determining the Weinberg angle from the empirical data perhaps some contributions have been left out, or (2) the calculated θ_W is its value at the Planck scale at which the internal symmetry space and spacetime could be discrete instead of continuous.

4 Anomaly cancellation

My introduction of a fourth quark family raises immediate suspicions regarding the cancellation of the triangle anomaly. The traditional cancellation procedure of matching each lepton family with a quark family "generation by generation" does produce the triangle anomaly cancellation by summing the appropriate $U(1)_Y$, $SU(2)_L$, and $SU(3)_C$ generators, producing the "generation" cancellation.

However, we now know that this "generation" conjecture is incorrect, because the derivation of the lepton and quark mixing matrices from the U_2 generators of the discrete binary subgroups of SU(2) above dictates that the 3 lepton families act as one collective lepton family for $SU(2)_L \times U(1)_Y$ and that the 4 quark families act as one collective quark family.

We have now created an effective single "generation" with one effective quark family matching one effective lepton family, so there is now the previously heralded "generation cancellation" of the triangle anomalies with the traditional summation of generator eigenvalues [8]. In the SU(3) representations the quark and antiquark contributions cancel. Therefore, there are no $SU(3) \times SU(3) \times U(1)$, $SU(2) \times SU(2) \times U(1)$, $U(1) \times U(1) \times U(1)$, or mixed U(1)-gravitational anomalies remaining.

There was always the suspicion that the traditional "generation" labeling was fortuitous because there was no specific reason for dictating the particular pairings of the lepton families to the quark families within the SM. Now, with the leptons and quarks representing the specific discrete binary rotation groups I have listed, a better understanding of how the families are related within the SM is possible.

5 Summary

The Weinberg angle derives ultimately from the third generator mismatch of specific discrete subgroups of SU(2) with the SU(2) quaternion generator k. The triangle anomaly cancellation occurs because 3 lepton families act collectively to cancel the contribution from 4 quark families acting collectively. Consequently, the SM may be an excellent approximation to the behavior of Nature down to the Planck scale.

Acknowledgements

The author thanks Sciencegems.com for generous support.

Submitted on December 17, 2014 / Accepted on December 18, 2014

References

1. Potter F. Geometrical Derivation of the Lepton PMNS Matrix Values. *Progress in Physics*, 2013, v. 9 (3), 29–30.
2. Potter F. CKM and PMNS mixing matrices from discrete subgroups of SU(2). *Progress in Physics*, 2014, v. 10 (1), 1–5.
3. Potter F. Our Mathematical Universe: I. How the Monster Group Dictates All of Physics. *Progress in Physics*, 2011, v. 7 (4), 47–54.
4. Potter F. Unification of Interactions in Discrete Spacetime. *Progress in Physics*, 2006, v. 2 (1), 3–9.
5. Potter F. Geometrical Basis for the Standard Model. *International Journal of Theoretical Physics*, 1994, v. 33, 279–305.
6. Coxeter H. S. M. Regular Complex Polytopes. Cambridge University Press, Cambridge, 1974.
7. Faessler M. A. Weinberg Angle and Integer Electric Charges of Quarks. arXiv: 1308.5900.
8. Bilal A. Lectures on Anomalies. arXiv: 0802.0634v1.

Can the Emdrive Be Explained by Quantised Inertia?

Michael Edward McCulloch

University of Plymouth, Plymouth, PL4 8AA, UK. E-mail: mike.mcculloch@plymouth.ac.uk

It has been shown that cone-shaped cavities with microwaves resonating within them move slightly towards their narrow ends (the emdrive). There is no accepted explanation for this. Here it is shown that this effect can be predicted by assuming that the inertial mass of the photons in the cavity is caused by Unruh radiation whose wavelengths must fit exactly within the cavity, using a theory already applied with some success to astrophysical anomalies where the cavity is the Hubble volume. For the emdrive this means that more Unruh waves are "allowed" at the wide end, leading to a greater inertial mass for the photons there. The gain of inertia of the photons when they move from the narrow to the wide end, and the conservation of momentum, predicts that the cavity must then move towards the narrow end, as observed. This model predicts the available observations quite well, although the observational uncertainties are not well known.

1 Introduction

It was first demonstrated by Shawyer (2008) that when microwaves are made to resonate within a truncated cone-shaped cavity a small, unexplained acceleration occurs towards the narrow end. In one example when 850 W of power was put into such a cavity with end diameters of 16 and 12 cm, and which had a Q value (dissipation constant) of 5900 the thrust measured was 16 mN towards the narrow end. The results from two of Shawyer's experiments are shown in Table 1 (rows 1-2). There is no explanation for this behaviour in standard physics, and it also violates the conservation of momentum, and Shawyer's own attempt to explain it using special relativity is not convincing, as this theory also should obey the conservation of momentum (Mullins, 2006).

Nethertheless, this anomaly was confirmed by a Chinese team (Juan et al., 2012) who put 80-2500 W of power into a similar cavity at a frequency of 2.45 GHz and measured a thrust of between 70 mN and 720 mN. Their result cannot however be fully utilised for testing here since they did not specify their cavity's Q factor or its geometry.

A further positive result was recently obtained by a NASA team (Brady et al., 2014) and three of their results are also shown in Table 1 (rows 3 to 5). They did provide details of their Q factor and some details of their cavity's geometry. The experiment has not yet been tried in a vacuum, but the abrupt termination of the anomaly when the power was switched off has been taken to show the phenomenon is not due to moving air.

McCulloch (2007) has proposed a new model for inertial mass that assumes that the inertia of an object is due to the Unruh radiation it sees when it accelerates, radiation which is also subject to a Hubble-scale Casimir effect. In this model only Unruh wavelengths that fit exactly into twice the Hubble diameter are allowed, so that a greater proportion of the waves are disallowed for low accelerations (which see longer Unruh waves) leading to a gradual new loss of inertia as accelerations become tiny, of order 10^{-10} m/s^2. This model, called MiHsC (Modified inertia by a Hubble-scale Casimir effect) modifies the standard inertial mass (m) as follows:

$$m_i = m\left(1 - \frac{2c^2}{|a|\Theta}\right) = m\left(1 - \frac{\lambda}{4\Theta}\right) \quad (1)$$

where c is the speed of light, Θ is twice the Hubble distance, a is the magnitude of the relative acceleration of the object relative to surrounding matter and λ is the wavelength of the Unruh radiation it sees. Eq. 1 predicts that for terrestrial accelerations (eg: 9.8 m/s^2) the second term in the bracket is tiny and standard inertia is recovered, but in low acceleration environments, for example at the edges of galaxies or in deep space (when a is small and λ is large) the second term in the bracket becomes larger and the inertial mass decreases in a new way.

In this way, MiHsC can explain galaxy rotation without the need for dark matter (McCulloch, 2012) and cosmic acceleration without the need for dark energy (McCulloch, 2007, 2010), but astrophysical tests like these can be ambiguous, since more flexible theories like dark matter can be fitted to the data, and so a controlled laboratory test like the EmDrive is useful.

Further, the difficulty of demonstrating MiHsC on Earth is the huge size of Θ in Eq. 1 which makes the effect very small unless the acceleration is tiny, as in deep space. One way to make the effect more obvious is to reduce the distance to the horizon Θ (as suggested by McCulloch, 2008) and this is what the emdrive may be doing since the radiation within it is accelerating so fast that the Unruh waves it sees will be short enough to be limited by the cavity walls in a MiHsC-like manner.

2 Method

The setup is a radio-frequency resonant cavity shaped like a truncated cone, with one round end then larger than the other. When the electromagnetic field is input in the cavity the microwaves resonate and we can consider the conservation of

momentum for the light

$$\frac{\partial(mv)}{\partial t} = 0 = m\frac{\partial v}{\partial t} + v\frac{\partial m}{\partial t}. \quad (2)$$

Interpreting the first term on the right hand side as the force (mass times acceleration) that must be exerted on the light to conserve its momentum, leads to

$$F = -c\frac{\partial m}{\partial t}. \quad (3)$$

So that

$$F = -c\frac{\partial m}{\partial x}\frac{\partial x}{\partial t} = -c^2\frac{\partial m}{\partial x}. \quad (4)$$

Normally, of course, photons are not supposed to have mass in this way, but supposing we consider this? We assume the inertial mass of the microwave photons (whatever its absolute value) is affected by MiHsC, but instead of the horizon being the far-off and spherically symmetric Hubble horizon as before, the horizon is now made by the asymmetric walls of the cavity. This is possible because the photons involved are travelling at the speed of light and are bouncing very fast between the two ends of seperation s and their acceleration ($a \sim v^2/s$) is so large that the Unruh waves that are assumed to produce their inertial mass are about the same size as the cavity, so they can be affected by it, unlike the Unruh waves for a terrestrial acceleration which would be far to long to be affected by the cavity. This dependence of the inertial mass on the width of the cavity means that the inertial mass is corrected by a MiHsC-like factor (Eq. 1). Using Eq. 4, the force is modified as follows

$$F = -c^2\left(\frac{m_{bigend} - m_{smallend}}{l}\right) \quad (5)$$

where l is the axial length of the cavity. Now using eq. 1 for the inertial masses and replacing the Hubble scale with the cavity width (W) assuming for simplicity the waves only have to fit laterally, and with subscripts to refer to the big and small ends, we get

$$F = \frac{-c^2 m}{l}\left(\frac{\lambda}{4W_{big}} - \frac{\lambda}{4W_{small}}\right) \quad (6)$$

where λ is the wavelength of the Unruh radiation seen by the photons because they are being reflected back and forth by the cavity$\lambda = 8c^2/a = 8c^2/(2c/(l/c)) = 4l$ so that

$$F = -4c^2 m\left(\frac{1}{4W_{big}} - \frac{1}{4W_{small}}\right). \quad (7)$$

Using $E = mc^2$ and $E = \int Pdt$ where P is the power, gives

$$F = -\int Pdt\left(\frac{1}{W_{big}} - \frac{1}{W_{small}}\right). \quad (8)$$

Table 1: Summary of EmDrive experimental data published so far, and the predicted (Eq. 10) and observed anomalous thrust.

Expt.	P	Q	l	w_{big}/w_{small}	F_{Pred}	F_{Obs}
	W	/1000	m	metres	mN	mN
S1	850	5.9	0.156	0.16/0.1275	4.2	16
S2	1000	45	0.345	0.28/0.1289	216	80-214
B1	16.9	7.32	0.332	0.397/0.244	0.22	0.091
B2	16.7	18.1	0.332	0.397/0.244	0.53	0.05
B3	2.6	22	0.332	0.397/0.244	0.1	0.055

Integrating P over one cycle (one trip of the photons from end to end) gives Pt where t is the time taken for the trip, which is l/c, so

$$F = \frac{-Pl}{c}\left(\frac{1}{W_{big}} - \frac{1}{W_{small}}\right). \quad (9)$$

This is for one trip along the cavity, but the Q factor quantifies how many trips there are before the power dissipates so we need to multiply by Q

$$F = \frac{-PQl}{c}\left(\frac{1}{W_{big}} - \frac{1}{W_{small}}\right) \quad (10)$$

where P is the power input as microwaves (Watts), Q is the Q factor measured for the cavity, l is the length of the cavity and W_{big} and W_{small} are the diameters of the wide and narrow ends of the cavity. MiHsC then predicts that a new force will appear acting towards the narrow end of the cavity.

3 Results

We can now try this formula on the results from Shawyer (2008) (from section 6 of their paper). This EmDrive had a cavity length of 15.6 cm, end diameters of 16 cm and 12.75 cm, a power input of 850 W and a Q factor of 5900, so

$$F = \frac{850 \times 5900 \times 0.156}{3 \times 10^8}\left(\frac{1}{0.16} - \frac{1}{0.1275}\right) = 4.2 \text{ mN}. \quad (11)$$

This predicts an anomalous force of 4.2 mN towards the narrow end, which is about a third of the 16 mN towards the narrow end measured by Shawyer (2008).

We can also try values for the demonstrator engine from section 7 of Shawyer (2008) which had a cavity length of 32.5 cm, end diameters of 28 cm and 12.89 cm, a power input of 1000 W and a Q factor of 45000. So we have

$$\begin{aligned} F &= \frac{1000 \times 45000 \times 0.325}{3 \times 10^8}\left(\frac{1}{0.28} - \frac{1}{0.1289}\right) \quad (12) \\ &= 216 \text{ mN}. \end{aligned}$$

This agrees with the observed anomalous force which was between 80 and 214 mN/kW (2008) (if we also take into account the uncertainties in the model due to the simplified 1-dimensional approach used).

Table 1 is a summary of various results from Shawyer (2008) in rows 1 and 2 and Brady et al. (2014) (see the Table on their page 18) in rows 3, 4 and 5. The Juan et al. (2012) data is excluded because they did not specify their Q factor or the exact geometry in their paper. Column 1 shows the experiment (S for Shawyer (2008) and B for Brady et al. (2014)). Column 2 shows the input power (in Watts). Column 3 shows the Q factor (dimensionless, divided by 1000). Column 4 shows the axial length of the cavity. Column 5 shows the width of the big and small ends (metres). Column 6 shows the thrust predicted by MiHsC and column 7 shows the thrust observed (both in milli-Newtons).

It is unclear what the error bars on the observations are, but they are likely to be wide, looking for example at the range of values for the case S2. MiHsC predicts the correct order of magnitude for cases S1, S2, B1 and B3 which is interesting given the simplicity of the model and its lack of adjustable parameters. The anomaly is case B2 where MiHsC overpredicts by a factor of ten. This case is anomalous in other ways since the Q factor in B2 was more than doubled from that in B1 but the output thrust almost halved.

More data is needed for testing, and a more accurate modelling of the effects of MiHsC will be needed. This analysis for simplicity, assumed the microwaves only travelled along the axis and the Unruh waves only had to fit into the lateral "width" dimension, but in fact the microwaves will bounce around in 3-dimensions so a 3-d model will be needed. This approximation would become a problem for a pointed cone shape where the second term in Eq. 10 would involve a division by zero, but it is a better approximation for a truncated cone, as in these experiments.

So far, it has been assumed that as the acceleration reduces, the number of allowed Unruh waves decreases linearly, but even a small change of frequency can make the difference between the Unruh waves fitting within a cavity, and not fitting and this could explain the variation in the observations, particularly in case B2.

4 Discussion

If confirmed, Equation 10 suggests that the anomalous force can be increased by increasing the power input, or the quality factor of the cavity (the number of times the microwaves bounce between the two ends). It could also be increased by boosting the length of the cavity and narrowing it. The effect could be increased by increasing the degree of taper, for example using a pointed cone. The speed of light on the denominator of Eq. 10 implies that if the value of c was decreased by use of a dielectric the effect would be enhanced (such an effect has recently been seen).

This proposal makes a number of controversial assumptions. For example that the inertial mass of photons is finite and varies in line with MiHsC. It is difficult to provide more backing for this beyond the conclusion that it is supported by the partial success of MiHsC in predicting the EmDrive with a very simple formula.

5 Conclusions

Three independent experiments have shown that when microwaves resonate within an asymmetric cavity an anomalous force is generated pushing the cavity towards its narrow end.

This force can be predicted to some extent using a new model for inertia that has been applied quite successfully to predict galaxy rotation and cosmic acceleration, and which assumes in this case that the inertial mass of photons is caused by Unruh radiation and these have to fit exactly between the cavity walls so that the inertial mass is greater at the wide end of the cavity. To conserve momentum the cavity is predicted to move towards its narrow end, as seen.

This model predicts the published EmDrive results fairly well with a very simple formula and suggests that the thrust can be increased by increasing the input power, Q factor, or by increasing the degree of taper in the cavity or using a dielectric.

Acknowledgements

Thanks to Dr Jose Rodal and others on an NSF forum for estimating from photographs some of the emdrives' dimensions.

Submitted on December 18, 2014 / Accepted on December 19, 2014

References

1. Brady D.A., White H.G., March P., Lawrence J.T. and Davies F.J. Anomalous thrust production from an RF test device measured on a low-thrust torsion pendulum. 50th AIAA/ASME/SAE/ASEE Joint Propulsion conference, 2014.
2. Juan Y. Net thrust measurement of propellantless microwave thrusters. *Acta Physica Sinica*, 2012, v. 61, 11.
3. McCulloch M.E. The Pioneer anomaly as modified inertia. *MNRAS*, 2007, v. 376, 338–342.
4. McCulloch M.E. Can the flyby anomaly be explained by a modification of inertia? *J. Brit. Interplanet. Soc.*, 2008, v. 61, 373–378.
5. McCulloch M.E. Minimum accelerations from quantised inertia. *EPL*, 2010, v. 90, 29001.
6. McCulloch M.E. Testing quantised inertia on galactic scales. *Astro. & Space Sci.*, 2012, v. 342, 575–578.
7. Mullins J. Relativity drive: the end of wings and wheels? *New Scientist*, 2006, no. 2568, 30–34.
8. Shawyer R. Microwave propulsion — progress in the emdrive programme. 59th International Astronautical conference (IAC-2008). Glasgow, UK.

Structures of Superdeforemed States in Nuclei with A ∼ 60 Using Two-Parameter Collective Model

N. Gaballah

Physics Department, Faculty of Science (Girls branch), Al-Azhar University, Cairo, Egypt. E-mail: nermgaballah@yahoo.com

Superdeformed (SD) states in nuclei in mass region $A \sim 60-90$ are investigated within the framework of two-parameter formula of Bohr and Motelson model. The concept of γ-ray transition energy E_γ over spin (EGOS) is used to assign the first order estimation of the bandhead spin. The model parameters and the true spin of bandhead have been obtained by adopted best fit method in order to obtain a minimum root-mean-square deviation between the calculated and the experimental γ-ray transition energies. The transition energies E_γ and the dynamical moment of inertia $J^{(2)}$ for data set include thirteen SD bands in even-even nuclei are calculated. The results agree with experimental data well. The behavior of $J^{(2)}$ as a function of rotational frequency $\hbar\omega$ are discussed. By using the calculated bandhead moment of inertia, the predicted quadrupole moments of the studied yrast SD bands are calculated and agree well with the observed data.

1 Introduction

Since the initial discovery of a superdeformed (SD) rotational band in ^{152}Dy [1], several SD bands were identified in different mass region [2]. The SD 60, 80 and 90 regions are of particular interest because they showed exciting new aspects of their large rotational frequency and they present experimental difficulties due to the increased doppler broading of γ-ray peaks and the decreased detection efficiency at large γ-ray transition energies. In $A \sim 60$, the negative-parity SD1 in ^{62}Zn was the first SD band [3], it assigned to configurations with two $ig_{9/2}$ protons (π) and three $ig_{9/2}$ neutrons (ν). It is formed in the $Z = 30$ deformed gap i.e with two $f_{7/2}$ proton holes [4,5]. The SD bands in $A \sim 60$ region are characterized by very large transition energies reaching 3.2 MeV or more. The yrast SD band in Sr was interpreted [6,7] as having the $\nu\, 5^2\pi 5^1$ configuration, i.e the excitation of two $N = 5$, $h_{11/2}$ intruder neutrons, which corresponding to the $N = 44$ shell gap with a large deformation, and a single proton excitation of the $N = 5$, $h_{11/2}$ intruder orbital. The predicted deformation for this band was $\beta_2 \simeq 0.55$ [6]. A systematic analysis on Sr nuclei shows that the quadrupole moment of the SD band in ^{82}Sr is the largest among these Sr isotopes. This may be an indication of the important role of $N = 44$ SD shell gap. For the region $A \sim 90$ SD states with large deformation $\beta_2 \simeq 0.6$ in ^{88}Mo were identified [8]. These findings were in agreement with cranked Woods-Saxon-Strutinsky calculations, which predicted $Z = 42$ and $Z = 43$ to be favored particle numbers at SD shapes in $A \sim 90$ nuclei [8,9].

As it is well known, the experimental data on SD bands consist only in a series of γ-ray transition energies linking levels of unknown spins. Spin assignment is one of the most difficult and unsolved problem in the study of superdeformation.This is due to the difficulty of establishing the deexcitation of a SD band into known yrast states of normal deformed band. Several approaches to assign the spins of SD bands were proposed [10–16]. For all such approaches an extrapolation fitting procedures was used. The purpose of the present paper is to predict the spins of the SD nuclear states in the $A \sim 60-90$ region and to study their properties by using the one-parameter and two-parameters Bohr-Mottelson model. The theoretical formalism is presented in section 2. The theoretical results and a comparison with experimental data are discussed in section 3. Finally a brief conclusion is given in section 4.

2 The formalism

For the strongly deformed nuclei, the collective excitations exhibit a spectrum of rotational character. In even-even nuclei, the spectrum is given by:

$$E(I) = A\,[I(I+1)] \tag{1}$$

where A is the inertial parameter $A = \hbar^2/2J$, with J denoting the effective moment of inertia, which is proportional to the square of the nuclear deformation, and expected to vary slowly with the mass number A. The γ-ray transition energies with the band are given by:

$$\begin{aligned} E_\gamma(I) &= E(I) - E(I-2) \\ &= 4A\left(I - \tfrac{1}{2}\right). \end{aligned} \tag{2}$$

It is interesting to discuss the energy levels by plotting the ratio $E_\gamma(I)$ to spin $(I-\frac{1}{2})$(EGOS)($E-Gamma$ Over Spin) [17] against spin. Therefore, the EGOS for rotational formula (2) can be written as:

$$EGOS = \frac{E_\gamma(I)}{\left(I - \frac{1}{2}\right)} = 4A. \tag{3}$$

Even in a first note on deformed nuclei, Bohr and Mottelson [18] remarked that the simple rotational formula equation (1) gives deviations from experimental data. They pointed out

Table 1: The calculated E Gamma Over Spin (EGOS) for $^{62}Z_n(\mathrm{SD}_1)$ compared to the experimental ones at three bandhead spins $I_0, I_0 \pm 2$ using the one-parameter formula.

$I(\hbar)$	$I_0 = 14.5$ $EGOS\,(\mathrm{keV}/\hbar)$		$I_0 = 16.5$ $EGOS\,(\mathrm{keV}/\hbar)$		$I_0 = 18.5$ $EGOS\,(\mathrm{keV}/\hbar)$	
	exp.	cal.	exp.	cal.	exp.	cal.
16.5	124.562	124.560				
18.5	123.055	124.560	110.722	110.720		
20.5	122.000	124.560	110.750	110.700	99.650	99.648
22.5	122.272	124.560	110.909	110.720	100.681	99.648
24.5	122.458	124.560	112.083	110.720	101.666	99.648
26.5	124.461	124.560	113.038	110.720	103.461	99.648
28.5			115.571	110.720	104.964	99.648
30.5					107.866	99.648

Table 2: The calculated E Gamma Over Spin(EGOS) for $^{62}Z_n(S\,D_1)$ compared to the experimental ones at three bandhead spins $I_0, I_0 \pm 2$ using the two-parameter formula.

$I(\hbar)$	$I_0 = 18$ $EGOS\,(\mathrm{keV}/\hbar)$		$I_0 = 20$ $EGOS\,(\mathrm{keV}/\hbar)$		$I_0 = 22$ $EGOS\,(\mathrm{keV}/\hbar)$	
	exp.	cal.	exp.	cal.	exp.	cal.
20	102.205	101.692				
22	103.023	102.901	92.697	92.477		
24	103.829	104.124	94.255	94.143	84.808	84.607
26	105.490	105.599	95.686	95.957	86.862	86.759
28	106.872	107.304	97.818	97.919	88.727	88.978
30	109.694	109.221	99.627	100.019	91.186	91.280
32			102.730	102.287	93.301	93.678
34					96.597	96.180

that agreement was improved by adding to it a second term (The Bohr-Mottelson two-term formula)

$$E(I) = A[I(I+1)] + B[I(I+1)]^2. \tag{4}$$

The new parameter B is almost negative and is 10^3 times less than that value of A.

$$E_\gamma(I) = A(4I-2) + B\left[2(4I-2)\left(I^2 - I + 1\right)\right], \tag{5}$$

and the EGOS can be written as:

$$\begin{aligned} EGOS &= \frac{E_\gamma(I)}{\left(I - \frac{1}{2}\right)} \\ &= 4A + 8B\left(I^2 - I + 1\right). \end{aligned} \tag{6}$$

For SD bands, one can determine the first-order estimation of the bandhead spin I_0 using equation (2) by calculating the ratio

$$\frac{E_\gamma(I_0+4)}{E_\gamma(I_0+2)} = \frac{E(I_0+4) - E(I_0+2)}{E(I_0+2) - E(I_0)} = \frac{2I_0+7}{2I_0+3}. \tag{7}$$

Let

$$E_{\gamma_1} = E_\gamma(I+2), \tag{8}$$

$$E_{\gamma_2} = E_\gamma(I+4), \tag{9}$$

$$J_0^2 = \frac{4}{E_{\gamma_2} - E_{\gamma_1}}, \tag{10}$$

we can find the bandhead spin I_0 as:

$$I_0 = \frac{1}{2}\left[E_{\gamma_1} J_0^2 - 3\right]. \tag{11}$$

Now, let us define the angular velocity ω as the derivative of the energy E with respect to the spin I

$$\omega = \hbar^{-1}\frac{dE}{d\hat{I}}; \quad \hat{I} = [I(I+1)]^{\frac{1}{2}}. \tag{12}$$

Two possible types of moments of inertia were suggested by Bohr and Mottleson [18] reflecting two different aspects of nuclear dynamics. The kinematic moment of inertia $J^{(1)}$ and the dynamic moment of inertia $J^{(2)}$:

$$J^{(1)} = \frac{\hbar^2}{2}\left[\frac{dE}{d[I(I+1)]}\right]^{-1} = \frac{\hbar}{\omega}[I(I+1)]^{\frac{1}{2}}, \tag{13}$$

Table 3: The bandhead spin proposition and the model parameters A and B adopted from the best fit procedures for the studied SD bands in the $A = 62 - 88$ mass region. The experimental bandhead moment of inertia are also given.

Z	N	Nuclear and the SD band	$E_\gamma(I_0+2\rightarrow I_0)$ (keV)	I_0 ($\hbar$)	A (keV)	B (keV)
30	32	^{62}Zn(SD1)	1993	20	20.997	2.313×10^{-3}
38	42	^{80}Sr(SD1)	1443	16	20.881	-1.873×10^{-4}
		^{80}Sr(SD2)	1688	18	22.106	-1.041×10^{-3}
		^{80}Sr(SD3)	1846	18	24.056	-4.466×10^{-4}
		^{80}Sr(SD4)	2140	20	26.371	-1.705×10^{-3}
38	44	^{82}Sr(SD1)	1429.8	17	19.292	1.770×10^{-4}
40	46	^{86}Zr(SD1)	1518	23	14.732	5.881×10^{-4}
		^{86}Zr(SD2)	1577	16	23.390	-1.354×10^{-3}
		^{86}Zr(SD3)	1866	25	19.082	-1.146×10^{-3}
		^{86}Zr(SD4)	1648	18	22.037	-1.021×10^{-3}
42	46	^{88}Mo(SD1)	1238.6	33	5.788	1.308×10^{-3}
		^{88}Mo(SD2)	1458.6	33	7.676	1.219×10^{-3}
		^{88}Mo(SD3)	1259.1	23	11.406	1.202×10^{-3}

$$J^{(2)} = \hbar^2 \left[\frac{d^2E}{d\left[[I(I+1)]^{\frac{1}{2}}\right]^2} \right] = \hbar \frac{d[I(I+1)]^{\frac{1}{2}}}{d\omega}. \quad (14)$$

$J^{(1)}$ is equal to the inverse of the slope of the curve of energy E versus $\hat{I}^2$ times $(\hbar^2/2)$, while $J^{(2)}$ is related to the curvature in the curve of E versus $\hat{I}$.

In terms of our two-parameter Bohr-Mottleson formula equation (4), yield

$$\hbar\omega(I) = 2\hat{I}\left(A + 2B\hat{I}^2\right), \quad (15)$$

$$J^{(1)}(I) = J_0\left(1 + \frac{2B}{A}\hat{I}^2\right)^{-1}, \quad (16)$$

$$J^{(2)}(I) = J_0\left(1 + \frac{6B}{A}\hat{I}^2\right)^{-1}, \quad (17)$$

with

$$J_0 = \frac{\hbar^2}{2A}. \quad (18)$$

Experimentally the dynamic moment of inertia $J^{(2)}$ is related to the difference ΔE_γ in consecutive transition energies E_γ along a band in the following way

$$\begin{aligned} J^{(2)} &= \frac{dI}{d\omega} \simeq \frac{\Delta I}{\Delta\omega} \simeq \frac{2}{\Delta\left(\frac{E_\gamma}{2}\right)} = \frac{4}{\Delta E_\gamma} \\ &= \frac{4}{E_\gamma(I+2\rightarrow I) - E_\gamma(I\rightarrow I-2)} \end{aligned} \quad (19)$$

remembering that $\omega \simeq E_\gamma/2$. Hence equal ΔE_γ's imply equal $J^{(2)}$'s.

The quadrupole deformation parameter β_2 are derived from the electric quadrupole transition probabilities $B(E_2)$. For this purpose, the well formula [18]

$$B(E_2, I\rightarrow I-2) = \frac{5}{16\pi} Q_0^2 \langle 2020|00\rangle^2, \quad (20)$$

was first applied to extract the intrinsic quadrupole moment Q_0. Then the deformation β_2 of the nuclear charge distribution was derived with the expression [19]

$$Q_0 = \frac{3}{\sqrt{5\pi}} ZR^2\beta_2(1 + 0.36\beta_2) \times 10^{-2}\text{eb} \quad (21)$$

where $R = 1.2\, A^{\frac{1}{3}}$ fm, and Z is the number of protons and A is the number of nucleons.

If X represents the ratio between the major to minor axis of an ellipsoid, then X can be deduced from Q by using the following formula [19]

$$Q = \frac{2}{5} ZR^2 \frac{X^2-1}{X^{\frac{2}{3}}} \times 10^{-2}\text{eb}. \quad (22)$$

The bandhead moment of inertia J_0 is related to the quadrupole deformation β_2 by the Grodzins formula [20]

$$J_0 = c(Z)A^{\frac{5}{3}}\beta_2^2. \quad (23)$$

c(Z) describes the calibration of this relationship between J_0 and β_2.

3 Results and discussions

For each SD band, we used the EGOS concepts of the one-parameter and the two-parameter models equations(3,6) to assign the bandhead spin I_0. Tables (1, 2) and Figure(1) presents

Table 4: Level spin I, γ-ray transition energies E_γ and the dynamical moment of inertia $J^{(2)}$ calculated by using the optimized best parameters listed in Table(3). The experimental γ-ray transition energies are also listed.

^{62}Zn(SD1)				^{80}Sr(SD3)			
E_γ^{exp}(keV)	$I(\hbar)$	E_γ^{cal}(keV)	$J^{(2)}(\hbar^2\text{MeV})^{-1}$	E_γ^{exp}(keV)	$I(\hbar)$	E_γ^{cal}(keV)	$J^{(2)}(\hbar^2\text{MeV})^{-1}$
1993	22	1988.275	17.849	1846	20	1849.857	21.806
2215	24	2212.375	17.054	2039	22	2033.287	22.028
2440	26	2446.915	16.269	2216	24	2214.874	22.275
2690	28	2692.781	15.499	2391	26	2394.445	22.549
2939	30	2950.862	14.750	2572	28	2571.830	22.853
3236	32	3222.048		2747	30	2746.857	
^{82}Sr(SD1)				^{86}Zr(SD1)			
E_γ^{exp}(keV)	$I(\hbar)$	E_γ^{cal}(keV)	$J^{(2)}(\hbar^2\text{MeV})^{-1}$	E_γ^{exp}(keV)	$I(\hbar)$	E_γ^{cal}(keV)	$J^{(2)}(\hbar^2\text{MeV})^{-1}$
1429.8	19	1436.598	25.385	1518	15	1513.088	29.361
1596.6	21	1594.170	25.273	1646	17	1649.323	28.729
1757.7	23	1752.439	25.151	1785	19	1788.551	28.081
1918.6	25	1911.473	25.020	1929	21	1930.996	27.417
2076.6	27	2071.340	24.880	2077	23	2076.886	26.745
2228.6	29	2232.107	24.731	2228	25	2226.446	26.066
2380.7	31	2393.844	24.574	2383	27	2379.901	25.384
2544.6	33	2556.616	24.408	2540	29	2537.478	24.702
2736	35	2720.494		2696	31	2699.403	
^{86}Zr(SD3)				^{86}Zr(SD4)			
E_γ^{exp}(keV)	$I(\hbar)$	E_γ^{cal}(keV)	$J^{(2)}(\hbar^2\text{MeV})^{-1}$	E_γ^{exp}(keV)	$I(\hbar)$	E_γ^{cal}(keV)	$J^{(2)}(\hbar^2\text{MeV})^{-1}$
1866	27	1851.803	36.037	1648	20	1658.218	25.696
1959	29	1962.798	38.197	1811	22	1813.881	26.412
2062	31	2067.518	40.815	1967	24	1965.327	27.241
2155	33	2165.521	44.030	2123	26	2112.163	28.202
2244	35	2256.368	48.048	2273	28	2253.996	29.317
2343	37	2339.618	53.181	2403	30	2390.435	30.615
2429	39	2414.832		2491	32	2521.086	
^{80}Sr(SD4)				^{88}Mo(SD2)			
E_γ^{exp}(keV)	$I(\hbar)$	E_γ^{cal}(keV)	$J^{(2)}(\hbar^2\text{MeV})^{-1}$	E_γ^{exp}(keV)	$I(\hbar)$	E_γ^{cal}(keV)	$J^{(2)}(\hbar^2\text{MeV})^{-1}$
2140	22	2132.134	23.600	1458.6	35	1460.250	29.582
2292.1	24	2301.619	24.723	1595.6	37	1595.465	27.823
2459	26	2463.411	26.068	1740.1	39	1739.226	26.182
2621.1	28	2616.854	27.693	1894.9	41	1892.002	24.652
2763	30	2761.294		2054.2	43	2054.260	23.227
				2224.3	45	2226.469	
^{80}Sr(SD2)				^{88}Mo(SD1)			
E_γ^{exp}(keV)	$I(\hbar)$	E_γ^{cal}(keV)	$J^{(2)}(\hbar^2\text{MeV})^{-1}$	E_γ^{exp}(keV)	$I(\hbar)$	E_γ^{cal}(keV)	$J^{(2)}(\hbar^2\text{MeV})^{-1}$
1688	20	1662.433	25.670	1238.6	35	1228.823	31.877
1821.1	22	1818.252	26.399	1342.1	37	1354.302	29.707
1950	24	1969.772	27.244	1480.7	39	1488.949	27.716
2090	26	2119.593	28.224	1633.5	41	1633.266	25.891
2256	28	2258.315	29.363	1795.5	43	1787.756	24.218
2364.1	30	2394.540	30.692	1962.2	45	1952.921	22.683
2573.9	32	2524.865		2133.4	47	2129.269	21.274
				2306.6	49	2317.284	

Table 6: The calculated quuadrupole deformation parameter β_2 and the major to minor axis ratio X in the yrast SD bands for even-even ^{62}Zn, ^{80,82}Sr, ^{86}Zn and ^{88}Mo nuclei. The experimental quadrupole moments Q^{exp} are also given for comparison.

	J_0 ($\hbar^2$MeV^{-1})	C(Z)	β_2	Q eb	X	Q^{exp} eb
^{62}Zn(SD1)	23.835	0.1261	0.4410	2.6178	1.52	2.70
^{80}Sr(SD1)	24.002	0.1106	0.3822	3.3438	1.44	3.42
^{82}Sr(SD1)	25.917	0.1089	0.3920	3.4973	1.45	3.54
^{86}Zr(SD1)	33.939	0.0996	0.4508	4.4512	1.54	4.60
^{88}Mo(SD1)	86.385	0.1707	0.5390	5.8295	1.66	6.00

Table 5: Level spin I, γ-ray transition energies E_γ and the dynamical moment of inertia $J^{(2)}$ calculated by using the optimized best parameters listed in Table(3). The experimental γ-ray transition energies are also listed.

^{80}Sr(SD1)			
E_γ^{exp}(keV)	$I(\hbar)$	E_γ^{cal}(keV)	$J^{(2)}(\hbar^2\text{MeV})^{-1}$
1443	18	1453.619	24.395
1611	20	1617.584	24.500
1775.1	22	1780.848	24.616
1948	24	1943.338	24.745
2118	26	2104.983	24.886
2284	28	2265.711	25.041
2440.9	30	2425.449	25.208
2595	32	2584.127	25.389
2743	34	2741.672	25.585
2680	36	2898.011	
^{86}Zr(SD3)			
E_γ^{exp}(keV)	$I(\hbar)$	E_γ^{cal}(keV)	$J^{(2)}(\hbar^2\text{MeV})^{-1}$
1577	18	1579.123	24.266
1730	20	1743.961	25.036
1890	22	1903.730	25.944
2056	24	2057.908	27.014
2227	26	2205.976	28.280
2392	28	2347.414	29.786
2514	30	2481.702	31.591
2562	32	2608.320	33.776
2708	34	2726.748	
^{88}Mo(SD3)			
E_γ^{exp}(keV)	$I(\hbar)$	E_γ^{cal}(keV)	$J^{(2)}(\hbar^2\text{MeV})^{-1}$
1259.1	25	1259.498	31.051
1382.6	27	1388.315	29.644
1522.9	29	1523.249	28.265
1669.4	31	1664.763	26.926
1817.0	33	1813.317	25.631
1976.0	35	1969.375	24.386
2134.0	37	2133.397	23.195
2297.0	39	2305.846	

the numerical values and graph of EGOS at three different values of bandhead spins I_0, $I_0 \pm 2$ for the yrast SD band in ^{62}Zn as example for our calculations. The model parameters

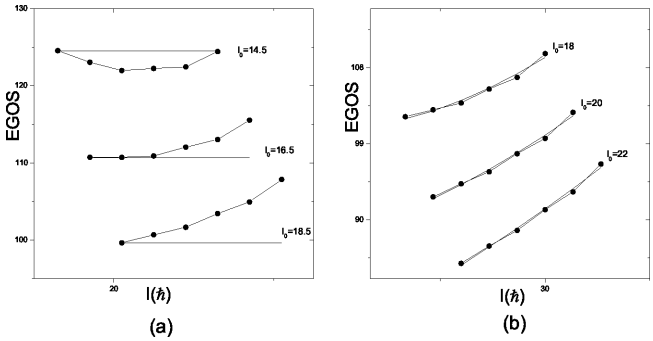

Fig. 1: Calculated (solid lines) and experimental (closed circles) EGOS against spin I for these different values of bandhead spin $I_0, I_0 \pm 2$. (a) for first order estimation of I_0 (b) for second order estimation of I_0.

A and B are then fitted to reproduce the observed transition energies E_γ. The procedure is repeated for several trail values of A and B and recalculate the true spin of the lowest observed level. In order to illustrate the sensitivity of the root mean square deviation, we employed the common definition of the chi squared

$$\chi^2 = \frac{1}{N}\sum_i \left[\frac{E_\gamma^{exp}(I_i) - E_\gamma^{cal}(I_i)}{\Delta E_\gamma^{exp}(I_i)}\right]^2 \qquad (24)$$

where N is the number of data points and ΔE_γ^{exp} is the experimental error in γ-ray transition energies. The experimental data are taken from the evaluated nuclear structure data file ENSDF [2]. Table (3) lists the bandhead spin proposition and the adopted model parameters. Using the best fitted parameters, the spins I, the γ-ray transition energies E_γ, the rotational frequency $\hbar\omega$ and the dynamical moment of inertia $J^{(2)}$ are calculated and listed in Table(4) compared to the observed E_γ.

Figures (2, 3, 4) shows the experimental and calculated dynamical moment of inertia $J^{(2)}$ as a function of rotational frequency $\hbar\omega$ for the SD bands in our even-even nuclei. The experimental and calculated values are denoted by solid circles and solid lines respectively.

By substituting the calculated bandhead moment of inertia J_0 in Grodzins formula equation (23), we adjusted the pro-

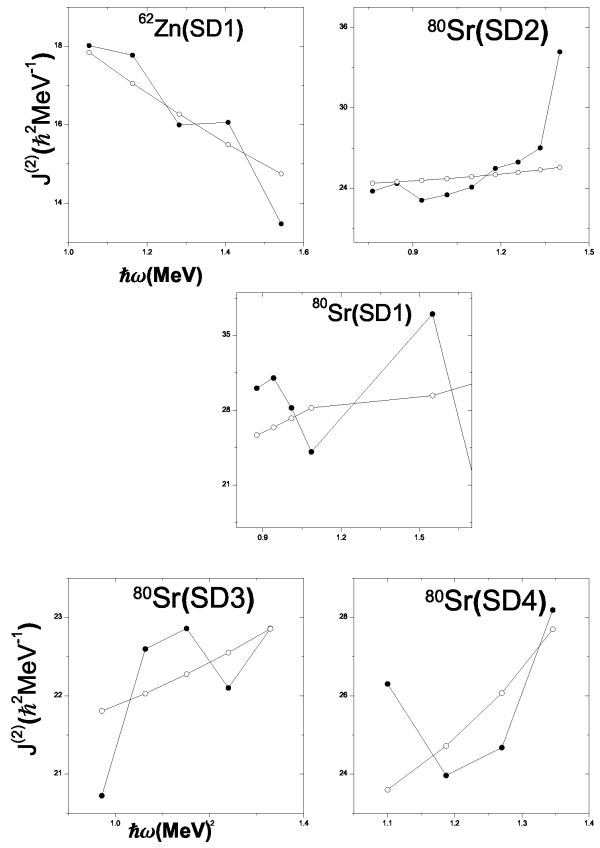

Fig. 2: Shows the experimental and calculated dynamical moment of inertia $J^{(2)}$ as a function of rotational frequency $\hbar\omega$ for even-even ^{62}Zn(SD1) and ^{80}Sr(SD1, SD2, SD3 and SD4). The experimental and calculated values are denoted by solid circles and solid lines respectively.

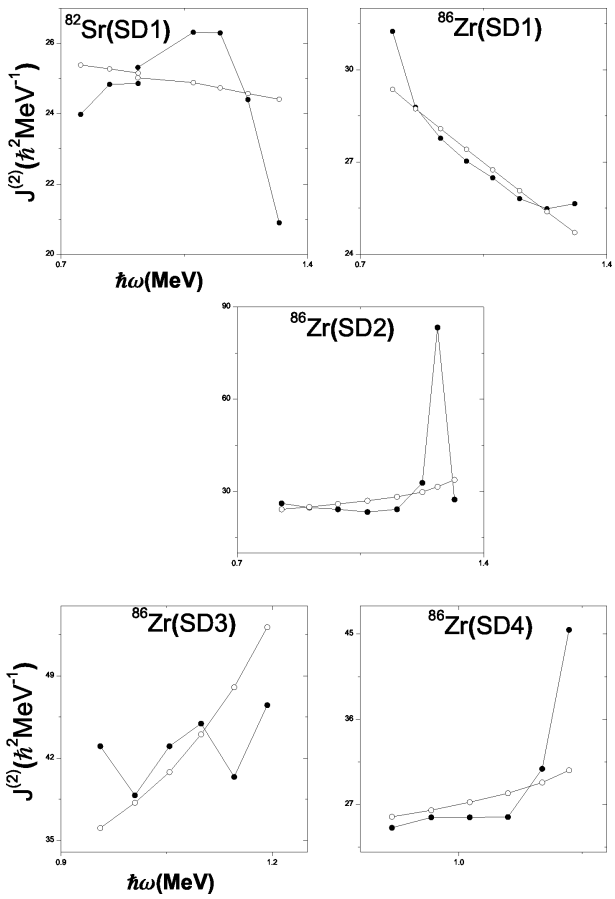

Fig. 3: Shows the experimental and calculated dynamical moment of inertia $J^{(2)}$ as a function of rotational frequency $\hbar\omega$ for even-even ^{82}Sr(SD1) and ^{86}Zn(SD1, SD2, SD3 and SD4). The experimental and calculated values are denoted by solid circles and solid lines respectively.

portional constant c(Z) for each yrast SD band and extracted the deformation parameter β_2 and then calculated the transition quadrupole moment Q which is related to the ratio X of the major to minor axis. The results are given in Table (5).

4 Conclusion

The structure of the SD bands in the mass region $A \sim 60-90$ have been investigated in the framework of two-parameter Bohr-Mottelson model. The bandhead spins have been extracted by using first order estimation method using the concept of EGOS. The model parameters have been determined by using a best fit method between the calculated and the experimental transition energies. The calculated transition energies E_γ, rotational frequency $\hbar\omega$ and dynamic moments of inertia $J^{(2)}$ are all well agreement with the experimental ones. This confirm that our model is a particular tool in studying the SD rotational bands. The behavior of $J^{(2)}$ as a function of $\hbar\omega$ have been discussed. The quadrupole deformation parameters are also calculated.

Submitted on December 5, 2014 / Accepted on December 12, 2014

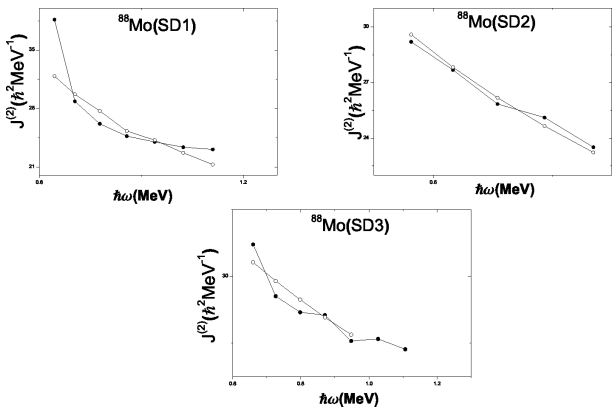

Fig. 4: Shows the experimental and calculated dynamical moment of inertia $J^{(2)}$ as a function of rotational frequency $\hbar\omega$ for even-even ^{88}Mo(SD1, SD2 and SD3). The experimental and calculated values are denoted by solid circles and solid lines respectively.

References

1. Twin P. J. , Nyak B. M. Observation of a Discrete Line Superdeformed Band up to $60\hbar$ in ^{152}Dy. *Physical Reveiw Letters*, 1986, v. 57, 811–814.
2. National Nuclear Data Center NNDC, Brookhaven National Laboratory, http.//www.nndc.bnl.gov/chart/
3. Svenssan C.E. et al. Observation and Quadrupole-Moment Measurement of the First Superdeformed Band in the $A \sim 60$ Mass Region. *Phys. Rev. Lett.*, 1997, v. 79, 1233.
4. C. H. Yu et al, Comparison of Superdeformation Bands in ^{61}Zn and ^{60}Zn: Possible evidence for $T = 0$ Pairing. *Phys. Rev.* 1999, v. 60C, 031305.
5. Johnasson E.K. et al. *Phys. Rev.*, 2008, v. C77, 064316.
6. Smith A.G. et al. Observation of Superdeformation in ^{82}Sr. *Phys. Lett.*, 1995, v. 355B, 32.
7. Yu C.H. et al. Lifetime Measurements of Normally Deformed and Superdeformed States in ^{82}Sr. *Phys. Rev.*, 1998, v. 57C, 113.
8. Bäck T. et al. Observation of Superdeformed States in ^{88}Mo. *Eur. Phys. J.*, 1999, v. 6A, 391.
9. Cederwall B. et al. Favoured Superdeformed States in ^{89}Tc. *Eur. Phys. J.*, 1999, v. 6A, 251.
10. Becker J.A. et al. Level Spin and Moment of Inertia in Superdeformed Nuclei Near $A = 194$. *Nucl. Phys.*, 1990, v. A520, C187–C194.
11. Droper J.E. et al. Spins in Superdeformed Bands in the Mass 190 region. *Phys. Rev.*, 1990, v. C42, R1791–R1795.
12. Zeng J.Z. et al. Critical of the spin Assignement of Rational Band. *Commun Theor. Phys.*, 1995, v. 24, 425.
13. Goel A. *Int. J. Scientific Research*, 2013, v. 21, 2277.
14. Hegazi A.M., Ghoniem M.H. and Khalaf A.M. Theoretical Spin Assignment for Superdeformed Rotational Bands in Mercury and Lead Nuclei. *Egyptian Journal of Physics*, 1999, v. 30, 293–303.
15. Khalaf A.M. et al. Description of Rotational Bands in Superdeformed Nuclei by Using Two-Parameter Empirical Formula. *Egyptian Journal of Physics*, 2003, v. 34, 159–177.
16. Khalaf A.M., Sirag M.M. and Taha M. Spin Assignement and Behavior of Superdeformed Bands in $A \sim 150$ Mass Region, *Turkish Journal of Physics*, 2013, v. 37, 49–63.
17. Khalaf A. and Okasha M. Properties of Nuclear Superdeformed Rotational Bands in $A \sim 190$ Mass Region. *Progress in Physics*, 2014, v. 10, 246–252.
18. Bohr A. and Mottelson B. Nuclear Structure v.2, Benjamin Inc, New York, 1975.
19. Clark R.M. et al. Very Extended Shapes in the $A \sim 110$ Region. *Phys. Rev. Lett.*, 2001, v. 87, 202502.
20. Grodzins I. *Phys. Lett.*, 1962, v. 2, 88.

ERRATA. NOTICE OF REVISION

Notice of Revision: "On the Equation which Governs Cavity Radiation I, II", by Pierre-Marie Robitaille

Pierre-Marie Robitaille
Department of Radiology, The Ohio State University, 395 W. 12th Ave, Columbus, Ohio 43210, USA
E-mail: robitaille.1@osu.edu

Professor Pierre-Marie Robitaille wishes to inform the readership of *Progress in Physics* that revisions were made on December 26, 2014 to the following two papers:

1. On the Equation which Governs Cavity Radiation I, *Progress in Physics*, 2014, v. 10, issue 2, 126–127.
2. On the Equation which Governs Cavity Radiation II, *Progress in Physics*, 2014, v. 10, issue 3, 157–162.

In addition to *Progress in Physics*, the electronic versions of these works have been archived on viXra.org and ResearchGate.

Submitted on December 29, 2014 / Accepted on December 29, 2014

Nuclear Power and the Structure of a Nucleus According to J. Wheeler's Geometrodynamic Concept

Anatoly V. Belyakov

E-mail: belyakov.lih@gmail.com

In this paper on a unified basis in terms of mechanistic interpretation of J. Wheeler's geometrodynamic concept the attempt to explain the nature of nuclear forces as the result of the complex nucleons structure and to submit the model of the structure of atomic nuclei is done. It is shown that the assumption of the existence of closed contours, including electron and proton quarks leads to a conclusion about the existence of W, Z-bosons and also the Higgs boson whose mass is calculated. Values of the coupling constants in the strong and weak interactions are calculated, and it is shown that they do not indicate the strength of the interaction, but indicate only the strength of bonds between the elements of nucleon structure. The binding energy of the deuteron, triton and alpha particles are defined. Dependence of the nucleon-nucleon interaction of the distance is explained. The structural scheme of nuclei is proposed, the inevitability of presence of envelopes in nuclei is proved, the formulas allowing to estimate the features of nuclear structure, as well as correctly to assess the binding energy of nuclei and their mass numbers are obtained. The results of calculations at the level of the model suggest the possibility to use this model for the construction of an appropriate theory.

1 Introduction

At present there is no a complete theory of the nuclear structure, which would explain all properties of atomic nuclei. To describe properties and behavior of atomic nuclei, different models are used, each of which is based on various experimental facts and explains some allocated properties of the nucleus. One reason for this is that the analytical dependences for the interaction forces between nucleons are until now not derived.

In the quantum theory, the interaction between the microparticles is described as an exchange of specific quanta (photons, pions, gluons, and vector bosons) associated with these types of interactions. The dimensionless parameter determining the relative strength of any interaction (an interaction constant or coupling constant α) is assumed proportional to the source interaction charge by analogy with the charge of an electron in the electromagnetic interaction:

$$\alpha_e = \frac{e^2}{\hbar c} = \frac{1}{137}, \qquad (1)$$

where e is the electron charge (in the CGSE).

But the problem consists in that for both strong and weak interactions the mechanism of interaction and, accordingly, a coupling constant strongly depend on the interaction energy (distance) and are determined experimentally.

In terms of the developed model based on the mechanistic interpretation of J. Wheeler's geometrodynamic concept [1], such a variety of types and mechanisms of interaction seems strange and unreasonable. In contrast to the quantum theory, which states that microphenomena in no way can be understood in the terms of our world scale, the mechanistic interpretation of Wheeler's idea above all assumes the existence of common or similar natural laws, which are reproduced at the different scale levels of matter that, in particular, allows using of macroscopic analogies in relation to the objects of microworld.

The proposed model of nuclear forces and nuclear structure as well as previous works [2–5] is based on the general conservation laws and balances between main interactions: electrical, magnetic, gravitational and inertial — with no additional coefficients or any arbitrary parameters introduced. Without using complicated mathematical apparatus, this work is not physical and mathematical one, but rather is the physical and logical model. However, application of Wheeler's ideas to this area of microphenomena gives the opportunity to clarify the cause and nature of nuclear forces and give a reasonable scheme of nuclear structure, which is confirmed by some of the examples of successful calculations made on the basis of the model.

2 Initial conditions

Recall that in this article, as well as in the earlier works, the charges in accordance with Wheeler's idea treated as singular points on the three-dimensional surface, connected by a "worm-hole" or vortical current tube similar to the source-drain principle, but in an additional dimension of space, constituting a closed contour as a whole.

The closest analogy to this model, in the scale of our world, could be the surface of ideal liquid, vortical structures in it and their interactions which form both relief of the surface and sub-surface structures (vortex threads and current tubes).

In this model, there is no place for a *charge* as a specific matter, it only manifests the degree of the nonequilibrium

state of physical vacuum; it is proportional to the momentum of physical vacuum in its motion along the contour of the vortical current tube. Respectively, the *spin* is proportional to the angular momentum of the physical vacuum with respect to the longitudinal axis of the contour, while the *magnetic interaction* of the conductors is analogous to the forces acting among the current tubes.

In such a formulation the electric constant ε_0 makes sense the linear density of the vortex current tube

$$\varepsilon_0 = \frac{m_e}{r_e} = 3.233 \times 10^{-16}\ \text{kg/m}, \tag{2}$$

and the value of *inverse magnetic constant* makes sense the centrifugal force

$$\frac{1}{\mu_0} = c^2\varepsilon_0 = 29.06\ \text{n}, \tag{3}$$

appearing by the rotation of a element of the vortex tube of the mass m_e and of the radius r_e with the light velocity c; this force is equivalent to the force acting between two elementary charges by the given radius, and electron charge makes sense the momentum of the vortex current tube (counter) with a mass of $m_e c_0^{2/3}$ and with velocity of $c_0^{2/3} \times [\text{m/sec}]$, the energy of which is equal to the maximum energy of the electron $m_e c^2$, i.e.

$$e = m_e c_0^{4/3} \cos q_w \times [\text{m/sec}] = 1.603 \times 10^{-19}\ \text{kg m/sec}, \tag{4}$$

where c_0 is the dimensionless light velocity $c \times [\text{m/sec}]^{-1}$, q_w is the Weinberg angle of mixing of the weak interaction, it equals 28.7°.

Vortex formations in the liquid can stay in two extreme forms — the vortex *at the surface* along the X-axis (let it be the analog of a fermion of the mass m_x) and the vortical current tube *under the surface* of the angular velocity v, the radius r and the length l_y along the Y-axis (let it be the analog of a boson of the mass m_y). These structures oscillate inside a real medium, passing through one another (forming an oscillation of oscillations). Probably, fermions conserve their boson counterpart with half spin, thereby determining their magnetic and spin properties, but the spin is regenerated up to the whole value while fermions passing through boson form. The vortex thread, twisting into a spiral, is able to form subsequent structures (current tubes). The possibility of reciprocal transformations of fermions and bosons forms shows that a mass (an energy) can have two states and pass from one form to another.

In paper [2] proceeding from conditions of conservation of charge and constancy parameters μ_0 and ε_0, parameters of the vortex thread m_y, v, r, for an arbitrary $p^+ - e^-$-contour defined as a proportion of the speed of light and electron radius as:

$$m_y = (an)^2, \tag{5}$$

$$v = \frac{c_0^{1/3}}{(an)^2}, \tag{6}$$

$$r = \frac{c_0^{2/3}}{(an)^4}, \tag{7}$$

where n is quantum number, a is inverse fine structure constant.

Wherein, referring to the constancy ε_0 (linear density), it is clear that the relative length of the tube current in the units of r_e is equal boson mass m_y in the units of m_e, i.e.

$$l_y = m_y = (an)^2. \tag{8}$$

In the model the particles themselves are a kind of a contour of subsequent order, formed by the intersection of the X-surface with the current tube, and they have their own quantum numbers defining the zone of influence of these microparticles. In [3] determined that for the proton

$$n_p = \left(\frac{2c_0}{a^5}\right)^{1/4} = 0.3338, \tag{9}$$

for an electron $n_e = \sqrt{n_p} = 0.5777$, and for the critical contour, when $r \to r_e$ and $v \to c$, $n_c = c_0^{1/6}/a = 0.189$.

Hereinafter all the numerical values of the mass, size and speed are given in dimensionless units: as a proportion of mass of the electron m_e, its radius r_e and speed of light c.

It is important to note that the contour or vortex tube, which the vortex thread fills helically, can be regarded as completely "stretched", i.e. elongated proportional to $1/r$ or, on the contrary, extremely "compressed", i.e. shortened proportional to $1/r$ and filling all the vortex tube of radius r_e. In the latter case its compressed length $L_p = l_y r$ is numerically equal to the energy of the contour boson mass in units of mass-energy.

Indeed, since $r = v^2$, then the above quantities values in dimensionless units are in all cases identical:

$$L_p = l_y r = m_y r = m_y v^2 = \frac{c_0^{2/3}}{(an)^2}. \tag{10}$$

It is obvious that an arbitrary boson mass in the units of mass-energy will match of its own value m_y only in the case of ultimate excitation of the vortex tube when $r \to r_e$ and $v \to c$.

Here are some of the parameters for mentioned three particular contours. Substituting in the formula (7) and (8) the parameters n_e, n_p, and n_c one can find the characteristic sizes of the vortex tubes: for an electron vortex thread radius $r = 0.0114$, the length of the vortex thread $l_y = 6267$, for the proton $r = 0.1024$, $l_y = 2092$, for a critical contour $r = 1$, $l_y = 670$.

As for the accepted *scheme of the nucleons structure*, in [3] it is shown that the proton has a complex structure, which

is revealed in process of transition to smaller scales with increasing the interaction energy, i.e., as if its "deepening" along the Y-axis; so to the outside observer the nuclear forces manifest themselves in a complex manner.

In the *inner area of the proton* there are three critical section (quarks), each of which is crossed by three force lines (charges 1, 1, −1). The presence of inverse circulation currents forming three closed contours leads to the fact that the intersection of the critical section by the lines of force inside the proton will for an outside observer be projected on the *outer proton surface* in the form of $\frac{2}{3}$, $\frac{2}{3}$, $-\frac{1}{3}$ of the total charge.

Along the Y-axis the proton boson vortex tube is located having parameters $m_{py} = 2092$ and $r_p = 0.1024$. The most "deep" along the Y-axis the quark vortex tubes are located with the parameters defined in [3]: the quantum number $n_k = 0.480$, the total fermion mass $m_{kx} = 12.9$, the total boson mass $m_{ky} = 4324$, the radius of the vortex tube $r_k = 0.024$.

It should be noted that the value of the parameter r_k is confirmed by works on studying of *neutron polarizability*. In [6] the lower limit the polarizability coefficient is specified of $a_p = 0.4\times10^{-42}\,\mathrm{cm}^3$. This means that the linear inhomogeneity parameter in the structure of the neutron coincides with the radius of the quark vortex tube as $(a_p)^{1/3} = 7.37\times10^{-15}$ cm or $0.026\,r_e$.

Neutron has three closed contour, i.e. six force lines instead of nine ones, which a proton has, and, therefore, the total neutron quark mass has the value of $12.9\times2/3 = 8.6$. Having in mind adopted direction and the possible distribution of the force lines in the neutron [3], one can expect that in the case of neutron polarization neutron may have the charges in the inner region of 1, −1, or −1, $\frac{2}{3}$, $\frac{1}{3}$, and in the projection of the outer surface of $-\frac{2}{3}$, $\frac{1}{3}$, $\frac{1}{3}$.

In the contour connecting the charged particles, the quarks are involved in the circulation and become an active part of the nucleon mass. It is assumed that in the critical section circulation velocity reaches the velocity of light, so quarks are actually dark matter, which is equivalent to the mass defect, reflecting the energy of bonds within nucleons or nuclei; the nominal mass-energy of a quark is $0.511\times\frac{12.9}{3} = 2.2$ MeV.

When considering the closed contour having contradirectional currents, from the balance of magnetic and gravitational forces recorded in a "Coulombless" form the characteristic size of a contour as a *geometrical mean* of two linear values is obtained:

$$l_k = \sqrt{l_i\, r_i} = \sqrt{\frac{z_{g_1} z_{g_2}}{z_{e_1} z_{e_2}}}\,\sqrt{2\pi\gamma\,\varepsilon_0}\;\times[\mathrm{sec}]\,, \qquad (11)$$

where z_{g_1}, z_{g_2}, z_{e_1}, z_{e_2}, r_i, l_i are gravitational masses and charges expressed through masses and charges of an electron, a distance between current tubes and theirs length.

Number of vortex thread constituting contour reflects the difference of material medium from vacuum, and their greatest value corresponds to the ratio of electrical forces to gravitational forces, i.e. value:

$$f = \frac{c^2}{\varepsilon_0\,\gamma} = 4.16\times10^{42}, \qquad (12)$$

where γ is the gravitational constant.

The contour can be considered located both in the X-area (for example, $p^+ - e^-$-contour in atom) and in the Y-area (vortex tube inside an atomic nucleus). When a proton and an electron come together (for example, when its contraction by the e-capture) a deformation of the contour takes place, energy and the fermion mass increase, while the boson mass decreases, but the impulse (charge) is conserved.

Formula (11) for unit charge taking $z_{g_2} = 1$ and after calculating the constants gets the form in the units of r_e and m_e:

$$m_k = z_{g_1} = b\,l_k^2\,, \qquad (13)$$

where m_k is the proton quark mass involved in the circulation contour, $b = 5.86\times10^{-5}$.

Parameter l_k is composite. If the contour (vortex tubes) is directed along the Y-axis, then $r_i = r$, $l_i = l_y$, if the contour is directed along the X-axis, then in calculating parameters are replaced, i.e. $r_i = l_y$, $l_i = r$. Having in mind (7), (8), (11), and (13)), replacing arbitrary parameters r_i and l_i by the sizes of short and long axes of the contour and calculating constants, we obtain the formulas relating the quark mass and the contour linear parameters:

$$m_k = \frac{26.25}{r} = 0.0392\,\sqrt{l_y}\,, \qquad (14)$$

and also

$$r\,\sqrt{l_y} = c_0^{1/3}. \qquad (15)$$

3 On boson masses

The circuit parameters in X-region and Y-region in the general case do not match, but both include the quark mass, which depends on the size of the contour. Let us compare the parameters of these contours for some specific cases.

Let us consider X-contour of own electron at $n_e = 0.5777$. Its size along the X-axis, as follows from (8), $r_i = l_y = 6267$. From (14) we find the quark mass $m_k = 3.10$. For having of the same value of mass-energy L_p, Y-contour, as follows from (10), should have a quantum number $n = 2.77$. The boson mass of such a contour according to (5) $m_y = 1.44\times10^5$, that is close to the mass of W-bosons.

Let us consider the contour of own proton at $n_p = 0.3338$. Its size along the X-axis $r_i = l_y = 2092$ and the quark mass $m_k = 1.795$. Y-contour having the same value of mass-energy has $n = 3.645$. Boson mass of such a contour $m_y = 2.494\times10^5$, that is almost exactly ***corresponds to the mass of the Higgs boson*** (125 GeV).

Let us consider the critical contour at $n_c = 0.189$. Its size along the X-axis $r_i = l_y = 672$ and the quark mass $m_k = 1.02$. That is, in the limiting case the ***quark mass becomes equal to the mass of an electron***. Y-contour having the same value of mass-energy has $n = 4.884$, i.e. it is a standard contour [2]. The boson mass of such a contour $m_y = 4.48 \times 10^5$, that is close to the total mass of W, Z-bosons.

Thus, these relations between the masses of the particles taking part in the weak interaction (quarks, bosons, protons, and electrons) to some extent clarify the nature of the weak interaction and the physical meaning of its interpretation as "the exchange of bosons". It turns out that W, Z-bosons and the Higgs boson are the vortex tube having the value of mass-energy equal to mass-energy of the quarks included in the circulation contours corresponding to their own electron, proton, and critical contours. And in the course of the weak interaction X-contour is reduced and when performing this condition, it is reoriented to Y-region, transmitting momentum (charge) to the proton while keeping the angular momentum (spin, in the case of e-capture, for example); then it is extracted as a neutrino [3]. From the above it implies that the *Higgs boson is not a unique particle in microcosm*.

4 The coupling constants

In [5] a formula is obtained, from which it follows that the unit contour or vortex tube having a *momentum equivalent to the electron charge* consist of three unit vortex threads. After transformation this formula can be written as:

$$n_i^3 = \frac{\frac{m_e c_0^{2/3} r_e}{\sqrt{2\pi} \times [\sec^2]}}{\frac{2\pi\gamma m_e^2}{r_e^2}} = 26.25. \qquad (16)$$

This formula represents the ratio of inertial forces occurring during acceleration of the standard contour boson mass and acting toward to periphery (as the value $\frac{r_e}{\sqrt{2\pi} \times [\sec]}$ is the rotational speed of the vortex thread relative to the longitudinal axis of the contour [3]) to the gravity forces acting between the masses of m_e at a distance of r_e. The numerator is constant, so the formula depends only on the force of gravity, i.e. from interacting masses and distances between them. This ratio (or its modification for arbitrary m_i and r_i) can be the equivalent of the coupling constant, as indicates the strength of the bonds between the elements of the proton structure (quarks).

4.1 Strong interaction

Suppose that quarks are located at the corners of an equilateral triangle at a distance r_e. In this case each of them is exposed of the sum of two projections forces, therefore the denominator into (16) should be corrected by multiplier $2 \sin 60°$. As a result, the formula (16) in the relative units of r_e and m_e after calculating of constants takes the form:

$$a_s = 15.15 \left(\frac{r_i}{m_i} \right)^2 . \qquad (17)$$

Consider the case of the strong interaction at low energies where the parameter r_i is greater than the nucleon size r_n. Let the mass of the proton quark takes a minimum value m_e (section 3), the distance between the quarks is r_e; substituting $r_i = 1$, $m_i = 1$ into (17), we obtain $a_s = 15.15$, which coincides with the known value determined at low energies $a_s \sim 15$.

It should be expected that at $a_s = 1$, there is a balance between the forces of gravity and peripheral inertia forces, which the nominal size of the proton can be determined from. Indeed, under this condition (17) it follows $r_i = 0.257$, and the size of the vortex tube, accordingly, is $0.257 / \sin 60° = 0.297$ or 0.84 fm, which coincides with the proton radius.

Consider the case of the strong interaction with $r_i < r_n$, where the energy of the interacting particles is high (about 100 GeV), and they approach each other at the minimum distance of the vortex proton tube $r_p = 0.1023$ (section 2). In this case, the distance between the quarks inscribed in the vortex proton tube is $r_i = r_p \sin 60° = 0.0887$. Substituting r_i and $m_i = 1$ into (17), we obtain $a_s = 0.119$. This calculated value coincides with the experimental data. Indeed, in [7] it was found that at the given energy $a_s = 0.1176 \pm 0.0024$.

Now it becomes clear physical meaning of the great difference in magnitudes of this type interaction. At low energies of the interacting particles affecting only the outer structure of nucleons ($r_i > r_n$, low "depth" along Y-axis) the peripheral inertial forces exceed the forces of gravity, so the elements of the structure (quarks) are weakly bonded to each other, can move away from the starting position and interact with nearby nucleon quarks. At high energies ($r_i < r_n$, more "depth" along Y-axis) interaction occurs at the level where the forces of mutual attraction holds the quarks in the bound state within the nucleon size, that leads to a decrease in the efficiency of the interaction of microparticles as a whole.

Note, that in the atoms nuclei quarks may also be in a bound state due to their large masses, which they acquire when entering into the $p^+ - e^-$-contours.

4.2 Weak interaction

When the weak interaction (such as in the case of e-capture, for example) the bosonic part of the proton quark or vortex tubes take part (section 3).

Let us assume that the mass of each of three quark tubes $m_i = m_{ky} = 4324/3 = 1441$ (section 2). Substituting m_i and $r_i = 1$ into (17), we find $a_w = 0.73 \times 10^{-5}$. This value agrees with the value of a_w, defined through Fermi constant (1×10^{-5}). At high interaction energies (about 100 GeV) the constant a_w increases to $\sim \frac{1}{40}$. In our model this increase can also be explained.

At the limit excitation of the contour vortex tube at the quarks level when $v \to c$ and $r \to r_e$ boson mass becomes equivalent to its mass-energy, but because the parameters ε_0 and μ_0 are constant then the radius of the vortex tube increases proportional to the ratio r_e/r_k. Since $r_e/r_k = 41.7$, then in this case $r_i = 41.7$, and the parameter a_w increases proportionally to the square of this ratio, i.e. $a_w = 0.73\times10^{-5}\times41.72^2 = \frac{1}{78}$, which is in agreement with the value of a_w determined at high energies.

4.3 On the electron

Suppose that the formula (17) is applied to the electron itself. Electron contains three vortex threads. Assuming $r_i = r_e$ and considering that the boson mass of an electron vortex threads is $m_i = \frac{1}{3}(an_e)^2 = 2089$, and it coincides with the proton boson mass, it is obvious that the *coupling constant for the electron in the weak interaction is identical to that of the proton*.

As for the strong interaction then in this case $m_i = \frac{1}{3}m_e$. Substituting into (17) $r_i = 1$ and $m_i = \frac{1}{3}$, we find $a_s = 136.4$, which almost coincides with the value of the reciprocal fine structure. Proceeding from the enormous value of the coupling constant a_s the electron structure cannot be in a bound state, and in equilibrium at $a_s = 1$ the size of the electron would be very small at $r_i = 0.086$. But having such a small radius the electron charge cannot place itself according to the classical definition, by which the potential energy of the electrostatic field is completely equivalent to the rest mass of an electron.

Thus, the electron to resolve this contradiction and be able to exist itself shall continuously oscillate between these states. Its pulsations provide the motion of medium along the p^+-e^--contours thereby confirming definition of the charge as the momentum.

Summing up the results of Chapter 4 one can say that the coupling constant defines neither the nature of nuclear forces, nor the interaction force, but only *indicates the strength of the bonds within the complex structure of nucleons*.

5 The nucleus

When considering nuclear forces hereinafter to take into account the Coulomb interaction at various energy levels (distances) proved sufficient, from which it can be concluded that the *introduction of any special nuclear forces is not required*, at least within the limits of this model.

As for scheme of nuclear structure, then the proposed scheme is, to a certain extent, associated with collective model (J. Rainwater, 1959, A. Bohr, and B. Mottelson, 1952). This model combines the provisions of the hydrodynamic and the envelope model and suggests that the nucleus consists of the inner stable part — the core formed the nucleons of filled envelopes and the outer nucleons moving in the field generated by the core nucleons.

5.1 Nuclear forces

Are there any special nuclear forces at all?

At high energies and short distances, i.e. when approaching nucleons to their radius $r_n = 0.842$ fm and overlapping of their *internal structures*, the interaction between nucleons occurs inside their total "quark bag" between oppositely quarks having inside the nucleon structure the charges of 1 and -1 at the distance of its vortex tube. Let us assume that the quark mass is minimal and equal to m_e, i.e. it is identical to an electron, then its vortex tube size is equal to the electron vortex tube size $r_k = 0.0114$ (section 2).

Write the formula for the potential in the units of MeV and the fractions of r_e. The depth of the attractive potential at the minimum distance for unit charges is

$$V = -\frac{0.511}{r_k}, \tag{18}$$

which gives -44.8 MeV (see Figure 1).

With further approach of nucleons at even higher energies (greater "depth" along Y-axis) the interaction at the level of boson vortex nucleons tubes is added. It is understood that the unidirectional vortex tubes are repelled, and as far as "deepening" along Y-axis their radius r decreases (here the role of magnetic attraction forces is negligible). Since the mass per unit length is reduced in proportion to the square of the radius, the local value of the electrical constant (linear density) ε_0 is reduced proportional to the ratio r/r_e. Thus repulsive potential as a result increases in inverse proportion to the square of the distance, and the resulting potential-distance dependence receives the form below:

$$V = 0.511\left(-\frac{1}{r_k} + \frac{1}{r^2}\right) \text{ MeV}. \tag{19}$$

Beyond "quark bag", at the distance of the nucleon diameter, the Coulomb interaction occurs between the fractional

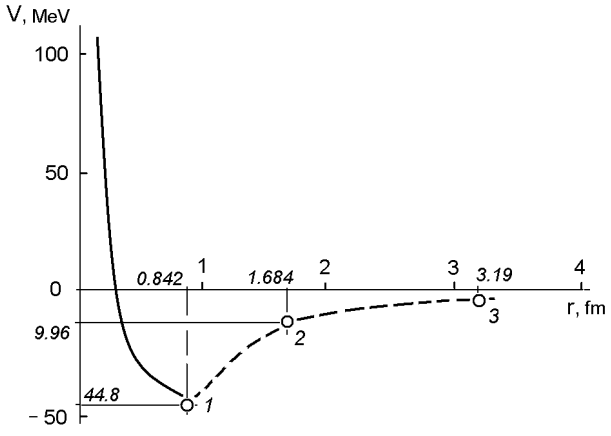

Fig. 1: Dependence of the nucleon-nucleon interaction on the distance between them.

charges of different signs, located on the *outer surface* of protons. Thus, attractive potential sharply decreases, for protons it is in proportion to the product of $\frac{1}{3} \times \frac{2}{3} = \frac{2}{9}$. Namely, at the distance $2r_n = 1.684$ fm attractive potential decreases to a value $\frac{2}{9} \times 44.8 = 9.96$ MeV.

Another reference point for plotting the dependence $V(r)$ can be found by equating the Coulomb repulsive forces between two protons at the distance between their centers to the residual attractive forces acting between the fractional charges located on the outer surface of the protons. In this case we have:

$$\frac{e^2}{\varepsilon_0 r^2} = \frac{2}{9} \frac{e^2}{\varepsilon_0 (r - 2r_n)^2}, \qquad (20)$$

from which we obtain $r = 2r_n \left(1 - \sqrt{\frac{2}{9}}\right)^{-1} = 3.78 r_n = 3.19$ fm, i.e. distance where the attractive forces between the nucleons can be neglected. The resulting dependence $V(r)$ is shown in Figure 1 and it as a whole corresponds to actual dependence.

Thus, it may be concluded that any special nuclear forces do not exist, and complex nuclear interaction is explained by the forces of unified nature (electrical) acting between the elements of the complex structure of nucleons at different levels (the "depths" along Y-axis), which are determined by the interaction energy.

5.2 The binding energy of deuterium, tritium and alpha particles

A deuterium nucleus — the deuteron is a rather loose formation, and therefore it can be assumed that the bond of two nucleons due to Coulomb forces between the proton having on its outer surface fractional charges of $\frac{2}{3}$, $\frac{2}{3}$, $-\frac{1}{3}$ and the polarized neutron with charges on the surface of $-\frac{2}{3}$, $\frac{1}{3}$, $\frac{1}{3}$. Let us assume that the nucleons form its own contour having at $n = n_p$ the parameters $l_y = 2092$ and $r = 0.1024$ (section 2). When substituting r into (18), we obtain the binding energy (potential) in the units of MeV bonding the nucleons in the deuteron: $E_d = 0.511 \times (\frac{2}{3} \times \frac{2}{3})/0.1024 = 2.22$ MeV that corresponds exactly to the actual binding energy of the deuteron.

Could this be an accidental coincidence? It is known that the good description of the characteristics of the deuteron provides the selection of the nucleon-nucleon n-p potential in the form of a rectangular pit of depth $V \sim 35$ MeV and of width $d = 2$ fm [8]. Assuming that d is the distance between the centers of nucleons, one can find that the distance between the fractional charges on the nucleon periphery is $d - 2r_n = 0.316$ fm or $0.112\, r_e$. The result is in good agreement with the proton vortex tube size, i.e. with parameter r, that confirms the correctness of calculation.

The tritium nucleus — triton consists of a proton and two neutrons attached. The mean square charge radius of the triton is 1.63 fm, so, obviously, the nucleons are in contact. Let us assume that the neutrons are polarized with charges of 1, -1. Binding energy can be determined by summing the mass-energy of the four quarks involved in creating bonds. As a result, we get $E_d = 2.2 \times 4 = 8.8$ MeV that is close to the actual triton binding energy (8.48 MeV).

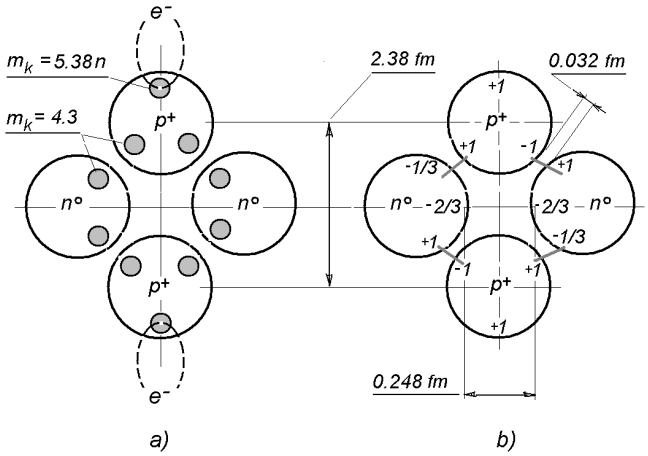

Fig. 2: Settlement scheme of the alpha particle: a — on the basis of the quark masses, b — on the basis of energy of the quarks.

An alpha-particle is a spherically symmetric object with radius of about 2 Fermi, and it is the most stable and compact structure (cluster) that can occur inside the atomic nucleus. If we assume that nucleons are in contact with each other, then for symmetrical arrangement of four nucleons having radii $r_n = 0.842$ fm and forming a closed system as a whole, in fact, the alpha-particles radius will be 2.04 fm, Figure 2.

The alpha particle emitted from a nucleus overcomes the potential barrier and, in addition, is a surplus energy in different ranges. Apparently, in addition to the mass-energy of eight quarks involved in the interaction, there is a necessity to take into account also the mass-energy of the two protons quarks included in $p^+ - e^-$-contours; this mass-energy depends on the quantum number of the contour, Figure 2a. It was revealed that alpha-clustering is most probable in the nucleus surface region where the density of nuclear matter is reduced to about one-third of density in the nucleus central part [9]. Therefore, we can assume that the protons of alpha-particles leaving the nucleus are associated with the second electron shell (the first one has only two electrons).

From (8), (13), and (14) it follows that the masses of quarks that are constituents in a $p^+ - e^-$-contour are proportional to the quantum number:

$$m_k = b\, a\, c_0^{1/3} n = 5.377\, n, \qquad (21)$$

i.e. for the second shell the quark mass is equal to 10.75. As a result, given the potential repulsion of two protons (~ 0.6 MeV at a specified distance 2.38 fm on the scheme), we obtain: $E_a = 0.511 \times (4.3 \times 8 + 10.75 \times 2) - 0.6 = 28.0$ MeV, which corresponds well to the actual alpha particles binding

energy (28.2 MeV).

One can determine the binding energy from another considerations by summing the energy of bonded opposite charges, assuming that the distance between them is equal to the radius of the electron vortex tube $r = 0.0114 = 0.032$ fm, Figure 2b. Other positive charges of the protons quarks are associated with the atom electrons, and the unaccounted negative neutrons charges create the repulsive potential. The bonds form a closed system, so one can assume that the alpha particle binding energy is the averaged binding energy of a link, since at destruction of a link the particle splits as a whole. Indeed, it is known that to remove of only a nucleon from alpha particles the energy about 20 MeV is required [9].

Given the above, referring to the adopted charges layout, the alpha particles geometry, and specified dimensions, one can write the final formula for the binding energy as the average energy per bond at subtracting the repulsive potentials of protons as whole units and the fractional charge repulsion potentials of neutrons:

$$E_a = \frac{1}{4}\left(1\times 1 + \frac{1}{3}\times 1 + 1\times 1 + \frac{1}{3}\times 1\right)\frac{0.511}{r} - \\ - 1\times 1\times\frac{0.511}{b} - \left(\frac{2}{3}\times\frac{2}{3}\right)\frac{0.511}{c}, \qquad (22)$$

where b and c are calculated from geometrical considerations: $b = 2r_n\sqrt{2} = 2.38$ fm or 0.845, $c = 2r_n(\sqrt{2}-1) = 0.697$ fm or 0.248. Substituting the values, we obtain $E_a = 28.3$ MeV, which coincides with the actual value.

It is known that the nuclei can be seen as the system of nucleons and at the same time as the system of the large number of clusters of different nature, which are in dynamic equilibrium, i.e. they disintegrate, are again formed and exchanged both nucleons and energy [10]. The closer to the nucleus center are protons, the higher energy they have, since the proton quarks mass-energy included in the $p^+ - e^-$-contours increases in proportion to the quantum number. When the transfer of energy from the center and from the inner envelopes to the periphery occurs, alpha-particles leaving the nucleus surface have the energy excess equal to the energy difference between the corresponding levels, i.e. referring to (22) and at changing to energy units $E_a = 2.75(n_2 - n_1)$ MeV.

Thus, when the excitation transfer from the third to the second envelope the energy of alpha-particles having two protons may be not more than $2\times 2.75 = 5.5$ MeV, and when the excitation transfer from the fourth to the second envelope — twice as much, not more than 11 MeV.

Indeed, for the emitted alpha particles there are two energy ranges: with the upper limit of 2–4 MeV for rare earth elements and 4–9 MeV for the elements heavier than lead [11]. Not numerous long-range alpha particles with higher energy get this energy after series of collisions with protons in the center of the nucleus, which are associated with the fifth, sixth, and seventh envelopes; accordingly, their maximum energy can reach $2\times 2.75(7-2) = 27.5$ MeV. The resulting value matches exactly the value of the maximum alpha particles energy, defined in during the study of heavy nucleus fission accompanied by the formation of three charged particles [12]. Moreover, in these particles energy spectrum there is no fine structure, which is understandable, since the energy of such particles is derived from protons homogeneously packed in the "quark bag" in the nucleus core, but not from the structural units in the nuclear envelopes composition having certain specificities.

It should be noted that the binding energies differences between neighboring isotopes for the nuclei of almost all elements are in the range of 20 MeV (for isotopes with the least number of neutrons) to 2 MeV (for isotopes with the greatest number of neutrons). That is, in the most cases these energy differences lie in the range from the nominal mass-energy of a cluster $2.2\times 8 = 17.6$ MeV to the mass-energy of a quark 2.2 MeV. This means that in the first case, with the excess of protons, addition of a neutron leads to the formation of an entire cluster (alpha-particles) and in the second case, with the excess of neutrons, — to another quark be only involved in a common bound nucleus structure.

Another fact confirming that clusters are only formed in the envelopes from the first to the fourth is the amount of isotopes depleted by neutrons. Typically, for most of elements (except radioactive ones) it is close to the number of clusters. The maximum amount of such isotopes Platinum has ($Pt^{195}\ldots Pt^{166}$), it is equal to the number of clusters in all four envelopes (30).

5.3 On the nucleus structure

In accordance with the model the packing density of alpha-clusters and of protons in particular increases toward the center of the nucleus, as the distance between the vortex tubes of $p^+ - e^-$- contours is reduced and the vortex tubes length increases. Therefore, the electrons located at the more distant orbits are associated with the protons located at the deeper nucleus levels; thus the *layers or envelopes are formed in the nucleus* that similarly to the electronic shells.

Suppose that the distance r_i between the vortex tubes cannot be less than the size of alpha-particles (4 Fermi). This condition limits the number of the electronic shell whose electrons can associate with the protons belonging to alpha-clusters and, accordingly, the nucleus envelope which deeper alpha-clusters are not formed. From (14) and (8) implies $n \geqslant 3.44$. Even if the diameter of the equivalent sphere equal to the volume of four alpha-particles nucleons ($\sim r_e$) to accept for limiting size, and even then $n < 5$. That is the electrons of the fifth and subsequent atom shells are associated with protons in the center of the nucleus; these protons are here not part of the alpha-clusters. Thus, the fourth layer (envelope) is the last in the nucleus.

It should be noted that a similar condition for the nu-

cleon size also determines the maximum possible number of the atom electron shell. Indeed, assuming $r_i \geqslant 2r_n$, we find $n_{max} \leqslant 8.1$.

Consider the heavy atom nucleus, for example, $_{82}Pb^{207}$, wherein there is a fourth filled electron shell with 32 electrons and, accordingly, the fourth layer of 16 clusters in the nucleus. It is not difficult calculate the outer and inner radii of the layer, assuming that one alpha-cluster has a volume equivalent to the volume of four nucleons, i.e. $4 \times (2r_n)^3 = 19.1$ fm^3. The inner radius is 2.93 fm. The remaining 22 protons are not part of the proton clusters; they are located in the center of the nucleus and have the volume equivalent to the sphere of exactly the same radius 2.93 fm. The outer diameter of the nucleus as a whole in the summation of the thickness of the four envelopes is $2.93 + 4 \times 2r_n = 9.66$ fm, which corresponds to the size of heavy nuclei.

Thus, it appears that for the elements heavier than lead, the protons taking part in the contours where electrons belong to the fifth and subsequent shells no longer completely go in the core of the nucleus. With increasing the number of protons the fourth nuclear envelope expands, additional neutrons are included in it, and radius of the nucleus increases.

Neutrons are not included in the cluster (for $_{82}Pb^{207}$ of such neutrons are 65) are placed in the free volume being forced out into the outer envelopes. One can assume that the average distance between them is not less r_e, accordingly, the average volume per a neutron exceeds 22.4 fm^3 that provides the nuclear attraction forces between neutrons to be absent and neutrons to move freely. Now it is possible to calculate the number of neutrons in the void volume (excluding the first envelope, which is the transition boundary structure, where the nuclear and charge density fall sharply down) and then the mass number. For lead the outer radius of the second envelope is $9.66 - 2r_n = 7.98$ fm, its volume is 2130 fm^3. Subtracting from this volume the volume of 30 clusters (120 nucleons) and subtracting the volume of 22 nucleons in the center of the nucleus, we obtain the volume 1452 fm^3, which can accommodate 65 neutrons. As a result, adding the number of protons (82) and neutrons in clusters (60), we obtain the exact mass number for the stable isotope of lead $A = 207$.

The highest density of nuclear matter exists in the nucleus center and in the inner envelopes. Assuming that the nucleons packing density in the nuclear core and in the adjoining envelope are identical, i.e. their nuclear density is the same, and on the basis of the above geometrical considerations, it is possible derive the relation between the number of nucleons in the nucleus core z_{cor} and their number in the adjoining envelope z_{env}, which provides this homogeneity condition:

$$z_{env} = c\left(1 + (\frac{z_{cor}}{c})^{1/3}\right)^3 - z_{cor}\,, \qquad (23)$$

were $c = \frac{4\pi}{3}$.

Equation (23) observed for the lead very precisely: 22 nucleons in the center correspond to 64 nucleons in the 4th

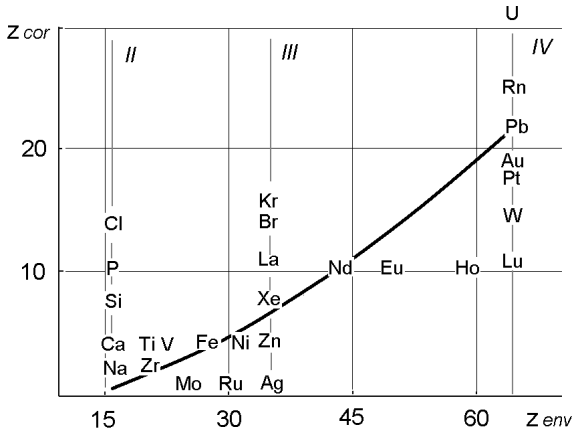

Fig. 3: Condition of the nucleus central part homogeneity with respect to the initial number of nucleons for the stable isotopes of some elements.

envelope (32 protons and 32 neutrons), so it turns out that in the nucleus core neutrons are absent. For the lighter nuclei the inner envelope volume including protons and neutrons can be considered as the core. Condition (23) is also satisfied of about for iron (4 nucleons in 4th envelope, 28 nucleons in 3d envelope), xenon (8 nucleons in the core 36 nucleons in 4th envelope) and for a few other elements. At that, for the nuclei of these elements the observed electric quadrupole moments are close to zero. For most other elements situation may be different; in the general case part of the neutrons or go in the nucleus core, or go in the adjacent envelope, and such nuclei may take a non-spherical shape.

Thus, for the condition (23) to be satisfied, it is necessary (for the metals heavier than iron having one or two electron at the fourth electronic shell) for the additional neutrons that are outside clusters to replenish the fourth inner nucleus envelope and (for the metals with $Z = 37 \ldots 52$, many of lanthanides, and heavy metals before lead) to instil into the nucleus core. For others, mainly non-metals and the elements heavier than lead, the neutrons must replenish the envelope adjoining to the nucleus inner part. Figure 3 shows the position of the curve $z_{cor}(z_{env})$ respect to the initial number of nucleons for stable isotopes of some elements.

Thus, knowing the structure of the atom electron shell and, accordingly, the number of protons in nucleus envelopes and its core, specifying the number of neutrons and having in mind the condition (23), one can try to reproduce the nucleus structure for different atoms and their isotopes. There is a question, how exactly the condition (23) should be satisfy during of additional neutrons distribution? That is whether equation (23) can be solved in integers, as it is done for lead? Perhaps this peculiarity defines some properties of the isotopes: lifetime and others.

To fill the outer nuclear envelopes neutrons there is usually no in enough. Therefore, for some nuclei its outer en-

Even numbered elements

Elements	$_4Be^9$	$_8O^{16}$	$_{14}Si^{28}$	$_{26}Fe^{56}$	$_{30}Zn^{65}$	$_{42}Mo^{96}$	$_{62}Sm^{150}$	$_{74}W^{184}$	$_{92}U^{238}$
Actual, MeV	58.2	128	237	492	567	831	1239	1473	1802
Calculated, MeV	62.6	131	244	487	566	822	1232	1479	1806
Calculated A	9	16	28	56	65	99	151	184	236

Odd numbered elements

Elements	$_5B^{11}$	$_{17}C^{l35}$	$_{21}Sc^{45}$	$_{29}Cu_{64}$	$_{39}Y^{89}$	$_{51}Sb^{122}$	$_{67}Ho^{165}$	$_{83}Bi^{209}$	$_{93}Np^{237}$
Actual, MeV	76.4	298	388	559	775	1033	1344	1640	1795
Calculated, MeV	79.7	303	388	544	757	1009	1344	1636	1821
Calculated A	11	35	45	63	90	123	165	208	238

velope must be squeezed, lose shape of a spherical layer and take the form of a polyhedron, in the corners of which alpha-clusters are. A similar phenomenon is starting to get a confirmation, for example, in [13].

5.4 The nuclei binding energies and the mass numbers

It is well known that nuclear binding energy E_n is calculated by the Weizsäcker semiempirical formula, based on the liquid drop model and consists of five members and empirical coefficients reflecting the contribution of various components in the total binding energy.

Presented above model allows calculating the nucleus binding energy without having to empirical coefficients. As mentioned in section 5.2, the nucleus energy is ultimately determined by the mass-energy of nucleon quarks. Represent this energy as the sum of the nominal energy of eight quarks in all clusters (Figure 2a), included in the envelopes from the first to the fourth as $8 \times 2.2\, z_{kl}$, the total energy of the proton quarks belonging to $p^+{-}e^-$-contour as $2.75(m_1 + 2m_2 + 3m_3 + \ldots)$, and the base energy of the first envelope as $2.75\, z$. The latter may be associated with a potential barrier.

Here it is denoted: z_{kl} is the clusters number, z is the protons total number, m_i is the electrons number in the i-th atom shell.

The final amount when changing the clusters number by the protons number in clusters has the form:

$$E_n = 8.8\, z_{pkl} + 2.75\,(m_1 + 2m_2 + 3m_3 + \ldots + z)\,,\ \text{MeV} \quad (24)$$

where z_{pkl} is the total protons number in the first — the fourth envelopes.

Formula (23) for the binding energy does not depend on the neutrons number; this indicates that for stable isotopes a certain optimum amount of neutrons are in accordance with protons. It turns out that it is possible to calculate the neutrons number based on energy balance considerations, using the dependences previously obtained.

It is considered that the neutrons and protons are different states of nucleons. This is true for the nominal quark masses of nucleons, since their mass-energies are identical and equal to $2 \times 2.2 = 4.4$ MeV. However, the mass-energy of neutron quarks must also comply with the mass-energy of proton quarks, which are included in the circulating $p^+{-}e^-$-contour $2.75(m_1 + 2m_2 + 3m_3 + \ldots)$, net of the basic energy of the unfilled first shell $2.75\, z$ and minus the nominal mass-energy of proton quarks, located in the nucleus center and not connected with neutrons $4.4(z{-}z_{pkl})$.

That is the balance of energy must be from which the neutrons number N and further the mass number $A = N + z$ can be determined:

$$2.75\,(m_1 + 2m_2 + 3m_3 + \ldots) - 2.75\, z - 4.4\left(z{-}z_{pkl}\right) = \\ = 4.4\, N\ \text{MeV}, \quad (25)$$

$$A = z_{pkl} + 0.625\,(m_1 + 2m_2 + 3m_3 + \ldots {-} z) + (4)_{A<140}\,. \quad (26)$$

For the mass number an amendment is necessary in some cases, which, it may be supposed, is the consequence of the presence of alpha-cluster four nucleons in the first envelope, which are split off when the nucleus reaches a certain mass. Thus, for light and medium nuclei the result of formula (26) should be increased by 4. For the heavier nuclei with $A > 140$, the amendment is not necessary, that seems to be due to their natural alpha decay. For the transuranic elements nuclei, as calculations are shown, their binding energy should also be reduced by the amount of the alpha particle binding energy.

Table 1 show the actual and calculated data of the binding energy and mass number rounded to the integer for the stable isotopes of certain elements according to the formulas (24) and (26). These formulas are obtained under the condition that the nuclei structure satisfies the condition (23). Existing slight variations in binding energy to the lower side for medium nuclei can be eliminated by considering their individual features, for example, with taking into account the energy bonds of additional neutrons, which replenish the core or adjoining nucleus envelope.

6 Conclusion

It seems surprising that the complex nature of nuclear forces and the structure of atomic nuclei proved possible to be largely understood without involving actual quantum concepts and complex mathematical apparatus.

The mass of equivalent to the Higgs boson mass are obtained, the coupling constants in different types of interactions, the binding energy of the deuteron, triton, and alpha particles are defined, the possible ranges of alpha particles energies are identified, and dependence of the nucleon-nucleon interaction from a distance is explained. Based only on the composition of the atom electron shells, it was possible to determine the nuclei binding energies, the nucleus neutron numbers, to reveal the important features of nuclei.

Obviously, these results indicate that the model adequately reflects the fundamental features of the atomic nucleus structure. These results give reason to believe that the foregoing model can become the basis of further theoretical developments for detailed describing the properties of nuclei and their behavior in nuclear reactions.

Submitted on December 19, 2014 / Accepted on December 25, 2014

References

1. DeWitt B.S. Quantum gravity. *Scientific American*, v. 249, December 1983, 112–129.
2. Belyakov A.V. Charge of the electron, and the constants of radiation according to J. A. Wheeler's geometrodynamic model. *Progress in Physics*, 2010, v. 4, 90–94.
3. Belyakov A.V. Macro-analogies and gravitation in the micro-world: further elaboration of Wheeler's model of geometrodynamics. *Progress in Physics*, 2012, v. 2, 47–57.
4. Belyakov A.V. On the independent determination of the ultimate density of physical vacuum. *Progress in Physics*, 2011, v. 2, 27–29.
5. Belyakov A.V. On materiality and dimensionality of the space. Is there some unit of the field? *Progress in Physics*, 2014, v. 10, 203–206.
6. Alexandrov Y.A. Polarizability of the neutron. The possibility of its determination of the neutron experiments. *Particle Physics and Nuclear Physics*, 2001, v. 2, issue 6.
7. Krivokhizhin V.G., Kotikov A.V. The structure functions of nucleons and the definition of the coupling constant of the strong interaction. *Particle Physics and Nuclear Physics*, 2009, v. 40, issue 7.
8. Ishkhanov B.S., Cabin E.I. Nuclear and Particle Physics. The Twentieth Century. Moscow University Publishers, Moscow, 2000.
9. Berezhnoy Y.A., Mikhailyuk V.P. Alpha-clustering in the scattering particles and light nuclei by nuclei. *Particle Physics and Nuclear Physics*, 2008, v. 39, issue 2.
10. Kadmensky S.G. Clusters in the Nucleus. *Soros Educational Journal*, 2000, issue 3.
11. Dulov E.N., Vagizov F.G., Bikchantaev M.M., Pyataev A.V. Gainov R.R. Spectra of Alpha-Particles, Semiconductor Detectors. Kazan State University, Institute of Physics, Kazan, 2013.
12. Perfilov N.A., Romanov Y.F., Solovyov Z.I. Fission of heavy nuclei with the emission of long-range α-particles. *Physics-Uspekhi*, July I960, v. LXXI, issue 3.
13. Dudek J., Curien D., Dubray N., Dobaczewski J., Pangon V., Olbratowski P., and Schunck N. Island of rare-Earth nuclei with tetrahedral and octahedral symmetries: possible experimental evidence. *Phys. Rev. Lett.*, 2006, v. 97, 072501.

Motion-to-Motion Gauge Entails the Flavor Families

Felix Tselnik
Ben-Gurion University of the Negev, P.O.B. 653, Beer-Sheva 84105, Israel
E-mail: tselnik@ee.bgu.ac.il

Charge and mass gauging procedure is carried out by means of counting the oscillation numbers of an auxiliary top-speed signal ("photons") between the appropriately ordered electrons and positrons, moving under their interaction along the diagonals of the cube toward its center (the "cube star"). Regular lattices composed of such stars transport the values of charge and mass over space-time regions. The gauge consists in detection of the cube symmetry in each star. However, the detected symmetry can also be observed, even if some particles of the basic electron/positron star are replaced with heavy mesons. These become an unavoidable byproduct of the gauge procedure. Two possible subsymmetries of the cube realizing such replacement correspond to two mesons, but the regularity of the whole lattice holds only for some particular values of their masses. Numerical solutions to the non-linear ODE systems describing this situation yield these masses in terms of electron mass, which are close to those of the μ- and τ-mesons.

1 Introduction

The existence of the three flavor families remains a mystery, and it appears rather artificial in the otherwise self-contained structure of the standard model of particle physics (see, for instance, [1]). As in all basic structures of physics, theories must agree with experimental facts, and, in turn, the performance of experiments depends on existing theoretical conceptions. The design of measuring devices includes their gauge, which is an intermediary between the measurement of interest and some standard test measurements. In order to eliminate clocks and rods in the gauge, which might hide some features of the desired correspondence, we suggested a direct motion-to-motion gauge [2, 3]. We shall show that the flavor families naturally arise from the particular way this gauge could be carried out. Since all related experiments are ultimately based on the observation of the trajectories of charged particles in external electromagnetic fields, the gauge of electric charges and masses of particles is at the heart of any measurement. A relevant gauge procedure could use a regular lattice comprised of elementary cells ("stars"), each one being a standard configuration of the trajectories of test particles that are identical, apart from the sign of their charges [2, 3]. Starting with the stars that are primary for the gauge lattice, the whole lattice is constructed in such a way that the primary stars completely define secondary ones. The resulting relay races make it possible to transport the initial values of charge and mass over a chosen space-time region. In an appropriate construction of the lattice, each star could be connected to a previous star along various sequences of intermediate stars. The preservation of charge and mass over such transports might be detected, provided various paths connecting a pair of stars reveal the same symmetry at both ends according to the dynamics of involved particles.

In order to realize this program one needs a method to construct standard stars unambiguously. For this purpose, it was proposed to count top signal oscillations between the particles of the star [2]. No rods or clocks are then needed, provided the elementary stars possess some symmetry belonging to the Platonic solids. In this communication, we confine ourselves to the lepton sector of elementary particles, corresponding to the cube subsystem of the full dodecahedron structure. To this end, consider electrons and positrons moving along the diagonals of the cube toward its center under mutual attraction — the "cube star". The cube consists of two interlaced tetrahedrons — one for electrons, another for positrons, and the star is thus electrically neutral as a whole. Charge is being gauged by means of detecting the cube symmetry as being seen in the equality of the related numbers of photon oscillations, so that the detection of even one extra oscillation is sufficient to find this symmetry broken. (It is convenient to replace formally the counting of inter-particle oscillations with that between the particle and an imaginary central body; the translation is straightforward.) Of particular interest is the limiting case of the finest lattice, in which only one photon oscillation is sufficient to detect the symmetry of the star. Just this finest star will be considered in what follows.

The regular lattice comprises the stars as elementary cells to form a whole charge gauging structure. For this to be possible, the electrons/positrons are bound to turn into neutrinos at the center: Otherwise, the exit potential together with the radiation reaction force would prevent their leaving the star, so destroying the lattice forming connections. We regard neutrinos massless (or having a mass that is negligible as compared to that of other involved particles), hence moving practically with the velocity of light independently of their kinetic energy.

Only the simplest case of cube star symmetry breaking was considered in the charge gauging procedure [2, 3], i.e. that in which asymmetry may occur only between the two opposite-charge tetrahedrons of the cube. The breaking of

cube symmetry in this case consists in this that particles belonging to different tetrahedrons have dissimilar masses m and/or absolute values of charge e, while these parameters remain identical within each tetrahedron. Perfect symmetry will be observed, provided all the involved particles have the same values of *both* m and $|e|$. In this case, the asymmetry to be detected is, in a sense, the weakest, and we assign it to the first flavor family, i.e. to that of the electron. We regard this — electron/positron — star as the basic one and ask whether or not our photon oscillations counting procedure might detect the symmetry as observed, even if some electrons/positrons in the star are being replaced with different particles. Detection of a perfect star with our method requires both charges and masses of the involved particles to be identical. Upon assuming the charges to remain equal, let us consider the lattice, in which some particles have a different mass. While electrons must turn into neutrinos in each star, these foreign particles ("mesons") are able to pass the center intact, since the exit barrier decreases there. They can then take part in the secondary stars. For this to be possible, they must satisfy three following requirements:

i. Preserve proper charge distribution in each star;

ii. Pass successfully the symmetry detection in the stars as carried out by counting photon oscillations;

iii. Yield the definite output velocity (e.g., equal to the input velocity) to be suitable over a long line of successive stars.

To fulfill these requirements, we have only two parameters at our disposal to be controlled over the whole lattice, that is, the mass and the velocity of the meson at the star entrance. We guess only much heavier mesons to be met with. Since the lattice is a ready structure and the slower mesons are just "impurities" in it, they will enter the next star with some time lag.

Besides the basic star, there exist only two configurations having weaker sub-symmetries. Depending on the mass found for the related foreign particle, one of the sub-symmetries will be ascribed to the τ-meson, and another to the μ-meson.

In the first sub-symmetry, only one pair of opposite electron and positron is replaced by the meson/anti-meson pair. Their diagonal is the natural axis of the star symmetry, since under the interaction in the star the mesons keep moving along this axis. The trajectories of the remaining three electrons and three positrons are curvilinear, though confined pair-wise to three planes (the members of each pair don't belong to a common diagonal of the cube). Then the absolute values of the Cartesian coordinates of all six electrons/positrons, both along and transverse the axis, will be the same. We refer to this case as (6:2) sub-symmetry. (In this notation, the electron/positron star is (8:0) sub-symmetry.) Contrary to the basic (8:0) case, magnetic part of the interaction is no longer cancelled on the curved trajectories in stars possessing only sub-symmetries, though the total resulting interaction still leaves the particles on the same planes they would move under the electric force alone.

In the second sub-symmetry, two identical meson/anti-meson pairs replace electron-positron pairs. Now all eight trajectories are curved though confined to the two mutually orthogonal planes, one of which carries only electrons and positrons, while another — only mesons and anti-mesons. Within each of these planes, the absolute values of the appropriately chosen Cartesian coordinates of its particles will be the same. We refer to this case as (4:4) sub-symmetry. Following the previous argument [2], we ignore the terms with retarded interaction in the equations describing the motion of the particles in the star, but radiation reaction of the accelerated particles may be important. However, even rough estimation of this multiple soft photons radiation will be sufficient to distinguish flavor families, provided the mesons are much heavier than the electron, and the mesons related to the two possible sub-symmetries strongly differ in their masses. As was found [2], the radius of the star is much smaller than the classical electron radius, still the smallest radius down to which the photon oscillations are being counted might be of the order or even larger than the classical radius r_0 of the meson. Therefore, the effect of radiation on the motion of the star particles should be estimated for the electrons and the mesons differently though the very motion of the center of the electron wave packet, which only matters in the photon oscillations counting procedure, might be described classically in virtue of the Ehrenfest theorem. In so complicated systems as the stars containing several interacting particles, accurate calculation of radiation would be rather complicated, and, moreover, it is well known [4] that r_0 is the limit of validity of the electrodynamics, while the trajectories for the finest star lie well deeper this value. Therefore, QED is needed to determine single photon radiation of electrons, pair production etc. in the very strong (even vacuum violating) electric field [5]. However, the motion of the electrons is of interest here only inasmuch as it influences that of the mesons, and we need not go into fine details for the electron component of the star. We thus choose to model radiation of the electrons with an appropriate functional factor S that tempers the energy increase of the accelerated electrons. This factor will depend on a parameter q, varying which one can match a solution for the mesons according to the threshold where the quantum single photon radiation reaction exceeds the driving force in the star. We assume that S depends only on the kinetic energy of the electron via the relativistic factor γ_e: $S = \exp[-(\gamma_e^{-2} - \gamma_{ei}^{-2})/q^2]$, where γ_{ei} is the initial value γ_e of in the star. So, $S = 1$ at the initial moment, while for appropriate solutions the value of q must be so chosen that its final value $\gamma_{e,f} \cong 5$, in accordance with the charge gauge [2] in the basic (8:0) star unperturbed by mesons.

The mesons are expected to move unchanged over many successive stars. Their motion should be analyzed in respect of the possibility to sustain a regular lattice, that is, of the

$$
\left.
\begin{aligned}
S^{-1}\frac{d\beta_{eu}}{d\chi} &= -4u_e\gamma_e^{-5}\left[4u_e^2+v_e^2-(2u_e\beta_{ev}+v_e\beta_{eu})^2\right]^{-\frac{3}{2}}-\frac{1}{4}u_e\gamma_e^{-5}\left[u_e^2+v_e^2-(u_e\beta_{ev}-v_e\beta_{eu})^2\right]^{-\frac{3}{2}}+\\
&+\left[(u_M-u_e)\left(1-\beta_{eu}^2\right)-v_e\beta_{ev}(\beta_M-\beta_{eu})\right]\gamma_M^{-2}\gamma_e^{-1}\left[(u_M-u_e)^2+v_e^2\gamma_M^{-2}\right]^{-\frac{3}{2}}+\\
&+\left[(u_M+u_e)\left(1-\beta_{eu}^2\right)+v_e\beta_{ev}(\beta_M-\beta_{eu})\right]\gamma_M^{-2}\gamma_e^{-1}\left[(u_M+u_e)^2+v_e^2\gamma_M^{-2}\right]^{-\frac{3}{2}}\\
S^{-1}\frac{d\beta_{ev}}{d\chi} &= -v_e\gamma_e^{-5}\left[4u_e^2+v_e^2-(2u_e\beta_{ev}+v_e\beta_{eu})^2\right]^{-\frac{3}{2}}-\frac{1}{4}v_e\gamma_e^{-5}\left[u_e^2+v_e^2-(u_e\beta_{ev}-v_e\beta_{eu})^2\right]^{-\frac{3}{2}}+\\
&+3^{-\frac{1}{2}}v_e^{-2}\gamma_e^{-5}\left(1-\beta_{eu}^2-\frac{1}{4}\beta_{ev}^2\right)^{-\frac{3}{2}}-\left[(u_M-u_e)\beta_{eu}\beta_{ev}+v_e\left(1-\beta_M\beta_{eu}-\beta_{ev}^2\right)\right]\gamma_M^{-2}\gamma_e^{-1}\times\\
&\times\left[(u_M-u_e)^2+v_e^2\gamma_M^{-2}\right]^{-\frac{3}{2}}-\left[(u_M+u_e)\beta_{eu}\beta_{ev}-v_e\left(1-\beta_M\beta_{eu}-\beta_{ev}^2\right)\right]\gamma_M^{-2}\gamma_e^{-1}\left[(u_M+u_e)^2+v_e^2\gamma_M^{-2}\right]^{-\frac{3}{2}}\\
\eta^{-1}\frac{d\beta_M}{d\chi} &= -3(u_M-u_e)\gamma_M^{-3}\gamma_e^{-2}\left[(u_M-u_e)^2+v_e^2\gamma_e^{-2}\right]^{-\frac{3}{2}}+\\
&+3(u_M+u_e)\gamma_M^{-3}\gamma_e^{-2}\left[(u_M+u_e)^2+v_e^2\gamma_e^{-2}\right]^{-\frac{3}{2}}-\frac{1}{4}u_M^{-2}\gamma_M^{-5}
\end{aligned}
\right\}. \quad (1)
$$

repeatability of their initial and final velocities either in each star or, at least, for a long sequence of successive stars. For each of the sub-symmetries this possibility depends on the mass of the related meson. Interaction of the electrons and the mesons results in that that the motion of the electrons depends on the meson mass as well, hence the ratio of electron to meson masses might be obtained from our condition of the whole lattice regularity. Motion of heavy mesons might be described classically.

Strictly speaking, one has to include explicitly the meson radiation reaction term in the equation of motion. It would be convenient however to use, wherever possible, perturbation methods to determine the radiation reaction, provided it is much less than the driving force: The equation of motion could be solved for the driving force alone, and then the radiated energy is found using this solution. The final kinetic energy of the meson is determined by subtracting the radiation loss from its value as obtained before (see, e.g., [4]). This estimation is certainly valid for a large enough mass, since the radiation cross section contains inverse square of the mass value. For this reason, we may use classical, that is, multiple soft photon emission value for the radiation of heavy mesons.

2 (6:2) sub-symmetry

In this case, the meson/anti-meson pair still moves along a straight line, whereas the curved trajectories of the three electron family pairs confine to three planes intersecting over the meson axis with the relative angles $\frac{2\pi}{3}$. It is convenient therefore to measure the z coordinate along the meson axis, and to choose the second coordinate ρ at each electron plane as the distance from this axis. Then the values of ρ for each particle of the electron family (each one measured in its own plane) are equal, and the absolute values of z are the same for all electrons. In dimensionless variables:

$$
\chi=\frac{ct}{r_0},\quad u_e=\frac{z_e}{r_0},\quad v_e=\frac{\rho}{r_0},\quad \beta_{eu}=\frac{du_e}{d\chi},
$$

$$
\beta_{ev}=\frac{du_v}{d\chi},\quad u_M=\frac{z_M}{r_0},\quad \beta_M=\frac{du_M}{d\chi},\quad \eta=\frac{m_e}{m_M},
$$

$$
\gamma_e=\left(1-\beta_{eu}^2-\beta_{ev}^2\right)^{-\frac{1}{2}},\quad \gamma_M=\left(1-\beta_M^2\right)^{-\frac{1}{2}},
$$

where the subscript e marks electrons, M means mesons, c is the speed of light. The system of three ODEs describes the motion of the electrons and the mesons in the star under their interaction. Using the well-known expression for the field of a fast moving charge [4], this system can be written as shown in Eqs. 1 on top of this Page 101.

This system should be numerically solved under the initial conditions taken from the solution for the basic electron family [2]: the initial radius of the electrons $r_{e,i}=0.24r_0$, and $\gamma_{e,i}=3.2$. In our variables, these correspond to:

$$
\left.
\begin{aligned}
&\chi_i=0,\quad u_{e,i}=\frac{r_i}{3r_0},\quad v_{e,i}=\frac{2\sqrt{2}r_i}{3r_0}\\
&\beta_{eu,i}=\frac{1}{3}\beta_{e,i},\beta_{ev,i}=\frac{2\sqrt{2}}{3}\beta_{e,i}\\
&\beta_{e,i}=\left(1-\gamma_{e,i}^{-2}\right)^{\frac{1}{2}},\quad \beta_{M,i}=\left(1-\gamma_{M,i}^{-2}\right)^{\frac{1}{2}}
\end{aligned}
\right\}. \quad (2)
$$

In the perturbation approach, the value of $\gamma_{M,i}$ for the regular lattice should be equal to the final $\gamma_{M,f}$ at the exit of the preceding star (or a group of stars) as obtained by subtracting the radiation term $\gamma_{M,rad}$ and the term of the exit potential barrier $\gamma_{M,ex}$ from the final value of the solution to the system (1). These terms are:

$$
\gamma_{M,rad}=\frac{2}{3}\eta\int_0^{\chi_f}d\chi\left(\frac{d\beta_M}{d\chi}\right)^2\gamma_M^3, \quad (3)
$$

$$\gamma_{M,ex} \cong 12^{-1}\eta u_{M,f}^{-1}\gamma_{M,i}^{-2}. \quad (4)$$

It is assumed in (4) that $\gamma_{M,ex} \ll \gamma_{M,f} - \gamma_{M,i}$, and $u_{M,f} \ll u_{M,i}$. (The first inequality holds since the deceleration from the opposite meson is at least an order of magnitude less than the acceleration from the electrons because of the relativistic anisotropy of the electric field of fast moving charges.)

Then the value of $u_{M,i}$ is: $u_{M,i} = \frac{r_i}{r_0}(2-\beta_{M,f})$, where $\beta_{M,f} = (1-\gamma_{M,f}^{-2})^{1/2}$.

The solution for (1) goes down to the final value $r_{e,2} = 0.002 r_0$, that is, $(u_{e,2}^2 + v_{e,2}^2 = 0.002)^{1/2}$. This value of $r_{e,2}$ corresponds to the average value of the weak Yukawa-type potential (instead of $r_{e,2} = 0.003 r_0$ found in the charge gauge procedure for (8:0) case [2]). We assume that the electrons and positrons disappear at $r < r_{e,2}$. The value of χ_f in (3) should be defined by the condition that the function $r_e(\chi_f) = r_{e,2}$ for the first time.

The solution must meet the requirement for the meson to be unrecognized with our method of symmetry detection, i.e., that the numbers of the photon oscillations remain equal for the electron and the meson. To this end, consider the photon emitted at $r_e(0) = r_i$ and reaching $r_{e,1} = r_e(\chi_{e,1})$ after being reflected at the star center. Then, $\chi_{e,1} = (u_{e,i}^2 + v_{e,i}^2)^{1/2} + (u_{e,1}^2 + v_{e,1}^2)^{1/2}$, where the last member should be taken from (1). Similarly for the meson: $\chi_{M,1} = u_{M,i} + u_{M,1}$. Neglecting the small (because $r_{M,1} \gg r_{M,2} \approx r_{M,i} - r_{e,i}$) difference in the initial positions, we write the condition for the second photon not to have enough time to oscillate between the electron and the center over the first oscillation of the meson as:

$$\left(u_{e,1}^2 + v_{e,1}^2\right)^{\frac{1}{2}} + 0.002 > u_{M,1}. \quad (5)$$

This inequality ensures that the electron annihilates within the time of the first oscillation for the meson. Since the meson doesn't annihilate, the opposite inequality preventing the second photon oscillation for the meson within the time of the first photon oscillation for the electron is:

$$u_{M,1} > \left(u_{e,1}^2 + v_{e,1}^2\right)^{\frac{1}{2}}. \quad (6)$$

Upon solving the system (1) with $q = 2$, it was found that only for $\eta = 0.0003$ there exists an "equilibrium cycle" that repeats itself over the series of the stars (possibly with small shift of $\gamma_{M,f}$ from a mean value in a star to be compensated with some opposite shift in the next star) under the conditions (5) and (6) for some particular value of $\gamma_{M,i}$. For $\gamma_{M,i} = 5.150408$, and $u_{M,i} = 0.244567$, the system (1) yields $\gamma_{M,f} = 5.248322 \neq \gamma_{M,i}$, but already in the next star with $u_{M,i}$, following from this $\gamma_{M,f} : u_{M,i} = 0.244397$ ($\gamma_{M,i} = 5.248322$), we obtain $\gamma_{M,f} = 5.150408$, and the solution for the whole trajectory of the meson repeats itself infinitely. For these two consecutive stars: $(u_{e,1}^2 + v_{e,1}^2)^{1/2} = 0.00437$ and 0.003782, $u_{M,1} = 0.004815$ and 0.003785 respectively, so both (5) and (6) are fulfilled for each of them; $u_{M,f} = u_{M,2} = 0.00214$, $(u_{e,1}^2 + v_{e,1}^2)^{1/2} = 0.002$, $\gamma_{e,f} = 5.280387$. According to (3) and (4), radiation decreases $\gamma_{M,f}$ by only $\gamma_{M,rad} \approx 10^{-4}$, and the exit potential by $\gamma_{M,ex} \approx 10^{-3}$. Both are small as compared to the variation in the energy of the meson along its trajectory: $\left|\gamma_{M,f} - \gamma_{M,i}\right| \approx 0.05$. Hence, our assumption for deceleration from the exit potential barrier to be negligible for (6:2) sub-symmetry is reasonable. No acceptable solutions exist for other values of η. Although at each η there is a value of $\gamma_{M,i}$, for which the electrons and the mesons meet at $(u_{e,2}^2 + v_{e,2}^2)^{1/2} \approx u_{M,2} \leqslant 0.002$, but $\gamma_{M,f} \neq \gamma_{M,i}$, tending to increase monotonously, when extended over the next stars. Eventually the electron radius $(u_{e,2}^2 + v_{e,2}^2)^{1/2}$ becomes larger than the weak interaction threshold 0.002 everywhere on the trajectory. E.g., for $\eta = 0.00015$ this happens at $\gamma_{M,i} \approx 5.46$, while for $\eta = 0.0004$ at $\gamma_{M,i} \approx 5.48$. (For $\eta = 0.0002$, only (6) is broken.) Then the annihilation of the electrons becomes impossible, and our lattice will be ruined.

This behavior of the solutions to (1) can be explained as follows. If in the immediate vicinity of the star center the positive, say, meson lags with respect to the three nearest electrons, it is accelerated, while the electrons are decelerated to be overtaken by the meson and vice versa. Which case is realized depends on η and on $\gamma_{M,i}$. The equilibrium along the whole series comes from balance in the interaction. If situation is far from the balance, the meson will move much ahead or behind the electrons. Then its attraction will not be able to compensate for the reciprocal repulsion of the electrons, resulting in the increase of $(u_{e,2}^2 + v_{e,2}^2)^{1/2}$, and this quantity becomes eventually larger than 0.002.

3 (4:4) sub-symmetry

In this case, electrons and mesons move in two orthogonal planes intersecting at some axis of the cube (z) that connects the centers of the pair of its opposite faces. In each of these planes, the absolute values of the two Cartesian coordinates of the particles are the same for its four particles — electrons or mesons — due to the (4:4) symmetry. It is convenient therefore to choose a coordinate frame with the (x) axis in the electron plane and the (y)axis in the meson plane.

We guess in this case $\eta \gg 0.0003$, since the effect of four electrons on four mesons is smaller than that of six electrons on two mesons. Hence, radiation is expected to be important, since the meson must radiate much more energy with main contribution coming from the close neighborhood of the star center. This effect owes to the smaller meson mass as well as to the curvature of the trajectory, since, given force, transverse acceleration scales as γ^{-1} while longitudinal one only as γ^{-3}. Although it was long shown [4, 6] that, in the relativistic case, the energy radiated by the particle might be even larger than that received under external acceleration, we cannot use this result directly. In these references, the accelerating field was considered given in advance, i.e. independent of the particle's motion, whereas in our case back influence of radiation

$$
\left.
\begin{aligned}
S^{-1}\frac{d\beta_{eu}}{d\chi} = &-\frac{1}{4}\left(1-\beta_{ev}^2\right)^{-\frac{1}{2}}\left(1-\beta_{eu}^2\right)\gamma_e^{-3}u_e^{-2}-\frac{1}{4}\left(1-\beta_{eu}^2\right)^{-\frac{1}{2}}\beta_{eu}\beta_{ev}\gamma_e^{-3}v_e^{-2}-\\
&-\frac{1}{4}\left[u_e\left(\gamma_e^{-2}+\beta_{eu}^2\beta_{ev}^2+\beta_{eu}\beta_{ev}^3\right)-v_e\left(2\beta_{eu}\beta_{ev}-\beta_{eu}^3\beta_{ev}^2-\beta_{eu}^2\beta_{ev}^2\right)\right]\gamma_e^{-3}\left[u_e^2+v_e^2-(u_e\beta_{ev}-v_e\beta_{eu})^2\right]^{-\frac{3}{2}}+\\
&+2\left[(u_M+u_e)\left(1-\beta_{ev}\beta_{Mu}\right)\left(1-\beta_{eu}^2\right)-v_e\left(1-\beta_{eu}\beta_{Mu}\right)\beta_{eu}\beta_{ev}\right]\gamma_e^{-1}\gamma_M^{-2}+\\
&+\left\{v_e^2\gamma_M^{-2}+w_M^2+(u_M+u_e)^2-\left[(u_M+u_e)\beta_{Mw}-w_M\beta_{Mu}\right]^2\right\}^{-\frac{3}{2}}+\\
&+2\left[(u_M-u_e)\left(1-\beta_{ev}\beta_{Mu}\right)\left(1-\beta_{eu}^2\right)-v_e\left(1-\beta_{eu}\beta_{Mu}\right)\beta_{eu}\beta_{ev}\right]\times\\
&\times\gamma_e^{-1}\gamma_M^{-2}\left\{v_e^2\gamma_M^{-2}+w_M^2+(u_M-u_e)^2-\left[(u_M-u_e)\beta_{Mw}-w_M\beta_{Mu}\right]^2\right\}^{-\frac{3}{2}}\\
S^{-1}\frac{d\beta_{ev}}{d\chi} = &-\frac{1}{4}\left\{u_e\beta_{ev}\left(\beta_{eu}+\beta_{ev}\right)\left(1-\beta_{ev}^2\right)+v_e\left[1-\beta_{ev}\left(\beta_{eu}+\beta_{ev}\right)\left(1-\beta_{eu}\beta_{ev}\right)\right]\right\}\gamma_e^{-3}\times\\
&\times\left[u_e^2+v_e^2-(u_e\beta_{ev}-v_e\beta_{eu})^2\right]^{-\frac{3}{2}}+\frac{1}{4}\left(1-\beta_{eu}^2\right)^{\frac{1}{2}}\left(1-\beta_{ev}^2\right)\gamma_e^{-3}v_e^{-2}+\frac{1}{4}\left(1-\beta_{eu}^2\right)^{-\frac{1}{2}}\beta_{eu}\beta_{ev}\gamma_e^{-1}u_e^{-2}+\\
&+2\left[(u_M+u_e)\left(1-\beta_{ev}\beta_{Mu}\right)\beta_{eu}\beta_{ev}-v_e\left(1-\beta_{eu}\beta_{Mu}\right)\left(1-\beta_{ev}^2\right)\right]\times\\
&\times\gamma_M^{-2}\gamma_e^{-1}\left\{v_e^2\gamma_M^{-2}+w_M^2+(u_M+u_e)^2-\left[(u_M+u_e)\beta_{Mw}-w_M\beta_{Mu}\right]^2\right\}^{-\frac{3}{2}}-\\
&-2\left[(u_M-u_e)\left(1-\beta_{ev}\beta_{Mu}\right)\beta_{eu}\beta_{ev}-v_e\left(1-\beta_{eu}\beta_{Mu}\right)\left(1-\beta_{ev}^2\right)\right]\gamma_M^{-2}\gamma_e^{-1}\times\\
&\times\left\{v_e^2\gamma_M^{-2}+w_M^2+(u_M-u_e)^2-\left[(u_M-u_e)\beta_{Mw}-w_M\beta_{Mu}\right]^2\right\}^{-\frac{3}{2}}\\
\frac{d^2\beta_{Mu}}{d\chi^2} = &\frac{3}{2}\left(\eta^{-1}\frac{d\beta_{Mu}}{d\chi}-U\right)\gamma_M^{-1}-2\left(\beta_{Mu}\frac{d\beta_{Mu}}{d\chi}+\beta_{Mw}\frac{d\beta_{Mw}}{d\chi}\right)\times\\
&\times\left[\frac{d\beta_{Mu}}{d\chi}-\gamma_M^{-2}\beta_{Mw}\left(\beta_{Mu}\frac{d\beta_{Mw}}{d\chi}-\beta_{Mw}\frac{d\beta_{Mu}}{d\chi}\right)\right]-2\gamma_M^{-2}\beta_{Mu}\left(\beta_{Mu}\frac{d\beta_{Mu}}{d\chi}+\beta_{Mw}\frac{d\beta_{Mw}}{d\chi}\right)^2\\
\frac{d^2\beta_{Mw}}{d\chi^2} = &\frac{3}{2}\left(\eta^{-1}\frac{d\beta_{Mw}}{d\chi}-W\right)\gamma_M^{-1}-2\left(\beta_{Mu}\frac{d\beta_{Mu}}{d\chi}+\beta_{Mw}\frac{d\beta_{Mw}}{d\chi}\right)\times\\
&\times\left[\frac{d\beta_{Mw}}{d\chi}+\gamma_M^{-2}\beta_{Mu}\left(\beta_{Mu}\frac{d\beta_{Mw}}{d\chi}-\beta_{Mw}\frac{d\beta_{Mu}}{d\chi}\right)\right]-2\gamma_M^{-2}\beta_{Mu}\left(\beta_{Mu}\frac{d\beta_{Mu}}{d\chi}+\beta_{Mw}\frac{d\beta_{Mw}}{d\chi}\right)^2
\end{aligned}
\right\},\quad (7)
$$

where the functions U and W are expressed as follows

$$
\begin{aligned}
U = &-\frac{1}{4}\left(1-\beta_{Mw}^2\right)^{-\frac{1}{2}}\left(1-\beta_{Mu}^2\right)\gamma_M^{-3}u_M^{-2}-\frac{1}{4}\left(1-\beta_{Mu}^2\right)^{-\frac{1}{2}}\beta_{Mu}\beta_{Mw}\gamma_{Mw}^{-3}w_M^{-2}-\\
&-\frac{1}{4}\left[u_M\left(\gamma_M^{-2}+\beta_{Mu}^2\beta_{Mw}^2+\beta_{Mu}\beta_{Mw}^3\right)-w_M\left(2\beta_{Mu}\beta_{Mw}-\beta_{Mu}^3\beta_{Mw}^2\right)\right]\gamma_M^{-3}\times\\
&\times\left[u_M^2+w_M^2-(u_M\beta_{Mw}-w_M\beta_{Mu})^2\right]^{-\frac{3}{2}}+2\left[(u_M+u_e)\left(1-\beta_{Mw}\beta_{eu}\right)\left(1-\beta_{Mu}^2\right)-w_M\left(1-\beta_{Mu}\beta_{eu}\right)\beta_{Mu}\beta_{Mw}\right]\times\\
&\times\gamma_M^{-1}\gamma_e^{-2}\left\{w_M^{-2}\gamma_e^{-2}+v_e^2+(u_M+u_e)^2-\left[(u_M+u_e)\beta_{ev}-v_e\beta_{eu}\right]^2\right\}^{-\frac{3}{2}}-\\
&-2\left[(u_M-u_e)\left(1-\beta_{Mw}\beta_{eu}\right)\left(1-\beta_{Mu}^2\right)-w_M\left(1-\beta_{Mu}\beta_{eu}\right)\beta_{Mu}\beta_{Mw}\right]\gamma_M^{-3}\times\\
&\times\left\{w_M^2\gamma_e^{-2}+v_e^2+(u_M-u_e)^2-\left[(u_e-u_M)\beta_{ev}-v_e\beta_{eu}\right]^2\right\}^{-\frac{3}{2}},
\end{aligned}
$$

$$W = -\frac{1}{4}\left\{u_M\beta_{Mw}\left(\beta_{Mu}+\beta_{Mw}\right)\left(1-\beta_{Mw}^2\right)+w_M\left[1-\beta_{Mw}\left(\beta_{Mu}+\beta_{Mw}\right)\left(1-\beta_{Mu}\beta_{Mw}\right)\right]\right\}\times$$
$$\times\ \gamma_M^{-3}\left[u_M^2+w_M^2-\left(u_M\beta_{Mw}-w_M\beta_{Mu}\right)^2\right]^{-\frac{3}{2}}+\frac{1}{4}\left(1-\beta_{Mu}^2\right)^{\frac{1}{2}}\left(1-\beta_{Mw}^2\right)\gamma_M^{-3}w_M^{-2}+$$
$$+\ \frac{1}{4}\left(1-\beta_{Mu}^2\right)^{-\frac{1}{2}}\beta_{Mu}\beta_{Mw}\gamma_M^{-1}u_M^{-2}+2\left[\left(u_M+u_e\right)\left(1-\beta_{Mw}\beta_{eu}\right)\beta_{Mu}\beta_{Mw}-w_M\left(1-\beta_{Mu}\beta_{eu}\right)\left(1-\beta_{Mw}^2\right)\right]\times$$
$$\times\ \gamma_e^{-2}\gamma_M^{-1}\left\{w_M^2\gamma_e^{-2}+v_e^2+\left(u_M+u_e\right)^2-\left[\left(u_M+u_e\right)\beta_{ev}-v_e\beta_{eu}\right]^2\right\}^{-\frac{3}{2}}+$$
$$+\ 2\left[\left(u_M-u_e\right)\left(1-\beta_{Mw}\beta_{eu}\right)\beta_{Mu}\beta_{Mw}-w_M\left(1-\beta_{Mu}\beta_{eu}\right)\left(1-\beta_{Mw}^2\right)\right]\times$$
$$\times\ \gamma_e^{-2}\gamma_M^{-1}\left\{w_M^2\gamma_e^{-2}+v_e^2+\left(u_M-u_e\right)^2-\left[\left(u_M-u_e\right)\beta_{ev}-v_e\beta_{eu}\right]^2\right\}^{-\frac{3}{2}}.$$

on the field-generating particles is important. We have thus to include the radiation reaction term explicitly in the equation of motion. But the value $\eta \approx 0.005$ is just at the boundary of self-contradiction of electrodynamics for the meson at the weak interaction threshold. Also quantum effects, however weaker than those for the electron, might alter radiation there. Moreover, deceleration of the meson at the exit potential barrier coming from other mesons as well as radiation accompanying this deceleration cannot be neglected now.

However, it would be inadequate merely to introduce a functional factor like that used above for the electron, because details of the meson trajectory are now in question. In order to trace the tendency, we shall instead try to approach the value $\eta = 0.005$ from below, i.e. from larger meson mass.

Again, in dimensionless variables

$$\chi=\frac{ct}{r_0},\quad u_e=\frac{z_e}{r_0},\quad v_e=\frac{x_e}{r_0},\quad \beta_{eu}=\frac{du_e}{d\chi},\quad \beta_{ev}=\frac{dv_e}{d\chi},$$
$$\gamma_e=\left(1-\beta_{eu}^2-\beta_{ev}^2\right)^{-\frac{1}{2}},$$
$$u_M=\frac{z_M}{r_0},\quad w_M=\frac{y_M}{r_0},\quad \beta_{Mu}=\frac{du_M}{d\chi},\quad \beta_{Mw}=\frac{dw_M}{d\chi},$$
$$\gamma_M=\left(1-\beta_{Mu}^2-\beta_{Mw}^2\right)^{-\frac{1}{2}},$$

the system of four ODE equations — Eqs. 7 shown in the previous Page 103, with the functions U and W explained on the same Page Page 103 and on top of this Page 104 — describes the relativistic motion of electrons and mesons in the (4:4) cubic star under their interaction.

This system will be numerically solved under following initial conditions:

$$u_{e,i}=u_{M,i}=\frac{r_i}{\sqrt{3}r_0},\quad v_{e,i}=w_{M,i}=\sqrt{\frac{2}{3}}\,\frac{r_i}{r_0},$$
$$\beta_{eu,i}=\frac{1}{\sqrt{3}}\,\beta_{e,i},\quad \beta_{Mu,i}=\frac{1}{\sqrt{3}}\,\beta_{M,i},\quad \beta_{ev,i}=\sqrt{\frac{2}{3}}\,\beta_{e,i},$$
$$\beta_{Mw,i}=\sqrt{\frac{2}{3}}\beta_{M,i},\quad \beta_{e,i}=\left(1-\gamma_{e,i}^{-2}\right)^{\frac{1}{2}},$$
$$\gamma_{e,i}=3.2,\quad \beta_{M,i}=\left(1-\gamma_{M,i}^{-2}\right)^{\frac{1}{2}}.$$

At the star exit, the contribution of radiation coming from meson-meson interaction is expected to be rather low. It is thus convenient to follow the method used in the previous section in order to separate the radiation part in the total decrease of kinetic energy there. So, we solve first the equations of motion ignoring radiation, and then compute $\gamma_{M,rad}$ over the confined to a plane meson trajectory corresponding to this solution:

$$\gamma_{M,rad}=\frac{2}{3}\,\eta\int_0^{\chi_f}d\chi\left[\left(\frac{d\beta_{Mu}}{d\chi}\right)^2+\left(\frac{d\beta_{Mw}}{d\chi}\right)^2-\right.$$
$$\left.-\left(\beta_{Mw}\frac{d\beta_{Mu}}{d\chi}-\beta_{Mu}\frac{d\beta_{Mw}}{d\chi}\right)^2\right]\gamma_M^3. \qquad (8)$$

The related ODE system is shown in Eqs. 9 on top of the next Page 104.

Since the lateral displacement of the heavy meson in a single star is expected to be small, the system (9) should be solved under the initial condition:

$$u_{Mi}=\frac{r_{M2}}{\sqrt{3}},\quad w_{Mi}=r_{M2}\sqrt{\frac{2}{3}},\quad r_{M2}=\left(u_{M2}^2+w_{M2}^2\right)^{\frac{1}{2}}, \qquad (10)$$

where r_{M2} is the final radius of the meson in the accelerating phase of the star. It was found that the condition (6) holds only for $\eta \geqslant 0.005$. With $\eta = 0.005$, the equilibrium cycle looks as follows. (We have to choose $q = 1.3$ to agree with the charge gauge condition $\gamma_{e,f} \approx 5$ as in [2]). Unlike (6:2) case, in which the full cycle of returning to the initial state takes two neighboring stars, now it takes four.

On the accelerating phase of the first star of the cycle: $r_{M,i} = 0.244912$; $r_{M,2} = 0.001923$; $\gamma_{M,i} = 4.927011$; $\gamma_{M,f} = 5.090523$; $\gamma_{e,f} = 5.353761$. On the decelerating phase: $\gamma_{M,f} = 4.925161$; $\gamma_{M,rad} = 0.014866$. Radiation energy decrease (8) is less than 0.1 of that from the exit potential barrier as found by subtraction the final energy for the deceleration phase (9) from that for the acceleration phase (7), the second being initial for the first. Hence, our approximation is appropriate. On the accelerating phase of the last star of the cycle: $r_{M,i} = 0.244921$; $r_{M,2} = 0.001934$; $\gamma_{M,i} = 4.926057$;

$$\left.\begin{aligned}
\eta^{-1}\frac{d\beta_{Mu}}{d\chi} &= \frac{1}{4}\left(1-\beta_{Mw}^2\right)^{-\frac{1}{2}}\left(1-\beta_{Mu}^2\right)\gamma_M^{-3}u_M^{-2} - \frac{1}{4}\left(1-\beta_{Mu}^2\right)^{-\frac{1}{2}}\beta_{Mu}\beta_{Mw}\gamma_M^{-3}w_M^{-2} - \\
&- \frac{1}{4}\left[u_M\left(\gamma_M^{-3}+\beta_{Mu}^2\beta_{Mw}^2+\beta_{Mu}\beta_{Mw}^3\right) - w_M\left(2\beta_{Mu}\beta_{Mw}-\beta_{Mu}^3\beta_{Mw}^2-\beta_{Mu}^2\beta_{Mw}^2\right)\right]\times \\
&\times\ \gamma_M^{-3}\left[u_M^2+w_M^2-(u_M\beta_{Mw}-w_M\beta_{Mu})^2\right]^{-\frac{3}{2}} \\
\eta^{-1}\frac{d\beta_{Mw}}{d\chi} &= -\frac{1}{4}\left\{u_M\beta_{Mw}\left(\beta_{Mu}+\beta_{Mw}\right)\left(1-\beta_{Mw}^2\right)+w_M\left[1-\beta_{Mw}\left(\beta_{Mu}+\beta_{Mw}\right)\left(1-\beta_{Mu}\beta_{Mw}\right)\right]\gamma_M^{-3}\times\right. \\
&\left.\times\left[u_M^2+w_M^2-(u_M\beta_{Mw}-w_M\beta_{Mu})^2\right]^{-\frac{3}{2}}+\frac{1}{4}\left(1-\beta_{Mu}^2\right)^{\frac{1}{2}}\left(1-\beta_{Mw}^2\right)\gamma_M^{-3}w_M^{-2}+\frac{1}{4}\left(1-\beta_{Mu}^2\right)^{-\frac{1}{2}}\beta_{Mu}\beta_{Mw}\gamma_M^{-1}u_M^{-2}\right.
\end{aligned}\right\}. \quad (9)$$

$\gamma_{M,f} = 5.089923$; $\gamma_{e,f} = 5.411567$. On its decelerating phase again: $\gamma_{M,f} = 4.927011$. The conditions (5) and (6) are satisfied in all four stars of the equilibrium cycle.

Contrary to the (6:2) case, both electron and meson energies have been found to increase in the close vicinity of the star center on the acceleration phase. Therefore, for (4:4) symmetry it is just meson radiation that dominates the mechanism to support equilibrium. An equilibrium cycle satisfying both (5) and (6) exists also for $\eta > 0.005$. Formal solution gives that only for $\eta > 0.02$ the condition (5) is broken. QED estimation with averaged Coulomb field [5] shows that for heavy meson ($\eta < 0.02$) quantum single photon corrections for radiation are small. However, classical electrodynamics is invalid for $\eta < 0.005$. Therefore $\eta = 0.005$ could only be accepted as the lowest value compatible with the above equations. This result by no means undermines the very fact of correspondence between the lepton families and the cube star sub-symmetries as detected with photon oscillation counting, which possesses its own meaning, independent of a particular theory to specify trajectories.

4 Concluding remarks

However imprecise, the obtained values for η strongly suggest the (6:2) and (4:4) sub-symmetries to be associated accordingly with the $\tau-$meson ($\approx 1.5\,\mathrm{GeV}/c^2$, $\eta = 0.0003$) and the meson ($\approx 100\,\mathrm{MeV}/c^2$, $\eta = 0.005$). Our estimations are reliable because of sufficiently big differences in mass values between the leptons. In order to find precise values, more complicated calculations of bremsstrahlung [5] are required for the star involving many Feynman diagrams for the mesons, interacting between themselves and with the electrons. Another approximation relates to the assumed sharp cut-off in the electroweak interaction at $r_{e,2}$.

We point out that the similar analysis might be carried out for quarks, which correspond to the three subsets of the complementary to the cube 12-particle part of the dodecahedron star in the full gauge lattice [2].

Although being presented here in the conventional form, the motion-to-motion gauge is actually coordinate-less, basing solely on the existence of the top velocity signal and symmetrical patterns of particles' trajectories. The existence of the flavor families could never be comprehended, unless the direct motion-to-motion gauge of charge is used, because the intermediary involving reference systems comprised of clocks and rods hides some important features of actual measurements. Just the same situation comes about in the weak interaction [3], where the obstructive role of reference systems stimulates the appearance of auxiliary "principles" like gauge invariance with its artificial group structure that can only explain the already known results of experiments rather than predict them. As a matter of fact, the very statement of the basic problem in mechanics, i.e. the contact problem, must be sufficient to substantiate all principles, including Lorentz covariance, gauge invariance and so on [7].

Submitted on December 23, 2014 / Accepted on December 28, 2014

References

1. Guidry M. Gauge Field Theories. A Wiley-Interscience Publication, 1991.
2. Tselnik F. *Communications in Nonlinear Science and Numerical Simulations*, 2007, v. 12, 1427.
3. Tselnik F. *Progress in Physics*, 2015, v. 1(1), 50.
4. Landau L.D., Lifshitz E.M. The Classical Theory of Fields. Oxford, Pergamon Press, 1962.
5. Akhiezer A.I, Berestetskii V.B. Quantum Electrodynamics. New York, Interscience Publishers, 1965.
6. Pomeranchuk I.Ya. Maximum energy that primary cosmic-ray electrons can acquire on the surface of the Earth as a result of radiation in the Earth's magnetic field. *JETP*, 1939, v. 9, 915; *J. Phys. USSR*, 1940, v. 2, 65.
7. Tselnik F. Preprint No. 89-166. Budker Institute of Nuclear Physics, Novosibirsk, 1989.

Progress in Physics is an American scientific journal on advanced studies in physics, registered with the Library of Congress (DC, USA): ISSN 1555-5534 (print version) and ISSN 1555-5615 (online version). The journal is peer reviewed and listed in the abstracting and indexing coverage of: Mathematical Reviews of the AMS (USA), DOAJ of Lund University (Sweden), Zentralblatt MATH (Germany), Scientific Commons of the University of St.Gallen (Switzerland), Open-J-Gate (India), Referential Journal of VINITI (Russia), etc. Progress in Physics is an open-access journal published and distributed in accordance with the Budapest Open Initiative: this means that the electronic copies of both full-size version of the journal and the individual papers published therein will always be acessed for reading, download, and copying for any user free of charge. The journal is issued quarterly (four volumes per year).

Electronic version of this journal: http://www.ptep-online.com

Postal address:
Department of Mathematics and Science, University of New Mexico,
705 Gurley Avenue, Gallup, NM 87301, USA